Hadronic corrections to electroweak observables from twisted mass lattice QCD

DISSERTATION

zur Erlangung des akademischen Grades

doctor rerum naturalium
(Dr. rer. nat.)

im Fach Physik

eingereicht an der
Mathematisch-Naturwissenschaflichen Fakultät
Humboldt-Universität zu Berlin

von
Frau M. Sc. Grit Pientka, geb. Hotzel

Präsident der Humboldt-Universität zu Berlin
Prof. Dr. Jan-Hendrik Olbertz

Dekan der Mathematisch-Naturwissenschaftlichen Fakultät
Prof. Dr. Elmar Kulke

Gutachter/innen:
1. **Prof. Dr. Marc Wagner, Goethe-Universität Frankfurt**
2. **Prof. Dr. Michael Müller-Preußker, Humboldt-Universität zu Berlin**
3. **PD Dr. Meinulf Göckeler, Universität Regensburg**

Tag der mündlichen Prüfung: 11.09.2015

To my birds of prey

Abstract

Among the most prominent benchmark quantities investigated to detect signs for new physics beyond the standard model of elementary particle physics are the weak mixing angle and the muon anomalous magnetic moment. For both quantities, new experiments aiming at a substantial error reduction are being constructed. Due to the great precision achieved by perturbative computations of the QED and electroweak contributions, the non-perturbative leading QCD contributions nowadays account for the largest uncertainties in the standard model predictions. They are usually extracted from results of other experiments by means of sophisticated phenomenological analyses. In this way the accuracy of the theoretical determination of these contributions is limited by the accuracy of the experimental data, and the resulting values cannot be regarded as pure standard model predictions.

Lattice QCD currently constitutes the only ab initio approach available at small momentum transfers for the computation of non-perturbative hadronic observables. We compute the leading QCD contribution to the muon anomalous magnetic moment by performing lattice QCD calculations on ensembles incorporating $N_f = 2 + 1 + 1$ dynamical twisted mass fermions. Considering active up, down, strange, and charm quarks, admits for the first time a direct comparison of the lattice data for the muon anomaly with phenomenological results because both the latter as well as the experimentally obtained values are sensitive to the complete first two generations of quarks at the current level of precision. Recently, it has been noted that improved measurements of the electron and tau anomalous magnetic moments might also provide ways of detecting new physics contributions. Therefore, we also compute their leading QCD contributions, which simultaneously serve as cross-checks of the value obtained for the muon.

Additionally, we utilise the obtained data to compute the leading hadronic contribution to the running of the fine structure constant, which enters all perturbative QED calculations. Furthermore, we show that even for the weak mixing angle the leading QCD contribution can be computed from this data. In this way, we identify a new prime observable in the search for new physics whose hadronic contributions can be obtained from lattice QCD. The phenomenological determination of the hadronic contributions to the running of the weak mixing angle is hampered by the necessity to perform a flavour separation of the experimental data, for which several possibilities exist. With the results obtained in this thesis, we are able to exclude unsuitable flavour separations and thus directly assist the presently more precise phenomenological determinations of this eminent quantity.

For all five electroweak observables, we perform the continuum limit and comprehensive analyses of the systematic uncertainties, including a first estimate of the influence of the light-quark disconnected contributions. The resulting values for all quantities are fully consistent with the results of various phenomenological analyses, thus representing a highly non-trivial cross-check of those values. Moreover, since they can systematically be improved, these first four-flavour lattice QCD determinations pave the way for obtaining more exact results in the future. The quantified systematic uncertainties of our computations enable us to outline the steps that are necessary in order to possibly surpass the phenomenological accuracies within the coming years.

Zusammenfassung

Zu den bedeutendsten Richtgrößen, die untersucht werden, um Hinweise auf Neue Physik jenseits des Standardmodells der Elementarteilchenphysik zu finden, gehören der schwache Mischungswinkel und das anomale magnetische Moment des Myons. Für beide Größen werden derzeit neue Experimente konstruiert, deren Ziel eine deutliche Fehlerreduzierung ist. Aufgrund der hohen Genauigkeit, die bei den perturbativen Berechnungen der QED- und der elektroschwachen Beiträge erzielt worden ist, weisen mittlerweile die nichtperturbativen führenden QCD-Beiträge die größten Unsicherheiten in den Standardmodellvorhersagen auf. Diese werden gewöhnlich mittels komplexer phänomenologischer Analysen aus anderen experimentellen Ergebnissen gewonnen. Somit wird die Genauigkeit der theoretischen Bestimmung dieser Beiträge durch die Genauigkeit der experimentellen Daten limitiert und die resultierenden Werte können nicht als reine Standardmodellvorhersagen betrachtet werden.

Die Gitter-QCD stellt zur Zeit den einzigen Ab-initio-Zugang für die Berechnung von nichtperturbativen hadronischen Observablen bei kleinen Impulsüberträgen dar. Wir bestimmen den führenden QCD-Beitrag zum anomalen magnetischen Moment des Myons mit Hilfe einer Gitter-QCD-Rechnung auf Ensemblen, die $N_f = 2 + 1 + 1$ dynamische Twisted-Mass-Fermionen berücksichtigen. Durch die Betrachtung aktiver up, down, strange and charm Quarks können erstmalig Gitter-QCD-Daten für die Myonanomalie direkt mit phänomenologischen Resultaten verglichen werden, da letztere genau wie die experimentellen Ergebnisse bei der derzeitigen Genauigkeit sensitiv auf die vollständigen ersten beiden Quarkgenerationen sind. Unlängst wurde darauf hingewiesen, dass es auch möglich sein könnte Beiträge Neuer Physik durch verbesserte Messungen der anomalen magnetischen Momente des Elektrons und des Tauons nachzuweisen. Aus diesem Grund berechnen wir auch deren führende QCD-Beiträge, was gleichzeitig eine Überprüfung des Wertes liefert, den wir für das Myon erhalten haben.

Zusätzlich nutzen wir die gewonnenen Daten, um den führenden hadronischen Beitrag zum Laufen der Feinstrukturkonstante zu berechnen, die in alle perturbativen QED-Rechnungen eingeht. Darüber hinaus zeigen wir, dass sogar für den schwachen Mischungswinkel der führende QCD-Beitrag mit Hilfe dieser Daten berechnet werden kann. Dadurch identifizieren wir eine neue grundlegende Observable für die Suche nach Neuer Physik, deren hadronische Beiträge mit Hilfe der Gitter-QCD beschafft werden können. Die phänomenologische Bestimmung der hadronischen Beiträge zum Laufen des schwachen Mischungswinkels werden durch die Notwendigkeit erschwert eine Flavourseparation der experimentellen Daten vorzunehmen, für welche es unterschiedliche Herangehensweisen gibt. Mit den Resultaten dieser Arbeit ist es uns gelungen ungeeignete Herangehensweisen auszuschließen und somit direkt die derzeit präziseren phänomenologischen Bestimmungen dieser bedeutsamen physikalischen Größe zu unterstützen.

Für alle fünf elektroschwachen Observablen führen wir den Kontinuumslimes und umfangreiche Analysen der systematischen Unsicherheiten durch, inklusive einer ersten Abschätzung des Einflusses der unverbundenen Beiträge der leichten Quarks. Die daraus resultierenden Werte sind für alle Größen vollkommen konsistent mit den Ergebnissen von verschiedenen phänomenologischen Analysen, was eine hochgradig nichttriviale Überprüfung dieser Werte darstellt. Zudem ebnen diese ersten Vier-Flavour-Gitter-QCD-Berechnungen den Weg um zukünftig genauere Resultate zu erhalten, da sie systematisch verbessert werden können. Die quantifizierten systematischen Unsicherheiten unserer Berechnungen ermöglichen es uns die Schritte zu skizzieren, die nötig sind, um möglicherweise die phänomenologischen Genauigkeiten innerhalb der nächsten Jahre zu übertreffen.

Contents

Chapter 1

Introduction

The known fundamental forces of nature comprise the strong, the electromagnetic, the weak, and the gravitational interaction. The latter is very successfully described by the laws of general relativity [Einstein 1916], whereas the standard model of elementary particle physics (SM) [Glashow 1961a, Weinberg 1967, Salam 1968] constitutes the theoretical framework for the first three and is extremely well tested, too. Despite their success, no consistent way has been found to combine the two. Hence, both theories are considered incomplete; general relativity because no consistent quantised version has been established so far and the SM because it does not account for a number of experimental observations as discussed below.

This thesis addresses prime candidate observables for detecting clues of new physics beyond the SM. In particular, we focus on the computation of hadronic vacuum polarisation contributions to electroweak quantities. These contributions are obtained from the investigation of hadronic current correlators in lattice QCD. Below, we will first of all describe a small selection of the great successes of the SM before taking a closer look at its main features. In order to motivate the calculations performed in this thesis, some phenomena that cannot be explained by the SM and thus point towards its incompleteness will be presented subsequently. The observables we investigate will be specified in the outline of this work as delineated at the end of this introduction.

The SM is a renormalisable quantum field theory based on the principle of local gauge invariance. It comprises matter and antimatter fields as well as fields mediating the forces and the Higgs boson. Among the big successes of the theory were the prediction of the existence and the quantum numbers of eight of those particles which have later been confirmed, the charm quark [Glashow et al. 1970] [SLAC-SP-017 1974, E598 1974], the τ-lepton [Tsai 1971] [Perl et al. 1975], the bottom quark [Kobayashi and Maskawa 1973] [E288 1977], the gluon [Gell-Mann 1962] [TASSO 1979], the W and the Z bosons [Glashow 1961b] [UA1 1983, UA2 1983], the top quark [Kobayashi and Maskawa 1973] [CDF 1995, D0 1995], and the Higgs boson [Higgs 1964] [ATLAS 2012, CMS 2012], where the first set of references refers to the theoretical predictions and the second one to the experimental observations. Another big achievement is that the SM has so far withstood all scrutinies by the Large Hadron Collider (LHC) where several processes predicted by the theory have been measured for the first time without detecting any significant deviations, e.g. those originating from quartic couplings of weak vector bosons [ATLAS 2015, CMS 2015].

The matter content of the theory is represented by spin-$\frac{1}{2}$ fermions which are divided into quarks and leptons. They are grouped in three families or generations consisting of two quarks, two antiquark, two leptons, and two antileptons each. The leptons are subdivided into an electrically charged, electronlike lepton and the respective neutrino; the same applies to the antileptons. The particle masses grow with increasing family number. Tab. 1.1 contains the matter content of the SM.

matter fields				gauge bosons	Higgs boson
quarks	$\begin{pmatrix} u \\ d \end{pmatrix}_L$	$\begin{pmatrix} c \\ s \end{pmatrix}_L$	$\begin{pmatrix} t \\ b \end{pmatrix}_L$	A, γ, $W^{\pm}$, Z	H
	u_R, d_R	c_R, s_R	t_R, c_R		
leptons	$\begin{pmatrix} \nu_e \\ e \end{pmatrix}_L$	$\begin{pmatrix} \nu_\mu \\ \mu \end{pmatrix}_L$	$\begin{pmatrix} \nu_\tau \\ \tau \end{pmatrix}_L$		
	e_R	μ_R	τ_R		

Table 1.1.: The field content of the SM. For simplicity the antimatter fields are omitted. The quark flavours are up (u), down (d), charm (c), strange (s), top (t), and bottom (b). The three electrically charged leptons are called electron (e), muon (μ), and τ-lepton (τ). Each comes with a corresponding neutrino ν_e, ν_μ, and ν_τ. Above, the fields are organised in left-handed (L) doublets and right-handed (R) singlets with respect to $SU(2)_I$. The bosonic gauge fields are known as gluons (A) mediating the strong interaction, photons (γ) mediating the electromagnetic, and W- and Z-bosons mediating the weak interaction. The scalar Higgs field is needed for the generation of quark masses and for electroweak symmetry breaking leading to massive W- and Z-bosons.

Besides the matter fields, there are spin-1 vector bosons originating from the requirement of local gauge invariance of the SM under the gauge group $SU(3)_c \times SU(2)_I \times U(1)_Y$. The $SU(3)_c$ Lie group represents the gauge group of the theory describing the strong interaction known as quantum chromodynamics (QCD) [Gell-Mann 1962, Zweig 1964, Fritzsch et al. 1973]. c denotes the conserved charge of this interaction called colour. The bosonic mediators of the strong interaction are dubbed gluons. They only act on quark fields. In contrast, the electroweak interaction governed by the gauge group $SU(2)_I \times U(1)_Y$ [Glashow 1961b, 't Hooft 1971], where I stands for the weak isospin and Y is the hypercharge, involves all matter fields, quarks as well as leptons. In fact, the renormalisability of the $U(1)_Y$ gauge group necessitates the lepton-quark family structure of the SM. Spontaneous electroweak symmetry breaking via the Higgs mechanism [Higgs 1964, Englert and Brout 1964, Guralnik et al. 1964] leaves the electromagnetic subgroup $U(1)_Q$, where Q denotes the electric charge, intact whose force mediator is the photon. This constitutes the gauge group of quantum electrodynamics (QED) [Feynman 1950]. The massive $SU(2)_I$ gauge bosons in the broken phase are the W- and the Z-boson. The Higgs boson is the massive mode of the complex Higgs doublet field responsible for their masses and also for the masses of the quarks through Yukawa interactions.

In spite of the magnificent achievements of the SM, it cannot explain all phenomena attributed to the realm of particle physics. Among the clearest signs for the necessity to extend the SM are the observations of neutrino oscillations in solar, reactor, atmospheric, and accelerator neutrino fluxes, see [PDG 2014] for a review. This implies that, contrary to the original SM prediction, individual lepton number is violated. It also means that neutrinos have non-zero masses suggesting the exciting possibility that, in contrast to all other known elementary fermionic particles, neutrinos could be their own antiparticles and thus Majorana fermions [Majorana 1937].

Further evidence for physics beyond the SM stems from cosmological observations, namely the existence of dark matter and the baryon asymmetry of the universe. The observation of the remnants of colliding galaxy clusters are among the most striking indi-

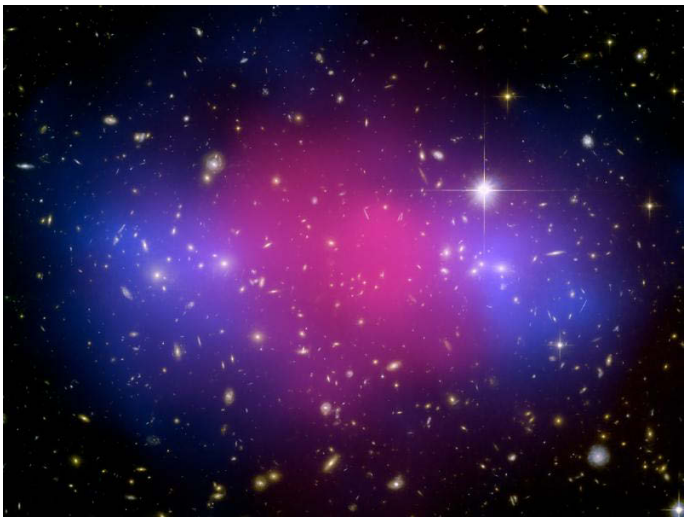

Figure 1.1.: Overlay of images obtained by the Hubble space telescope using gravitational lensing to map the matter distribution (blue) and by the Chandra X-ray observatory determining the position of ordinary matter (pink). The object known as MACS J0025.4-1222 is a remnant of a gigantic collision of galaxy clusters [Bradac et al. 2008], image from [NASA et al. 2013].

cations for dark matter. Here, the strong X-ray emission of baryonic matter occurs in a distinctly different region than where the majority of the mass is concentrated according to weak gravitational lensing [Clowe et al. 2006, Bradac et al. 2008]. An example is shown in Fig. 1.

In addition, there is a number of other clues pointing towards the existence of dark matter, e.g. the rotation curves of stars and galaxies and other gravitational lensing effects to name only a few, for a review see [Garrett and Duda 2011]. To allow for structure formation in the early universe this dark matter needs to be cold, i.e. non-relativistic. In fact, anisotropies in the cosmic microwave background radiation [Planck 2015], predictions from big bang nucleosynthesis [PDG 2014] as well as the analysis of the large-scale structure of the universe suggest that normal matter constitutes only about 15% of the matter content of the universe whereas 85% appears to be dark matter. The only stable, electrically neutral particles in the SM are neutrinos. Thus, they are the only SM particles representing possible dark matter candidates. However, due to their small mass they can only account for a tiny fraction of the dark matter content of the universe. This means that the origin of the majority of the matter in the universe remains unsettled.

The puzzle related to the baryon asymmetry of the universe can be summarised by the fact that there is hardly any antimatter in the observable universe, the only traces being compatible with secondary production in various astrophysical processes. Currently, no generally accepted explanation exists as to why this should be the case [Canetti et al. 2012, Balazs 2014]. Here again, big bang nucleosynthesis [PDG 2014] as well as the power spectrum of the cosmic microwave background [Planck 2015] allow us to quantify the initial baryon asymmetry at the time of recombination to be

$$\eta = \frac{n_b - n_{\overline{b}}}{n_\gamma} = \mathcal{O}\left(10^{-10}\right) ,$$

where n_b denotes the number of baryons, $n_{\bar{b}}$ the number of antibaryons, and n_γ the number of photons. This suggests that the baryon asymmetry might have been dynamically generated in the past. However, scrutinising the Sakharov conditions [Sakharov 1967] the baryon asymmetry of the universe cannot be explained within the SM mainly due to a too small violation of combined charge and parity symmetry (CP) and too small deviations from thermal equilibrium.

In addition to those well-established experimental hints pointing to the necessity for physics beyond the SM, there are several conceptional questions theorists would like to be able to answer. For example, there is no generally accepted explanation as to why there appear to be only three fermion families or why the values of their masses and mixing constants are as they are. Furthermore, there is the so-called strong CP problem. This comprises the experimental finding that a CP violating term, which is theoretically allowed for the strong interactions, appears to be absent. Another conceptional issue often used to motivate new physics is the hierarchy or naturalness problem related to the very different scales of electroweak symmetry breaking and the Planck scale. In order to solve these questions different new physics models have been devised.

The aim of contemporary particle physics is to inspect whether one of the proposed scenarios can explain the existing observations. Experimentally, this is done in two complementary ways. One is the so-called energy frontier currently presented by the LHC where particles collide at the highest attainable energies in order to directly produce and detect hypothetical particles not present in the SM thus providing a crystal clear proof of their existence. This approach is currently sensitive to particles with masses of up to $\mathcal{O}(10\,\mathrm{TeV})$. Another research direction deals with high precision experiments mostly at lower energies representing what is known as intensity frontier. This approach compares ultra-precise measurements with theoretical SM predictions in order to detect tiny deviations due to particles beyond the SM present in loop effects. In this way, present experiments are sensitive to about an order of magnitude higher energies than direct searches. Actually the values of the charm, the bottom, and the top quark masses have been sufficiently constrained by such experiments to enable their subsequent direct observation.

Nowadays, these indirect searches are performed with spectacular precision, the most prominent example being the anomalous magnetic moment of the electron, which has been measured by the Harvard group [Hanneke et al. 2008] with a precision of 0.24 ppb. In the past, this quantity has been essential for establishing QED as the correct theory of the electromagnetic interactions. The current experimental accuracy necessitates an extremely involved tenth-order perturbative QED calculation [Aoyama et al. 2015] and is even sensitive to electroweak and to QCD contributions. Convincing agreement between the experimental result and the SM prediction has been established. Thus, due to brilliant experimental techniques and truly outstanding perturbative calculations it is meanwhile possible to test the complete SM including QCD in the low-energy region.

The anomalous magnetic moment of the muon represents another observable, which has been measured with tremendous accuracy. Due to the muon being about 200 times heavier than the electron, it is unstable. Therefore, the determination of its magnetic moment is even more complicated. Nevertheless, the E821 experiment performed at BNL has achieved an impressive precision of 0.5 ppm [Muon (g-2) 2006, Roberts 2010a] for this quantity, which shows a deviation from the SM prediction of about three standard deviations [Jegerlehner and Nyffeler 2009, Hagiwara et al. 2011]. Since in many models

for physics beyond the SM, the contributions of new physics to the anomalous magnetic moments of the leptons are proportional to the squared lepton mass, the discrepancy could very well be caused by yet unknown physics.

Currently, there is, however, some ambiguity in the determination of the QCD contributions originating from the fact that QCD is inherently non-perturbative at low energies. The reason lies in the non-Abelian nature of the unbroken $SU(3)_c$ gauge group, which allows for gluon self-interactions and the fact that gluons carry colour charge, contrary to the photon, which is electrically neutral. This leads to two striking properties of QCD: asymptotic freedom [Gross and Wilczek 1973, Politzer 1973] and confinement [Wilson 1974]. Asymptotic freedom means that the theory can be described perturbatively at high energies because the strong coupling constant, α_s, decreases with increasing energy. On the contrary, α_s becomes large at small energies. This leads to the confinement of quarks in colourless bound states known as hadrons, for which perturbation theory is not applicable. Fortunately, the largest QCD contributions to the lepton anomalous magnetic moments can be related to experimental data from electron-positron scattering and τ-decays via a dispersion relation. However, these data sets are plagued by different systematic uncertainties, and the results obtained for the theoretical prediction of the anomalous magnetic moments depend to a certain extent on the choice of the data sets, cf. [Benayoun et al. 2012b].

In this situation lattice QCD [Wilson 1974], the approach employed in this thesis, might be valuable since it constitutes a very successful non-perturbative tool to obtain quantitative results in the low-energy domain of the strong interaction. In fact, it is the only purely theoretical first-principle approach solely based on QCD available for such calculations. As we will see upon introducing lattice QCD in chapter 2, the numerical computations can be systematically improved such that more accurate results can be expected by investing more computing time, improved algorithms, and conceptually better approaches. Therefore, lattice QCD can provide a real ab-initio prediction of the hadronic contributions to the lepton anomalous magnetic moments and other electroweak observables.

The utility of lattice QCD has been tremendously increased during the last decade by the steady advent of more and more powerful computing architectures and great algorithmic and conceptual advances. Thus, lattice QCD is now capable of producing results with accuracies that are useful for intensity-frontier searches for new physics. In particular, it is now possible to perform simulations involving the complete first two quark families, which, for the observables investigated in this thesis, is indispensable in order to draw a comparison with the real world.

In this work, we employ the twisted mass formulation of lattice QCD [Aoki and Gocksch 1989, Alpha 2001, Frezzotti and Rossi 2004a, Frezzotti and Rossi 2004b, Frezzotti and Rossi 2004c], which offers the big advantage of automatic $\mathcal{O}(a)$ improvement [Frezzotti and Rossi 2004a]. This means that effects caused by the discretisation of the four-dimensional spacetime to a lattice with lattice spacing a scale with a rate of $\mathcal{O}\left(a^2\right)$, contrary to Wilson's original formulation of lattice QCD, which features $\mathcal{O}(a)$ effects. Automatic refers to the situation that all physical observables are on-shell $\mathcal{O}(a)$ improved by tuning only one parameter in the simulations. This avoids the demanding task of computing operator specific improvement coefficients, which substantially eases the computations. Twisted mass lattice QCD will be introduced in chapter 2 after briefly discussing continuum QCD and Wilson's original formulation of lattice QCD.

The central object of the computations reported in this thesis is the hadronic vacuum

polarisation (HVP) function, which constitutes the principal ingredient in the determination of leading hadronic contributions for several electroweak observables. As outlined in chapter 3, it can be obtained from the correlator of two electromagnetic vector currents. In this chapter, we will also present our lattice definition of the HVP function and demonstrate that automatic $\mathcal{O}(a)$ improvement is retained despite the occurrence of off-shell contributions.

Subsequently, in chapter 4 it will be discussed how we analyse the procured data for the HVP function and also alternative approaches will be exemplified. Since our standard analysis employs the spectral information of the lowest lying vector meson states, the corresponding results in the physical and continuum limit will also be presented there.

Having laid the foundation, we will proceed with the discussion of the leading-order hadronic contributions to the running of the electroweak coupling constants in chapter 5. These include the fine structure constant α_{QED} and the $SU(2)_I$ coupling constant α_2, which are related by the weak mixing angle whose leading hadronic contribution we have also computed. The determination of these hadronic contributions is useful for many low-energy experiments measuring the weak mixing angle in order to obtain hints on the nature of new physics. In particular, the parity violating deep inelastic scattering experiment to be conducted with the SoLID spectrometer at Jefferson Lab [SoLID 2014] will be sensitive to the QCD contribution computed in this work. Perturbative QED and weak calculations performed for other observables can also benefit from our calculations since the values of the coupling constants represent important input parameters in such computations. In this way, our results are even expected to be valuable for future high-energy colliders since the precision of the values of the coupling constants will be limited by the accuracy to which their hadronic contributions at low energies are known [Jegerlehner 2011].

Chapter 6 is devoted to the lepton anomalous magnetic moments already mentioned above. Similarly to the weak mixing angle, they constitute physical observables which might indicate the scale and the nature of physics beyond the standard model. In fact, for the muon, a deviation of the experimental result from the SM prediction has been persistent for more than a decade now. Furthermore, new experiments aiming at a reduction of the experimental uncertainty by a factor of four are currently constructed. This provides the exciting possibility of a $5\,\sigma$ evidence for new physics if the SM calculation can be rendered equally precise. Due to very accurate predictions accomplished within perturbation theory for the weak and the QED contributions, the by far dominant uncertainty in the SM calculation stems from the leading-order QCD contribution. It will be very difficult for the standard phenomenological approach to further reduce this uncertainty, and it also presents an enormous challenge for lattice QCD. Through the first four-flavour lattice QCD calculation, we will show that such a calculation might indeed be feasible. Moreover, we will identify the necessary next steps to possibly achieve the required precision within the next years. If this procedure is successful, the computation of hadronic corrections to electroweak parameter shifts will contribute to strengthening the position of lattice QCD as one of the prime tools needed for the identification of the laws of new physics and thus to providing answers to some of the biggest questions of particle physics.

Our conclusions follow in chapter 7. Besides summarising and interpreting the results obtained in this thesis, we will provide an outlook on possible improvements and further important quantities which can be computed utilising the data procured for the electroweak observables discussed in this work.

Chapter 2

From continuum QCD to twisted mass lattice QCD at maximal twist

The purpose of this chapter is twofold. First of all, we want to present the method employed in this thesis to procure physically meaningful results, namely lattice QCD and in particular twisted mass lattice QCD. Secondly, we try to convince the reader of some of the advantages inherent in these approaches. To this end, we first provide a very short introduction to QCD in general and afterwards discuss its regularisation to a four-dimensional space-time lattice known as lattice QCD. Subsequently, a succinct introduction to twisted mass lattice QCD follows covering only the most relevant aspects for the computations of the observables discussed in subsequent chapters. Among those is automatic $\mathcal{O}(a)$ improvement which is realised for the condition known as maximal twist.

2.1. QCD fundamentals

QCD is a quantised, relativistic, local, and renormalisable field theory [Gell-Mann 1962, Zweig 1964, Fritzsch et al. 1973]. The basic ingredients of QCD are the matter content - six fermionic spin-$\frac{1}{2}$ quark fields in the fundamental representation of the non-Abelian group $SU(3)_c$ - and the principle of local gauge invariance under this gauge group. These requirements lead to a unique determination of QCD up to eight parameters, the masses of the six quarks, the value of the coupling constant g_s, and the θ-angle which is related to the amount of CP violation of the theory. Experimentally, the latter has been found to be absent or at least extremely small and the unsolved strong CP problem constitutes the question why this is the case. With this small number of parameters, QCD is able to describe a plethora of physical phenomena encountered not only in particle physics but also in nuclear physics, astrophysics, and cosmology. In particular, QCD constitutes the dynamical theory leading to the formation of colour singlet bound states known as hadrons. Proofs for the latter assertion mainly stem from comparisons of experimental data with analyses performed within lattice QCD. For a recent guide through the literature on this vast field we recommend [Kronfeld and Quigg 2010].

2.1.1. The Lagrangian

The main building blocks of QCD are the quark and antiquark fields which are represented by Dirac 4-spinors and colour triplets such that several indices have to be assigned to the quark fields

$$\psi^f(x)_{\alpha,c}\,,\ \overline{\psi}^f(x)_{\alpha,c}\,. \tag{2.1}$$

$f \in \{1,2,3,4,5,6\}$ denotes the so-called flavour index stating whether ψ describes an up, down, charm, strange, top, or bottom quark, and similarly for the antiquark $\overline{\psi}$. The space-

time position of the field is marked by x. $\alpha \in \{1,2,3,4\}$ is the Dirac spinor index. The colour index is given by $c = 1,2,3$. The latter two will soon be considered to be understood and thus dropped. Quarks are also subject to electroweak interactions and thus possess non-trivial quantum numbers with respect to $SU(2)_I$ and $U(1)_Y$ which, however, are not needed to follow the remainder of this thesis. The only additional characteristic we need are their fractional electric charges, namely for u, c, and t quarks $Q_q = +\frac{2}{3}$ whereas d, s, and b carry $Q_{q'} = -\frac{1}{3}$ in units of the positron charge e. Antiquarks are oppositely charged.

Requiring the fermion action to be locally gauge-invariant under $SU(3)_c$ leads to the introduction of gluon fields

$$A_\mu(x)_{cd} \tag{2.2}$$

which constitute vector fields in Minkowski space-time characterised by the diagonal metric tensor $g_{\mu\nu} = \mathrm{diag}(1,-1,-1,-1)$. Hence, they possess a Lorentz index $\mu \in \{0,1,2,3\}$ and a space-time argument x. Additionally they are in the adjoint representation of $SU(3)_c$ and thus form hermitian 3×3 matrices indicated by the colour indices c and d each running from 1 to 3. Altogether there exist eight gluon fields.

With these components the QCD Lagrangian reads

$$\mathcal{L}_{\mathrm{QCD}}[\overline{\psi},\psi,A_\mu] = -\frac{1}{2}\mathrm{tr}\left[F_{\mu\nu}(x)F^{\mu\nu}(x)\right] + \sum_f \overline{\psi}^f(x)\left(i\gamma^\mu\mathcal{D}_\mu - m_f\right)\psi^f(x)\,. \tag{2.3}$$

Here we have already dropped colour and spinor indices. $F_{\mu\nu}$ denotes the gluon field strength tensor

$$F_{\mu\nu} = \partial_\mu A_\nu - \partial_\nu A_\mu + ig_s[A_\mu, A_\nu]\,, \tag{2.4}$$

γ_μ are the Dirac matrices, $\mathcal{D}_\mu = \partial_\mu + ig_sA_\mu$ is the covariant derivative, and m_f is the bare mass of fermion flavour f. From Eq. (2.4) we see that gluon self interactions governed by their kinetic term in Eq. (2.3) are due to their non-Abelian nature.

This together with the simple matter content of the theory and the renormalisability of its coupling constant g_s is the origin of one of the most striking features of QCD known as asymptotic freedom [Gross and Wilczek 1973, Politzer 1973]. It means that the coupling decreases with decreasing distance or equivalently increasing energy. This not only allows for perturbative computations in the high energy regime but is also a precondition for the existence of the continuum limit of lattice QCD as we will elucidate in the next section. In several applications like in perturbative calculations it is necessary to fix a gauge for Eq. (2.3), but since this is not the case in our non-perturbative investigation of gauge-invariant observables we omit the details of such gauge fixing procedures.

2.1.2. The quark model

One important proposition of QCD is that only colour neutral states, i.e. $SU(3)_c$ singlets, have finite energy and thus exist as free particles. This leads to quark confinement since only combinations of quarks and gluons can form states which are trivial under $SU(3)_c$. These combinations are known as hadrons. Additionally, states consisting solely of gluons have been predicted. For this thesis it is, however, sufficient to consider only one class of hadrons known as mesons. In the quark model [Gell-Mann 1962, Zweig 1964], mesons are bound states formed by a valence quark and a valence antiquark. Besides, also combinations of three quarks or three antiquarks exist which are called baryons or antibaryons,

respectively. The best known baryons are the proton and the neutron which form the nuclei of atomic elements and are thus also called nucleons. A review of the quark model is contained in [PDG 2014].

Due to being combinations of two fermionic fields, mesons obey bosonic statistics. Depending on the quantum numbers, one distinguishes pseudoscalar, pseudovector (or axial vector), scalar, vector, and tensor mesons. In the course of this work only the pseudoscalar mesons known as pions ($\pi^{\{0,+,-\}}$), kaons ($K^{\{0,+,-\}}$, $\overline{K}^0$), and D-mesons ($D^{\{0,+,-\}}$, $\overline{D}^0$) and several vector mesons will appear. Therefore, we limit the discussion to those. An overview of the mesons mentioned in this thesis is provided in Tab. 2.1.

meson	J^P	I_3	quark content	mass [MeV]
π^0	0^-	0	$\frac{1}{\sqrt{2}}(u\overline{u} - d\overline{d})$	135
π^+	0^-	1	$u\overline{d}$	140
π^-	0^-	-1	$d\overline{u}$	140
K^0	0^-	$-\frac{1}{2}$	$d\overline{s}$	498
$\overline{K}^0$	0^-	$\frac{1}{2}$	$s\overline{d}$	498
K^+	0^-	$\frac{1}{2}$	$u\overline{s}$	494
K^-	0^-	$-\frac{1}{2}$	$s\overline{u}$	494
D^0	0^-	$-\frac{1}{2}$	$c\overline{u}$	1865
$\overline{D}^0$	0^-	$\frac{1}{2}$	$u\overline{c}$	1865
D^+	0^-	$\frac{1}{2}$	$c\overline{d}$	1870
D^-	0^-	$-\frac{1}{2}$	$d\overline{c}$	1870
ρ^0	1^-	0	$\frac{1}{\sqrt{2}}(u\overline{u} - d\overline{d})$	775
ρ^+	1^-	1	$u\overline{d}$	775
ρ^-	1^-	-1	$d\overline{u}$	775
ω	1^-	0	$\frac{1}{\sqrt{2}}(u\overline{u} + d\overline{d})$	783
ϕ	1^-	0	$s\overline{s}$	1019
J/ψ	1^-	0	$c\overline{c}$	3097

Table 2.1.: Quantum numbers, quark content, and masses of mesons relevant for this work. The electric charge of the mesons is indicated by the superscripts {0,+,-} in their names. J^P denotes the quantum numbers associated with total angular momentum J and parity P. I_3 is the third component of the isospin.

Pseudoscalar mesons are characterised by the quantum numbers $J^P = 0^-$ where J denotes the total angular momentum and P indicates the behaviour under parity transformation, i.e. spatial reflection. They also carry other quantum numbers which are not necessary for the distinction we discuss here. Pions consists only of the two light quarks, up and down. They are the pseudo Goldstone bosons [Goldstone 1961, Goldstone et al. 1962] of chiral symmetry breaking which makes them the lightest of all hadrons. Kaons in contrast contain a light and a strange quark or antiquark in the valence sector. Similarly, the pseudoscalar D-mesons are composed of light and charm quark and antiquark fields.

The vector mesons of considerable importance for this thesis are the ρ-, the ω-, the ϕ-, and the J/ψ mesons. They feature $J^P = 1^-$. Similarly to the pions, the ρ-mesons are entirely composed of light quarks and form an isospin triplet, but since they are not related to any symmetry of the Lagrangian and possess non-vanishing angular momentum they are much heavier than the pions. The ω is predominantly the isospin singlet combination of

the light quarks whereas ϕ is mainly composed of a strange quark and a strange antiquark. Since the ρ^0 and the Φ mesons both exhibit $I_3 = 0$, they can mix with the ω meson. The J/ψ vector meson consists only of charm and anticharm quarks.

2.2. Lattice QCD

The lattice formulation of QCD is based on Feynman's path integral formulation of quantum field theories [Feynman 1950] and the idea of solving problems formulated in Minkowski space-time by analytical continuation to Euclidean space-time [Wick 1954, Symanzik 1966]. In the early 1970s it has been rigorously proven that for any local, relativistic theory satisfying a given set of conditions the Hilbert space of the theory formulated in Minkowski space can be constructed from the Euclidean correlation functions [Osterwalder and Schrader 1973, Osterwalder and Schrader 1975]. Those axioms are equivalent to the well-known Wightman axioms for quantum field theories formulated in Minkowski space [Wightman 1956], cf. [Reed and Simon 1975]. The main requirement is reflection positivity of the Euclidean correlation functions also known as Schwinger functions, which corresponds to unitarity in Minkowski space and thus naturally is of utmost importance. According to [Ukawa 2015], Wilson was well aware of these developments when he established the discretisation of QCD on a four-dimensional Euclidean grid known as lattice QCD [Wilson 1974]. By merging these ingredients and adding his knowledge about critical phenomena in statistical mechanics and the principle of local gauge invariance he created a non-perturbative re-gularisation and thus a mathematically well-defined theory. The latter statement and the compliance with the Osterwalder-Schrader axioms have been proven in [Lüscher 1977, Osterwalder and Seiler 1978] for the practically relevant parts of parameter space bringing lattice QCD on firm mathematical ground. The perturbative renormalisability of lattice QCD has been proven in a series of publications by Reisz [Reisz 1988a, Reisz 1988b, Reisz 1989]. For further details, we recommend [Weisz 2010]. Below we briefly sketch the most relevant points in the construction of lattice QCD which is based on our favourite text books of the field [Montvay and Münster 1994, Gattringer and Lang 2010, Rothe 1992].

In the path integral formulation of QCD the vacuum expectation value of some operator $\hat{\mathcal{O}}$ at space-time position x is expressed by a path integral of the form

$$\langle \hat{\mathcal{O}}(x) \rangle = \frac{1}{Z} \int \mathcal{D}\overline{\psi}\mathcal{D}\psi\mathcal{D}A \, \mathcal{O}[\overline{\psi}, \psi, A_\mu](x) \, e^{i \int d^4x \mathcal{L}_{\mathrm{QCD}}[\overline{\psi}, \psi, A_\mu]} \, , \tag{2.5}$$

where $\mathcal{L}_{\mathrm{QCD}}$ is the QCD Lagrangian given in Eq. (2.3) and $S = \int d^4x \mathcal{L}_{\mathrm{QCD}}[\overline{\psi}, \psi, A_\mu]$ is the action in Minkowski space-time. The integral is over all field configurations of the quark ψ, antiquark $\overline{\psi}$, and gluon fields A_μ which leads to the occurrence of infinities that have to be renormalised by introducing a suitable regulator for the integrals and a well-defined prescription of how to adjust the parameters of the theory when removing the regulator such that a finite limiting theory independent on the regularisation is procured. The normalisation factor Z is the vacuum to vacuum transition amplitude

$$Z = \int \mathcal{D}\overline{\psi}\mathcal{D}\psi\mathcal{D}A \, e^{iS} \, . \tag{2.6}$$

The operator $\hat{\mathcal{O}}$ is constructed from field operators and their conjugate momenta. In the

path integral expression on the right-hand side of Eq. (2.5) it appears as functional of the classical field variables.

Performing the Wick rotation to Euclidean space-time by replacing the temporal component of the position 4-vector in Minkowski space $x_0 \to -i\tilde{x}_0$ leads to the expression for the Euclidean correlation function

$$\langle \hat{O}(\tilde{x}) \rangle = \frac{1}{\tilde{Z}} \int \mathcal{D}\overline{\psi}\mathcal{D}\psi\mathcal{D}A \, O[\overline{\psi}, \psi, A_\mu](\tilde{x}) \, e^{-S_E} \, , \tag{2.7}$$

where S_E denotes the Euclidean action

$$S_E = \int d^4\tilde{x} \left[\frac{1}{2} \mathrm{tr} \left[F_{\mu\nu}(\tilde{x}) F_{\mu\nu}(\tilde{x}) \right] + \sum_f \overline{\psi}^f(\tilde{x}) \left(\gamma_\mu^E \mathcal{D}_\mu + m_f \right) \psi^f(\tilde{x}) \right] = S_G + S_F \, . \tag{2.8}$$

S_G and as S_F stand for the gauge and the fermion action, respectively. The Euclidean γ-matrices γ_μ^E are defined such that they satisfy the Clifford algebra

$$\{\gamma_\mu^E, \gamma_\nu^E\} = 2\delta_{\mu\nu} \tag{2.9}$$

with the Euclidean metric $\delta_{\mu\nu}$. We employ the same chiral representation for the γ-matrices as has been used in [Shindler 2008]. From now on we will omit the index E as well as the $\tilde{}$-symbol on continuum space-time arguments. $\tilde{Z}$ can now be identified with the partition function of a statistical ensemble

$$\tilde{Z} = \int \mathcal{D}\overline{\psi}\mathcal{D}\psi\mathcal{D}A \, e^{-S} \, . \tag{2.10}$$

This immediately reveals the close relation between Euclidean field theory and statistical mechanics when e^{-S} is interpreted as (Boltzmann) probability distribution.

2.2.1. Wilson's original formulation

Due to the appearance of divergences, the expression in Eq. (2.7) is still only formally defined. To remedy this deficiency Wilson formulated the theory on a discrete hypercubic, equidistant space-time lattice Λ:

$$\Lambda = \{ n = (n_0, n_1, n_2, n_3) \, | \, n_\mu = 1, \ldots, N \}$$

where the vectors $n \in \Lambda \simeq \mathbb{Z}^4$ label points separated by the lattice spacing a as shown in Fig. 2.1.

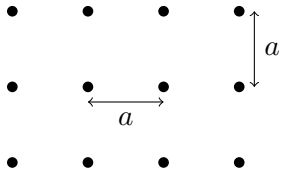

Figure 2.1.: A plane section of a hypercubic, equidistant lattice with lattice spacing a.

Thus the action integral turns into a finite sum $\int d^4x \to a^4 \sum_{n\in\Lambda}$ and a natural momentum cutoff $|p_\mu| \leq \frac{\pi}{a}$ is introduced that regulates ultraviolet divergences. Introducing

only a finite number of lattice sites N in every direction μ implies an additional infrared cutoff $|p_\mu| \geq \frac{2\pi}{L}$, where $L = N\,a$.

Due to the introduction of a space-time lattice, the Grassmann-valued spinor fields $\psi^f(n)$ and $\overline{\psi}^f(n)$ representing the fermionic degrees of freedom get constrained to the lattice sites n. Thus, the integration measure for the fermions in the path integral becomes

$$\mathcal{D}\overline{\psi}\mathcal{D}\psi = \prod_{n\in\Lambda}\prod_{f,\alpha,c} d\overline{\psi}^f(n)_{\alpha,c} \prod_{n\in\Lambda}\prod_{f,\alpha,c} d\psi^f(n)_{\alpha,c}\ . \tag{2.11}$$

When discretising the partial derivative appearing in the fermionic part of Eq. (2.8), e.g. in a symmetric way

$$\partial_\mu \psi^f(n) = \frac{1}{2a}(\psi^f(n + a\hat{\mu}) - \psi^f(n - a\hat{\mu}))\ , \tag{2.12}$$

bilocal terms of the form $\overline{\psi}^f(n)\psi^f(n\pm a\hat{\mu})$ emerge where $\hat{\mu}$ denotes the lattice unit vector in μ direction. These are rendered gauge invariant by introducing the gluons as path-ordered Schwinger line integrals or gauge transporters

$$U(n+\hat{\mu}, n) = \mathcal{P} e^{ig_s \int_n^{n+\hat{\mu}a} A_\mu(x) dx_\mu} = e^{ig_s a A_\mu(n)} \equiv U_\mu(n) \tag{2.13}$$

which are elements of the $SU(3)_c$ group rather than its algebra. They are referred to as link variables or simply links and can be represented graphically as depicted in Fig. 2.2.

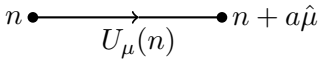

Figure 2.2.: Directed link variable $U_\mu(n)$ from lattice site n to adjacent lattice site $n + a\hat{\mu}$.

The resulting covariant symmetric lattice derivative reads

$$\tilde{\nabla}_\mu \psi^f(n) = \frac{1}{2}(\nabla_\mu + \nabla^*_\mu)\psi^f(n) = \frac{1}{2a}(U_\mu(n)\psi^f(n + a\hat{\mu}) - U_\mu(n - a\hat{\mu})^\dagger \psi^f(n - a\hat{\mu})) \tag{2.14}$$

and the covariant forward and backward derivatives appearing in the above expression are defined by

$$\nabla_\mu \psi^f(n) = \frac{1}{a}(U_\mu(n)\psi^f(n + a\hat{\mu}) - \psi^f(n)) \tag{2.15}$$

$$\nabla^*_\mu \psi^f(n) = \frac{1}{a}(\psi^f(n) - U_\mu(n - a\hat{\mu})^\dagger \psi^f(n - a\hat{\mu}))\ , \tag{2.16}$$

respectively.

Furthermore, in accordance with the Nielsen-Ninomiya theorem [Nielsen and Ninomiya 1981] Wilson added a term to the naively discretised fermion action which explicitly breaks chiral symmetry and leads to additive mass renormalisation in order to avoid the well-known fermion doubling problem. In general, any term which can be made dimensionless by multiplication with suitable powers of the lattice spacing, can be added to the lattice action, since these constitute irrelevant terms which disappear in the limit of vanishing lattice spacing. Thus the discretised gauge invariant Euclidean action for Wilson fermions

takes the form [Wilson 1975]

$$S_F = a^4 \sum_{n\in\Lambda} \sum_{f=1}^{N_f} \overline{\psi}^f(n)(D_W + m_f)\psi^f(n) \tag{2.17}$$

$$D_W = \frac{1}{2}(\nabla_\mu + \nabla^*_\mu)\gamma_\mu - ar\nabla^*_\mu\nabla_\mu \tag{2.18}$$

N_f denotes the number of fermion flavours, 6 in continuum QCD, and r is known as Wilson parameter. The typical choice is $r = 1$. $D^f_W = D_W + m_f$ is the Wilson-Dirac operator. As in the continuum, the inverse of the Dirac operator constitutes the fermion propagator.

Having introduced link variables $U_\mu(n)$ to render operators formed by products of quark and antiquark fields on the lattice gauge-invariants, we additionally need pure gluonic gauge-invariant expressions to construct a discretised version of the gauge action in Eq. (2.8). These can be constructed by taking the trace of a product of link variables forming a closed loop. The simplest such loop is called elementary plaquette

$$U_P(n) \equiv U_{\mu\nu}(n) = U_\mu(n)U_\nu(n + a\hat{\mu})U^\dagger_\mu(n + a\hat{\nu})U^\dagger_\nu(n) \tag{2.19}$$

and is shown in Fig. 2.3.

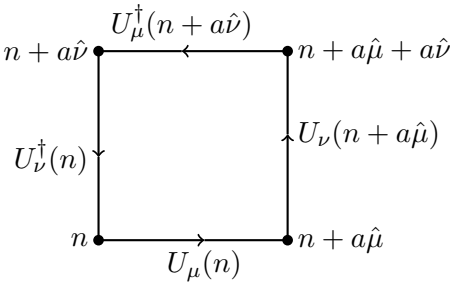

Figure 2.3.: Elementary plaquette $U_P(n) = U_{\mu\nu}(n)$ in the $\mu\nu$-plane at point n.

Inserting $U_\mu(n) = e^{ig_s aA_\mu(n)}$ and expanding in the lattice spacing a leads to

$$U_{\mu\nu}(n) = \mathbb{1} + ig_s a^2 F_{\mu\nu}(n) + \mathcal{O}(a^3)\ . \tag{2.20}$$

Hence, up to $\mathcal{O}\left(a^2\right)$ the continuum gauge action in Eq. (2.8) can be obtained in the limit $a \to 0$ from the Wilson gauge action

$$S_G = \frac{6}{g_s^2} \sum_P \left[1 - \frac{1}{6}\mathrm{Tr}\left(U_P + U^\dagger_P\right)\right] \tag{2.21}$$

where the sum is over all oriented plaquettes. In practice, the gauge coupling constant is often given by $\beta = \frac{6}{g_s^2}$. Using the Wilson gauge as well as the Wilson fermion action in the expression of the Euclidean action in Eq. (2.7) and replacing the integral measures by a finite number of differentials leads to mathematically well-defined expressions for expectation values of physical observables. Thanks to asymptotic freedom, there exists a fixed point for $g_s \to 0$ such that the continuum limit of physical observables generates

the right results provided no other intervening critical points are passed. The equivalence to perturbative QCD in the continuum limit has been proven in [Karsten and Smit 1981, Bochicchio et al. 1985]. Thus, lattice QCD in principle provides a means to compute any QCD observable, albeit usually only numerically relying on Monte Carlo methods [Metropolis 1949] which have originally been developed to study problems in statistical mechanics.

2.2.2. Numerical calculations and their costs

In this subsection we briefly sketch how those expectation values are computed and why massively parallel computations are necessary in order to get quantitative results. Furthermore, we want to point out that such results can systematically be improved.

From the discussion in the preceding subsection we know that expectation values of observables O can be evaluated as follows

$$\langle O \rangle = \frac{\int \mathcal{D}U e^{-S_G} \prod_{n\in\Lambda} \prod_{f,\alpha,c} d\overline{\psi}^f(n)_{\alpha,c} \prod_{n\in\Lambda} \prod_{f,\alpha,c} d\psi^f(n)_{\alpha,c} e^{-S_F} O[\overline{\psi},\psi,U]}{\int \mathcal{D}U e^{-S_G} \prod_{n\in\Lambda} \prod_{f,\alpha,c} d\overline{\psi}^f(n)_{\alpha,c} \prod_{n\in\Lambda} \prod_{f,\alpha,c} d\psi^f(n)_{\alpha,c} e^{-S_F}} \tag{2.22}$$

where the integrals are over a finite number of variables. The integral measure for the gluon fields $\mathcal{D}U$ is known as Haar measure. It is gauge-invariant and finite due to the compactness of $SU(3)$. It is normalised in such a way that

$$\int \mathcal{D}U = \int \prod_{n\in\Lambda} \prod_{\mu=0}^{3} dU_\mu(n) = 1 \; . \tag{2.23}$$

Due to the fermion action being bilinear in $\bar{\psi}$ and ψ as we have seen in Eq. (2.17), the Grassmann integrals can be performed analytically yielding a product of determinants of Dirac operators for each flavour as well as the Wick contractions of the operator O which typically result in products of fermion propagators. Denoting the resulting functional by $\tilde{O}[U]$ to indicate that the dependence on the fermionic degrees of freedom has been integrated out, we are left with

$$\langle O \rangle = \frac{\int \mathcal{D}U e^{-S_G} \prod_f \det\left(D_W^f\right) \tilde{O}[U]}{\int \mathcal{D}U e^{-S_G} \prod_f \det\left(D^f\right)} = \frac{1}{\tilde{Z}} \int \mathcal{D}U e^{-S_G} \prod_f \det\left(D_W^f\right) \tilde{O}[U] \; . \tag{2.24}$$

This expression can only be evaluated analytically for extremely small lattices. Instead by considering $\frac{1}{\tilde{Z}} \mathcal{D}U e^{-S_G} \prod_f \det\left(D_W^f\right)$ as Gibbs measure $dP[U]$, the expectation value can be approximated by ensemble averages over N_{conf} gauge link configurations that have been generated by Monte Carlo algorithms based on importance sampling with this measure

$$\langle O \rangle = \int dP[U] \tilde{O}[U] \tag{2.25}$$

$$= \frac{1}{N_{\text{conf}}} \sum_{i=1}^{N_{\text{conf}}} \tilde{O}[U]|_{\{U\}_i} + \mathcal{O}\left(\frac{1}{\sqrt{N_{\text{conf}}}}\right) \; . \tag{2.26}$$

Computationally most demanding is the computation of the determinants of the Wilson-Dirac operators, since the Dirac operators are $12V \times 12V$ matrices, where $V = N^4$ denotes

the total number of lattice sites and 12 results from having a four-component Dirac spinor with three colours at every lattice point. The typical lattice volumes V used in our calculations are $V = 64 \cdot 32^3 = 2,097,152$ and $V = 96 \cdot 48^3 = 10,616,832$, where the temporal extent is twice the spatial extent for reasons which will become clear in Sect. 4.1. The second most expensive operation is inverting this huge matrix required for the computation of the fermion propagators. Additionally, there are four $SU(3)_c$ gluon fields per site which are each described by eight parameters. Thus, obviously the lattice extent L that is feasible for numerical calculations is limited as the costs scale roughly like L^5 and the simulations are also cheaper the smaller the number of dynamical fermions, i.e. fermion species for which the determinants of the Dirac operators are taken into account in the probability distribution.

Besides those obvious limitations, also the mass m_l of the lightest fermions in the simulation and the lattice spacing a influence the algorithmic performance. Standard simulation algorithms slow down with a rate of $\left(\frac{1}{m_l}\right)^{1...3} \rightarrow \left(\frac{1}{m_{\mathrm{PS}}}\right)^{2...6}$ and $\left(\frac{1}{a}\right)^{5...7}$ [Del Debbio et al. 2007, Gattringer and Lang 2010] where m_{PS} denotes the often unphysically large pion masses that have to be employed in the simulation. Furthermore, autocorrelation times increase with decreasing lattice spacing such that more configurations have to be generated in order to obtain the same number of statistically independent configurations. Therefore, generating the gauge link configurations is a formidable task which nowadays employs ingenious algorithms and the fastest and in terms of the number of cores and of memory biggest available supercomputers. For the use of massively parallel software the locality of the action is an important prerequiste. As mentioned before, major algorithmic improvements have been achieved in recent years but it is still rather expensive to perform simulations at the physical value of the pion mass, m_π, and at small lattice spacings. More details about general concepts needed for the generation of lattice gauge field ensembles can be found in [Lüscher 2010].

Here, we only want to mention that a computation of physical observables in lattice QCD typically proceeds in two steps:

- generation of gauge field ensembles with several volumes, lattice spacings, and pion masses (if not directly the physical value)
- measurement of physical observables and statistical analysis of the results

Several lattice volumes are needed in order to check for finite size effects and to ultimately perform the limit $V \rightarrow \infty$. When taking the continuum limit, at the same time the lattice spacing has to be taken to zero. In order to allow for an extrapolation to $a \rightarrow 0$, simulations at different values of the lattice spacing have to be performed. Additionally, for simulations not directly at the physical point several pion masses are required to be able to extrapolate to the physical one. This requires a lot of computing power but with the help of those ensembles the expectation values of many different QCD observables can be computed. One of the advantages of lattice QCD is that the limiting procedure is precisely defined and the results can be systematically improved by investing more computing time either to increase statistics or to produce more ensembles with different parameters. Furthermore, it also allows to determine the systematic uncertainties due to the lattice discretisation in a well-defined manner. Fortunately, for the computations carried out in this thesis we can rely on the four-flavour gauge field configurations generated by the European Twisted Mass Collaboration (ETMC) [ETMC 2010a, ETMC 2011] comprising several volumes,

lattice spacings, and pion masses. Therefore, we are only concerned with the last step which consists in the determination of physical observables and their statistical as well as systematic uncertainties.

2.3. Twisted mass lattice QCD

As we have seen above, simulations at very small lattice spacings constitute a major numerical burden and are often simply not feasible. The expression for the Wilson-Dirac operator Eq. (2.18) obviously exhibits $\mathcal{O}(a)$ effects. Hence, when performing the continuum limit a linear dependence on the small lattice spacing parameter a is expected and thus rather big disretisation effects. These impair the accuracy of the final results. Furthermore, for the system to undergo a second order phase transition as required when taking the continuum limit where the correlation length $\xi \propto \frac{1}{m}$ diverges we need to have

$$a \ll \frac{1}{m} \ll L \,, \tag{2.27}$$

for all fermion masses m. Several possibilities have been devised to reduce the size of lattice artefacts and thus accelerate the convergence to the continuum limit by improving the continuum limit scaling to $\mathcal{O}\left(a^2\right)$. Such procedures are known as $\mathcal{O}\left(a\right)$ improvement. Due to the requirement in Eq. (2.27) the improvement is in some situations even necessary to arrive at meaningful results at all.

One particular realisation of $\mathcal{O}\left(a\right)$ improvement, known as automatic $\mathcal{O}\left(a\right)$ improvement [Frezzotti and Rossi 2004a], is accomplished by utilising the twisted mass formulation for the fermionic action [Aoki and Gocksch 1989, Alpha 2001, Frezzotti and Rossi 2004a, Frezzotti and Rossi 2004b, Frezzotti and Rossi 2004c]. The big advantage compared to other options is that by tuning a single parameter in the simulation, the bare quark mass m_f, the approach of the continuum limit is on-shell improved for all physical observables without the need to compute additional improvement coefficients. How this is achieved will be shown in Sect. 2.3.2. Additonally, there are various other advantages twisted mass fermions offer like simpler renormalisation patterns for composite operators compared to standard Wilson quarks. More details are given in the review articles [Sint 2007, Shindler 2008].

Before discussing the most striking property of twisted mass fermions, automatic $\mathcal{O}\left(a\right)$ improvement, we introduce the expressions for the fermion actions and thereby define the twisted mass formulation of lattice QCD.

2.3.1. Fermion actions and observables

In good approximation the light quarks, up and down, are regarded as mass-degenerate throughout this thesis. This implies that we are neglecting isospin symmetry breaking effects originating from their mass difference. For such a mass-degenerate fermion doublet with respect to the flavour group $SU(2)_f$ in the twisted-basis, $\{\chi_l, \bar{\chi}_l\}$, the twisted mass lattice action has the form

$$S_{F,D}^{(\omega)}[\chi_l, \bar{\chi}_l, U] = a^4 \sum_{n\in\Lambda} \bar{\chi}_l(n) \left(D_W \mathbb{1}_2 + m_f \mathbb{1}_2 + i\mu\gamma_5\tau^3\right) \chi_l(n) \tag{2.28}$$

where μ denotes the twisted quark mass, which serves as infrared regulator of the Dirac operator, and τ^3 is the third Pauli matrix in flavour space. The additional term in Eq. (2.28) does not alter the power counting and hence does not impair the renormalisability proofs valid for standard Wilson fermions.

In the continuum limit, the twisted-mass action in Eq. (2.28) reads

$$S_{F,D}^{(\omega)}[\chi_l, \bar{\chi}_l, U] = \int d^4\, x\, \bar{\chi}_l(x) \left(\gamma_\mu D_\mu \mathbb{1}_2 + m_q \mathbb{1}_2 + i\mu\gamma_5\tau^3\right) \chi_l(x) \tag{2.29}$$

where the bare continuum quark mass m_q is related to the bare lattice quark mass by additive renormalisation due to the Wilson term

$$m_q = m_f - m_{\text{crit}}\ . \tag{2.30}$$

The renormalisation constant is called critical mass m_{crit} for reasons which will become clear subsequently. Performing a change of variables with twist angle ω according to

$$\chi_l \to \psi_l = e^{i\omega\gamma_5\tau^3}\chi_l\,, \qquad \overline{\chi_l} \to \overline{\psi_l} = \overline{\chi_l} e^{i\omega\gamma_5\tau^3} \tag{2.31}$$

leads to the expression in the physical basis, $\{\psi_l, \bar{\psi}_l\}$,

$$S_{F,D}^{(\omega)}[\psi_l, \bar{\psi}_l, U] = \int d^4\, x\, \bar{\psi}_l(x) \left(\gamma_\mu D_\mu \mathbb{1}_2 + M\mathbb{1}_2\right) \psi_l(x) \tag{2.32}$$

with $M = \sqrt{m_q^2 + \mu^2}$ known as polar mass and $\omega = \arctan\frac{\mu}{m_q}$. Hence,

$$m_q\mathbb{1}_2 + i\mu\gamma_5\tau^3 = M e^{i\omega\gamma_5\tau^3} \text{ with } m_q = M\cos\omega,\ \mu = M\sin\omega\ . \tag{2.33}$$

The special case $\omega = \frac{\pi}{2}$, for which $m_q = 0$ and $\mu = M > 0$, is called maximal or full twist and implies automatic $\mathcal{O}(a)$ improvement as we will see below. The corresponding lattice action reads

$$\begin{aligned} S_{F,D}[\psi_l, \bar{\psi}_l, U] &= a^4 \sum_{n\in\Lambda} \bar{\psi}_l(n) \left(D_{\text{tm}}\mathbb{1}_2 + m_{\text{crit}}\mathbb{1}_2 + \mu\mathbb{1}_2\right) \psi_l(n) \\ D_{\text{tm}} &= \frac{1}{2}(\nabla_\mu + \nabla_\mu^*)\gamma_\mu - are^{-i\omega\gamma_5\tau^3}\nabla_\mu^*\nabla_\mu\ . \end{aligned} \tag{2.34}$$

Eq. (2.34) has the same form as the ordinary Wilson action Eq. (2.17) and we see that in the Dirac operator only the Wilson term is rotated. As we have already mentioned, this term constitutes an irrelevant operator as it vanishes in the naive continuum limit. Since both lattice actions are exactly related by Eq. (2.31), also the symmetries of both actions are. Hence, for $a \to 0$ both actions share the same symmetries, namely those of continuum QCD. This is not true at finite a due to the rotation of the Wilson term. In particular, the $SU(2)_V$ flavour symmetry of Wilson's original formulation of lattice QCD is broken to the subgroup $U(1)_3$ generated by the third Pauli matrix τ^3 such that properties of observables forming an isospin triplet like the masses of the two charged pions and the neutral pion are no longer degenerate in twisted mass lattice QCD, $m_{\pi^0} < m_{\pi^\pm}$. Besides flavour symmetry, also continuum-like parity symmetry is broken to a subgroup such that operators possessing different parity quantum numbers in the continuum can mix at finite lattice spacing. A list of the remaining symmetries of the twisted mass formulation of

lattice QCD is given in appendix A.

When considering the first two generation of quarks, the strange and the charm quark can obviously not be regarded as mass-degenerate. The notation used to indicate that the light quarks possess the same mass whereas strange and charm both have different masses is $N_f = 2 + 1 + 1$. For simulations involving $N_f = 2 + 1 + 1$ dynamical flavours, we employ Eq. (2.28) for the light quarks whereas the second-generation quarks, strange and charm, also reside in a fermion doublet, χ_h. The twisted mass action for such a mass non-degenerate fermion doublet reads [Frezzotti and Rossi 2004c]

$$S^{(\omega)}_{F,ND}[\chi_h, \overline{\chi}_h, U] = \sum_{n\in\Lambda} \overline{\chi}_h(n) \left[D_W + i\mu_\sigma \gamma_5 \tau^1 + \mu_\delta \tau^3 \right] \chi_h(n) \tag{2.35}$$

Here, the twist term with mass parameter μ_σ is orthogonal to the mass splitting in flavour space characterised by μ_δ. Both μ_σ and μ_δ can be chosen to be positive and the bare quark masses are then obtained from $\mu_{c,s} = \mu_\sigma \pm \mu_\delta$. It has been shown that this provides a real, positive quark determinant with non-zero eigenvalues for non-zero quark masses, thus allowing for Monte Carlo simulations with meaningful probability distributions [Frezzotti and Rossi 2004c]. Therefore, this action is chosen to govern the behaviour of the heavy sea quarks. As shown in [Frezzotti and Rossi 2004c], automatic $\mathcal{O}(a)$ improvement at maximal twist prevails. In practice this is achieved by using the same critical mass as in the light-quark sector [Chiarappa et al. 2007, ETMC 2010a].

Provided the renormalised sea and valence quark masses of the same flavour coincide, due to automatic $\mathcal{O}(a)$ improvement it is legitimate to use a different action for the valence fermions than for the sea quarks [Frezzotti and Rossi 2004b]. The valence quark action utilised in this work is known as Osterwalder-Seiler action [Osterwalder and Seiler 1978, Frezzotti and Rossi 2004b]

$$S_{F,OS}[\chi_h, \overline{\chi}_h, U] = \sum_{n\in\Lambda} \overline{\chi}_h(n) \left[D_W + i \begin{pmatrix} \mu_c & 0 \\ 0 & -\mu_s \end{pmatrix} \gamma_5 \right] \chi_h(n) \ . \tag{2.36}$$

Since it entails a complex fermion determinant, it cannot be used for the gauge field generation. In our calculations the bare twisted mass parameters for the valence strange and charm quarks, μ_s and μ_c, are tuned in such a way that the physical value for $2m_K^2 - m_{\mathrm{PS}}^2$ and the D-meson mass, respectively, are reproduced. Here, m_K denotes the kaon mass. Why it is beneficial for our computations to describe the heavy valence quarks by this action will be mentioned in the next chapter. Here, we only note that in this case $\mathcal{O}(a)$ improvement is maintained and no wrong flavour or parity mixing in physical amplitudes occurs [Frezzotti and Rossi 2004b].

Employing the transformation Eq. (2.31) also for the operators, it can be shown that standard QCD correlation functions can be expressed as linear combinations of correlation functions obtained in the twisted formulation [Alpha 2001]. Here, we only want to mention the example of the vector current, since we investigate two-point vector-current correlators in the subsequent chapters of this thesis. The local vector current in the physical basis

$$J'^a_\mu = \bar{\psi} \gamma_\mu \frac{\tau^a}{2} \psi \ , \tag{2.37}$$

with the three Pauli matrices τ^a, $a = 1, 2, 3$, acting in flavour space, can be expressed by

the vector and axial vector currents in the twisted basis as follows

$$J'^{a}_{\mu} = \begin{cases} \cos\omega J^{a}_{\mu} + \varepsilon^{3ab} J^{b}_{\mu 5} & a = 1, 2 \\ J^{3}_{\mu} & a = 3 \, . \end{cases} \tag{2.38}$$

Note that this explicitly shows the flavour symmetry breaking $SU(2)_V \to U(1)_3$ inherent in the twisted mass formulation of lattice QCD. The vector and axial vector currents in the twisted basis are given by the usual quark bilinears

$$J^{a}_{\mu} = \bar{\chi}\gamma_{\mu}\frac{\tau^{a}}{2}\chi \tag{2.39}$$

$$J^{a}_{\mu 5} = \bar{\chi}\gamma_{\mu}\gamma_{5}\frac{\tau^{a}}{2}\chi \, . \tag{2.40}$$

Additionally, the Ward identities for the axial current also known as partially conserved axial current (PCAC) and the vector current assume a different form in the twisted basis

$$\partial_{\mu} J^{a}_{\mu 5} = 2 m_f J^{a}_{5} + i\mu\delta^{3a} J \tag{2.41}$$

$$\partial_{\mu} J^{a}_{\mu} = -2\mu\varepsilon^{3ab} J^{b}_{5} \, . \tag{2.42}$$

Here $J^{a}_{5} = \bar{\chi}\gamma_5\frac{\tau^a}{2}\chi$ is the pseudoscalar and $J = \bar{\chi}\chi$ the scalar current. The expression in Eq. (2.41) will later be used to define the PCAC mass. Eq. (2.42) reveals that only the vector currents trivial or diagonal in flavour space are conserved for non-zero bare twisted mass μ.

2.3.2. Automatic $\mathcal{O}(a)$ improvement

Similarly to the well-known concept of effective field theories [1] where effects of a more fundamental theory present at larger energy scales are described by adding higher-dimensional operators to the Lagrangian of the theory valid at lower energies, it is conjectured that also the lattice theory at finite lattice spacing can be regarded as effective field theory of a theory with smaller lattice spacing and thus ultimately of the continuum theory, since by refining the discretisation new degrees of freedom are introduced.

In this sense, the action of the low-energy effective field theory also known as Symanzik's effective theory [Symanzik 1983a,Symanzik 1983b,Lüscher and Weisz 1985] can be written as

$$S_{\text{eff}} = \int d^4x (\mathcal{L}_4(x) + a\mathcal{L}_5(x) + a^2\mathcal{L}_6(x) + a^3\mathcal{L}_7(x) + \ldots) \, , \tag{2.43}$$

where $\mathcal{L}_4$ is the Lagrangian of the continuum theory and the $\mathcal{L}_k$ with $k \geq 5$ are linear combinations of operators with dimensions k. Those operators are required to share the same symmetries as the lattice action. Here, we only consider the fermion action since even the simplest lattice gauge action represented by the Wilson action in Eq. (2.21) possesses only $\mathcal{O}\left(a^2\right)$ lattice artefacts.

Analogously to the action, multiplicatively renormalised fields can be expanded close to the continuum

$$\phi_{\text{eff}} = \phi_0 + a\phi_1 + a^2\phi_2 + \ldots . \tag{2.44}$$

Combining Eq. (2.43) and Eq. (2.44), renormalised Green functions of fields at separate

[1] For an introduction to effective field theories we recommend the lecture notes [Pich 1998].

space-time points x_i read up to $\mathcal{O}(a)$

$$Z_\phi^{r/2}\langle\phi(x_1)\dots\phi(x_r)\rangle_{\text{latt}} = \langle\phi_0(x_1)\dots\phi_0(x_r)\rangle_{\text{cont}} - a\int d^4x\langle\mathcal{L}_5\phi_0(x_1)\dots\phi_0(x_r)\rangle_{\text{cont}} + a\sum_{k=1}^{r}\langle\phi_0(x_1)\dots\phi_1(x_k)\dots\phi_0(x_r)\rangle_{\text{cont}} + \mathcal{O}\left(a^2\right) . \quad (2.45)$$

Simplifying the notation by regarding $\phi(x_1)\dots\phi(x_r)$ as one multilocal composite operator O, we have

$$\langle O_R\rangle = \langle O_R\rangle_{\text{cont}} - a\langle S_5 O_R\rangle_{\text{cont}} + a\langle O_1\rangle_{\text{cont}} + \mathcal{O}\left(a^2\right) . \quad (2.46)$$

As mentioned before, the operators that can arise in the higher-dimensional Lagrangians in Eq. (2.43) are restricted by the requirement that they have to be invariant under the symmetries of the target continuum theory for which the twisted mass lattice action for a mass-degenerate fermion doublet in the twisted basis reads

$$S_4 = \int d^4x\bar{\chi}(x)(\gamma_\mu D_\mu + i\mu\gamma_5\tau^3)\chi(x) . \quad (2.47)$$

Here, we have already assumed that the theory has been tuned to maximal twist by setting $m_f = m_{\text{crit}}$ such that the renormalised quark mass

$$m_R = \frac{m_q}{Z_S} = \frac{m_f - m_{\text{crit}}}{Z_S} = 0 . \quad (2.48)$$

As we have briefly mentioned when discussing Wilson's original formulation of lattice QCD, the Wilson term breaks chiral symmetry and thus leads to the additive mass renormalisation shown above. Let us remark that the argumentation for the mass non-degenerate fermion action in Eq. (2.35) proceeds along the same lines and can be found in [Frezzotti and Rossi 2004b].

One of the symmetries of S_4 in Eq. (2.47) is the combined transformation $\mathcal{R}_5^{1,2}\times\mathcal{D}\times[\mu\to-\mu]$ with

$$\begin{aligned}\mathcal{R}_5^{1,2}:&\chi(x)\to i\,\gamma_5\,\tau^{1,2}\,\chi(x)\\ &\bar{\chi}(x)\to i\,\bar{\chi}(x)\,\gamma_5\,\tau^{1,2}\\ \mathcal{D}:&U_\mu(x)\to U_\mu(-x-a\hat{\mu})^\dagger\\ &\chi(x)\to -i\,\chi(-x)\\ &\bar{\chi}(x)\to -i\,\bar{\chi}(-x) ,\end{aligned}$$

where $\mathcal{R}_5^{1,2}$ is a discrete chiral symmetry and $\mathcal{D}$ effectively measures the parity of the dimensions of the operators. It can be shown that all possible operators appearing in $\mathcal{L}_5$ are odd under the above transformation such that for an operator O even under $\mathcal{R}_5^{1,2}\times\mathcal{D}\times[\mu\to-\mu]$ the second term on the right-hand side of Eq. (2.46) vanishes. Since the operator O_1 is one dimension higher than O_0, it has to be odd under $\mathcal{R}_5^{1,2}$ such that also its expectation value with respect to the continuum action and thus the third term in Eq. (2.46) vanishes. Hence, renormalised Green functions of operators even under $\mathcal{R}_5^{1,2}\times\mathcal{D}\times[\mu\to-\mu]$ are $\mathcal{O}(a)$ improved provided the theory has been tuned to maximal

twist, whereas the expectation values of odd operators vanish in the continuum limit

$$\langle O_R^+ \rangle = \langle O_R^+ \rangle_{\text{cont}} + \mathcal{O}\left(a^2\right) \tag{2.49}$$

$$\langle O_R^- \rangle = \mathcal{O}\left(a\right) \ . \tag{2.50}$$

This is regarded as automatic $\mathcal{O}(a)$ improvement since in contrast to other actions no further improvement coefficients for the operators are needed.

The condition of maximal twist can be achieved by requiring some correlator violating the $\mathcal{R}_5^{1,2} \times \mathcal{D} \times [\mu \to -\mu]$ or a related symmetry to vanish [Frezzotti et al. 2006]. In practice, monitoring the PCAC quark mass defined at large Euclidean times τ by

$$m_{\text{PCAC}} = \frac{1}{2} \frac{\sum_{\vec{x}} \langle \partial_0^* J_{0\,5}^{1,2}(\tau, \vec{x}) J_5^{1,2}(y) \rangle}{\langle J_5^{1,2}(\tau, \vec{x}) J_5^{1,2}(y) \rangle} \tag{2.51}$$

has been found to be advantageous [XLF 2005a, XLF 2005b] and the parameters of the simulations are tuned in such a way that m_{PCAC} becomes zero, usually to within 0.1μ, since it has been found that it is sufficient to only enforce this condition to $\mathcal{O}(a)$ [ETMC 2008, ETMC 2010b].

With this relatively easy prescription for achieving $\mathcal{O}(a)$ improvement of physical observables and the numerous other advantages of which only some have been mentioned in this section, twisted mass lattice QCD represents an attractive and fruitful formulation of lattice QCD.

Chapter 3

The hadronic vacuum polarisation function

The hadronic vacuum polarisation function constitutes the prime ingredient for the calculation of hadronic corrections of several SM parameters including all observables discussed in this thesis. The leading-order hadronic contributions to the running of electroweak coupling constants which are discussed in chapter 5 are directly proportional to the renormalised hadronic vacuum polarisation function, whereas the leading hadronic contributions to the lepton anomalous magnetic moments presented in chapter 6 are convolutions of the renormalised vacuum polarisation with a known kernel function. Therefore, we devote this chapter to the introduction of this pivotal quantity.

Figure 3.1.: The hadronic vacuum polarisation depicted as the shaded blob contributes to the photon self-energy.

The hadronic vacuum polarisation characterises the impact virtual quarks, antiquarks, and gluons have on the propagation of the photon. The corresponding Feynman diagram is shown in Fig. 3.1. Similarly to the vacuum polarisation of QED which entails charge screening by virtual lepton pairs, also the hadronic or QCD vacuum polarisation function receives charge screening contributions from quark-antiquark pairs. This screening, however, is overcompensated by the self-interactions of the gluons such that, in contrast to the QED case, we observe the amplification of colour charges leading to the properties of confinement for small momenta and asymptotic freedom at small distances. Studying the Callan-Symanzik β-function for QCD to leading order [Peskin and Schroeder 1995, Srednicki 2007]

$$\beta(\alpha_s) = -\frac{\alpha_s^2}{2\pi}\left(11 - \frac{2}{3}N_f\right) + \mathcal{O}\left(\alpha_s^3\right) \ , \tag{3.1}$$

where α_s is the strong coupling constant and N_f denotes the number of active flavours, reveals that to overcome this antiscreening by the gluons many more quark species than are currently known would be needed. Since this is not the case in the SM, the hadronic vacuum polarisation at low energies represents an inherently non-perturbative quantity which we investigate in the framework of twisted mass lattice QCD.

In the following, we present the definition of the hadronic vacuum polarisation function in continuum as well as lattice QCD and in both cases summarise how it is computed in practice. The continuum part in Sect. 3.1 is mainly based on material provided by Jegerlehner in his excellent reviews on the muon anomalous magnetic mo-

ment [Jegerlehner 2008b, Jegerlehner and Nyffeler 2009]. After constructing our lattice definition in Sect. 3.2.1, we sketch a proof in Sect. 3.2.2 demonstrating that with this specific definition automatic $\mathcal{O}(a)$ improvement of the hadronic vacuum polarisation function is ensured at maximal twist despite the occurrence of short-distance contributions [Burger et al. 2015b]. Only after having established the utility of our definition we discuss the basics of the practical implementation of the lattice calculations by providing the necessary contraction formulae in Sect. 3.2.3.

3.1. The hadronic vacuum polarisation function in the continuum

The external photons, $\tilde{A}_\mu(x)$, in Fig. 3.1 couple to the electromagnetic vector current of the quark fields ψ^f

$$j_\mu^{\mathrm{em}}(x) = \sum_{f=1}^{N_f} Q_f \bar{\psi}^f(x)\gamma_\mu\psi^f(x) \,, \tag{3.2}$$

where Q_f denotes the charge of fermion flavour f in units of the positron charge e, via $i\,e\,j_\mu^{\mathrm{em}}(x)\tilde{A}_\mu(x)$. Hence, by amputating the external photon lines the one-particle irreducible self-energy function of the photon, as the hadronic vacuum polarisation tensor is often called in the context of perturbation theory, can be represented as a time-ordered correlator of two electromagnetic currents

$$\Pi_{\mu\nu}(q) = ie^2 \int d^4x e^{iqx} \langle 0|T\{j_\mu^{\mathrm{em}}(x) j_\nu^{\mathrm{em}}(y)\}|0\rangle \,, \tag{3.3}$$

where q are timelike momenta. Diagrammatically this is depicted in Fig. 3.2.

Figure 3.2.: The hadronic vacuum polarisation tensor as the correlator of two vector currents marked by the crossed circles.

According to Noether's theorem [Noether 1918], the global gauge symmetry of QED implies that the total charge of the system and thus the electromagnetic current is conserved, $\partial_\mu j_\mu^{\mathrm{em}} = 0$. Using this in the Lorentz-covariant decomposition of a general rank-2 tensor in Minkowski space-time implies that the hadronic vacuum polarisation tensor in Eq. (3.3) is transverse

$$\Pi_{\mu\nu}(q) = (q_\mu q_\nu - q^2 g_{\mu\nu})\Pi(q^2) \,. \tag{3.4}$$

$\Pi(q^2)$ is the scalar hadronic vacuum polarisation function which as mentioned above is the central quantity for the calculations performed in this thesis. The wave function renormalisation of the photon, which removes a logarithmic ultraviolet divergence at vanishing momentum transfer, implies that the hadronic vacuum polarisation function is renormalised by subtracting its value at zero momentum

$$\Pi_R(q^2) = \Pi(q^2) - \Pi(0) \,. \tag{3.5}$$

Among the most important properties of the vacuum polarisation function are analyticity and unitarity. Since time-ordered Green functions are products of causal propagators, the Fourier transforms of such Green functions are analytic. Thus causality of a quantum field theory implies analyticity. Being derived from a time-ordered Green function in position space, the hadronic vacuum polarisation function defined in Eqs. (3.3) and (3.4) is evidently analytic which is the prerequisite for a well-defined result after Wick rotation and thus also for the possibility to compute the hadronic vacuum polarisation function on the lattice as described in Sect. 3.2 below. Another important consequence of analyticity is the validity of a dispersion relation which relates the real part of the hadronic vacuum polarisation function with its imaginary one. Due to the necessity of subtracting the value at zero momentum, we have to use for the renormalised vacuum polarisation function a once-subtracted dispersion relation, namely

$$\Pi(q^2) - \Pi(0) = \frac{q^2}{\pi} \int_0^\infty ds \frac{\operatorname{Im}\Pi(s)}{s(s - q^2 - i\varepsilon)} \,. \tag{3.6}$$

Combining this with unitarity, which ensures the conservation of quantum mechanical transition probabilities, allows to obtain a value for the hadronic vacuum polarisation function in Minkowski space-time by analysing hadronic e^+e^- scattering data. The reason is that in the limit of elastic forward scattering the optical theorem

$$\operatorname{Im}\Pi(s) = \frac{e^2}{12\pi} R^{\mathrm{had}}(s) \tag{3.7}$$

directly follows from unitarity. It relates the imaginary part of the vacuum polarisation function to the hadronic cross-section ratio

$$R^{\mathrm{had}}(s) \equiv \frac{\sigma(e^+e^- \to \text{hadrons})}{\sigma(e^+e^- \to \mu^+\mu^-)} \,. \tag{3.8}$$

Additionally, the unitarity condition reveals that physical states with $s < 4m_\pi^2$ are forbidden by energy and momentum conservation. Hence, it follows from Eqs. (3.6) and (3.7) that the renormalised hadronic vacuum polarisation function can be procured from hadronic e^+e^- cross-section data according to

$$\Pi_R(q^2) = \frac{\alpha_0 q^2}{3\pi} \int_{4m_\pi^2}^\infty ds \frac{R^{\mathrm{had}}(s)}{s(s - q^2 - i\varepsilon)} \,, \tag{3.9}$$

where the fine structure constant $\alpha_0 = \frac{e^2}{4\pi}$ has been introduced.

Eq. (3.9) looks like a straightforward prescription for obtaining the hadronic vacuum polarisation function, but since the integral involves a huge range of momentum transfers s, the results of many different measurements have to be combined such that one should know more or less precisely what has been measured by the individual experiments and how this has been done to correctly take the different systematic uncertainties into account. Another obstacle are the sharp vector meson resonances appearing in this ratio, cf. Sect. 2.1.2, and also the treatment of various other structures not directly related to resonances appearing in $R^{\mathrm{had}}(s)$. The low-energy part of the latest data for $R^{\mathrm{had}}(s)$ [PDG 2014] is shown in Fig. 3.3. In order to determine the resonance characteristics their shapes have to be fitted. However, for example the ρ and the ω resonance overlap and thus the

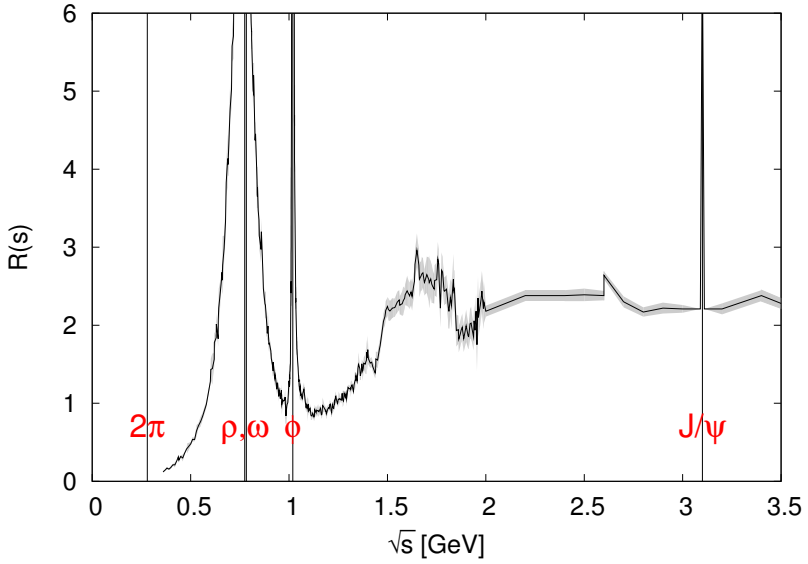

Figure 3.3.: The hadronic cross-section ratio $R^{\text{had}}(s)$. The quark content of the vector mesons and their masses can be found in Tab. 2.1.

ideal Breit-Wigner shapes of the individual resonances get distorted such that more elaborate fit functions like the Gounaris-Sakurai function [Nambu and Sakurai 1962, Gell-Mann et al. 1962] are required. However, this is not gauge invariant for $s \neq 0$ [Jegerlehner and Szafron 2011] and there are also other issues which complicate the phenomenological analysis.

At large enough energies $q^2 \gtrsim 4\,\text{GeV}^2$, the property of asymptotic freedom allows for reliable perturbative QCD calculations of the hadronic vacuum polarisation which nowadays have been obtained up to four loops in massless QCD [Baikov et al. 2012], up to three loops including mass effects [Chetyrkin et al. 2000], and have additionally been numerically implemented in the RHAD package [Harlander and Steinhauser 2003]. A collection of recent results can be found in the review [Baikov et al. 2015]. However, according to [Jegerlehner 2008b, Jegerlehner and Nyffeler 2009] one might miss some non-perturbative contributions when utilising perturbative QCD results in place of the data at intermediate q^2 leading to an unknown systematic error. Fortunately, there exists an overlap region in which both lattice QCD and perturbative QCD yield reliable results for the hadronic vacuum polarisation function such that cross-checking the results is feasible. Usually, good agreement is observed, see e.g. [Boyle et al. 2012, Herdoiza et al. 2014]. However, some difficulties arise due to lattice artefacts, which have to be handled appropriately in the large-Q^2 region on the lattice. In Ref. [Herdoiza et al. 2014], the scale parameter $\Lambda^{Nf=2}_{\overline{\text{MS}}}$ has been determined from a comparison with the operator product expansion of the HVP function. Comparisons with perturbative results can also be used to determine the strong coupling constant α_s and the quark masses as has been done e.g. in [HPQCD 2008, Jansen et al. 2011]. A dedicated comparison with perturbative results is beyond the scope of this thesis. Nevertheless, it appears to be clear that lattice QCD, which provides an ab initio, non-perturbative calculation of the hadronic vacuum polarisation function, can provide a very valuable cross-check of the different phenomenological analyses at low momenta.

3.2. The hadronic vacuum polarisation function in twisted mass lattice QCD

3.2.1. Definition

On the lattice the hadronic vacuum polarisation function is computed for space-like momenta Q in Euclidean space-time. As we have seen in Sect. 2.3, in twisted mass lattice QCD physical quantities are usually defined in terms of doublet quark fields. Arranging the electromagnetic charges appearing in Eq. (3.2) in a $SU(2)$ flavour matrix, results in

$$Q_{\mathrm{em}} = \begin{pmatrix} \frac{2}{3} & 0 \\ 0 & -\frac{1}{3} \end{pmatrix} = \frac{1}{6}\mathbb{1} + \frac{1}{2}\tau^3 \,, \tag{3.10}$$

where we have also included the decomposition in irreducible isospin components represented by the Pauli matrices $\tau^0 = \mathbb{1}$ and τ^3. From Eq. (2.38) we thus see that, since no $\tau^{1,2}$ is involved in the definition of the electromagnetic vector current, the form of the current is the same expressed in the physical and in the twisted basis. Therefore, we will exclusively work in the twisted basis where the local electromagnetic vector current reads

$$j_\mu^{\mathrm{em}}(n) = \sum_{j=l,h} \bar{\chi}_j(n) Q_{\mathrm{em}} \gamma_\mu \chi_j(n) \tag{3.11}$$

and the sum is over the light and the heavy fermion doublets. Checking the current conservation of the local vector current reveals that it does not satisfy the Ward identity of its continuum counterpart and thus requires renormalisation. The difference is proportional to the lattice spacing implying that the reason for the non-conservation of the local vector current at finite lattice spacing is the reduced space-time symmetry due to the lattice discretisation. However, the actions employed for the light quarks Eq. (2.28) and for the heavy valence quarks Eq. (2.36) are invariant under transformations generated by Q_{em} whose linearised, infinitesimal version for a generic fermion doublet χ reads

$$\begin{aligned} \chi(x) \to \chi'(n) &= \chi(n) + i\alpha Q_{\mathrm{em}} \chi(n) \\ \bar{\chi}(x) \to \bar{\chi}'(n) &= \bar{\chi}(n) - i\alpha \bar{\chi}(n) Q_{\mathrm{em}} \end{aligned} \tag{3.12}$$

such that Noether's theorem [Noether 1918] implies the existence of a conserved current. This current can be determined by requiring the lattice action to be invariant under the local version of Eq. (3.12), which entails assigning a space-time dependence to the infinitesimal parameter α. This results in the lattice Ward identity

$$\langle \partial_\mu^* J_\mu^C(n) \rangle = 0 \,, \tag{3.13}$$

where ∂_μ^* denotes the backward derivative defined in Eq. (2.16) and $J_\mu^C(n)$ is the conserved, 1-point split, lattice vector current

$$\begin{aligned} J_\mu^C(n) = \frac{1}{2} \Big\{ & \bar{\chi}(n) \left(\gamma_\mu - r\right) U_\mu(n) \, Q_{\mathrm{em}} \, \chi(n + a\hat{\mu}) \\ & + \bar{\chi}(n + a\hat{\mu}) \left(\gamma_\mu + r\right) U_\mu(n)^\dagger \, Q_{\mathrm{em}} \chi(n) \Big\} \,. \end{aligned} \tag{3.14}$$

The presence of the gauge links $U_\mu(n)$ guarantees the gauge-invariance of this current and since it only differs from the local vector current in Eq. (3.11) by terms proportional to a

$$J_\mu^C(n) = j_\mu^{\mathrm{em}}(n) + \frac{a}{2}\left[\bar{\chi}\,\gamma_\mu\,Q_{\mathrm{em}}\left(\overrightarrow{\nabla}_\mu + \overleftarrow{\nabla}_\mu\right)\chi\right](n) - \frac{ar}{2}\left[\bar{\chi}\,Q_{\mathrm{em}}\left(\overrightarrow{\nabla}_\mu - \overleftarrow{\nabla}_\mu\right)\chi\right](n)\,, \tag{3.15}$$

it approaches the electromagnetic current in Eq. (3.2) in the continuum limit.

The action of the heavy sea quarks Eq. (2.35) is not invariant under the transformation given in Eq. (3.12) because the twisted mass term involves the first Pauli matrix τ^1. Hence, no conserved lattice vector current exists in this case. This is the reason for employing a mixed-action setup for the second-generation quarks and using the Osterwalder-Seiler action Eq. (2.36) for the heavy valence quarks instead which is diagonal in flavour space. In the valence sector we thus formally introduce three doublets of quarks: the light quark pair $\chi_l = (\chi_l^+, \chi_l^-) = (u, d)$, a strange quark pair $\chi_s = (\chi_s^+, \chi_s^-)$ and a charm quark pair $\chi_c = (\chi_c^+, \chi_c^-)$. The superscript sign refers to the sign of the twisted quark mass for the corresponding field in the valence Dirac operator. Since we employ the Osterwalder-Seiler action Eq. (2.36) in the heavy sector, the complete valence action can be written concisely as a sum over standard twisted mass action terms for the fermion doublets [Frezzotti and Rossi 2004a],

$$S_F^{\mathrm{val}} = \sum_{q=l,s,c}\sum_n \bar{\chi}_q(n)\left[D_W + i\mu_q\gamma_5\tau^3\right]\chi_q(n)\,. \tag{3.16}$$

For non-conserved vector currents as the local one given in Eq. (3.11) multiplicative renormalisation factors Z_V have to be computed and even for non-anomalous transformations Ward-Takahashi identities

$$\langle\delta\mathcal{O}\rangle - \langle\mathcal{O}\delta S\rangle = 0\,, \tag{3.17}$$

which for $\mathcal{O} = 1$ reduces to the Ward identity in Eq. (3.13), are not valid at finite lattice spacing. However, since we want to avoid additional uncertainties related to current renormalisation and we want to rely on the Ward identity for the hadronic vacuum polarisation

$$\langle\partial_\mu^* J_\mu^C(m) J_\nu^C(n)\rangle - a^{-3}\partial_\mu^*\delta_{\mu\nu}\delta_{mn}\langle S_\nu(n)\rangle = 0 \tag{3.18}$$

to check our calculations configurationwise, we employ conserved vector currents in the definition of the hadronic vacuum polarisation tensor on the lattice. The second term in Eq. (3.18) is a contact term only contributing when the space-time position as well as the Lorentz indices are the same for both currents. The field S_ν in the contact term in Eq. (3.18) reads

$$\begin{aligned} S_\nu(n) =& \frac{1}{2}\sum_{j=l,s,c}\Big\{\bar{\chi}_j(n)\,(\gamma_\nu - r)\,U_\nu(n)\,{Q_{\mathrm{em}}}^2\,\chi_j(n+a\hat{\nu}) \\ & -\bar{\chi}_j(n+a\hat{\nu})\,(\gamma_\nu + r)\,U_\nu(n)^\dagger\,{Q_{\mathrm{em}}}^2\,\chi_j(n)\Big\}\,. \end{aligned} \tag{3.19}$$

Eq. (3.18) implies that in order to have a transverse hadronic vacuum polarisation tensor also in Euclidean space-time, not only the conserved vector current but also the contact term has to be included in the definition. Hence, we define the lattice hadronic vacuum

polarisation tensor in position space according to

$$\Pi_{\mu\nu}(n,m) \equiv \langle J^C_\mu(m)\, J^C_\nu(n)\rangle - a^{-3}\,\delta_{\mu\nu}\,\delta_{mn}\,\langle S_\nu(n)\rangle \tag{3.20}$$

in contrast to the naive bare polarisation tensor obtained from the 2-point current correlator of the local vector current in Eq. (3.11)

$$\Pi^L_{\mu\nu}(m,n) = \langle j^{\rm em}_\mu(m)\, j^{\rm em}_\nu(n)\rangle\,. \tag{3.21}$$

Due to the point-split nature of the conserved vector current $J^C(n)$, it can be considered to 'live' at a lattice site $n+\frac{a}{2}\hat{\mu}$ such that transversality in momentum space can be ensured by performing the Fourier transformation with the spacetime arguments in the Fourier phase shifted by half a lattice spacing

$$\Pi_{\mu\nu}(Q) = a^4 \sum_m \mathrm{e}^{iQ\cdot(m+a\hat{\mu}/2-n-a\hat{\nu}/2)}\,\Pi_{\mu\nu}(m,n)\;, \tag{3.22}$$

where Q denotes discrete lattice momenta. The Fourier transform in Eq. (3.22) is only realised in the variable m. Therefore, the Ward identity in momentum space

$$\hat{Q}_\mu\Pi_{\mu\nu}(Q) = 0 \quad \text{with} \quad \hat{Q}_\mu = \frac{2}{a}\sin(aQ_\mu/2) \quad \text{for} \quad Q_\mu = \frac{2\pi k_\mu}{L_\mu}\;, \tag{3.23}$$

where L_μ is the lattice extent in μ direction and k_μ denotes an integer with $1 \le k_\mu \le \frac{L_\mu}{a}$, is configurationwise valid only for the index μ.

In contrast to the continuum case discussed in Sect. 3.1, the step from the hadronic vacuum polarisation tensor to the hadronic vacuum polarisation function is not unique on the lattice, because in general the tensor is only transverse up to $\mathcal{O}\,(a)$

$$\Pi_{\mu\nu}(Q) = (\hat{Q}_\mu\hat{Q}_\nu - \hat{Q}^2\delta_{\mu\nu})\Pi(Q^2) + \mathcal{O}(a)\;, \tag{3.24}$$

where $\delta_{\mu\nu}$ is the Euclidean metric given by the unit element. The reason for the $\mathcal{O}(a)$ lattice artefacts is the reduction of the Euclidean space-time symmetry to a hypercubic one by the lattice discretisation. However, as we will prove in Sect. 3.2.2, $\mathcal{O}\,(a)$ effects are removed in twisted mass lattice QCD at maximal twist when deploying the following definition of the vacuum polarisation. Projecting first with $P_{\mu\nu}(Q)$ on the transverse part of the tensor,

$$\begin{aligned} P_{\mu\nu}(Q) &= \hat{Q}_\mu\,\hat{Q}_\nu - \delta_{\mu\nu}\,\hat{Q}^2 \\ \Pi(\hat{Q}^2) &= \Pi_{\mu\nu}(Q)P_{\mu\nu}(Q)\,(P_{\mu\nu}(Q)P_{\mu\nu}(Q))^{-1}\;, \end{aligned} \tag{3.25}$$

noting that $P_{\mu\nu}P_{\mu\nu} = 3\,(\hat{Q}^2)^2$ and using the Ward identity in Eq. (3.23) we define a real and momentum-averaged polarisation function

$$\Pi^{(\rm av)}(\hat{Q}^2) = \mathrm{Re}\left(\frac{1}{\#\mathcal{G}(Q)}\sum_{Q'\,\in\,\mathcal{G}(Q)}\Pi(Q')\right) \equiv \Pi(\hat{Q}^2) \tag{3.26}$$

$$\text{with} \quad \Pi(Q) = \frac{1}{3\,(\hat{Q}^2)^2}P_{\mu\nu}(Q)\,\Pi_{\mu\nu}(Q)\;, \tag{3.27}$$

where $\hat{Q}^2 = \sum_\mu \hat{Q}_\mu^2$. By explicitly taking the real part, we project on isospin symmetry sectors. This will be further discussed in Sect. 3.2.2. $\mathcal{G}(Q)$ is the set which contains all momenta obtained from Q by applying discrete rotations and reflections of the 4-dimensional lattice. We also include rotations mixing time and spatial coordinates, whenever they are possible, although our configurations feature $T = 2\,L$ for the lattice time direction T and spatial extent L. Moreover, in practice we also average over momenta with the same $\hat{Q}^2$ which are only related by a spacetime transformation in the continuum. Correspondingly, $\#\mathcal{G}(Q)$ denotes the number of elements of this set. This concludes our definition of the scalar vacuum polarisation function as a function of the squared lattice 4-momentum.

3.2.2. $\mathcal{O}(a)$ improvement

Before utilising our definition of the hadronic vacuum polarisation function Eq. (3.26), we want to ascertain that $\mathcal{O}(a)$ improvement holds in this case. As we have discussed in Sect. 2.3.2, for twisted mass fermions at maximal twist automatic on-shell $\mathcal{O}(a)$ improvement has been established for current correlators at non-zero physical distances towards the continuum limit [Frezzotti and Rossi 2004a]. The hadronic vacuum polarisation function in momentum space, $\Pi_{\mu\nu}(\hat{Q}^2)$, however, also receives short-distance contributions arising from the Fourier summation of the 2-point vector current correlator in Eq. (3.22) for $n - m \to 0$. In the following, we focus on the impact of such contributions to the Fourier sum from small and zero distance.

By extending Symanzik's effective theory [Symanzik 1983a,Symanzik 1983b] introduced in Sect. 2.3.2 to also include the case of coinciding space-time points, we show in the following that with our definition of the hadronic vacuum polarisation function and at maximal twist these short-distance contributions do not spoil the automatic $\mathcal{O}(a)$ improvement of the vacuum polarisation function in the twisted mass formulation of lattice QCD. The reasoning presented below is a summary of our proof published in [Burger et al. 2015b].

We proceed in two steps:

1. We examine the possible mixing of the polarisation tensor in position space with operators of equal and lower dimension due to renormalisation and short-distance contributions. The occurrence of such a mixing requires the definition of a subtracted operator.

2. We use the Symanzik expansion technique with reference to the twisted mass lattice action and the subtracted operator to show that all contributions of $\mathcal{O}(a)$ vanish at maximal twist.

As in Sect. 2.3.2 the identification of the mixing pattern and of the terms in the Symanzik expansion relies on the symmetries of the lattice and the continuum theory. Automatic $\mathcal{O}(a)$ improvement means that no improvement coefficients are needed in twisted mass lattice QCD in order to eliminate $\mathcal{O}(a)$ terms. The only parameter ultimately assumed to be tuned is the bare quark mass such that maximal twist is realised. See Refs. [Frezzotti et al. 2006, Chiarappa et al. 2007, ETMC 2010a, ETMC 2011] for details how this has been achieved for the $N_f = 2 + 1 + 1$ setup we are interested in here. For our purposes, we only need to recall that maximal twist corresponds to having a vanishing bare quark mass $m_q = 0$ in the Wilson Dirac operator such that the twisted mass μ_q takes the role of the physical one.

Symmetry projections

Our discussion of operator mixing and the Symanzik expansion given below proceeds in position space, yet the position space current correlators given in Eq. (3.20) and (3.21) do not have a definite transformation behaviour under the symmetries of the lattice theory. To remedy this shortcoming, our definition of the hadronic vacuum polarisation function in momentum space given in Eq. (3.26) incorporates projections on the space-time symmetry sector as well as on the isospin symmetry sectors by taking the real part. Since for the following discussion it is desirable to have definite transformation properties in position space as well, we show in this section that the projections defined in momentum space automatically imply the corresponding properties for the correlators in position space.

Space-time transformation group The momentum projector $P_{\mu\nu}(Q)$ given in Eq. (3.25) transforms like a rank-2 tensor. Restricting the set of momenta to a representative set we can extend the average over $\mathcal{G}(Q)$ to the complete space-time transformation group. As outlined in appendix B we can realise this average equivalently in position space. This amounts to defining the projected polarisation tensor

$$\left[\Pi_{\mu'\nu'}(m',n')\right]^{(av)} = \frac{1}{N_{\mathcal{G}}} \sum_{R\in\mathcal{G}} \Lambda(R)^{\mu'}_{\mu}\, \Lambda(R)^{\nu'}_{\nu}\, \Pi_{\mu\nu}(\Lambda(R)m', \Lambda(R)n')\,, \tag{3.28}$$

where $\Lambda(R)$ are the representation matrices of the lattice rotations and reflections and $N_{\mathcal{G}}$ is the total number ot elements in the group. In this form the vacuum polarisation tensor in position space exhibits the transformation behaviour of a true rank-2 tensor. We will leave out the brackets $[\quad]^{(\mathrm{av})}$ from position space operators and assume this exact rank-n tensor transformation behaviour for all operators in the following sections

In anticipation of the subsequent discussion, we note that in particular we have invariance of the tensor under space-time inversion $Q \to -Q$ or $m \to -m$. This is one of the key transformations in the discussion of automatic $\mathcal{O}(a)$ improvement. Moreover, with the definition in Eq. (3.28) the average over momentum orbits becomes trivial as in the continuum.

Isospin For $SU(2)_I$ isospin relations we use the flavour matrices $\tau^{\pm} = \frac{1}{2}\left(\tau^1 \pm i\,\tau^2\right)$ and τ^3 formed of the Pauli matrices, and $\tau^0 = \mathbb{1}$. Correspondingly, with $J^{\tau} = \bar{\chi}\,\gamma_\mu \tau\,\chi$ we denote the isospin component of the current for any of the three doublets.

The implications of taking the real part of the polarisation tensor in momentum space can be immediately seen by using the relation

$$\langle J^{f_1}_{\mu}(m)\, J^{f_2}_{\nu}(n)\rangle^* = \langle J^{\bar{f}_2}_{\mu}(m)\, J^{\bar{f}_1}_{\nu}(n)\rangle \tag{3.29}$$

of the current correlator in position space and the corresponding relation

$$\Pi^{f_1 f_2\,*}_{\mu\nu}(Q) = \Pi^{\bar{f}_2 \bar{f}_1}_{\mu\nu}(-Q) \tag{3.30}$$

for the polarisation tensor in momentum space. Here (f_1, f_2) denotes a pair of quark flavour indices and the index with a bar $\bar{f}_{1,2}$ denotes the flavour with opposite sign of the twisted mass parameter compared to flavour $f_{1,2}$.

Given the electromagnetic charge matrix we can split the electromagnetic current in all

three sectors into its irreducible isospin components

$$\begin{aligned} J_l^{\mathrm{em}} &= \frac{2}{3}\, J^{\mathrm{u}} - \frac{1}{3}\, J^{\mathrm{d}} = \frac{1}{6}\, J^{\tau^0} + \frac{1}{2}\, J^{\tau^3} \\ J_s^{\mathrm{em}} &= -\frac{1}{3}\, J^{\bar{s}} = -\frac{1}{6}\, J^{\tau^0} - \frac{1}{6}\, J^{\tau^3} \\ J_c^{\mathrm{em}} &= \frac{2}{3}\, J^{c} = \frac{1}{3}\, J^{\tau^0} + \frac{1}{3}\, J^{\tau^3}\,. \end{aligned} \tag{3.31}$$

With $\bar{s}$ we denote the upper component of the valence strange quark doublet. Hence, we only need the components with flavour structure τ^0 and τ^3. Using the relation (3.29) the correlator of two such isospin currents $J^{a,b} = J^f + \sigma_{a,b}\, J^{\bar{f}}$ with $\sigma_{a,b} \in \{\pm 1\}$ in momentum space can be decomposed according to

$$\begin{aligned} \Pi_{\mu\nu}^{ab}(Q) &= \langle J^a J^b \rangle \\ &= \Pi_{\mu\nu}^{ff}(Q) + \sigma_b\, \Pi_{\mu\nu}^{f\bar{f}}(Q) + \sigma_a\, \Pi_{\mu\nu}^{\bar{f}f}(Q) + \sigma_a\sigma_b\, \Pi_{\mu\nu}^{\bar{f}\bar{f}}(Q) \\ &= \Pi_{\mu\nu}^{ff}(Q) + \sigma_b\, \Pi_{\mu\nu}^{f\bar{f}}(Q) + \sigma_a\, \Pi_{\mu\nu}^{f\bar{f}\,*}(-Q) + \sigma_a\sigma_b\, \Pi_{\mu\nu}^{ff\,*}(-Q) \\ &\xrightarrow{[\quad]^{(\mathrm{av})}} 2\,\mathrm{Re}\left(\left[\Pi_{\mu\nu}^{ff}(Q)\right]^{(\mathrm{av})}\right)(1+\sigma_a\sigma_b) + 2\,\mathrm{Re}\left(\left[\Pi_{\mu\nu}^{f\bar{f}}(Q)\right]^{(\mathrm{av})}\right)(\sigma_a+\sigma_b) \\ &\quad + 2i\,\mathrm{Im}\left(\left[\Pi_{\mu\nu}^{ff}(Q)\right]^{(\mathrm{av})}\right)(1-\sigma_a\sigma_b) + 2i\,\mathrm{Im}\left(\left[\Pi_{\mu\nu}^{f\bar{f}}(Q)\right]^{(\mathrm{av})}\right)(-\sigma_a+\sigma_b)\,. \end{aligned} \tag{3.32}$$

As before, $[\quad]^{(\mathrm{av})}$ denotes the average over equivalent momenta, in particular averaging over Q and $-Q$. From Eq. (3.32) we find that the contributions from the current-current correlator with equal isospin components for both currents are purely real ($\sigma_a = \sigma_b$), whereas the mixed isospin combinations are purely imaginary ($\sigma_a = -\sigma_b$). The latter contributions are isospin symmetry breaking lattice artefacts originating from the breaking of flavour symmetry due to the twist term. Retaining only the real part of the averaged momentum space correlator removes these terms explicitly. In the continuum the hadronic vacuum polarisation function for space-like momenta is manifestly real and $\Pi^u = \Pi^d$ if both quarks have the same mass as is the case in our setup. The twisted mass γ_5-hermiticity relation

$$\gamma_5 (D_W^u)^\dagger \gamma_5 = D_W^d \tag{3.33}$$

implies $\Pi^u(\hat{Q}^2) = (\Pi^d(\hat{Q}^2))^*$ which again amounts to the imaginary part of the vacuum polarisation function being a pure lattice artefact and shows that it is sufficient to compute $\Pi(\hat{Q}^2)$ for only one, say the upper, component of the flavour doublet. Our definition in Eq. (3.26) thus removes any explicit signs of flavour-symmetry breaking and we only need to consider the correlators $\langle J^\tau J^\tau \rangle$ with $\tau \in \{\mathbb{1}, \tau^3\}$.

Knowing that we only need to consider correlators of same isospin, we can infer that in position space we always get correlators for flavour pairs $(f_1,\, f_2)$ which are symmetrised in the indices $(1, 2)$ and the bar operation. These combinations are manifestly real. The operator in the contact term Eq. (3.19) contains the squared electromagnetic charge matrix. Thus, it also consists of two isospin components given by τ^0 and τ^3. Again the isospin component τ^3 is purely imaginary whereas the component with τ^0 is purely real. Thus, for the contact term we may limit our considerations to the component with $\tau^0 = \mathbb{1}$.

Mixing of the polarisation tensor

When renormalising the vacuum polarisation it will in general mix with operators of equal and lower dimension possessing the same symmetry transformation properties. Moreover, Fourier sums on the lattice and the Fourier integrals in the Symanzik effective theory extend over all distances of operator products. This can give rise to additional terms that need to be subtracted. They are accounted for by allowing additional contributions of contact terms, again of equal and lower dimension and with same transformation properties.

The polarisation tensor in position space is of mass dimension 6. We thus write a general subtracted polarisation tensor in position space as

$$\begin{aligned}\left[J^\tau_\mu(m)\, J^\tau_\nu(n)\right]_{\text{sub}} = &\sum_{k=0}^{6}\sum_{i\geq 0}\frac{Z^{(0)}_{ki}}{a^{6-k}}\, O_{ki\,\mu\nu}(m,n) + a^{-4}\,\delta_{mn}\sum_{k=0}^{6}\sum_{i\geq 0}\frac{Z^{(1)}_{ki}}{a^{2-k}}\, B^{(1)}_{ki\,\mu\nu}(n)\\ &+ a^{-4}\,\partial^{(m)}_\mu\,\delta_{mn}\sum_{k=0}^{6}\sum_{i\geq 0}\frac{Z^{(2)}_{ki}}{a^{1-k}}\, B^{(2)}_{ki\,\nu}(n)\\ &+ a^{-4}\,\partial^{(m)}_\kappa\,\partial^{(m)}_\lambda\,\delta_{mn}\sum_{k=0}^{6}\sum_{i\geq 0}\frac{Z^{(3)}_{ki}}{a^{-k}}\, B^{(3)}_{ki\,\mu\nu\kappa\lambda}(n)\\ &+ \dots . \end{aligned} \tag{3.34}$$

With index k we label the dimension of the operators and index i runs over the possible operators within each dimension. As a lattice version of the Dirac δ function we use $a^{-4}\,\delta_{mn} \xrightarrow{a\to 0} \delta(x-y)$. The parity-odd symmetric lattice derivative ∂_μ has been defined in Eq. (2.12) and $O_{ki\,\mu\nu} = J^\tau_\mu\, J^\tau_\nu$ for $k=6$, $i=0$.

When enumerating the operators O_{ki}, $B^{(n)}_{ki}$, we keep explicit factors of Wilson and twisted quark mass, m_q and μ_q, respectively, as well as of the dimensionless Wilson parameter r at zeroth and first power. With the parametrisation in Eq. (3.34), i.e. the explicit factoring out of powers of the lattice spacing and of quark masses, the dimensionless coefficients $Z^{(n)}_{ki}$ do not have a power dependence on the lattice spacing [Lüscher et al. 1996, Weisz 2010]. The detailed form of these factors would be fixed by a proper set of renormalisation conditions. We will not formulate such conditions, but stay on the level of a general subtracted operator. This is sufficient for our purposes.

Taking the Fourier transform of Eq. (3.34), the contributions from the operators $B^{(1)}$ are momentum independent, while those from $B^{(2)}$ and $B^{(3)}$ generate terms that depend on the external momentum. For $B^{(2)}$ there are no operators to give rise to $\mathcal{O}(a)$ terms. The general notation for $B^{(3)}_{ki\,\mu\nu\kappa\lambda}$ is meant to include various Lorentz structures, $B^{(3)}_{ki\,\mu\nu\kappa\lambda} \propto B^{(3)}_{ki}\,\delta_{\mu\nu}\,\delta_{\kappa\lambda}$, $B^{(3)}_{ki}\,\delta_{\mu\kappa}\,\delta_{\nu\lambda}$, $B^{(3)}_{ki\,\mu\kappa}\,\delta_{\nu\lambda}$, etc.. The sets of operators for the $B^{(n)}$ that can mix with the polarisation tensor via short-distance contributions can be constructed from the mass parameters, the Wilson parameter r, quark bilinears and products of those as well as the lattice covariant derivative and the lattice gauge field strength tensor $C_{\mu\nu}$ for which the expression given in [Sheikholeslami and Wohlert 1985] can be taken. The set is restricted by the symmetries of the lattice theory. For twisted mass lattice QCD we use the following list of symmetry transformations,

- twisted time reversal:

$$\begin{aligned}
&\mathcal{T} \times [\mu_q \to -\mu_q] : \\
&\qquad \text{with } \mathcal{T} : \qquad x \to Tx = (-x_0, \vec{x}) \\
&\qquad\qquad \chi(x) \to i\,\gamma_0\,\gamma_5\,\chi(Tx) \\
&\qquad\qquad \bar{\chi}(x) \to -i\bar{\chi}(Tx)\,\gamma_5\,\gamma_0 \\
&\qquad\qquad U_0(x) \to U_0(Tx - a\hat{0})^\dagger\,,\; U_i(x) \to U_i(Tx)
\end{aligned}$$

$$\begin{aligned}
\mathcal{T}_{1,2} : \qquad & x \to Tx = (-x_0, \vec{x}) \\
& \chi(x) \to i\tau^{1,2}\,\gamma_0\,\gamma_5\,\chi(Tx) \\
& \bar{\chi}(x) \to -i\bar{\chi}(Tx)\,\tau^{1,2}\,\gamma_5\,\gamma_0 \\
& U_0(x) \to U_0(Tx - a\hat{0})^\dagger\,,\; U_i(x) \to U_i(Tx)
\end{aligned}$$

- twisted parity:

$$\begin{aligned}
&\mathcal{P} \times [\mu_q \to -\mu_q] : \\
&\qquad \text{with } \mathcal{P} : \qquad x \to Px = (x_0, -\vec{x}) \\
&\qquad\qquad \chi(x) \to i\,\gamma_0\,\chi(Px) \\
&\qquad\qquad \bar{\chi}(x) \to -i\bar{\chi}(Px)\,\gamma_0 \\
&\qquad\qquad U_0(x) \to U_0(Px)\,,\; U_i(x) \to U_i(Px - a\hat{i})^\dagger \\
&\qquad \mathcal{P}_{1,2} : \qquad \chi(x) \to i\tau^{1,2}\,\gamma_0\,\chi(Px) \\
&\qquad\qquad \bar{\chi}(x) \to -i\bar{\chi}(Px)\,\tau^{1,2}\,\gamma_0 \\
&\qquad\qquad U_0(x) \to U_0(Px)\,,\; U_i(x) \to U_i(Px - a\hat{i})^\dagger
\end{aligned}$$

- charge conjugation:

$$\begin{aligned}
\mathcal{C} : \qquad & \chi(x) \to C^{-1}\,\bar{\chi}(x)^T \\
& \bar{\chi}(x) \to -\chi(x)^T\,C \\
& U_\mu(x) \to U_\mu(x)^*
\end{aligned}$$

- $\mathcal{P} \times \mathcal{D} \times [m_q \to -m_q] \times [r \to -r]$
- $\mathcal{R}_5^{1,2} \times \mathcal{D} \times [\mu_q \to -\mu_q]$

The details of these transformations are described in the review [Shindler 2008] and for completeness a brief listing is also given in appendix A.

We start our considerations with the local vector current correlator $\Pi^L_{\mu\nu}(m,n)$ given in Eq. (3.21), which is symmetry projected as described in the previous section and in Eq. (3.26). To investigate the mixing pattern for $\Pi^L_{\mu\nu}(m,n)$ in the continuum limit, we distinguish the two cases $m = n$ and $m \neq n$ for the space-time arguments in the Fourier

sum

$$\Pi^L_{\mu\nu}(Q) = a^4 \sum_{m\neq n} \langle \left[j^{\rm em}_\mu(m)\right]_R \left[j^{\rm em}_\nu(n)\right]_R\rangle \, {\rm e}^{iQ(m-n)} + a^4 \, \langle \left[j^{\rm em}_\mu(n)\, j^{\rm em}_\nu(n)\right]_R\rangle$$
$$= \Pi^{(2)}_{\mu\nu}(Q) + \Pi^{(4)}_{\mu\nu} \,, \tag{3.35}$$

where $[\ \ ]_R$ denotes a given renormalisation scheme. The two terms in Eq. (3.35) have to be considered individually due to their different behaviour under renormalisation in the continuum limit.

Case $m \neq n$**:** $\Pi^{(2)}_{\mu\nu}(Q)$ is composed of a product of two vector currents in position space at non-zero distance $m \neq n$. This is exactly the situation encountered in Sect. 2.3.2. For this operator neither mixing nor additive renormalisation occurs. The local current operators are renormalised multiplicatively with a factor Z_V, which can be determined non-perturbatively [Martinelli et al. 1995] in a lattice calculation. Thus,

$$\left[j^{\rm em}_\mu(m)\right]_R = Z_V \, j^{\rm em}_\mu(m) \tag{3.36}$$
$$\left[\Pi^{(2)}_{\mu\nu}(Q)\right]_R = a^4 \sum_{m\neq n} \left[j^{\rm em}_\mu(m)\right]_R \left[j^{\rm em}_\nu(n)\right]_R \ {\rm e}^{iQ(m-n)} \,. \tag{3.37}$$

In the language of Eq. (3.34) we have $Z_{ki} \neq 0$ only for $(k = 6,\, i = 0)$ and zero else. For automatic $\mathcal{O}(a)$ improvement of the latter correlator for physical distances $m \neq n$ the on-shell improvement conditions are sufficient within twisted mass lattice QCD at maximal twist [Frezzotti and Rossi 2004a].

Case $m = n$**:** $\Pi^{(4)}_{\mu\nu}$ is the lattice vacuum expectation value of a four-quark operator of mass dimension 6. We recall, that τ is either τ^0 or τ^3. Additional $\mathcal{O}(a)$ terms and terms with negative powers of the lattice spacing can also arise through singularities in the limit $m \to n$ when performing the continuum limit in the Symanzik effective theory. In the continuum these terms can be identified by expanding the operator product in terms having the form of a ratio $\langle O^{(k)}(y)\rangle / ||x-y||^k$ of a condensate over a power of the distance $||x-y||^k$ with k a positive integer (up to logarithms) [Wilson 1969, Shifman et al. 1979]. These contributions emerge when applying the Fourier transform over a region extending to one lattice spacing around n.

We capture these short-distance contributions by subtracting from the current-current correlator in position space all possible local operators of equal and lower dimension, which are allowed to appear constrained by the lattice symmetries. This involves contributions in the form of the $B^{(n)}_{ki}$ given in Eq. (3.34). The candidate mixing operators $B^{(n)}_{ki}$ have been separated into those that include and do not include covariant derivatives. They are listed in tables {C.1}, and {C.2} in appendix C.

Symanzik expansion for the local case

The operators allowed in the mixing pattern when using the local light quark current $j^{\rm em}_\mu(x)$ are listed in tables {C.1} and {C.2} in appendix C. According to this collection

the subtracted operator reads

$$\begin{aligned}\left[J^\tau_\mu(m)\, J^\tau_\nu(n)\right]_{\text{sub}} &= J^\tau_\mu(m)\, J^\tau_\nu(n) + \frac{Z^{\mathbb{1}}}{a^6}\,\delta_{\mu\nu}\,\delta_{mn} + \frac{Z^{rm}\, rm_q}{a^5}\,\delta_{\mu\nu}\,\delta_{mn} \\ &+ \frac{Z^{m^2}\, m_q^2 + Z^{\mu^2}\,\mu_q^2}{a^4}\,\delta_{\mu\nu}\,\delta_{mn} + \frac{Z^{r\bar\chi\chi}}{a^3}\, r\,\bar\chi\chi\,\delta_{\mu\nu}\,\delta_{mn} + \frac{Z^{rm^3}\, rm_q^3}{a^3}\,\delta_{\mu\nu}\,\delta_{mn} \\ &+ \frac{1}{a^4}\left(Z^{Q^2}\,\delta_{\mu\nu}\,\bar\partial^2 + Z^{QQ}\,\bar\partial_\mu\,\bar\partial_\nu\right)\delta_{mn} + \frac{rm_q}{a^3}\left(Z^{rmQ^2}\,\delta_{\mu\nu}\,\bar\partial^2 + Z^{rmQQ}\,\bar\partial_\mu\,\bar\partial_\nu\right)\delta_{mn} \\ &+ \text{ operators of dimension } \geq 4\,. \end{aligned} \tag{3.38}$$

The expansion of the lattice action close to the continuum limit follows from the local effective action given in Eq. (2.43). We expand its exponential up to $\mathcal{O}(a^3)$. The corrections to the gauge field Lagrangian in the continuum limit start with $\mathcal{O}\left(a^2\right)$ and in fact contain only even powers of the lattice spacing [Lüscher and Weisz 1985]. We thus concentrate on the corrections to the fermion action. The operators that can appear in $\mathcal{L}_5$ and $\mathcal{L}_6$, cf. Eq. (2.43), have been listed in Refs. [Sheikholeslami and Wohlert 1985, Lüscher et al. 1996].

From the expansion of the operator Eq. (3.38) and $\exp\left(-S_{eff}\right)$ in Eq. (2.43) the full Symanzik expansion in momentum space is obtained and reads

$$\begin{aligned}\Pi^\tau_{\mu\nu}(Q) = a^4\,\langle J^\tau_\mu(n)\, J^\tau_\nu(n)\rangle_0 &+ \frac{\tilde Z^{\mathbb{1}}}{a^2}\,\delta_{\mu\nu} \\ &+ \frac{\tilde Z^{\mathbb{1}}}{a}\,\langle -S_5\rangle_0\,\delta_{\mu\nu} + \frac{\tilde Z^{rm}\, rm_q}{a}\,\delta_{\mu\nu} \\ &+ \tilde Z^{\mathbb{1}}\,\langle -S_6 + \frac{1}{2}S_5^2\rangle_0\,\delta_{\mu\nu} + \tilde Z^{rm}\,\langle -rm_q\, S_5\rangle_0\,\delta_{\mu\nu} + \left(\tilde Z^{m^2}\, m_q^2 + \tilde Z^{\mu^2}\,\mu_q^2\right)\,\delta_{\mu\nu} \\ &+ a\,\tilde Z^{\mathbb{1}}\,\langle -S_7 + S_5S_6 - \frac{1}{6}S_5^3\rangle_0\,\delta_{\mu\nu} + a\,\langle\left(\tilde Z^{rm}\, rm_q\right)\,\left(-S_6 + \frac{1}{2}S_5^2\right)\rangle_0\,\delta_{\mu\nu} \\ &+ a\,\langle -\left(\tilde Z^{m^2}\, m_q^2 + \tilde Z^{\mu^2}\,\mu_q^2\right)\, S_5\rangle_0\,\delta_{\mu\nu} + a\,\tilde Z^{r\bar\chi\chi}\,\langle r\,\bar\chi\chi\rangle_0\,\delta_{\mu\nu} + a\,\tilde Z^{rm^3}\, r\, m_q^3\,\delta_{\mu\nu} \\ &+ \left(\tilde Z^{Q^2}\,\delta_{\mu\nu}\,\hat Q^2 + \tilde Z^{QQ}\,\hat Q_\mu\,\hat Q_\nu\right) + arm_q\,\left(\tilde Z^{rmQ^2}\,\delta_{\mu\nu}\,\hat Q^2 + \tilde Z^{rmQQ}\,\hat Q_\mu\,\hat Q_\nu\right) \\ &+ \left\{\mathcal{O}\left(a^2\right)\,,\ \text{operators of higher dimension}\ \right\}\,. \end{aligned} \tag{3.39}$$

Since we are working at maximal twist $m_q \to 0$, we may drop all terms involving the untwisted quark mass. Using the $\mathcal{R}_5^{1,2}$-symmetry [Shindler 2008] we see that the vacuum expectation values $\langle\ \rangle_0$ of S_5, S_5S_6 as well as of $\mu_q^2 S_5$ and $\bar\chi\chi$ vanish as these merely contain $\mathcal{R}_5^{1,2}$-odd operators. Similarly all terms in S_7 disappear by either the $\mathcal{R}_5^{1,2}$- or the $\mathcal{P}\times[\mu_q\to-\mu_q]$ symmetry as is demonstrated in appendix D.

We may then conclude that at maximal twist there are no $\mathcal{O}(a)$ lattice artefacts stemming from the contributions in Eq. (3.39) to $\Pi^\tau_{\mu\nu}$, whose Symanzik expansion we write again for this case,

$$\begin{aligned}\Pi^\tau_{\mu\nu}(Q) = a^4\,\langle J^\tau_\mu(n)\, J^\tau_\nu(n)\rangle_0 &+ \frac{\tilde Z^{\mathbb{1}}}{a^2}\,\delta_{\mu\nu} + \tilde Z^{\mathbb{1}}\,\langle -S_6 + \frac{1}{2}S_5^2\rangle_0\,\delta_{\mu\nu} + \left(\tilde Z^{\mu^2}\,\mu_q^2\right)\,\delta_{\mu\nu} \\ &+ \left(\tilde Z^{Q^2}\,\delta_{\mu\nu}\,Q^2 + \tilde Z^{QQ}\,Q_\mu\,Q_\nu\right) + \left\{\mathcal{O}\left(a^2\right)\,,\ \text{operators of higher dimension}\ \right\}\,. \end{aligned} \tag{3.40}$$

Application to the conserved current correlator

As we have seen in Eq. (3.15) which we repeat below for the reader's convenience, the conserved vector current is a sum of the local current operator and two local operators of mass dimension 4,

$$J_\mu^C(m) = j_\mu^{\mathrm{em}}(m) + \frac{a}{2}\left[\bar{\chi}\,\gamma_\mu\,Q_{\mathrm{em}}\left(\overrightarrow{\nabla}_\mu + \overleftarrow{\nabla}_\mu\right)\chi\right](m) - \frac{ar}{2}\left[\bar{\chi}\,Q_{\mathrm{em}}\left(\overrightarrow{\nabla}_\mu - \overleftarrow{\nabla}_\mu\right)\chi\right](m)\,. \tag{3.41}$$

Similarly, for the field in the lattice contact term in Eq. (3.20) we have

$$S_\nu^\tau(n) = \frac{a}{2}\left[\bar{\chi}\,\tau\,\gamma_\nu\left(\overrightarrow{\nabla}_\nu^f - \overleftarrow{\nabla}_\nu^f\right)\chi\right](n) - \frac{ar}{2}\left[\bar{\chi}\,\tau\left(\overrightarrow{\nabla}_\nu^f + \overleftarrow{\nabla}_\nu^f\right)\chi\right](n) - r\,\bar{\chi}\,\tau\,\chi(n)\,. \tag{3.42}$$

Hence, both the conserved current as well as the lattice contact term are a sum of local quark-bilinear operators for whose correlators we can use the Symanzik expansion.

Having written the conserved current as the local current plus two operators containing derivatives that are of dimension 4 implies that there is no principle alteration of the mixing with lower dimensional operators for $\langle J_\mu^C\, J_\nu^C\rangle$ compared to the local case, since $J_\mu^C\, J_\nu^C$ can be expressed as a sum of the local-current correlator and additional terms of dimension 7 and 8. Moreover, for the short-distance part of the vacuum polarisation tensor formed from the conserved current the appearance of mixing operators is further constrained by the vector Ward identity Eq. (3.18). Thus, the considerations for the occurrence of $\mathcal{O}(a)$ terms are basically the same as for the local case.

The only addition is the lattice contact term where we have $r\bar{\chi}\,\tau\,\chi$. As stated earlier, due to the symmetry projections $\bar{\chi}\,\tau\,\chi$ with $\tau = \tau^3$ is excluded and only $\tau = \mathbb{1}$ needs to be considered. At maximal twist, when $\mathcal{R}_5^{1,2}$ is a symmetry of the continuum theory, this term will vanish, since it is odd under $\mathcal{R}_5^{1,2}$.

Combining the above arguments, the hadronic vacuum polarisation function formed from the conserved vector current according to Eq. (3.20), Eq. (3.25) and Eq. (3.26) exhibits no $\mathcal{O}(a)$ contributions.

3.2.3. Wick contractions

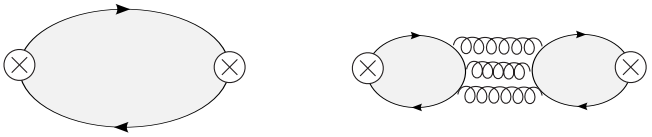

Figure 3.4.: Quark-connected (left) and leading gluon exchange diagram for the disconnected (right) Wick contractions. The crosses represent vector current insertions.

Having ensured the desired properties of our definition of the hadronic vacuum polarisation function, we now perform the Wick contractions of the vector current two-point function in Eq. (3.20) to obtain the expressions for the lattice correlation functions to be computed. As usual, two kinds of diagrams emerge: One in which the two vector current insertions are connected by valence quark propagators, these are the (quark-)connected

contributions, and one in which the quark propagators return to their starting points such that the quark loops are only connected by gluon exchanges. The latter contributions are known as (quark-)disconnected or singlet contributions. For both pieces of the full vacuum polarisation tensor representative Feynman diagrams are drawn in Fig. 3.4. The tensor takes the form

$$\Pi_{\mu\nu}(m,n) = C_{\mu\nu}(m,n) + D_{\mu\nu}(m,n) - a^{-3}\,\delta_{\mu\nu}\,\delta_{mn}\,\langle S_\nu(n)\rangle \tag{3.43}$$

where $C_{\mu\nu}$ denotes the connected and $D_{\mu\nu}$ the disconnected contributions. The methods used for their computations as well as the associated numerical costs differ substantially as we outline below and discuss further in appendix F. The third term in Eq. (3.43) is the contact term which we have already encountered in Eq. (3.20).

The connected Wick contraction for a single flavour in Eq. (3.20) reads without the charge factors

$$\begin{aligned} C^f_{\mu\nu}(m,n) = \; & -\frac{1}{4}\,\mathrm{tr}_{\mathrm{cs}}\Big\{S^f(n,m+a\hat{\mu})(1+\gamma_\mu)U^\dagger_\mu(m)S^f(m,n+a\hat{\nu})(1+\gamma_\nu)U^\dagger_\nu(n) \\ & -S^f(n+a\hat{\nu},m+a\hat{\mu})(1+\gamma_\mu)U^\dagger_\mu(m)S^f(m,n)(1-\gamma_\nu)U_\nu(n) \\ & -S^f(n,m)(1-\gamma_\mu)U_\mu(m)S^f(m+a\hat{\mu},n+a\hat{\nu})(1+\gamma_\nu)U^\dagger_\nu(n) \\ & +S^f(n+a\hat{\nu},m)(1-\gamma_\mu)U_\mu(m)S^f(m+a\hat{\mu},n)(1-\gamma_\nu)U_\nu(n)\Big\}\,. \end{aligned} \tag{3.44}$$

$S^f(m,n)$ denotes the propagator of quark flavour f. We use $\mathrm{tr}_{\mathrm{cs}}$ to denote the trace over colour and spin indices. Utilising again γ_5-hermiticity Eq. (3.33) we can arrange the space-time arguments depending on n to be the second argument of all propagators such that the connected contributions can be computed using point-to-all propagators. This requires the inversion of the twisted mass Dirac matrices for all different masses, up and down components of the quark doublet, 4 spins, 3 colours, and all 5 space-time position n, $n+a\hat{\nu}$. The latter factor of five is absent in calculations using the local current at the source position n. However, as we have mentioned before in this case also the renormalisation factor Z_V has to be determined. Having found the physical masses for strange and charm quark, our approach amounts to $3\cdot2\cdot4\cdot3\cdot5 = 360$ inversions per gauge field configuration. The four-flavour connected part of the hadronic vacuum polarisation tensor in position space then including the corresponding charges Q_f is given by

$$C_{\mu\nu}(m,n) = (Q_u)^2 C^u_{\mu\nu}(m,n) + (Q_d)^2 C^d_{\mu\nu}(m,n) + (Q_c)^2 C^c_{\mu\nu}(m,n) + (Q_s)^2 C^s_{\mu\nu}(m,n)\,, \tag{3.45}$$

which can be further simplified by taking the relation $(C^f_{\mu\nu})^*(m,n) = C^{\bar{f}}_{\mu\nu}(m,n)$ into account which again follows from γ_5-hermiticity Eq. (3.33) and implies that the real parts of the connected contributions of the upper and lower flavour doublet components are the same. Thus, we have in total

$$C_{\mu\nu}(m,n) = \mathrm{Re}\left(\frac{5}{9}C^{ud}_{\mu\nu}(m,n) + \frac{4}{9}C^c_{\mu\nu}(m,n) + \frac{1}{9}C^{\bar{s}}_{\mu\nu}(m,n)\right)\,. \tag{3.46}$$

The expression for a single flavour combination ff' entering the disconnected contribu-

tion reads again without the charge factors

$$\begin{aligned} D_{\mu\nu}^{ff'}(m,n) =& \frac{1}{4}\Big\{ \mathrm{tr_{cs}}\left(S^f(m,m+a\hat{\mu})(1+\gamma_\mu)U_\mu^\dagger(m)\right)\mathrm{tr_{cs}}\left(S^{f'}(n,n+a\hat{\nu})(1+\gamma_\nu)U_\nu^\dagger(n)\right) \\ &- \mathrm{tr_{cs}}\left(S^f(m,m+a\hat{\mu})(1+\gamma_\mu)U_\mu^\dagger(m)\right)\mathrm{tr_{cs}}\left(S^{f'}(n+a\hat{\nu},n)(1-\gamma_\nu)U_\nu(n)\right) \\ &- \mathrm{tr_{cs}}\left(S^f(m+a\hat{\mu},m)(1-\gamma_\mu)U_\mu(m)\right)\mathrm{tr_{cs}}\left(S^{f'}(n,n+a\hat{\nu})(1+\gamma_\nu)U_\nu^\dagger(n)\right) \\ &+ \mathrm{tr_{cs}}\left(S^f(m+a\hat{\mu},m)(1-\gamma_\mu)U_\mu(m)\right)\mathrm{tr_{cs}}\left(S^{f'}(n+a\hat{\nu},n)(1-\gamma_\nu)U_\nu(n)\right)\Big\} . \end{aligned} \tag{3.47}$$

Like for the connected parts, γ_5-hermiticity Eq. (3.33) implies $(D_{\mu\nu}^{ff})^*(m,n) = D_{\mu\nu}^{\bar{f}\bar{f}}(m,n)$ such that the real parts coincide and due to explicitly taking the real part in our definition of the hadronic vacuum polarisation function Eq. (3.26) we only have to compute the disconnected contributions for either the upper or the lower component of the flavour doublets χ_l, χ_s, χ_c. Since in each term one of the loops contains only m and $m + a\hat{\mu}$ it is obviously no longer possible to have the source position n as second argument of all propagators such that all-to-all propagators have to be computed which is rather expensive in terms of computing time. In practice, we use stochastic Gaussian distributed volume sources. Since there is no longer a fixed source position, the Fourier transform for the disconnected pieces can be carried out in both space-time arguments m and n.

Whereas the expression for the connected contributions of the four flavours present in our calculation Eq. (3.46) only involves three terms due to the fact that flavour is conserved along the propagators and the mass-degeneracy of up and down quarks, expanding the products of the two electromagnetic vector currents leads to the four-flavour expression

$$D_{\mu\nu} = \sum_f^4 (Q_f)^2 D_{\mu\nu}^{ff}(m,n) + \sum_f^4 \sum_{f'\neq f}^4 Q_f Q_{f'} D_{\mu\nu}^{ff'}(m,n) . \tag{3.48}$$

Using again γ_5-hermiticity Eq. (3.33) valid for $m_u = m_d$ gives the simplified expression only involving the upper components of the flavour doublets

$$\begin{aligned} D_{\mu\nu}(m,n) =& \mathrm{Re}\left(\frac{1}{9}D_{\mu\nu}^{uu}(m,n) + \frac{2}{3}D_{\mu\nu}^{uc}(m,n) + \frac{1}{3}D_{\mu\nu}^{u\bar{s}}(m,n)\right. \\ &+\frac{2}{3}D_{\mu\nu}^{cu}(m,n) + \frac{4}{9}D_{\mu\nu}^{cc}(m,n) + \frac{2}{9}D_{\mu\nu}^{c\bar{s}}(m,n) \\ &\left.+\frac{1}{3}D_{\mu\nu}^{\bar{s}u}(m,n) + \frac{2}{9}D_{\mu\nu}^{\bar{s}c}(m,n) + \frac{1}{9}D_{\mu\nu}^{\bar{s}\bar{s}}(m,n)\right) . \end{aligned} \tag{3.49}$$

There are several reasons for believing that the quark-disconnected contributions to the hadronic vacuum polarisation function are small. As can be seen in Fig. 3.4, in perturbation theory they are at least of $\mathcal{O}\left(\alpha_s^3\right)$ in contrast to the connected contribution which is of $\mathcal{O}(1)$. The pure charm quark contribution, for which perturbation theory probably is already applicable, has been shown to be suppressed by a factor $\left(\frac{q^2}{4\ m_c^2}\right)^4$ [Groote and Pivovarov 2002], where q^2 is the relevant energy scale of the problem. Furthermore, the disconnected contributions would be identically zero for three mass-degenerate light fermions. However, there are also indications that quark-disconnected contributions are

non-negligible like an analysis performed within partially quenched chiral perturbation theory estimating the light quark disconnected contributions to be $-\frac{1}{10}$ times the connected contributions [Della Morte and Jüttner 2010]. The same result can be obtained by a straightforward investigation of the charge factors associated with the Wick contractions in the very low momentum region $2m_\pi < Q < 3m_\pi$ [Francis et al. 2013a]. Additionally, in nature the strange quark is, of course, heavier than the light quarks and we also have to take mixed quark contributions from the second term in Eq. (3.48) into account. Hence, it is a priori not clear that disconnected contributions can be neglected. Therefore, we aim at an explicit calculation of these contributions, parts of which will already be presented in this work.

Chapter 4

Analysing the hadronic vacuum polarisation function

The computation of the hadronic vacuum polarisation (HVP) function along the lines of the previous chapter results in a scalar function $\Pi(\hat{Q}^2)$ depending on discrete lattice momenta $\hat{Q}^2 = \sum_\mu \hat{Q}_\mu^2$ with $\hat{Q}_\mu = \frac{2}{a}\sin(aQ_\mu/2)$ and $Q_\mu = \frac{2\pi k_\mu}{L}$ valid for lattices with periodic boundary conditions and integer values $k_\mu = 1, \ldots, N$ in μ-direction. Hence, due to the finiteness of the lattice extent $L = N\,a$, also the lowest achievable momentum on the lattice is finite if standard techniques are used. However, it follows from Eq. (3.5) that the value at vanishing momentum transfer is needed in order to renormalise the hadronic vacuum polarisation function. The standard way to procure this value is to fit the vacuum polarisation function in order to extrapolate it to zero momentum. Fitting the hadronic vacuum polarisation function is also advantageous for the computation of the hadronic contributions to the electroweak observables considered in this thesis. As usual, there are various types of possible fit functions such that the fitting procedure needs to be carefully chosen. In this chapter, we want to present three different possibilities of treating the raw data.

We begin the discussion in Sect. 4.1 with a presentation of the procedure we have chosen for the determination of the leading-order hadronic contributions to the electroweak observables investigated in this thesis. To this end, we first describe the setup used for all numerical calculations in this work in Sect. 4.1.1. Afterwards, the fit functions employed when fitting the hadronic vacuum polarisation function are presented in Sect. 4.1.2. Those fits require the evaluation of the vector meson spectral properties. Therefore, Sect. 4.1.3 is devoted to their discussion and to the exposition of these first numerical results of this thesis. Afterwards, we introduce Padé fit functions in Sect. 4.2.1 which have been utilised by other collaborations working on a lattice determination of the muon anomalous magnetic moment. We discuss why we have refrained from using them at this stage of our lattice calculations. The last section contains a potentially even more promising procedure we have proposed in [Feng et al. 2013, Jansen et al. 2014] which enables the evaluation of $\Pi(0)$ without extrapolation. Its usage is, however, only considered beneficial once more precise data on larger lattices than are currently available has been obtained.

4.1. Standard procedure

4.1.1. Setup

As mentioned before, the calculations are performed employing gauge field configurations generated by the ETMC with $N_f = 2 + 1 + 1$ dynamical quark flavours [ETMC 2010a, ETMC 2011]. These sets of configurations are obtained at different values of the lattice

Ensemble	β	a[fm]	$\left(\frac{L}{a}\right)^3 \times \frac{T}{a}$	m_{PS}[MeV]	L[fm]
D15.48	2.10	0.061	$48^3 \times 96$	227	2.9
D30.48	2.10	0.061	$48^3 \times 96$	318	2.9
D45.32sc	2.10	0.061	$32^3 \times 64$	387	1.9
B25.32t	1.95	0.078	$32^3 \times 64$	274	2.5
B35.32	1.95	0.078	$32^3 \times 64$	319	2.5
B35.48	1.95	0.078	$48^3 \times 96$	314	3.7
B55.32	1.95	0.078	$32^3 \times 64$	393	2.5
B75.32	1.95	0.078	$32^3 \times 64$	456	2.5
B85.24	1.95	0.078	$24^3 \times 48$	491	1.9
A30.32	1.90	0.086	$32^3 \times 64$	283	2.8
A40.32	1.90	0.086	$32^3 \times 64$	323	2.8
A50.32	1.90	0.086	$32^3 \times 64$	361	2.8

Table 4.1.: Parameters of the $N_f = 2 + 1 + 1$ flavour gauge field configurations that have been analysed in this work. β denotes the gauge coupling, a the lattice spacing, $\left(\frac{L}{a}\right)^3 \times \frac{T}{a}$ the space-time volume, and m_{PS} is the unphysical value of the pion mass. The values for m_{PS} have been determined in [ETMC 2010a]. The approximate lattice spacings given here are taken from a first analysis of the used gauge field configurations [ETMC 2010b].

spacing and several volumes enabling us to perform the continuum limit and to estimate discretisation and finite size effects as systematic uncertainties in our lattice calculation. In addition, at each value of the lattice spacing configurations exist at several values of the pion mass, ranging from $230\,\mathrm{MeV} \lesssim m_\pi \lesssim 490\,\mathrm{MeV}$ thus allowing for an extrapolation to the physical point. Our calculations are not only the first four-flavour lattice computations of the leading hadronic contributions to electroweak parameter shifts but also constitute the first lattice computations of those quantities in which the continuum limit is taken and apart from the isospin breaking effects all systematic uncertainties can be estimated.

It has been observed that for Wilson-like fermions there is a first-order phase transition close to the chiral point for coarse lattices [Aoki 1984,Sharpe and Singleton 1998,Farchioni et al. 2005a] and that the strength of this transition can be weakened by not only using plaquettes but also 1×2 rectangular Wilson loops U_R in the gauge action [Farchioni et al. 2005b]. Similarly to the Wilson term and the twisted mass term, those rectangular loops constitute irrelevant operators. For the generation of gauge field configurations with $N_f = 2+1+1$ dynamical twisted mass fermions, numerical tests have revealed the Iwasaki gauge action [Iwasaki 1985]

$$S_G = \frac{\beta}{3} \sum_{n \in \Lambda} \left(c_0 \sum_{P \in \Lambda} \Re\left[\mathrm{tr}(\mathbb{1} - U_P(n))\right] + c_1 \sum_{R \in \Lambda} \Re\left[\mathrm{tr}(\mathbb{1} - U_R(n))\right] \right) \tag{4.1}$$

with $c_1 = -0.331$ and $c_0 = 1 - 8c_1$ to be particularly effective in smoothening the dependence on the bare quark mass of observables that are sensitive to the phase transition [ETMC 2010a]. Therefore this is the gauge action of choice for the gauge field ensembles used in this work.

Besides the gauge action, for the generation of the gauge field ensembles the twisted mass lattice actions for a degenerate fermion doublet Eq. (2.28) for the light quarks and the twisted mass action for a non-degenerate fermion doublet Eq. (2.35) for the second-generation quarks are implemented. Both have been tuned to maximal twist as detailed in [Frezzotti et al. 2006, ETMC 2010a, ETMC 2011]. Some properties of the ensembles we have studied are given in Tab. 4.1.

Since the Noether current is only conserved for actions diagonal in flavour space, we employ an action for the heavy valence quarks different from the sea quark action given in Eq. (2.35), namely the so-called Osterwalder-Seiler action in Eq. (2.36). How to achieve $\mathcal{O}(a)$ improvement in this situation is discussed in Ref. [Frezzotti and Rossi 2004b] and in the previous chapter we have explicitly shown based on [Burger et al. 2015b] that $\mathcal{O}(a)$ effects are absent when defining the hadronic vacuum polarisation function as detailed there. The bare twisted mass parameters for the valence strange and the charm quarks, μ_s and μ_c, are tuned in such a way that the physical values for $2m_K^2 - m_{\mathrm{PS}}^2$ and the D-meson mass, respectively, are reproduced. Here, m_K denotes the kaon mass. This leads to the values collected in Tab. 4.2.

β	$a\mu_s$	$a\mu_c$
1.90	0.01815(10)	0.2360(10)
1.95	0.01685(10)	0.2150(20)
2.10	0.014165(10)	0.1755(20)

Table 4.2.: Results for the bare strange and charm quark mass parameters in Eq. (2.36) from matching $2m_K^2 - m_{\mathrm{PS}}^2$ and m_D with their physical values.

When determining physical observables on the ETMC's $N_f = 2{+}1{+}1$ ensembles [ETMC 2010a, ETMC 2011] one potential source of a systematic error is the chiral extrapolation to the physical pion mass. Meanwhile an ensemble with $N_f = 2$ dynamical quarks directly at the physical point [Abdel-Rehim et al. 2013, Abdel-Rehim et al. 2014] has been generated thus overcoming a longstanding limitation in lattice QCD calculations. We have checked our chiral extrapolations of the light quark contributions to the physical observables studied in this thesis by comparing the results with those obtained on this ensemble featuring the physical pion mass. This appears to be admissible since for the light-quark contributions lattice artefacts as well as finite size effects have been found to be small on the four-flavour ensembles.

In the gauge sector again the Iwasaki action Eq. (4.1) is employed. In order to reduce lattice artefacts caused by the mass splitting of the neutral and the charged pions a clover-term known from [Sheikholeslami and Wohlert 1985] is added to the twisted mass action for a degenerate fermion doublet such that the fermion action in the twisted basis now reads

$$S_F[\chi, \overline{\chi}, U] = \sum_x \overline{\chi}(x) \left[D_W + m_0 + i\mu_q \gamma_5 \tau^3 \right] \chi(x) + c_{\mathrm{SW}} \sum_x \overline{\chi}(x) \left[\frac{i}{4} \sigma_{\mu\nu} \mathcal{C}_{\mu\nu} \right] \chi(x) \ , \quad (4.2)$$

where $\sigma^{\mu\nu} = \frac{i}{2}[\gamma_\mu, \gamma_\nu]$ and c_{SW} is the non-perturbatively determined Sheikoleslami-Wohlert improvement coefficient [CP-PACS, JLQCD 2006]. The parameters of this ensemble determined in [Abdel-Rehim et al. 2013, Abdel-Rehim et al. 2014] are given in Tab. 4.3.

β	c_{SW}	a[fm]	$\left(\frac{L}{a}\right)^3 \times \frac{T}{a}$	m_{PS}[MeV]	L[fm]
2.10	1.57551	0.094	$48^3 \times 96$	128	4.6

Table 4.3.: Parameters of ensemble featuring $N_f = 2$ twisted mass fermions at the physical point.

4.1.2. Fit functions

In this section, we specify the fit functions used for the quark-connected contributions to the hadronic vacuum polarisation function. According to our investigations of the B55.32 ensemble, see Tab. 4.1 for details, leaving out the quark-disconnected contributions seems to be acceptable at our current level of precision attained for the quark-connected contributions to the hadronic vacuum polarisation function. In fact, using the local vector current we have for the first time ever detected a momentum dependence of the disconnected contributions of the light quark part of the vacuum polarisation function when using 24 stochastic volume sources on 1548 configurations and 48 stochastic volume sources on 4996 configurations for the computation of the rather expensive all-to-all propagators necessary for their determination. This data has been generated in the course of the investigations of the η and η' mass difference by the authors of [Michael et al. 2013]. Employing the one-end trick [ETMC 2008], the isovector part

$$\Pi^3_{\mu\nu}(x,y) = \langle J^3_\mu(x) J^3_\nu(y) \rangle \tag{4.3}$$

with $J^3_\mu = \frac{1}{2}\overline{\chi}\gamma_\mu\tau^3\chi$ is significantly different from zero. However, this is a pure lattice artefact and will not contribute in the continuum limit. On the other hand, the more interesting isoscalar part

$$\Pi^0_{\mu\nu}(x,y) = \frac{1}{9}\langle J^0_\mu(x) J^0_\nu(y) \rangle \tag{4.4}$$

with $J^0_\mu = \frac{1}{2}\overline{\chi}\gamma_\mu \mathbb{1}\chi$ is compatible with zero. The connected and disconnected pieces of the polarisation function for the light flavours are depicted in Fig. 4.1.

Since the connected pieces are almost two orders of magnitude larger than the disconnected contributions, they already seem to provide a sufficient estimate of the complete hadronic vacuum polarisation function. However, the impact of the quark-disconnected contributions of the heavy flavours still needs to be explored. In the following we denote the left-hand sides of the fit functions by $\Pi(Q^2)$ despite it only being the connected contributions to the complete vacuum polarisation function. As we have seen in Sect. 3.2.3, there are no mixed-flavour contributions for the quark-connected Feynman diagrams. Hence, we can obtain the total vacuum polarisation tensor by adding the vacuum polarisation tensors of the single-flavour contributions including the appropriate charge factors

$$\Pi_{\mu\nu}(Q) = \frac{5}{9}\Pi^{\mathrm{ud}}_{\mu\nu}(Q) + \frac{1}{9}\Pi^{\mathrm{s}}_{\mu\nu}(Q) + \frac{4}{9}\Pi^{\mathrm{c}}_{\mu\nu}(Q)\,. \tag{4.5}$$

Notice that we have defined the single-flavour contributions to $\Pi_{\mu\nu}(Q)$ excluding the factors of the squared charges. In the following we will generically denote them by $\Pi^f_{\mu\nu}(Q)$ and the respective vacuum polarisation function by $\Pi^f(Q^2)$.

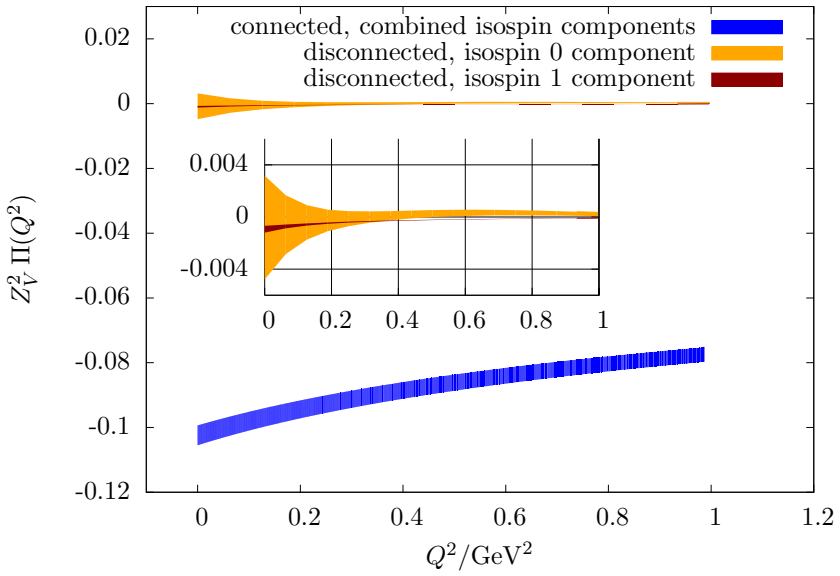

Figure 4.1.: Comparison of the light quark contributions to the unsubtracted hadronic vacuum polarisation function from quark-connected and disconnected diagrams of the local current correlator. Z_V has been obtained from the ratio of the connected part of the conserved and local current-current correlators. The values have been computed with the analytical continuation method [Feng et al. 2013] described in Sect. 4.2.2 without correcting for finite-size effects.

Due to the renormalisation of the vacuum polarisation function given in Eq. (3.5), the calculation for each flavour involves both an interpolation of $\Pi^f(Q^2)$ in between discrete lattice momenta as well as an extrapolation to zero momentum. Our standard fit of the low-momentum dependence of the vacuum polarisation function involves two different terms. The first is inspired by vector meson dominance with M vector meson mass poles

$$\Pi^f_{\mathrm{low}}(Q^2) = \sum_{i=1}^{M} \frac{f_i^2}{m_i^2 + Q^2} + \sum_{j=0}^{N-1} a_j (Q^2)^j \,, \tag{4.6}$$

whereas the second term parametrises remaining deviations in the low-momentum region which extends up to a matching momentum Q^2_{match}. Here, m_i denotes the mass of the vector meson states and f_i their decay constants. They are determined before fitting the vacuum polarisation from the same vector correlation functions partially Fourier transformed in the spatial directions on the same bootstrap samples as will be described in the next subsection 4.1.3. Thus, the a_j are the only parameters fitted here.

The high-momentum part of $\Pi^f(Q^2)$ for $Q^2 > Q^2_{\mathrm{match}}$ is interpolated using a polynomial in Q^2 and a polynomial multiplied by a logarithmic term

$$\Pi^f_{\mathrm{high}}(Q^2) = \log(Q^2) \sum_{k=0}^{B-1} b_k (Q^2)^k + \sum_{l=0}^{C-1} c_l (Q^2)^l \,. \tag{4.7}$$

Here, the fit parameters are b_k and c_l. Since this function is only needed to interpolate the numerous data points we have in the high Q^2 region in a finite interval, it is not necessary

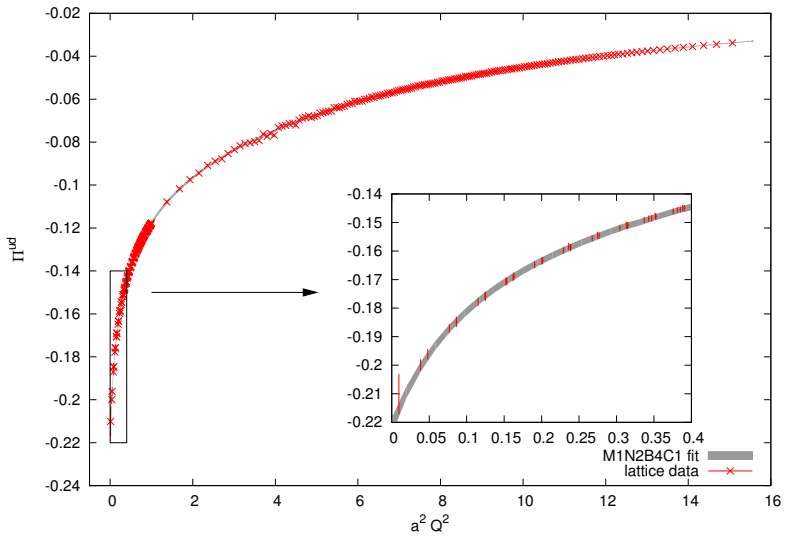

Figure 4.2.: Unsubtracted vacuum polarisation function of the light quarks $\Pi^{\mathrm{ud}}(Q^2)$ for ensemble B25.32t (see table 4.1 for details). For better readability the lattice data has been thinned out.

to use the available perturbative expressions. In this way, we arrive at pure lattice results without external input.

The total vacuum polarisation function for each flavour is then obtained from

$$\Pi^f(Q^2) = (1 - \Theta(Q^2 - Q^2_{\mathrm{match}}))\Pi^f_{\mathrm{low}}(Q^2) + \Theta(Q^2 - Q^2_{\mathrm{match}})\Pi^f_{\mathrm{high}}(Q^2) \tag{4.8}$$

with $\Theta(Q^2)$ denoting the Heaviside step function. For the matching of low and high momentum fit functions, we have chosen $Q^2_{\mathrm{match}} = 2$ GeV^2 since in this region both model functions $\Pi^f_{\mathrm{low}}(Q^2)$ as well as $\Pi^f_{\mathrm{high}}(Q^2)$ describe the lattice data very well. We would like to stress that similarly to Padé approximants, which will be introduced in Sect. 4.2.1, the description of the data can be systematically improved by including more terms, especially more dipole terms, in the fit function once more precise data becomes available.

For the light and the strange quark contributions to $\Pi(Q)$, our standard fit for the $N_f = 2 + 1 + 1$ ensembles is characterised by $M = 1$, $N = 2$, $B = 4$, and $C = 1$. An example fit for the vacuum polarisation for one of our lightest pion masses (B25.32t in table 4.1) is shown in Fig. 4.2. Since we have for the physical point ensemble more than three times the statistics than for the typical four-flavour ensembles we have in contrast chosen $N = 3$ in the standard fit for the new ensemble. The curvature of the vacuum polarisation function for the charm quark contribution is much smaller such that more parameters are needed in the high-momentum domain in order to ensure smooth contact between the fit functions in the low and high momentum regions. Thus, we employ for the charm quark contribution $M = 1$, $N = 2$, $B = 3$, and $C = 5$ in our standard fit.

To minimise finite-size effects, we have excluded the points with the lowest lattice momentum in the vacuum polarisation fits which due to the comparatively big uncertainty of these points has only a very mild influence on the fits. This has been suggested by a tree-level study showing that except for the lowest momentum point all other data points for different volumes fall on top of each other, cf. [Petschlies 2013].

4.1.3. Results for spectral properties of vector mesons

Since Eq. (4.6) involves the masses and decay constants of the vector meson states and since the ρ-meson mass will also be needed for the chiral extrapolations of the analysed observables as will be described in subsequent chapters, we determine these basic quantities from the same vector-vector current correlators, i.e. using the vector currents as interpolating operators for the vector mesons. Employing the same bootstrap samples as in the vacuum polarisation fits, the uncertainties of the determination of the vector meson properties can be correctly propagated to $\Pi(Q^2)$ and later on to the physical observables.

In principle, the vector mesons should be treated as resonances, since they can decay when the fermions are included dynamically in the lattice QCD simulations. Computationally demanding methods for a rigorous treatment exist [Lüscher 1986a, Lüscher 1986b] and have been successfully applied [Feng et al. 2011b, Dudek et al. 2013]. However, due to angular momentum conservation the decay products, two pions in the case of the ρ-meson, can only be produced if the kinematical condition $m_{\mathrm{V}} \geq 2\sqrt{m_{\mathrm{PS}}^2 + \vec{p}^2}$ is satisfied with $\vec{p} \neq 0$. Since on the lattice with finite spatial extent L, the momenta are quantised, the above condition becomes

$$m_{\mathrm{V}} \geq 2\sqrt{m_{\mathrm{PS}}^2 + \left(\frac{2\pi}{L}\right)^2} \,. \tag{4.9}$$

This condition is not fulfilled for all but one of the 4-flavour ensembles (D15.48 of table 4.1) where the vector meson mass m_{V} and the energy of the 2-pion state with non-zero momentum become consistent within errors. We nevertheless treat the lightest vector meson as a stable asymptotic state for all ensembles [1] and obtain the spectral information from the large-time behaviour of the correlator projected to zero momentum in order to utilise it in the vacuum polarisation fits. However, this is obviously no longer justified for the ensemble at the physical point. Therefore, we have additionally performed Padé fits which will be introduced in Sect. 4.2.1 below for which the spectral properties of the vector mesons are not needed. For the $N_f = 2 + 1 + 1$ ensembles for which our standard procedure is applicable we consider the determination of the vector meson properties as a first test of the validity of our data.

Besides the masses, m_V, the vector meson states $|V, \vec{p}, \epsilon\rangle$, where ϵ denotes their polarisations, are characterised by their couplings $g_{V,\mathrm{em}}$ to the electromagnetic vector current j_μ^{em} known from Eq. (3.2) and their decay constants f_V which are determined with respect to the isospin currents defined similarly to Eq. (3.31) as we will see shortly. For the vector mesons relevant for this work, the experimental values are tabulated in Tab. 4.4.

The defining relation for the electromagnetic coupling constants $g_{V,\mathrm{em}}$ reads

$$\langle 0|j_\mu^{\mathrm{em}}(0)|V, \vec{p}, \epsilon\rangle = m_V^2 \, g_{V,\mathrm{em}} \, \epsilon_\mu(\vec{p}) \,, \tag{4.10}$$

where $\epsilon_\mu(\vec{p})$ denotes the boosted polarisation of the vector meson and $\vec{p} \neq 0$ its spatial momentum. The electromagnetic coupling can be inferred from the experimental values for the partial leptonic decay widths $\Gamma(V \to l^+ l^-)$ with $l = e \,\mathrm{or}\, \mu$ collected in [PDG 2014]

[1] We do not expect a significant effect of taking the resonance mass or the correlator mass in our analysis, since in the 2-flavour case a comparison between [Feng et al. 2011b] and [Feng et al. 2011a] gave consistent results.

V	m_V [MeV]	$\Gamma(V \to e^+e^-)$ [MeV]	$g_{V,\mathrm{em}}$	f_V [MeV]
ρ	775.26(25)	0.00704(6)	0.20177(86)	221.2(0.9)
ω	782.65(12)	0.00060(2)	0.05862(98)	194.6(3.2)
Φ	1019.46(02)	0.00126(2)	0.07443(59)	227.7(1.8)
J/Ψ	3096.916(11)	0.00555(14)	0.0896(11)	416.4(5.3)

Table 4.4.: Masses of vector mesons, their partial decay widths [PDG 2014] and electromagnetic coupling constants as well as decay constants computed from the decay widths.

according to [Dumbrajs et al. 1983]

$$\Gamma(V \to l^+l^-) = \frac{4\pi}{3}\,\alpha^2\, g_{V,\mathrm{em}}^2\, m_V\, \left(1 + \frac{2m_l^2}{m_V^2}\right)\sqrt{1 - \frac{4m_l^2}{m_V^2}} \tag{4.11}$$

by substituting the appropriate vector meson mass m_V and lepton mass m_l.

Alternatively, the vector meson couplings are often expressed as dimensionful decay constants in a basis of isospin currents

$$J_\mu^{I=0} = \frac{1}{\sqrt{2}}(\bar{u}\gamma_\mu u + \bar{d}\gamma_\mu d),\ J_\mu^{I=1} = \frac{1}{\sqrt{2}}(\bar{u}\gamma_\mu u - \bar{d}\gamma_\mu d),\ J_\mu^s = -\frac{1}{3}\bar{s}\gamma_\mu s,\ J_\mu^c = \frac{2}{3}\bar{c}\gamma_\mu c\,. \tag{4.12}$$

Employing those currents, the decay constants f_V are defined by

$$\langle 0|J_\mu^I(0)|V,\vec{p},\epsilon\rangle = m_V f_V \epsilon_\mu(\vec{p})\,. \tag{4.13}$$

Comparing Eqs. (4.10) and (4.13), we see that we can simply define an isospin coupling constant by $g_V = \frac{f_V}{m_V}$. The decay constants for the vector mesons are obtained by decomposing the four-flavour electromagnetic vector current in terms of the isospin currents

$$j_\mu^{\mathrm{em}} = \frac{1}{3\sqrt{2}}J_\mu^{I=0} + \frac{1}{\sqrt{2}}J_\mu^{I=1} - \frac{1}{3}J_\mu^s + \frac{2}{3}J_\mu^c \tag{4.14}$$

and associating the corresponding mesons with the isospin currents, $J_\mu^{I=0} \to \omega$, $J_\mu^{I=1} \to \rho$, $J_\mu^s \to \Phi$, and $J_\mu^c \to J/\Psi$. Note, that we treat the Φ-meson as pure $\bar{s}s$ state despite its mixing with the ω. In this situation the decay constants of the three light vector mesons in Tab. 4.4 roughly agree as expected from $SU(3)$ chiral perturbation theory.

Following the analysis described in [Jansen et al. 2009], the time-dependent vector meson correlator at vanishing spatial momentum is constructed from the diagonal spatial elements of the hadronic vacuum polarsation tensor and we adopt the following fit function for the lattice data at large time separations

$$\begin{aligned} C(t) &= \sum_{\vec{x}}\sum_{k=1}^{3}\langle J_k^C(t,\vec{x})J_k^C(0)\rangle \\ &\xrightarrow{t\to\infty} 3m_V f_V^2 e^{-m_V\frac{T}{2}}\cosh\left(\left(\frac{T}{2}-t\right)m_V\right) \end{aligned} \tag{4.15}$$

for our correlated fits to extract m_V and f_V from it. The factor three arises from the polarisation sum of the vector meson. Likewise fits including $M-1$ excited state contributions are performed with

$$C(t;M) = \sum_{i=1}^{M} 3 m_i f_i^2 e^{-m_i \frac{T}{2}} \cosh\left(\left(\frac{T}{2} - t\right) m_i\right) \tag{4.16}$$

in an appropriate fit range. The statistical uncertainties of the fit parameters are estimated using the bootstrap method. When neglecting the disconnected contributions in the light-quark sector, the interpolating operators in Eqs. (4.15) and (4.16) are the same for the ρ^0 and the ω such that their masses and decay constants are indistinguishable at the current level of precision.

For single-state fits, the initial timeslice of the fit should be large enough such that the first excited state is sufficiently suppressed. The final fitting timeslice should be small enough to avoid the noisiest part of the correlator which, as mentioned before, is obtained from simple point sources in our calculation. Taking those restrictions into account we have selected fixed time ranges in physical units for the single-state fits by requiring the mean χ^2/dof for all the ensembles to be close to 1. To fit the ρ-meson properties our standard fit range is $0.7\,\text{fm} < t < 1.2\,\text{fm}$. For the $\bar{s}s$-state we have chosen $0.9\,\text{fm} < t < 1.4\,\text{fm}$ and for the J/Ψ fits $1.2\,\text{fm} < t < 1.7\,\text{fm}$. For fits with $M = 2$ done to check systematic effects of choosing a MNBC fit function, we have used $0.3\,\text{fm} < t < 1.2\,\text{fm}$ in the light sector, $0.35\,\text{fm} < t < 1.4\,\text{fm}$ in the strange sector, and $0.4\,\text{fm} < t < 1.7\,\text{fm}$ in the charm sector. We include the systematic effect of choosing different intervals for fitting the vector meson properties in our total error budgets for the investigated electroweak observables.

In tables E.1 and E.2 in appendix E, we list the results for m_V and f_V obtained with single-state fits in our standard fit ranges for all the ensembles. The data for the light vector meson mass is shown in the left panel of Fig. 4.3. From this, we see that some curvature is needed in the chiral extrapolation in order to arrive at the experimental value of the ρ-meson mass. This is indicated by the broken line obtained from a cubic fit in the squared pion mass, which has been constrained to reproduce the correct experimental result. The same is true for the decay constant $f_V = m_V\, g_V$. This behaviour has been observed before [Jansen et al. 2009, Feng et al. 2011b] and a strong curvature in the vicinity of the physical point is expected. In contrast, the data for the dimensionless isospin coupling constant g_V depicted in the right panel of Fig. 4.3 exhibit a linear pion mass dependence and are thus easily extrapolated to the physical point yielding a value compatible with the experimental one

$$g_V = 0.2862(34) \quad \text{this work} \tag{4.17}$$

$$g_V = 0.2853(12) \quad \text{experiment}\,, \tag{4.18}$$

where the experimental value is $g_V = \sqrt{2} g_{V,\text{em}}$ displayed in Tab. 4.4. Only lattice artefacts negligible compared to the statistical uncertainty could be detected by using an additional a^2-term in the fit function.

Verifying the results for the spectral properties of the strange quark vector meson obtained in our lattice calculation is impeded by the fact that due to $SU(3)_f$ breaking caused by the mass difference of the light and the strange quark masses there is no pure $\bar{s}s$-vector meson in nature. In fact, the Φ-meson mixes with the ω-meson, i.e. the ω also receives

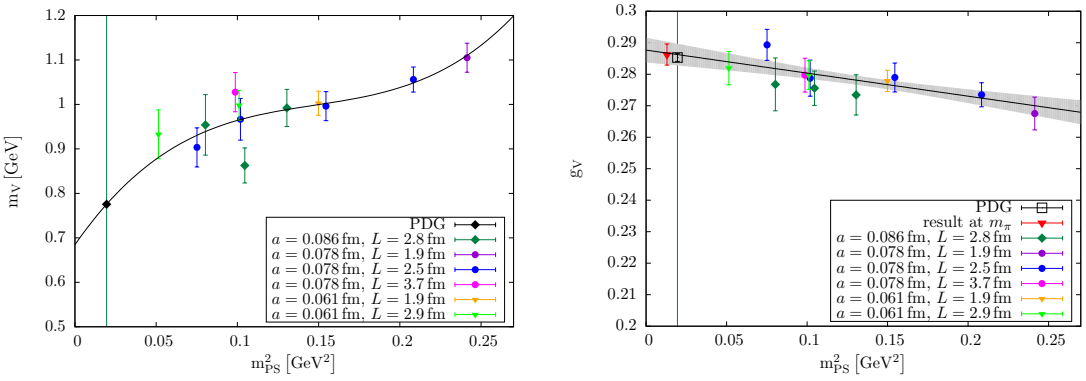

Figure 4.3.: Mass (left) and isospin coupling (right) of the ρ-vector meson as a function of the squared pion mass. The lattice result for the coupling constant at the physical pion mass is depicted as the red inverted triangle which has been displaced to the left to facilitate the comparison with the experimental value represented by the black square.

a small $\bar{s}\gamma_\mu s$ contribution resulting in a slightly larger mass than the ρ as can be seen in Tab. 4.4 and the Φ-meson also features a light quark admixture which makes it lighter than a pure $\bar{s}s$-vector meson would be. In fact, a mass difference is observed when comparing our lattice results for the mass of a pure $\bar{s}s$-state with the experimental values for the Φ-meson [PDG 2014] in the left panel of Fig. 4.4. The final value for the $\bar{s}s$-mass

$$m_{\bar{s}s} = 1.108(22)\,\text{GeV} \tag{4.19}$$

has been obtained from a combined chiral and continuum extrapolation according to

$$m_{\bar{s}s}(m_{\text{PS}}, a) = A + B\ m_{PS}^2 + C\ a^2 \tag{4.20}$$

with A, B, C denoting the free parameters of the fit. However, also a mistuning of the strange quark mass could contribute to the difference observed for the mass of the strange vector meson. What we can exclude is a non-linear pion mass dependence as we have found for the ρ above, since even when comparing the isospin coupling $g_{\bar{s}s}$ with the experimental result, we find that our lattice result does not match the measured value for the Φ-meson. This is shown in the right panel of Fig. 4.4. Here, we used a constant fit in the extrapolation, since linear and quadratic fits in the squared pion mass as well as fits including a^2-terms result in parameters which are 0 within the errors. Our result for the isospin coupling constant is

$$g_{\bar{s}s} = 0.2479(17)\ . \tag{4.21}$$

We have refrained from repeating the experimental values for the Φ-meson given in Tab. 4.4, since the Φ is not a pure $\bar{s}s$-state in nature and thus we cannot directly compare our pure $\bar{s}s$ results with those values.

Similarly to the strange quark vector meson, the data obtained for the mass and the decay constant of the J/Ψ meson naturally do not depend on the squared pion mass and are thus easily extrapolated to the physical point. However, due to the large mass of the charm quark, lattice spacing effects are clearly visible, especially for the J/Ψ-mass as shown in the left panel of Fig. 4.5, and thus here also an extrapolation to vanishing lattice

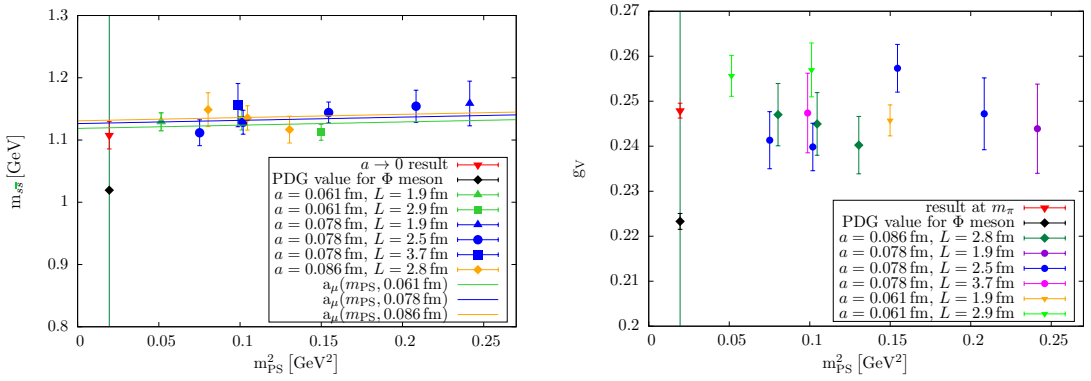

Figure 4.4.: Mass (left) and isospin coupling (right) of the $\bar{s}s$-vector meson as a function of the squared pion mass.

spacing is required in order to arrive at a meaningful comparison with the experimental values. We have applied the same combined chiral and continuum extrapolation as given in Eq. (4.20) simply replacing the $\bar{s}s$ mass by the J/Ψ mass or its decay constant, respectively, and obtained

$$m_{J/\psi} = 3.1001(61)\,\text{GeV} \qquad f_{J/\psi} = 0.4183(93)\,\text{GeV} \qquad \text{this work} \tag{4.22}$$

$$m_{J/\psi} = 3.09692(1)\,\text{GeV} \qquad f_{J/\psi} = 0.4164(53)\,\text{GeV} \qquad \text{experiment}\,, \tag{4.23}$$

where the experimental values are those from Tab. 4.4. The lattice QCD results fully agree with the experimental values and are depicted in Fig. 4.5.

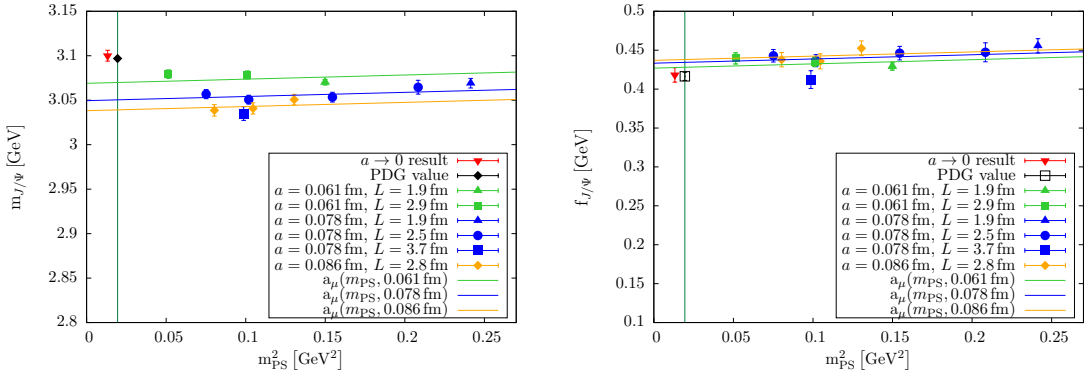

Figure 4.5.: Mass and electromagnetic coupling of the J/Ψ-vector meson as a function of the squared pion mass. The lattice results at the physical pion mass in the continuum limit are depicted as the red inverted triangles which have been displaced to the left to facilitate the comparison with the experimental values represented by the black squares.

4.2. Alternative approaches

In the following, we want to outline two alternative approaches for treating the lattice data obtained for the hadronic vacuum polarisation function. The first one, which consists in

fitting the data by using Padé approximants, is mathematically well-motivated and can actually be shown to be equivalent to our standard procedure up to lattice artefacts. The second possibility involves analytically continuing the data obtained for spacelike momenta into the timelike region. The corresponding section 4.2.2 is based on our publications [Feng et al. 2013, Jansen et al. 2014] in which we have developed this method.

4.2.1. Padé approximants

In [Aubin et al. 2012, Golterman et al. 2013] the usage of Padé approximants to fit the hadronic vacuum polarisation function has been advocated in order to avoid systematic errors related to the choice of fit function. In principle, this can be achieved by expressing $\Pi(Q^2)$ in terms of a Stieltjes function $\Phi(Q^2)$ using the once-subtracted dispersion relation from Eq. (3.6)

$$\Pi(Q^2) = \Pi(0) - Q^2\Phi(Q^2) \tag{4.24}$$

$$\Phi(Q^2) = \int_{4m_\pi^2}^{\infty} ds \frac{\rho(s)}{s(s+Q^2)} \,, \tag{4.25}$$

where $\rho(s)$ is the spectral function which is proportional to the cross-section ratio that we have encountered in Sect. 3.1. Such a Stieltjes function can be constructed by a convergent series of other Stieltjes functions [Baker 1969] which in turn can then be rationally approximated by Padé approximants of the form

$$R_M^N(Q^2) = \frac{\sum_{n=0}^{N} a_n Q^{2n}}{\sum_{n=0}^{M-1} b_n Q^{2n} + Q^{2M}} \,. \tag{4.26}$$

Since $\Phi(Q^2)$ is an analytic function except for $Q^2 < 0$, all poles have to be on the negative real axis such that the types of Padé fits that can adequately approximate this function are further restricted. One possibility are rational functions of the form [Barnsley 1973]

$$\Phi(Q^2) \approx R_{\lfloor P/2 \rfloor}^{\lfloor (P-1)/2 \rfloor}(Q^2) = a_0 + \sum_{n=1}^{\lfloor P/2 \rfloor} \frac{a_n}{b_n + Q^2} \tag{4.27}$$

with $a_0 = 0$ for even P and

$$\begin{aligned} a_n > 0, \qquad & n \in 1, \ldots, \lfloor P/2 \rfloor, \\ b_{\lfloor P/2 \rfloor} > b_{\lfloor P/2 \rfloor - 1} > \cdots > b_1 \geq 0 \,. & \end{aligned} \tag{4.28}$$

Here, $\lfloor x \rfloor$ denotes the floor function, i.e. the integer less or equal to x, and P counts the number of discrete Q^2 points. If the values of $\Phi(Q_i^2)$ for $i \in 1, \ldots, P$ are known exactly, then the series in Eq. (4.27) converges uniformly to the correct result as the number of points is increased, $P \to \infty$, on any closed and bounded domain in the complex Q^2-plane excluding the branch cut.

Therefore, the authors of [Aubin et al. 2012] suggest to fit the values for the hadronic vacuum polarisation function at discrete lattice momenta with

$$\Pi(Q^2) = \Pi(0) - Q^2 \left(a_0 + \sum_{n=1}^{N} \frac{a_n}{b_n + Q^2} \right) \,, \tag{4.29}$$

where $\Pi(0)$ as well as the a_n and b_n constitute the parameters of the fit. The nomenclature is such that when a_0 is taken to be $a_0 = 0$ the result is an $[N-1, N]$ Padé approximant whereas also fitting a_0 results in a $[N, N]$ Padé fit. The idea is to successively obtain better approximations to the true value of the vacuum polarisation by increasing N, the number of terms in the sum.

However, there are several practical limitations. First of all, the lattice data are not exact at the discrete Q^2 points such that an exact multipoint Padé approximation as given in Eq. (4.27) cannot be constructed. Secondly, the number of dipole terms N that can actually be fitted with realistic lattice data is currently limited to at most three, which is far below half of the typical number of lattice momenta available $\left\lfloor \frac{P}{2} \right\rfloor$ that would be needed according to Eq. (4.27). Conversely, the number of lattice points to be fitted could be decreased but then fitting e.g. four data points with a [1,2] Padé fit would involve five free parameters. Hence, we have observed that Padé approximants can only be applied in a very small momentum region. This finding is in accordance with investigations of [Golterman et al. 2014] in which it has been suggested to use Padé approximants only up to $Q^2 \leq 0.1\,\mathrm{GeV}^2$ where we unfortunately do not have a single data point for some of the ensembles. Recently, the RBC-UKQCD also reported problems in determining the maximum Q^2 up to which to fit the hadronic vacuum polarisation function and the corresponding degree N of the Padé approximants to use for it [Marinkovic et al. 2015].

Comparing Eq. (4.29) and Eq. (4.6) we see that the main difference between Padé fits and our standard procedure in the low-momentum region is whether the parameters in the pole terms are treated as free fit parameters in the vacuum polarisation fit or are determined before from the temporal correlator. Another difference is that our MN fits can accommodate differences from the dipole fits beyond the linear term in Q^2. However, as we have stated above, our standard fits on the four-flavour ensembles also feature only a linear term in Q^2 such that only the difference in the determination of the a_n and b_n in Eq. (4.29) remains. It has already been shown in Ref. [Boyle et al. 2012] that leaving the b_n as free parameters results in compatible values as obtained for the masses from the temporal correlator. The reason is that Fourier transforming the correlator in Eq. (4.16) and neglecting terms $\mathcal{O}\left(e^{-m_i T/2}\right)$ when letting $a \to 0$ leads to the pole structure of Eq. (4.29) with a_n replaced by the squared decay constants f_V and b_n replaced by the squared masses of the vector meson states, m_V. Various tests have shown that determining a_n, $n > 1$, and b_n as f_V^2 and m_V^2 from the temporal correlator leads to a weaker dependence of the results for the remaining fit parameters, a_0 and $\Pi(0)$, on the upper limit of the fit interval such that we prefer to employ the procedure introduced in Sect. 4.1. Nevertheless, performing Padé fits provides valuable cross-checks of our standard procedure, especially for the ensemble at the physical point, for which our standard approach might not be applicable due to the unstable ρ-meson. Furthermore, once data on much larger lattices with drastically reduced statistical uncertainties can be produced, Padé approximants will become beneficial due to their solid mathematical foundation.

4.2.2. Analytic continuation

As we have seen above, in our standard lattice calculation the hadronic vacuum polarisation function is determined at discrete spacelike momenta by performing a Fourier transform of the Euclidean vector-vector current correlation function. However, this computation suffers from a generic difficulty, namely, that low momenta are not directly accessible. Accessing the hadronic vacuum polarisation function at zero momentum is, however, nec-

essary for obtaining its renormalised value. To address this problem, efforts to approach the low momentum region by using partially twisted boundary conditions have been undertaken [Della Morte et al. 2012]. A new approach to directly obtain the zero momentum contribution has been discussed in Ref. [De Divitiis et al. 2012] where it was suggested to calculate the derivative of the relevant correlation function by using the sequential source propagator method. Very recently, another very promising method for computing the hadronic vacuum polarisation function in the low-momentum region relying on the determination of magnetic susceptibilities has been proposed [Bali and Endrődi 2015].

In this subsection, we present an alternative approach that enables us to compute the hadronic vacuum polarisation function for continuous momenta, both in the spacelike and timelike regions. Following the ideas of [Ji and Jung 2001], this is achieved by starting with the Euclidean vector-vector correlation function and performing a Fourier transform only in the spatial directions and an integration (in practice, a summation) in the time direction with a factor of $e^{\omega t}$. In this way, we are able to calculate the hadronic vacuum polarisation function at very small spacelike momenta, covering also the zero momentum value and even extending the calculation into the timelike region. Below, we reproduce only the derivation using temporal moments from our article [Feng et al. 2013] to show that this leads to a proper evaluation of the hadronic vacuum polarisation function. Ref. [Feng et al. 2013] comprises additionally a demonstration using the photon-vector current transition amplitude, a classification of the correlators, and results from $N_f = 2$ twisted mass fermions at unphysically high pion masses.

The advantage of this approach is that assumptions on the analytic form used to describe the hadronic vacuum polarisation function can be avoided. However, as we will see below, it currently does not lead to an increased precision in the calculation of the HVP function. Nevertheless, the approach has already been proven to be advantageous for the computation of other observables like the isovector magnetic form factor of the nucleon [Alexandrou et al. 2014] and it will clearly be beneficial for the computation of electroweak parameter shifts once larger lattices are available since finite size effects currently are the source of largest uncertainty of this method.

Alternative method

By modifying

$$\Pi(Q^2)(Q_\mu Q_\nu - \delta_{\mu\nu} Q^2) = e^2 \int d^4x \; e^{i\,Q\,x} \; \langle 0|T\{J_\mu(x) J_\nu(0)\}|0\rangle \; , \tag{4.30}$$

we propose to calculate the hadronic vacuum polarisation function by using a complex temporal momentum component. Hence, we effectively perform a Fourier transform only in the spatial directions but integrate in the time direction with a factor of $e^{\omega t}$,

$$\bar{\Pi}(K^2)(K_\mu K_\nu - \delta_{\mu\nu} K^2) = e^2 \int dt \; e^{\omega t} \int d^3\vec{x} \; e^{i\vec{k}\vec{x}} \; \langle 0|T\{J_\mu(t,\vec{x}) J_\nu(0,\vec{0})\}|0\rangle \; . \tag{4.31}$$

In Eq. (4.31), the momentum K is given by $K = (-i\omega, \vec{k})$, with $\vec{k}$ the spatial momentum and ω the photon energy which can be viewed as a free input parameter. By varying ω, we can achieve values for $K^2 = -\omega^2 + \vec{k}^2$ that enter both the spacelike and timelike momentum regions. In particular, using Eq. (4.31) we can compute $\bar{\Pi}(K^2)$ at zero momentum without

any extrapolation. A very important restriction is that the energy ω must satisfy

$$-K^2 = \omega^2 - \vec{k}^2 < m_V^2 \ , \quad \text{or} \quad \omega < E_V \ , \tag{4.32}$$

where E_V is the energy of the lowest state in the vector channel and m_V is the corresponding invariant mass. Restricting the values of ω in this way, a mixing between the photon state and the hadronic states is avoided. Furthermore, the divergence caused by $e^{\omega t}$ at infinitely large t is eliminated by a suppression factor $e^{-E_V t}$ arising from the asymptotic time dependence of the temporal correlator Eq. (4.15) thus rendering the integral of Eq. (4.31) convergent. In the following subsection, we will demonstrate that Eq. (4.31) is the analytic continuation of Eq. (3.3) from Minkowski space-time to Euclidean space-time, and therefore $\bar{\Pi}(K^2)$ defined in Eq. (4.31) can be used directly to compute the hadronic vacuum polarisation function as well as physical quantities derived thereof.

Demonstration from temporal moments

Here, we demonstrate the validity of Eq. (4.31) by a Taylor expansion and the introduction of temporal moments. This technique has previously been employed for lattice [HPQCD 2008] and perturbative calculations [Kühn et al. 2007, Chetyrkin et al. 2012]. In Ref. [Bernecker and Meyer 2011] it has been proposed to also use it for the calculation of the hadronic vacuum polarisation function. Further details can also be found in [Petschlies 2013].

We write Eq. (4.30) as follows:

$$\begin{aligned} \Pi(Q^2)F_{\mu\nu}(Q) &= e^2 \int dt\, e^{iQ_t t} \int d^3\vec{x}\, e^{i\vec{q}\vec{x}} \, \langle J_\mu(t,\vec{x}) J_\nu(0,\vec{0})\rangle \ , \\ &= e^2 \int dt\, e^{iQ_t t}\, C_{\mu\nu}(t,\vec{q}) \ , \end{aligned} \tag{4.33}$$

where $F_{\mu\nu}(Q) = Q_\mu Q_\nu - \delta_{\mu\nu} Q^2$ is the Lorentz factor.

The temporal moments of the correlation function $C_{\mu\nu}(t,\vec{q})$ are defined as

$$\begin{aligned} G^{\vec{q}}_{n,\mu\nu} &\equiv \frac{(i)^n}{n!} \int dt\, t^n\, C_{\mu\nu}(t,\vec{q}) \\ &= \frac{1}{n!} \frac{\partial^n [\Pi(Q^2) F_{\mu\nu}(Q)]}{\partial (Q_t)^n}\bigg|_{Q_t=0} \\ &= \begin{cases} M^{\vec{q}}_m F_{\mu\nu}(Q)\Big|_{Q_t=0} + \frac{1}{2} M^{\vec{q}}_{m-1} \frac{\partial^2 F_{\mu\nu}(Q)}{\partial {Q_t}^2}\Big|_{Q_t=0} \ , & \text{for } n = 2m, \\ M^{\vec{q}}_m \frac{\partial F_{\mu\nu}(Q)}{\partial Q_t}\Big|_{Q_t=0} \ , & \text{for } n = 2m+1, \end{cases} \end{aligned} \tag{4.34}$$

where m is an integer and the coefficients $M^{\vec{q}}_m$ are given by

$$M^{\vec{q}}_m = \frac{1}{m!} \frac{\partial^m \Pi(Q^2)}{\partial (Q_t^2)^m}\bigg|_{Q_t=0} \ . \tag{4.35}$$

Here we have used that odd temporal derivatives of the HVP function vanish since the

correlator is even under time reversal.

According to the definition in Eq. (4.34), the temporal moments $G^{\vec{q}}_{n,\mu\nu}$ are the coefficients in the Taylor expansion of the function $\Pi(Q^2)F_{\mu\nu}(Q)$ at $Q_t = 0$. Using again a once-subtracted dispersion relation and the optical theorem

$$\begin{aligned} \Pi(Q^2) - \Pi(0) &= -\frac{Q^2}{\pi} \int ds \, \frac{\mathrm{Im}[\Pi(s)]}{s(s+Q^2)} \, , \\ \mathrm{Im}[\Pi(s)] &= \frac{e^2 \, R(s)}{12\pi} \, , \quad R(s) \equiv \frac{\sigma(e^+e^- \to \mathrm{hadrons})}{4\pi\alpha(s)^2/(3s)} \, , \end{aligned} \tag{4.36}$$

we can relate $M^{\vec{q}}_m$ to the experimental observables $R(s)$,

$$\begin{aligned} M^{\vec{q}}_{m=0} &= \Pi(0) - \frac{e^2 \, \vec{q}^2}{12\pi^2} \int ds \, \frac{R(s)}{s(s+\vec{q}^2)} \, , \\ M^{\vec{q}}_{m\neq 0} &= (-1)^{m+1} \frac{e^2 \, \vec{q}^2}{12\pi^2} \int ds \, \frac{R(s)}{s(s+\vec{q}^2)^{m+1}} + (-1)^m \frac{e^2}{12\pi^2} \int ds \, \frac{R(s)}{s(s+\vec{q}^2)^m} \, . \end{aligned} \tag{4.37}$$

Note that $M^{\vec{q}}_m$ is suppressed by a factor of $(s+\vec{q}^2)^{-m} \leq (m_V^2 + \vec{q}^2)^{-m} = (E_V^2)^{-m}$ with $E_V \equiv \sqrt{m_V^2 + \vec{q}^2}$ the lowest energy level in the vector channel; see the previous subsection. We can construct a convergent series by

$$S^{\vec{q}}(\omega^2) = \sum_m M^{\vec{q}}_m (-\omega^2)^m \, , \quad \text{if } \omega^2 < m_V^2 + \vec{q}^2 \ \ (\omega < E_V) \, . \tag{4.38}$$

Putting Eq. (4.37) into the series and using $\Pi(0) = \Pi^M(0)$, with Π^M denoting the hadronic vacuum polarisation function in Minkowski space, we find that $S^{\vec{q}}(\omega^2)$ satisfies the dispersion relation

$$S^{\vec{q}}(\omega^2) - \Pi^M(0) = \frac{e^2 \, (\omega^2 - \vec{q}^2)}{12\pi^2} \int ds \, \frac{R(s)}{s \, (s - (\omega^2 - \vec{q}^2))} \, , \tag{4.39}$$

which indicates that $S^{\vec{q}}(\omega^2)$ is equivalent to $\Pi^M(q^2)$ at $q^2 = \omega^2 - \vec{q}^2$.

On the other hand, we can construct another series through

$$\begin{aligned} S^{\vec{k}}_{\mu\nu}(\omega) &= \sum_n G^{\vec{k}}_{n,\mu\nu} (-i\omega)^n \\ &= S^{\vec{k}}(\omega^2) \left(F_{\mu\nu}(K)\Big|_{K_t=0} + (-i\omega) \frac{\partial F_{\mu\nu}(K)}{\partial K_t}\Big|_{K_t=0} + \frac{(-i\omega)^2}{2} \frac{\partial^2 F_{\mu\nu}(K)}{\partial (K_t)^2}\Big|_{K_t=0} \right) \\ &= \Pi^M(k^2)\Big|_{k=(\omega,\vec{k})} (K_\mu K_\nu - \delta_{\mu\nu} K^2)\Big|_{K=(-i\omega,\vec{k})} \, . \end{aligned} \tag{4.40}$$

$S^{\vec{k}}_{\mu\nu}(\omega)$ is nothing but $\bar{\Pi}(K^2)(K_\mu K_\nu - \delta_{\mu\nu} K^2)$ as given in Eq. (4.31). We thus have demonstrated the equivalence between $\bar{\Pi}(K^2)$ and $\Pi^M(q^2)$ using temporal moments of the Euclidean vector correlation function.

In the special case $\vec{k} = \vec{0}$ and $\mu = \nu = z$, we have

$$G^{\vec{0}}_{0,zz} = 0 \ , \quad G^{\vec{0}}_{2m+1,zz} = 0 \ , \quad G^{\vec{0}}_{2m+2,zz} = \frac{1}{2} M^{\vec{0}}_m \neq 0 \ . \tag{4.41}$$

The hadronic vacuum polarisation function can then be constructed by

$$\begin{aligned} \bar{\Pi}(-\omega^2) &= -\frac{1}{\omega^2} \sum_m G^{\vec{0}}_{2m+2,zz} (-i\omega)^{2m+2} = -\int dt \ \frac{e^{\omega t} - 1}{\omega^2} C_{zz}(\vec{0}, t) \ , \\ \bar{\Pi}(-\omega^2) - \bar{\Pi}(0) &= -\int dt \ \left[\frac{e^{\omega t} - 1}{\omega^2} - \frac{t^2}{2} \right] C_{zz}(\vec{0}, t) \ . \end{aligned} \tag{4.42}$$

Eq. (4.42) is the analytic continuation of the formula

$$\Pi(K_t^2) - \Pi(0) = \int dt \ \left[\frac{e^{iK_t t} - 1}{K_t^2} + \frac{t^2}{2} \right] C_{zz}(\vec{0}, t) \tag{4.43}$$

given in Ref. [Bernecker and Meyer 2011].

Computation of $\bar{\Pi}(K^2)$

The analytic continuation method described in the previous subsections has been successfully applied in lattice QCD calculations of pion and charmonium radiative decay [Feng et al. 2012a, Dudek and Edwards 2006]. Below, we present the first lattice calculation of the hadronic vacuum polarisation function using this technique.

On a finite lattice, Eq. (4.31) takes the form

$$\begin{aligned} &\bar{\Pi}(K^2; t_{\max}) \left(K_\mu K_\nu - \delta_{\mu\nu} K^2 \right) = \bar{\Pi}_{\mu\nu}(\omega, \vec{k}; t_{\max}) \ , \\ &\bar{\Pi}_{\mu\nu}(\omega, \vec{k}; t_{\max}) = \sum_{t=-t_{\max}}^{t_{\max} - a(\delta_{t,\mu} - \delta_{t,\nu})} e^{\omega(t + a(\delta_{t,\mu} - \delta_{t,\nu})/2)} C_{\mu\nu}(t, \vec{k}) \ , \end{aligned} \tag{4.44}$$

where $K = (i\hat{\omega}, \hat{k}_1, \hat{k}_2, \hat{k}_3)$, with $\hat{k}_i \equiv (2/a) \sin(k_i a/2)$ and $\hat{\omega} \equiv (2/a) \sinh(\omega a/2)$, is the standard lattice definition of four-momentum. The correlator $C_{\mu\nu}(t, \vec{k})$ is defined by

$$C_{\mu\nu}(t, \vec{k}) = \sum_{\vec{x}} e^{-i\vec{k}(\vec{x} + a\hat{\mu}/2 - a\hat{\nu}/2)} \ \langle J^C_\mu(t, \vec{x}) J^C_\nu(0, \vec{0}) \rangle \ , \tag{4.45}$$

with $J^C_\mu(t, \vec{x})$ the point-split conserved vector current introduced in Eq. (3.14). The value of $t_{\max}$ can be taken up to $T/2$, where T is the temporal extent of the lattice.

In Eq. (4.44) we assume that the hadronic vacuum polarisation tensor carries a Lorentz factor $K_\mu K_\nu - \delta_{\mu\nu} K^2$. For some values of ω, we have $K_\mu K_\nu - \delta_{\mu\nu} K^2 = 0$. We denote these special values by ω_0. At $\omega = \omega_0$ and in the large-$t_{\max}$ limit, the hadronic vacuum polarisation tensor $\bar{\Pi}_{\mu\nu}(\vec{k}, \omega; t_{\max})$ is supposed to be consistent with zero up to space-time symmetry breaking effects. In our calculation, we have verified this for each spatial momentum $\vec{k}$ and polarisation direction $\{\mu, \nu\}$. We therefore calculate $\bar{\Pi}(K^2, t_{\max})$ from

$$\bar{\Pi}(K^2; t_{\max}) = \frac{\bar{\Pi}_{\mu\nu}(\omega, \vec{k}; t_{\max}) - \bar{\Pi}_{\mu\nu}(\omega_0, \vec{k}; t_{\max})}{K_\mu K_\nu - \delta_{\mu\nu} K^2} \ . \tag{4.46}$$

Finite-size effects

While Eq. (4.31) requires us to compute an integral in the range from $t = -\infty$ to $t = +\infty$, with a given finite lattice volume we can only perform a summation over t values from $t = -T/2$ to $+T/2$ as shown in Eq. (4.44). Thus, our calculations are contaminated by finite-size effects, which vanish in the limit $T \to \infty$.

It would be desirable to use the complete t range on the lattice. However, in practice the correlator $C_{\mu\nu}(t, \vec{k})$ at $|t|$ close to $T/2$ shows very large fluctuations and often no useful information can be extracted for these large values of $|t|$. Therefore, we define a maximal t value, $t_{\max} = \eta(T/2)$ with $\eta = 3/4$ in the following. Note that, in principle, any value of η would provide a well-defined choice for our method.

Of course, on a finite lattice the above value of η will induce a finite-size effect. This systematic effect is given by

$$\bar{\Pi}(K^2; t > t_{\max})(K_\mu K_\nu - \delta_{\mu\nu} K^2) = \bar{\Pi}_{\mu\nu}(\omega, \vec{k}; t > t_{\max}) \tag{4.47}$$

$$\bar{\Pi}_{\mu\nu}(\omega, \vec{k}; t > t_{\max}) \equiv \left(\sum_{t=t_{\max}+a-a(\delta_{\mu,t}-\delta_{\nu,t})}^{+\infty} + \sum_{t=-\infty}^{-t_{\max}-a} \right) e^{\omega(t+a(\delta_{\mu,t}-\delta_{\nu,t})/2)} C_{\mu\nu}(t, \vec{k}) \; .$$

In order to obtain an estimate of this finite-size effect, we assume that for $t > t_{\max}$, the vector correlator is dominated by the ground state. We believe that this provides a good estimate of the finite-size effects in our calculation for the following reasons: First, for all our ensembles, the contribution given in Eq. (4.47) is already exponentially suppressed and thus contributes only little to the total vacuum polarisation function. Second, even if for $t > t_{\max}$ other states may contribute, they provide only a correction to a correction and thus should not change our conclusions significantly. Note that the situation might change if one uses large ω and makes K^2 approach the hadron production threshold. In this case, the $t > t_{\max}$ contribution becomes dominant. Besides this, both the energy and the amplitude extracted from $C_{\mu\nu}(t, \vec{k})$ are affected by the finite lattice volume. Such effects should be treated properly using the Lellouch−Lüscher method [Lellouch and Lüscher 2001] and Meyer's proposal in Ref. [Meyer 2011], which is, however, beyond the scope of this work.

We evaluate the hadronic vacuum polarisation function only in the region of spacelike or low timelike momenta. Our strategy comprises regarding the values extracted from $\bar{\Pi}(K^2; t_{\max})$ as our results and estimating the finite-size effects by computing the contribution of $\bar{\Pi}(K^2; t > t_{\max})$ given in Eq. (4.47). Doing so it turns out that with our current lattice setup, the finite-size effects are comparable to the statistical error and thus cannot be neglected in our calculation. Of course, the calculation can be systematically improved in the future by using larger volumes and higher statistics.

Results for $\bar{\Pi}(K^2)$

In Fig. 4.6 we show the results obtained for the renormalised vacuum polarisation function procured according to Eq. (4.44) for our $N_f = 2 + 1 + 1$ ensembles. For results obtained on the old $N_f = 2$ with unphysically large pion masses, the interested reader is referred to [Feng et al. 2013]. We have added the $t > t_{\max}$ contribution to the renormalised hadronic vacuum polarisation function $\Pi_R(K^2) = \bar{\Pi}(K^2) - \bar{\Pi}(0)$ and extrapolated it to the physical pion mass using the modified extrapolation method proposed in [Renner et al. 2012] which we introduce in the next chapter. In the timelike region, especially the region

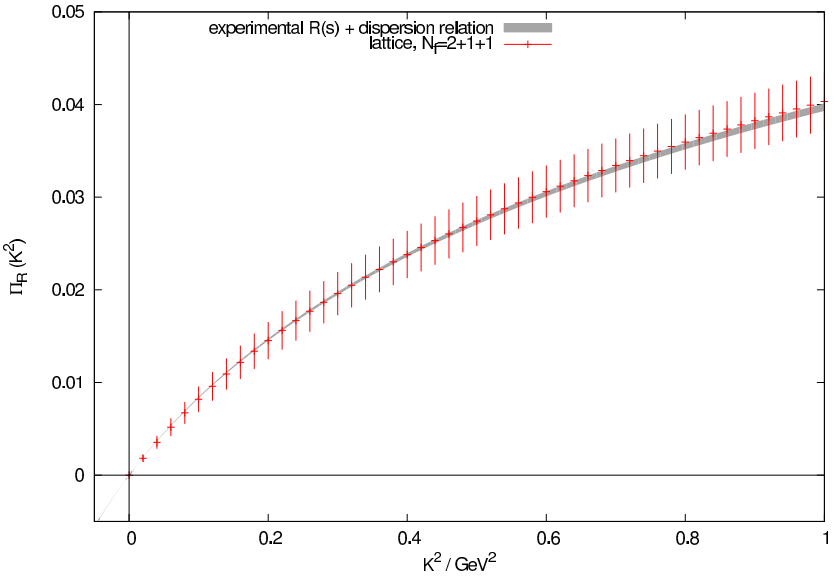

Figure 4.6.: A comparison between $N_f = 2 + 1 + 1$-flavour lattice results for $\Pi_R(K^2)$ calculated using the analytic continuation method proposed in this work and the experimental results compiled using the cross sections $R(s)$ as input together with the dispersion relation [Jegerlehner 2011]. The lattice results are shown by the red sparse error bars and the experimental data are shown by the grey condensed error band.

where K^2 approaches the hadron production threshold, it is very difficult to reproduce $\Pi_R(K^2)$ due to the significant finite-size effects. We have therefore restricted the calculation of $\Pi_R(K^2)$ to the spacelike region. The experimental results for $\Pi_R(K^2)$ are compiled using Jegerlehner's package alphaQED [Jegerlehner 2011], where the dispersion relation is used to relate the experimental data of $R(s)$ (last updated in 2012) to $\Pi_R(K^2)$. As illustrated in Fig. 4.6, the lattice results for $\Pi_R(K^2)$ are consistent with the experimental data but with presently available statistics the corresponding fluctuations are much larger. Nevertheless, the found agreement demonstrates that we can describe the hadronic vacuum polarisation function in the low-momentum region utilising the analytic continuation method. Later we will see that currently our standard procedure results in much smaller overall uncertainties which is the reason for its application. However, the analytical continuation method presented here features the big advantage of avoiding the systematic uncertainty related to the choice of fit function since no fit is involved. Hence, especially for the hadronic contributions to the electroweak coupling constants presented in the next chapter it might soon prove favourable to employ the analytic continuation method when ensembles with larger lattice extents have been generated.

Shortly after our proposal for computing the hadronic vacuum polarisation by analytic continuation had appeared, the Mainz group has suggested a very similar approach which they call mixed or time-momentum representation method [Francis et al. 2013a]. In a follow-up study [Francis et al. 2014a], they have also found completely consistent results for the hadronic vacuum polarisation function when compared to the standard approach and have suggested that both methods provide a means to quantify the systematic effects inherent in the other analysis strategy.

Chapter 5

Leading hadronic contribution to the running of electroweak coupling constants

In the preceding chapters, we have introduced twisted mass lattice QCD, the computational framework of our calculations, as well as their main ingredient, the hadronic vacuum polarisation function, and its definition on the lattice along with a definite procedure to treat the obtained results. Hence, we are now well prepared for the upcoming discussion of the computations of the leading-order hadronic contributions to electroweak precision observables. In this chapter, we cover the electroweak coupling constants whose leading QCD contributions are directly proportional to the vacuum polarisation. The exposition below to a large extent reproduces our recent article [Burger et al. 2015c] but further details have been added like a comparison of the light-quark contributions with the results obtained for the $N_f = 2$ ensemble at the physical point which support the validity of the chiral extrapolation. However, the main point of our analysis is that considering the contributions including the first two generations of quarks as active degrees of freedom enables us for the very first time to unambiguously compare lattice results for the leading QCD contributions to electroweak parameter shifts with those of phenomenological analyses. Naturally, the contributions from heavy flavours become more important the higher the considered momenta. Moreover, it is shown how to compute the leading hadronic contribution to the running of the weak mixing angle and the first lattice QCD computation of this important quantity is performed.

5.1. Overview

As we have indicated in chapter 1, finding hints for new physics beyond the standard model (SM) has been a major objective of particle physics over the past decades. A very promising strategy to detect such effects are high precision experimental measurements which are matched by equally precise theoretical predictions. An important ingredient for the precision attainable in a perturbative calculation is the knowledge of the coupling constants since they enter the quantum loop corrections.

In this chapter, we investigate the leading-order hadronic contributions for two of these couplings, the electromagnetic fine structure constant, α_{QED}, and the $SU(2)_I$ coupling constant, α_2, both related by the weak mixing angle due to electroweak symmetry breaking. An accurate knowledge of these hadronic contributions is mandatory to accomplish sufficiently precise predictions for future high-energy colliders [Jegerlehner 2011] and also the low-energy experiments [Hewett et al. 2012] measuring these observables.

The hadronic contributions to the running of α_{QED} turn out to be only poorly known at the scale of the Z-boson mass. This is reflected in a five orders of magnitude loss of precision when α_{QED} is taken at the Z-scale compared to α_{QED} at zero momentum transfer

turning $\alpha_{\rm QED}(M_Z^2)$ into one of the least determined input parameters of the SM [Hagiwara et al. 2011].

Phenomenologically, the leading-order hadronic contribution to the running of $\alpha_{\rm QED}$ originating from hadronic vacuum polarisation effects, $\Delta\alpha^{\rm hvp}_{\rm QED}$, is determined by using a dispersion relation and experimental e^+e^- scattering data for the hadronic cross-sections [Jegerlehner 2008c, Jegerlehner 2011, Hagiwara et al. 2011] along the lines of Sect. 3.1. Although new data has recently become available, the present analysis does not lead to a sufficient improvement of the error which would be needed for the requirements of future collider experiments [Hagiwara et al. 2011].

In principle, lattice QCD calculations constitute an ideal tool to determine the low-energy hadronic contributions to electroweak observables from first principles. However, presently the precision that can be achieved by lattice QCD computations is usually still lower than that of the phenomenological analyses. Nevertheless, the steady progress which is taking place in lattice QCD calculations promises to make it an expedient alternative to the phenomenological results in the future. In fact, as we will demonstrate below, even with our present simulations the statistical uncertainty is already close to the phenomenological error of $\alpha_{\rm QED}$ and the weak mixing angle.

The leading QCD contribution $\Delta\alpha^{\rm hvp}_{\rm QED}$ has first been investigated on the lattice for two dynamical twisted mass fermions [Renner et al. 2012]. Preliminary results incorporating also dynamical strange and charm quarks for one selected momentum value have been reported in [Feng et al. 2012b]. Another determination of $\Delta\alpha^{\rm hvp}_{\rm QED}$ employing two dynamical light and two quenched heavy clover-improved Wilson fermions has been performed in [Francis et al. 2014c] following the approach suggested in [Jegerlehner 2008c].

Here, we present our results obtained on the $N_f = 2+1+1$ ensembles which have been detailed in Sect. 4.1.1. We include estimates of the systematic uncertainties originating from the continuum limit, from the extrapolation to the physical point as well as from vector meson fit ranges, and the choice of fit functions for energies ranging from 0 to $10\,\mathrm{GeV}^2$. At higher energies perturbative QCD can be applied and is expected to yield more precise determinations of QCD contributions to electroweak parameter shifts.

In contrast to $\Delta\alpha^{\rm hvp}_{\rm QED}$, the hadronic contributions to the running of the weak mixing angle, θ_W, have not been studied on the lattice so far. This calculation is potentially even more important than the one for $\alpha_{\rm QED}$ since the phenomenological determination at low energies cannot solely be based on data but also requires several assumptions to perform at least a partial flavour separation of the cross-section data [Jegerlehner 1986a] which, in contrast to the continuum case, is straightforward on the lattice.

As we will demonstrate in Sect. 5.3, lattice calculations can actually provide a first-principle evaluation of the weak mixing angle in the low-momentum region, where several measurements exist [Wood et al. 1997, SLAC E158 2005, PVDIS 2014, Qweak 2014]. In addition, due to the great potential of such low-energy measurements for unveiling the nature of physics beyond the SM, there are also newly planned or currently constructed experimental facilities [MOLLER 2014, SoLID 2014, Becker et al. 2013], see also [Kumar et al. 2013, PDG 2014] for a recent review.

5.2. The fine structure constant $\alpha_{\rm QED}$

Radiative corrections lead to charge renormalisation and thus to the running of the fine structure constant obtained by summing the one-particle irreducible bubble insertions in

the photon propagator [Jegerlehner 1986a]

$$\alpha_{\mathrm{QED}}(Q^2) = \frac{\alpha_0}{1 - \Delta\alpha_{\mathrm{QED}}(Q^2)} \,. \tag{5.1}$$

Here, α_0 is the value at vanishing momentum transfer $Q^2 = 0$ obtained from the electron anomalous magnetic moment, $\alpha_0^{-1} = 137.035999173(35)$ [Aoyama et al. 2012b]. The leading-order hadronic contribution is given by [Jegerlehner 2011]

$$\Delta\alpha_{\mathrm{QED}}^{\mathrm{hvp}}(Q^2) = -4\pi\alpha_0 \Pi_{\mathrm{R}}\left(Q^2\right) \tag{5.2}$$

and is thus directly proportional to the subtracted vacuum polarisation function which we have introduced in chapter 3. As mentioned before, this is usually [Jegerlehner 1986a, Davier et al. 2011, Jegerlehner 2011] determined by a phenomenological approach relying on the once-subtracted dispersion relation [Jegerlehner and Nyffeler 2009] and experimental cross-section data for

$$R_{\mathrm{had}}(s) = \frac{\sigma(e^+e^- \to \mathrm{hadrons})}{\frac{4\pi\alpha_{\mathrm{QED}}^2(s)}{3s}} \,. \tag{5.3}$$

In Sect. 3.2 we have seen that lattice QCD represents an ab-initio alternative for the calculation of $\Pi_{\mathrm{R}}(Q^2)$, since the hadronic vacuum polarisation tensor can be obtained directly in Euclidean space-time from the correlator of two electromagnetic vector currents.

5.2.1. Lattice calculation

The computational strategy for the procurement and analysis of the hadronic vacuum polarisation function has been described in Sect. 4.1. In particular, we employ the set of ensembles presented in Sect. 4.1.1, the conserved point-split vector current at source and sink and we restrict our considerations to the quark-connected contributions.

For each flavour, we first fit the temporal vector current correlator to determine the vector meson mass, m_V, and its decay constant, f_V, obtaining the results given in appendix E and discussed in Sect. 4.1.3. Subsequently, we fit the hadronic vacuum polarisation function obtained from the current correlator as detailed in Sect. 4.1.2 separately for each flavour and each ensemble. The number of terms and thus the fit function is characterised by M, N, B, and C. In the following, we use $Q^2_{\mathrm{max}} = 100\,\mathrm{GeV}^2$ for the fit but we perform the extrapolations in the light quark mass and the lattice spacing only for momenta up to $10\,\mathrm{GeV}^2$. We choose as momentum dividing the low- and high-momentum parts of the fit $Q^2_{\mathrm{match}} = 2\,\mathrm{GeV}^2$. We have checked that varying Q^2_{match} by up to $1\,\mathrm{GeV}^2$ to the left and to the right gives compatible results.

Since our four-flavour ensembles feature unphysically large pion masses, an extrapolation to the physical point has to be performed. The pion mass dependence of the single-flavour contributions can be assessed by looking at the leading vector meson contribution obtained in resonance chiral perturbation theory [Ecker et al. 1989]

$$\Pi^{\mathrm{f}}(Q^2) \propto g_V^2 \frac{m_V^2}{Q^2 + m_V^2} \,. \tag{5.4}$$

As we have seen in Sect. 4.1.3, the spectral properties of the heavy vector mesons hardly

depend on the pion mass and also g_V of the ρ-meson has been found to be linear in the squared pion mass, m_{PS}^2. However, the ρ-meson mass, m_V, strongly depends on the value of the light quark masses, taken to be mass-degenerate in our calculation, and thus the squared pion mass. This has already been found in the two-flavour calculations [Feng et al. 2011a] and as a further illustration is shown in Fig. 5.1 below.

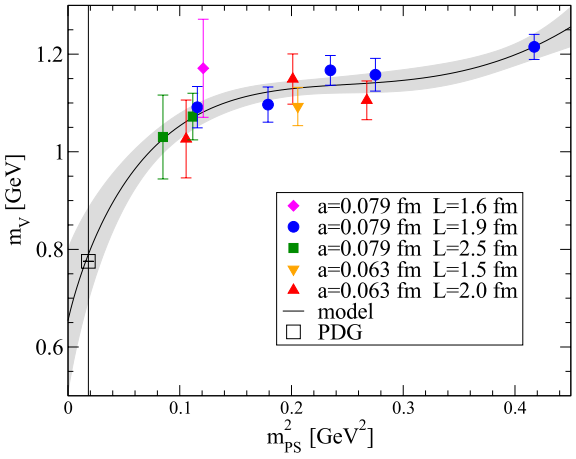

Figure 5.1.: Dependence of ρ-meson mass, m_V, on squared pion mass, m_{PS}, determined on $N_f = 2$ twisted mass ensembles [Feng et al. 2011a].

Eq. (5.4) implies that this non-linear dependence on the squared pion mass can be eliminated to a large extent by employing the lattice redefinition [Renner et al. 2012]

$$\Delta\overline{\alpha}_{\mathrm{QED}}^{\mathrm{hvp}}(Q^2) = -4\pi\alpha_0\Pi_{\mathrm{R}}\left(Q^2\frac{H^2}{H_{\mathrm{phys}}^2}\right) \tag{5.5}$$

in the light sector, if we use $H = m_V$, i.e. the ρ-meson mass at unphysically large up and down quark masses. This will be done in the following. Obviously, for any hadronic scale H that assumes its physical value in the limit $m_{\mathrm{PS}} \to m_\pi$, Eq. (5.5) leads to the correct result at the physical point when $\frac{H}{H_{\mathrm{phys}}} = 1$. For the contributions of heavy flavours we use the standard definition given in Eq. (5.2). This enables us to linearly extrapolate the sum of the single-flavour results in the squared pion mass to the physical point.

5.2.2. Results

In order to show that the above redefinition in Eq. (5.5) indeed provides the expected benefit for the chiral extrapolation of the light quark contribution to the running of the fine structure constant, we show the data for both Eqs. (5.2) and (5.5) with $H = m_V$ in Fig. 5.2 for a single momentum value $Q^2 = 1\,\mathrm{GeV}^2$. The upper set of data points obtained with the redefinition Eq. (5.5) evidently is much easier to extrapolate to the physical value of the pion mass than the lower points procured from the standard definition Eq. (5.2). In fact, while the linear fit in the squared pion mass, m_{PS}^2, shown in the figure yields a reduced $\chi^2/\mathrm{dof} = 0.76$ and well-determined fit parameters, introducing a quadratic term or a term proportional to the squared lattice spacing results in values for the additional parameters which are compatible with zero such that only the linear fit seems to be applicable.

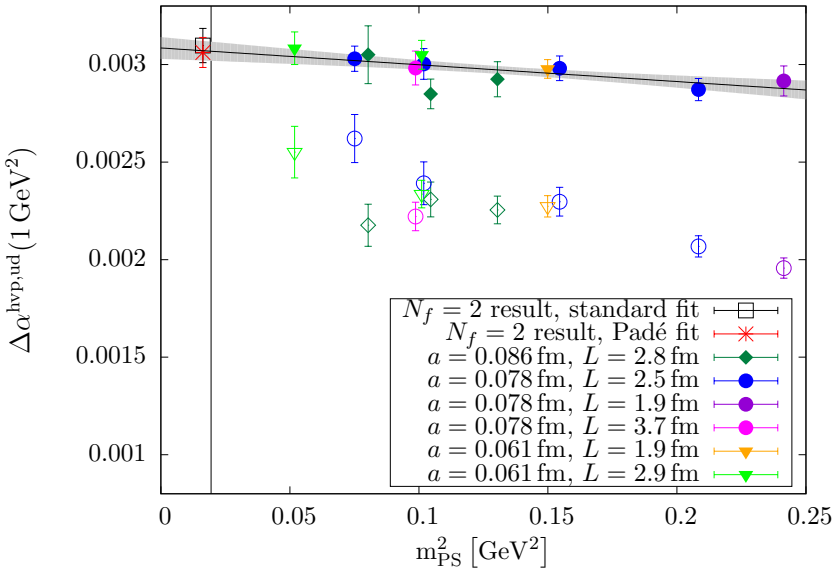

Figure 5.2.: Light-quark contribution to $\Delta\alpha^{\mathrm{hvp}}_{\mathrm{QED}}$ with filled symbols representing points obtained with Eq. (5.5) using $H = m_V$, open symbols refer to those obtained with Eq. (5.2), i. e. $H = 1$ in Eq. (5.5). In particular, the two-flavour results at the physical point have been computed with the standard definition. The grey errorband displays the uncertainty of the linear fit represented by the black dotted line.

Since we do neither observe lattice spacing artefacts nor finite size effects in these data at $Q^2 = 1\,\mathrm{GeV}^2$, we can actually compare our results computed on the four-flavour ensembles linearly extrapolated in the squared pion mass, m^2_{PS}, with those obtained from the $N_f = 2$ ensemble featuring the physical pion mass. As we have discussed in Sect. 4.1.3, treating the ρ-meson as stable particle is no longer justified at the physical point. Therefore, we have additionally to the standard analysis performed a correlated $[1,1]$ Padé fit possessing the same number of parameters up to $Q^2_{\mathrm{max}} = 1.5\,\mathrm{GeV}^2$ such that $Q^2 = 1\,\mathrm{GeV}^2$ is safely covered. As expected from the discussion at the end of Sect. 4.2.1, the values for the pole parameters determined from the temporal correlator in our standard approach and from the Padé fit are compatible

$$a^2\, m_V^2 = 0.153(35) \qquad b_n = 0.1575(81) \tag{5.6}$$

and also the results of both analyses of the leading hadronic contribution to the running of the fine structure constant at the physical point completely agree with each other and with the extrapolated result obtained on the four-flavour ensembles indicating that the systematic uncertainty caused by the chiral extrapolation is small. The results at the physical value of the pion mass which are depicted in Fig. 5.2 are summarised in Tab. 5.1 below.

An interesting feature of the results at the physical point is that the value obtained from the Padé fit actually has a smaller statistical uncertainty than obtained by our standard analysis in contrast to Refs. [Aubin et al. 2012, Golterman et al. 2013] where it has been suspected that the uncertainties of the parameters obtained by Padé approximants would be larger than those from our MNBC fits and thus would take a systematic uncertainty

$N_f = 2+1+1$ extrapolated	$N_f = 2$ standard	$N_f = 2$ [1, 1] Padé
0.003068(50)	0.003097(88)	0.003062(77)

Table 5.1.: Comparison of the chirally extrapolated result for $\Delta\alpha^{\mathrm{hvp,ud}}_{\mathrm{QED}}(1\,\mathrm{GeV}^2)$ obtained on the $N_f = 2+1+1$ ensembles with those obtained on the $N_f = 2$ ensemble at the physical point. For the latter, we have performed our standard analysis but without the redefinition and also tested a [1,1] Padé fit.

allegedly present in our standard analysis into account. The above comparison indicates that this suspicion is not true in general. The reason is that our standard analysis is not just the pure vector meson dominance model plus a linear term investigated in [Golterman et al. 2013]. In contrast to the procedure studied there, we properly propagate all uncertainties by using the same bootstrap samples for the determination of the vector meson properties and the vacuum polarisation fits.

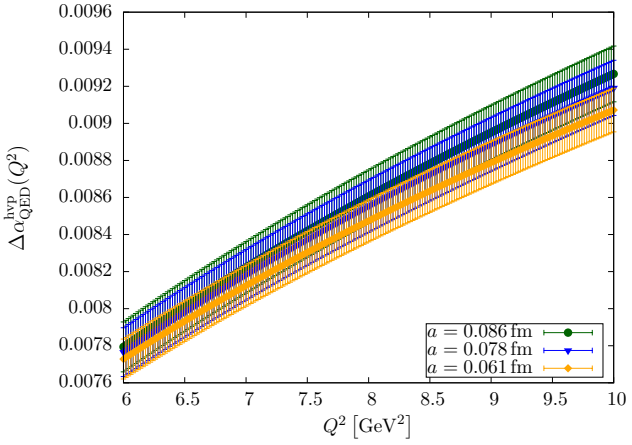

Figure 5.3.: $N_f = 2+1+1$ contribution to $\Delta\alpha^{\mathrm{hvp}}_{\mathrm{QED}}$ for the three lattice spacings at a fixed pion mass of $m_{\mathrm{PS}} \approx 320\,\mathrm{MeV}$.

Including also the heavy quark contributions by summing the single-flavour pieces and including the appropriate charge factors, a dependence on the lattice spacing is clearly visible, especially in the high-Q^2 region shown in Fig. 5.3. This is accounted for by combining the chiral extrapolation with taking the continuum limit and employing the following fit function

$$\Delta\alpha^{\mathrm{hvp}}_{\mathrm{QED}}(Q^2)^{\mathrm{hvp}}(m_{\mathrm{PS}}, a) = A + B\; m^2_{\mathrm{PS}} + C\; a^2 \tag{5.7}$$

with fit parameters A, B, C different for each momentum value

$$Q^2 \in \{0, 0.02, 0.04, \ldots, 10\}\,\mathrm{GeV}^2\,.$$

In Sect. 3.2.2 we have shown that automatic $\mathcal{O}(a)$ improvement is at work for our definition of the hadronic vacuum polarisation function presented in Sect. 3.2.1. Thus, performing the continuum extrapolation without a term linear in the lattice spacing a in Eq. (5.7) is justified.

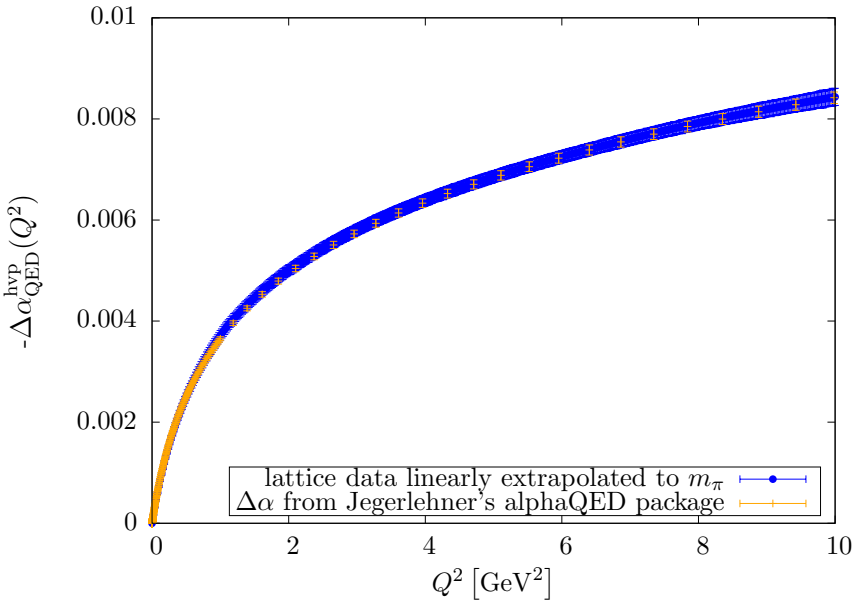

Figure 5.4.: $N_f = 2+1+1$ contribution to $-\Delta\alpha^{\text{hvp}}_{\text{QED}}$ compared to the data collected in [Jegerlehner 2012] employing the dispersion relation in Eq. (3.6). The lattice data are extrapolated to the physical point and the continuum limit (CL).

The results are depicted in Fig. 5.4 together with the results obtained by a phenomenological analysis [Jegerlehner 2011, Jegerlehner 2012]. Over the whole momentum range, perfect agreement with comparable uncertainties is found. In the figure we show only the statistical errors and discuss the systematic uncertainties further below. An updated phenomenological analysis including all experimental e^+e^- scattering data published till the end of 2014 will soon be available [Jegerelehner 2015]. A preliminary analysis shows that the lattice data also agree with those results featuring even smaller uncertainties.

Additionally, let us remark that comparing Fig. 5.4 with Fig. 4.6 where the lattice data is compared with exactly the same phenomenological results, it is evident that our standard procedure currently entails a much smaller statistical uncertainty than the analytic continuation method and is therefore preferable for the analyses conducted on the currently available $N_f = 2+1+1$ ensemles.

Systematic uncertainty from the choice of vector meson fit ranges

As mentioned before, the first step in our analysis is the determination of the masses and the coupling constants of the vector mesons from the 0-momentum vector two-point functions. The values of the spectral parameters differ when varying the fit range. We have repeated the complete analysis for various vector meson fit ranges for the light, strange, and charm quark currents propagating the uncertainty to the final results.

In the light quark sector depicted in Fig. 5.5, we observe systematic differences depending on whether we start fitting the vector meson correlator at 0.6 fm or at 0.7 fm whereas changing the upper bound of the fit interval by 0.1 fm does not lead to observable effects. The dependence on the lower starting point of the fit can be attributed to excited state contamination of the ρ-meson correlator. When stating the final results for selected

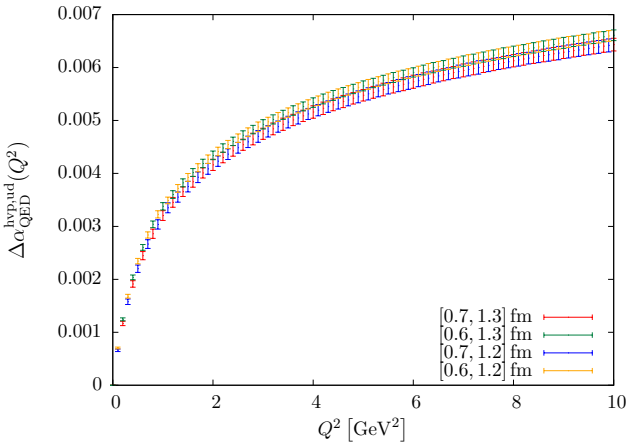

Figure 5.5.: Light quark contribution to $\Delta\alpha_{\mathrm{QED}}^{\mathrm{hvp}}$ obtained with different fit ranges for the ρ-meson mass, m_V, and coupling, g_V. The standard fit range is [0.7 fm, 1.2 fm].

momentum values below, we take for these systematic uncertainties half the difference between the central values that are furthest apart from each other. In this way, we obtain a conservative estimate since we do not account for correlations present between the fits.

For the heavy flavours changing the fit interval by 0.1 fm to the left and to the right of both the lower and the upper time slice of the fit ranges does not lead to observable differences as illustrated in Fig. 5.6.

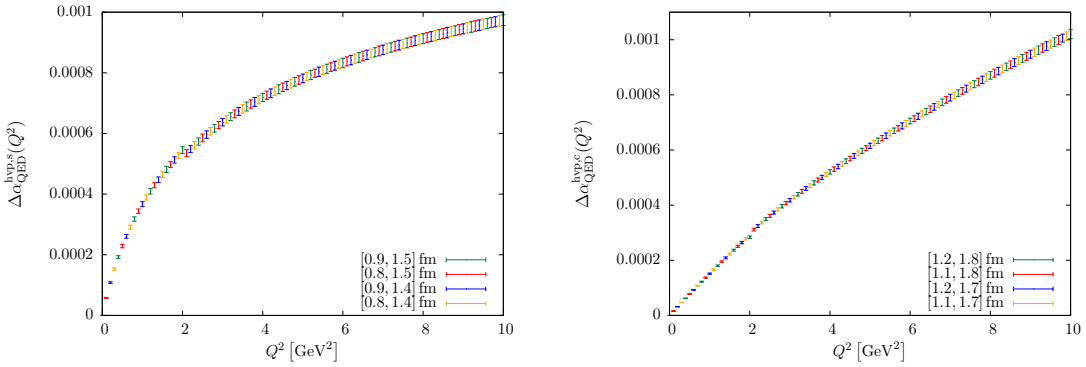

Figure 5.6.: Dependence of the single-flavour contributions to $\Delta\alpha_{\mathrm{QED}}$ on the fit range of the $\bar{s}s$-correlator (left panel) and of the J/Ψ-correlator (right panel). The standard $\bar{s}s$-correlator fit range is [0.9 fm, 1.4 fm], whereas the one for the charm quark correlator is [1.2 fm, 1.7 fm]. The minor discontinuities at $Q^2 = 2\,\mathrm{GeV}^2$ arise from connecting the low-momentum Eq. (4.6) and high-momentum Eq. (4.7) fit functions at this point by a simple step function as shown in Eq. (4.8). Due to the subdominance of the heavy flavour contributions those discontinuities do not influence the final result.

Systematic uncertainty from the choice of vacuum polarisation fit function

Performing the whole analysis with different numbers of terms in our vacuum polarisation fit functions also leads to observable differences in the light quark contribution as shown in

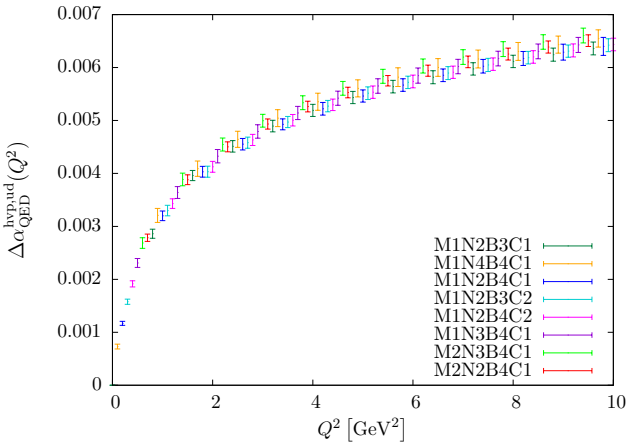

Figure 5.7.: Light quark contribution to $\Delta\alpha_{\mathrm{QED}}^{\mathrm{hvp}}$ obtained from different fit functions. The standard fit is M1N2B4C1.

Fig. 5.7. These are larger than the effects from the fit ranges of the vector meson fits discussed in the preceding subsection and thus present the dominant systematic uncertainty in our calculation. It might be possible to improve the situation by e.g. the method of analytic continuation presented in Sect. 4.2.2 or by taking momentum derivatives of the vacuum polarisation function [De Divitiis et al. 2012].

The results for the heavy quarks are presented in Fig. 5.8. Here, almost no systematic deviations are visible. Furthermore, the contributions from the heavy quarks are about an order of magnitude smaller than the light-quark one. Hence, we do not take systematic effects from the variation of the second-generation quark fit functions into account in our final error estimates.

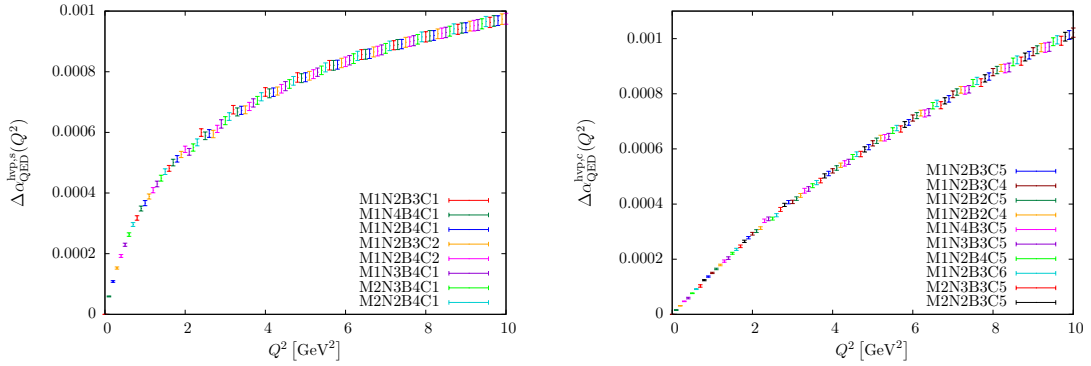

Figure 5.8.: Dependence of the single-flavour contributions to $\Delta\alpha_{\mathrm{QED}}$ on the choice of fit function for the strange (left panel) and for the charm (right panel) quark pieces. For the strange quark the standard fit is M1N2B4C1, whereas the one for the charm quark correlator is M1N2B3C5.

Finite size effects

In lattice QCD, typically $m_{\mathrm{PS}}\, L \gtrsim 4$ is required to minimise systematic effects due to the finite lattice volumes, where L denotes the spatial extent of the lattice. The $N_f = 2+1+1$

ensembles analysed in this work feature $3.35 < m_{\mathrm{PS}}\, L < 5.93$. Restricting our data to the condition $m_{\mathrm{PS}}L > 3.8$ yields the picture shown in the left panel of Fig. 5.9. Hence, we do not associate a systematic uncertainty to the usage of ensembles possessing smaller $m_{\mathrm{PS}}L$ values. This finding is corroborated by a dedicated finite volume study of the Budapest-Marseille-Wuppertal collaboration with $m_{\mathrm{PS}}\, L$ as big as 12.3 [BMW 2015]. There it was shown that the vacuum polarisation function renormalised as described in Eq. (3.5) only shows negligible finite size effects.

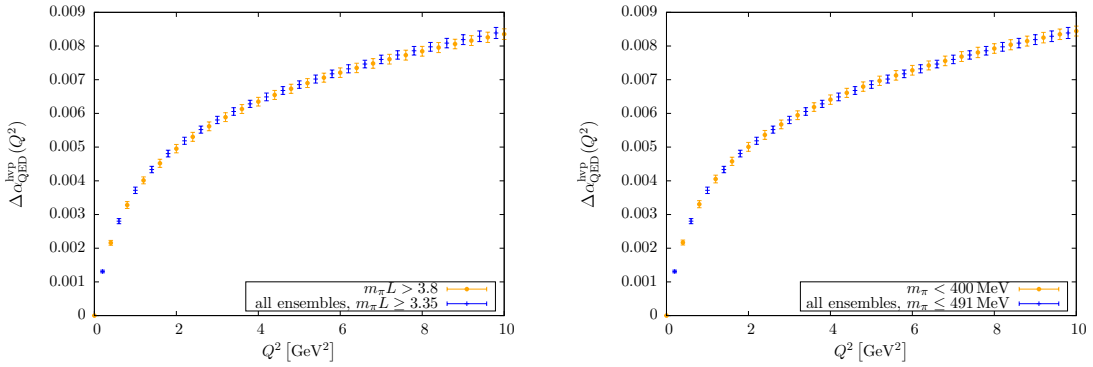

Figure 5.9.: Four-flavour contribution to $\Delta\alpha^{\mathrm{hvp}}_{\mathrm{QED}}$ obtained with (left panel) $m_{\mathrm{PS}}L \geq 3.35$ [standard] and $m_{\mathrm{PS}}L > 3.8$ and (right panel) $m_{\mathrm{PS}} \leq 491\,\mathrm{MeV}$ [standard] and $m_{\mathrm{PS}}L < 400\,\mathrm{MeV}$.

Systematic uncertainty from including heavy pion masses

In order to extrapolate to the physical point, $m_\pi \approx 140\,\mathrm{MeV}$, often not too high pion masses should be included in the fit. The ensembles entering the standard analysis comprise pion masses up to $m_{\mathrm{PS}} \approx 491\,\mathrm{MeV}$. Due to the usage of the redefinition in Eq. (5.5) in the light-quark sector, the dependence on the squared pion mass is linear for all single-flavour contributions such that the chiral extrapolation can be performed in a straightforward manner. In fact, employing only the ensembles with $m_{\mathrm{PS}} < 400\,\mathrm{MeV}$ yields fully compatible results for $\Delta\alpha^{\mathrm{hvp}}_{\mathrm{QED}}$ as can be seen in the right panel of Fig. 5.9. Therefore, we do not account for a systematic uncertainty related to the computation of $\Delta\alpha^{\mathrm{hvp}}_{\mathrm{QED}}$ on ensembles with pion masses above 400 MeV. This finding is strongly supported by the comparison of the results for the light quark contribution obtained by chirally extrapolating the values of the $N_f = 2+1+1$ ensembles with those computed directly at the physical point from the $N_f = 2$ ensemble which we have discussed above.

Final results for selected momentum values

Table 5.2 contains our final results compared to those of a phenomenological analysis [Jegerlehner 2011] utilising the once-subtracted dispersion relation Eq. (3.6) and experimental e^+e^- scattering data. The first error denotes the statistical and the second error the systematic uncertainty of our values. Evidently, the latter constitutes the dominant source of uncertainty of which the biggest part originates from the choice of the vacuum polarisation fit function. This might change when lowering the statistical uncertainty, because then the vacuum polarisation fits get more constrained. Alternatively, as mentioned before avoiding to fit the vacuum polarisation might be considered. Taken together,

the current uncertainty of the lattice determination still exceeds the one attained by the phenomenological analysis. Nevertheless, this first comparison between dynamical four-flavour lattice QCD and phenomenological results for the leading hadronic contribution to the shift of α_{QED} in the low-momentum region represents an important cross-check of the phenomenological results and opens up the possibility to reach or even surpass their accuracy by future lattice QCD calculations.

Q^2 [GeV^2]	this work	dispersive analysis [Jegerlehner 2011]
0.02	$0.163(05)(09) \cdot 10^{-3}$	$0.174(02) \cdot 10^{-3}$
1.00	$3.721(96)(145) \cdot 10^{-3}$	$3.651(40) \cdot 10^{-3}$
2.00	$4.993(102)(144) \cdot 10^{-3}$	$4.916(61) \cdot 10^{-3}$
3.00	$5.800(111)(151) \cdot 10^{-3}$	$5.725(74) \cdot 10^{-3}$
4.00	$6.396(108)(156) \cdot 10^{-3}$	$6.333(84) \cdot 10^{-3}$
6.00	$7.264(114)(159) \cdot 10^{-3}$	$7.223(98) \cdot 10^{-3}$
8.00	$7.906(124)(151) \cdot 10^{-3}$	$7.850(107) \cdot 10^{-3}$
10.0	$8.419(130)(159) \cdot 10^{-3}$	$8.420(114) \cdot 10^{-3}$

Table 5.2.: $\Delta\alpha^{\mathrm{hvp}}_{\mathrm{QED}}(Q^2)$ for selected values of Q^2. The first error of the lattice results is statistical, the second systematic. The phenomenological values of $\Delta\alpha^{\mathrm{hvp}}_{\mathrm{QED}}(Q^2)$ have been obtained from the dispersive analysis of Ref. [Jegerlehner 2011].

5.3. The weak mixing angle $\sin^2\theta_W$

The weak mixing or Weinberg angle, θ_W, constitutes one of the fundamental parameters of the electroweak standard model. It is introduced when describing electroweak symmetry breaking via the Higgs mechanism [Higgs 1964, Englert and Brout 1964, Guralnik et al. 1964] and is defined by

$$\sin^2\theta_W = \frac{g'^2}{g'^2+g^2} = \frac{e^2}{g^2} = \frac{\alpha_{\mathrm{QED}}}{\alpha_2}\,, \tag{5.8}$$

where g is the $SU(2)_I$ coupling constant and g' the $U(1)_Y$ coupling constant. The second equality is the electroweak unification condition $e^2 = g^2\sin^2\theta_W$ for the positron charge e. Thus, the running of the weak mixing angle can be obtained from the running of the fine structure constant and the $SU(2)_I$ coupling α_2. In the leading logarithmic approximation this is given by [Jegerlehner 1986b]

$$\sin^2(\theta)(q^2) = \sin^2(\theta_0)\frac{1-\Delta\alpha_2(q^2)}{1-\Delta\alpha_{\mathrm{QED}}(q^2)} = \sin^2(\theta_0)(1+\Delta(q^2)) \tag{5.9}$$

where $\sin^2(\theta_0) = \frac{\alpha^0}{\alpha_2^0}$, and $\Delta(q^2) = \Delta\alpha_{\mathrm{QED}}(q^2) - \Delta\alpha_2(q^2)$ is an abbreviation for $\Delta\sin^2\theta(q^2)$. The value of $\sin^2(\theta_0)$ has essentially been measured by the Boulder group studying atomic parity violation in Cesium [Wood et al. 1997], the latest value is $\sin^2(\theta_0) = 0.2356(20)$ [Dzuba et al. 2012]. The standard model prediction in the $\overline{\mathrm{MS}}$ scheme is $\sin^2(\theta_0) = 0.23871(9)$ [Erler and Ramsey-Musolf 2005, Kumar et al. 2013]. This is the value employed

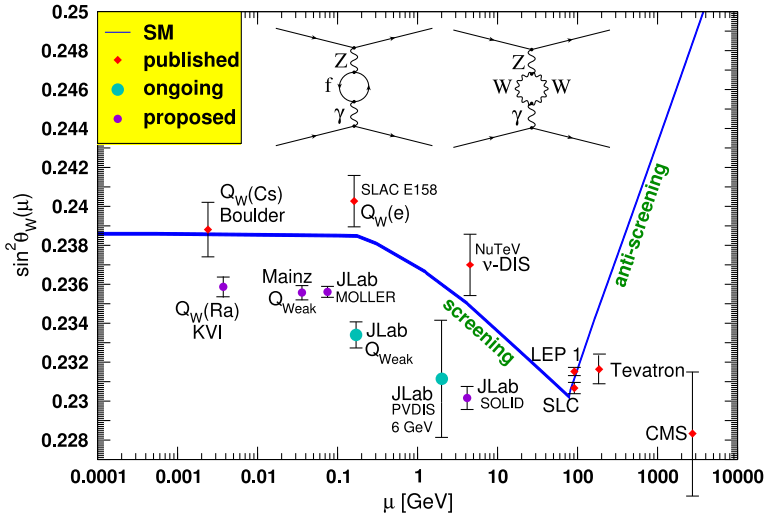

Figure 5.10.: Predicted running of the weak mixing angle compared to results of current and future experiments measuring it at various momentum transfers. This figure has been published in [Erler 2012].

in the analysis below in order to gain fully theoretical results without experimental input. For the latest computation [Kumar et al. 2013] of this value, the Higgs boson mass determined by the LHC experiments [ATLAS 2012, CMS 2012] has been used.

The current phenomenological value of the leading hadronic contribution to the running of $\sin^2\theta_W$ between 0 and the Z-scale has been computed for the first time in [Marciano 1993] relying on the dispersion relation Eq. (3.6) and results from [Jegerlehner 1990]. The method has been described and used with an older dispersive analysis [Wetzel 1981] before [Marciano and Sirlin 1984]. In [Erler and Ramsey-Musolf 2005], the error has been reduced with respect to the original rather conservative estimate of the uncertainty by about an order of magnitude.

Due to the great sensitivity of the weak mixing angle to physics beyond the SM over a wide range of momenta, several experiments have measured, are measuring or will measure the electroweak mixing angle indirectly from various parity violating processes. An overview is shown in Fig. 5.10 and further details of experiments taking data in the momentum region studied in this work will be given when presenting our final results for this eminent quantity. The blue line in Fig. 5.10 shows the theoretical prediction from [Erler and Ramsey-Musolf 2005]. Its thickness represents the theoretical uncertainty. In [Erler 2012] it is, however, admitted that this might be underestimated in the hadronic transition region between 0.1 GeV and 2 GeV where perturbation theory cannot be applied. Fortunately, as we will see shortly, lattice QCD is capable of providing reliable results there.

The leading hadronic contribution to the running of the $SU(2)_I$ coupling constant originates from Z-γ mixing depicted in Fig. 5.11.

Figure 5.11.: Hadronic vacuum polarisation $\Pi^{Z\gamma}$ from Z-γ mixing.

From the expressions for the hadronic currents of up-type (u) and down-type (d) quarks

$$J_\mu^Z = J_\mu^3 - \sin^2(\theta_W) J_\mu^\gamma \tag{5.10}$$

$$J_\mu^3 = \frac{1}{4}\sum_f \left(\overline{u_f}\gamma_\mu(1-\gamma_5)u_f - \overline{d_f}\gamma_\mu(1-\gamma_5)d_f\right) \tag{5.11}$$

$$J_\mu^\gamma = \sum_f \left(\frac{2}{3}\overline{u_f}\gamma_\mu u_f - \frac{1}{3}\overline{d_f}\gamma_\mu d_f\right) \tag{5.12}$$

where 3 refers to the third component of the weak isospin current and γ to the electromagnetic current denoted j_μ^{em} before, we see that to leading order

$$\Pi^{Z\gamma} \approx \Pi^{3\gamma} = \langle J_\mu^3 J_\mu^\gamma \rangle \tag{5.13}$$

and thus the leading hadronic contribution to the running of α_2 is given by [Jegerlehner 1986a, Jegerlehner 2011]

$$\Delta\alpha_2^{\mathrm{hvp}}(q^2) = -g^2\left(\Pi^{3\gamma}(q^2) - \Pi^{3\gamma}(0)\right) . \tag{5.14}$$

As for the purely electromagnetic current correlator, $\Pi^{3\gamma}$ denotes the transverse part of the vacuum polarisation function.

Beyond the leading logarithmic approximation, $\Delta\alpha_{\mathrm{QED}}^{\mathrm{hvp}}$ and $\Delta\alpha_2^{\mathrm{hvp}}$ become renormalisation scheme dependent. Additional hadronic contributions to these corrections at the scale of the W-mass and the Z-mass originate from chiral symmetry breaking. They have been shown to be calculable in perturbation theory and to be at least two orders of magnitude smaller and thus negligible compared to the leading contributions [Jegerlehner 1986a]. Thus, having computed $\Delta\alpha_{\mathrm{QED}}$ before, all that is left to do to leading order is to compute $\Delta\alpha_2$ as given in Eq. (5.14).

5.3.1. Lattice calculation

Since our ensembles feature mass-degenerate up and down quarks, $m_u = m_d$, light-quark disconnected contributions cannot occur in $\Pi^{3\gamma}$ due to the isospin symmetry of the vacuum. Without those interference terms, single-flavour contributions to Eq. (5.13) have the generic structure $\Pi^{3\gamma,f} =< (V-A)V >$, where V and A denote vector and axial vector currents, respectively. Since QCD conserves parity, no mixing between vector and axial vector currents occurs such that we obtain for up-type quarks twice the contribution of down-type quarks

$$\Pi_{\mu\nu}^{3\gamma,u} = \frac{1}{6}\sum_f \langle (\overline{u_f}\gamma_\mu u)\,(\overline{u_f}\gamma_\nu u)\rangle = 2\Pi_{\mu\nu}^{3\gamma,d} . \tag{5.15}$$

Combining this with the connected contributions to $\Delta\alpha_{\mathrm{QED}}$, the leading-order hadronic

contribution to the running of the weak mixing angle from the two light flavours reads

$$\Delta^{\mathrm{hvp,ud}}(q^2) = -\Delta\alpha_2^{\mathrm{hvp,ud}}(q^2) + \Delta\alpha_{\mathrm{QED}}^{\mathrm{hvp,ud}}(q^2) = \frac{1}{4}g^2\Pi^{uu}(q^2) - \frac{5}{9}e^2\Pi^{uu}(q^2)\,. \tag{5.16}$$

Neglecting quark-disconnected contributions also for the heavy flavours, we have for the strange and the charm quark contributions

$$\Delta^{\mathrm{hvp,s}}(q^2) = -\Delta\alpha_2^{\mathrm{hvp,s}}(q^2) + \Delta\alpha_{\mathrm{QED,s}}^{\mathrm{hvp}}(q^2) \quad = \tfrac{1}{12}g^2\Pi^{ss}(q^2) - \tfrac{1}{9}e^2\Pi^{ss}(q^2) \tag{5.17}$$

$$\Delta^{\mathrm{hvp,c}}(q^2) = -\Delta\alpha_2^{\mathrm{hvp,c}}(q^2) + \Delta\alpha_{\mathrm{QED,c}}^{\mathrm{hvp}}(q^2) \quad = \tfrac{1}{6}g^2\Pi^{cc}(q^2) - \tfrac{4}{9}e^2\Pi^{cc}(q^2)\,, \tag{5.18}$$

respectively. Hence, the single flavour contributions are all proportional to the hadronic vacuum polarisation function but with different prefactors than for $\Delta\alpha_{\mathrm{QED}}^{\mathrm{hvp}}$. In order to treat both contributions to $\Delta^{\mathrm{hvp}}\sin\theta_W$ consistently, we use in the light sector the same redefinition of the vacuum polarisation function for $\Delta\alpha_2^{\mathrm{hvp}}$ as for $\Delta\alpha_{\mathrm{QED}}^{\mathrm{hvp}}$

$$\Delta\overline{\alpha_2}^{\mathrm{hvp}}(Q^2) = -4\pi\alpha_0\Pi_{\mathrm{R}}^{3\gamma}\left(Q^2\frac{H^2}{H^2_{\mathrm{phys}}}\right)\,. \tag{5.19}$$

As stated above, the leading hadronic contribution to the running of the weak mixing angle in the leading logarithmic approximation is obtained from the difference of the corresponding contributions of the electromagnetic and the $SU(2)_I$ coupling constants, α_{QED} and α_2. In contrast to $\Delta\alpha_{\mathrm{QED}}^{\mathrm{hvp}}$, it is not straightforward to extract $\Delta\alpha_2^{\mathrm{hvp}}$ from experimental $e^+e^- \to$ hadrons data, since the data comprising the three lightest quarks would have to be separated either e.g. in up-type (u) and down-type (d and s) quarks or assuming isospin symmetry in light and strange quark contributions. This problem has no unique solution. For example, final states involving kaons could either originate directly from a strange quark current or from a gluon that could be radiated off light quarks. Another possibility is to assume $SU(3)_f$ symmetry and thus only split the data into information attributed to the three lightest quarks and the rest. The contributions from charm and heavier quarks can be computed in perturbation theory.

5.3.2. Results

$\Delta\alpha_2^{\mathrm{hvp}}$

Fig. 5.12 shows our four-flavour results after combined extrapolation to the physical point and to vanishing lattice spacing in the same way as for $\Delta\alpha_{\mathrm{QED}}^{\mathrm{hvp}}$ compared to the results of a phenomenological analysis [Jegerlehner 2011]. This is the first lattice QCD calculation of $\Delta\alpha_2^{\mathrm{hvp}}$. To arrive at a meaningful comparison, we have multiplied the data from [Jegerlehner 2012] with $\sin^2\theta_W(M_Z)/\sin^2(\theta_0)$ to account for the different reference values employed. As mentioned before we use $\sin^2(\theta_0) = 0.23871(9)$ and the value used by Jegerlehner is $\sin^2\theta_W(M_Z) = 0.23153(16)$ which has been measured at LEP [LEPEWWG 2010].

In [Jegerlehner 2012], two ways of flavour separation have been implemented, one is assuming approximate $SU(3)_f$ and the other one $SU(2)_f$ symmetry neglecting OZI violating terms. Our results clearly prefer the $SU(3)_f$ flavour separation and thus indicate that the latter assumption is not tenable as has also been observed in [Francis et al. 2013b] in a different context. Being able to distinguish between results from different flavour sep-

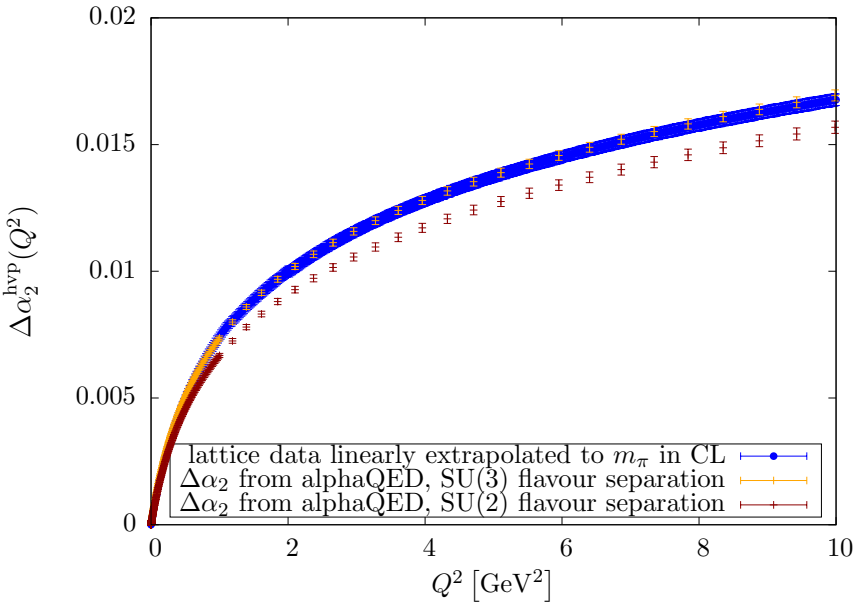

Figure 5.12.: $N_f = 2+1+1$ contribution to $\Delta\alpha_2^{\mathrm{hvp}}$ compared to the data collected in [Jegerlehner 2012] for all quarks except the top. The lattice data are extrapolated to the physical point and to the continuum limit (CL).

arations, our lattice QCD calculation can even provide guidance for the currently more precise phenomenological analyses in order to arrive at a reliable value for the running $SU(2)_I$ coupling constant and thus the weak mixing angle. Consequently, the flavour separation performed for the data set including very recent e^+e^- measurements no longer assumes flavour non-diagonal elements to be small but is instead based on isospin symmetry relations [Jegerelehner 2015]. The results are much closer to the ones based on $SU(3)_f$ flavour separation in Fig. 5.12 than to the $SU(2)_f$ curve. Thus, our lattice results are also compatible with the newest phenomenological analysis. This is shown in Fig. 5.13.

$\Delta^{\mathrm{hvp}} \sin^2\theta_W$

Having determined the four-flavour contributions to $\Delta\alpha_{\mathrm{QED}}^{\mathrm{hvp}}$ and $\Delta\alpha_2^{\mathrm{hvp}}$, it is straightforward to obtain the leading-order hadronic vacuum polarisation contribution to the running of the weak mixing angle

$$\Delta^{\mathrm{hvp}} \sin^2\theta_W(Q^2) = \Delta\alpha_{\mathrm{QED}}^{\mathrm{hvp}}(Q^2) - \Delta\alpha_2^{\mathrm{hvp}}(Q^2) \tag{5.20}$$

for $Q^2 \in [0, 10]\,\mathrm{GeV}^2$. As mentioned several times before, this is the central observable measured in various low-energy experiments in order to gain hints on beyond the SM physics. Below, a selection of such experiments operating at momentum transfers investigated in this work will be listed.

The physical results for the light-quark contribution for each momentum value can again be obtained from extrapolations in the squared pion mass as shown in Fig. 5.14 for $Q^2 = 1\,\mathrm{GeV}^2$. In contrast to the case of α_{QED} depicted in Fig. 5.2, for the weak mixing angle combining the redefinitions of α_{QED} in Eq. (5.5) and α_2 in Eq. (5.19) leads to lower values than obtained with the standard definitions. The common feature of the

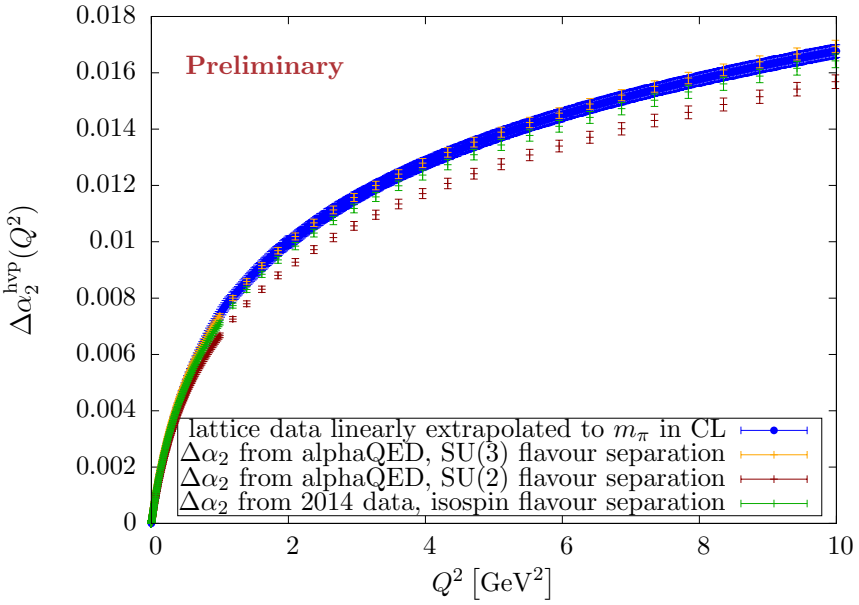

Figure 5.13.: Same as Fig. 5.12 with additional preliminary results of a phenomenological analysis of recent e^+e^- scattering data employing an $SU(2)$ flavour separation based on isospin symmetry relations [Jegerelehner 2015] represented by the green points. [new data generously provided by Fred Jegerlehner]

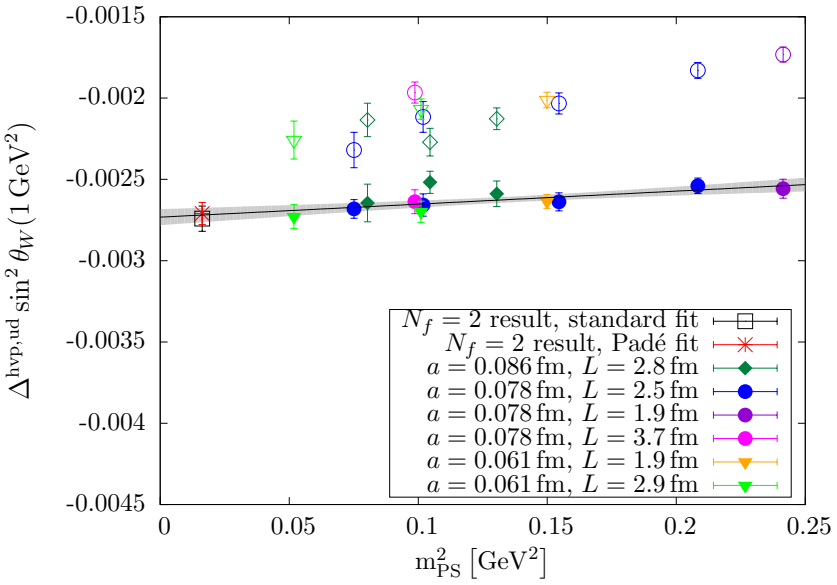

Figure 5.14.: Light-quark contribution to $\Delta^{\rm hvp}\sin^2\theta_W$ with filled symbols representing points obtained with Eqs. (5.5) and (5.19), open symbols refer to those obtained with Eqs. (5.2) and (5.14). In particular, the two-flavour results at the physical point have been computed with the standard definitions. The grey errorband displays the uncertainty of the linear fit represented by the black dotted line.

$N_f = 2+1+1$ extrapolated	$N_f = 2$ standard	$N_f = 2$ [1, 1] Padé
-0.002717(43)	-0.002742(78)	-0.002710(68)

Table 5.3.: Comparison of results for $\Delta^{\mathrm{hvp,ud}} \sin^2\theta_W(1\,\mathrm{GeV}^2)$ at the physical point. The same analyses as indicated below Tab. 5.1 have been performed.

leading-order hadronic contributions of both quantities is that the values procured with the redefinitions can be linearly extrapolated in the squared pion mass to the physical point yielding a result which is compatible with those of the standard analysis as well as the one from Padé approximants on the ensemble of two dynamical quarks at the physical point. The results at the physical value of the pion mass are given in Tab. 5.3.

When incorporating the heavy quarks, the chiral extrapolation is again combined with taking the continuum limit according to

$$\Delta^{\mathrm{hvp}} \sin^2\theta_W(Q^2)(m_{\mathrm{PS}}, a) = A + B\ m_{\mathrm{PS}}^2 + C\ a^2\ . \tag{5.21}$$

The results are shown in Fig. 5.15. Complying with the indication from the previous subsection, we have employed the published results for $\Delta\alpha_2^{\mathrm{hvp}}$ obtained from $SU(3)$ flavour separation [Jegerlehner 2011] in Fig. 5.15 together with the factor needed to take the different reference values into account. Since we do not have information on the correlation of the data in [Jegerlehner 2012], we have simply added the uncertainties of $\Delta\alpha_{\mathrm{QED}}^{\mathrm{hvp}}$ and $\Delta\alpha_2^{\mathrm{hvp}}$ in quadrature thus clearly overestimating the errors of the phenomenological determination. The results are again completely compatible with each other.

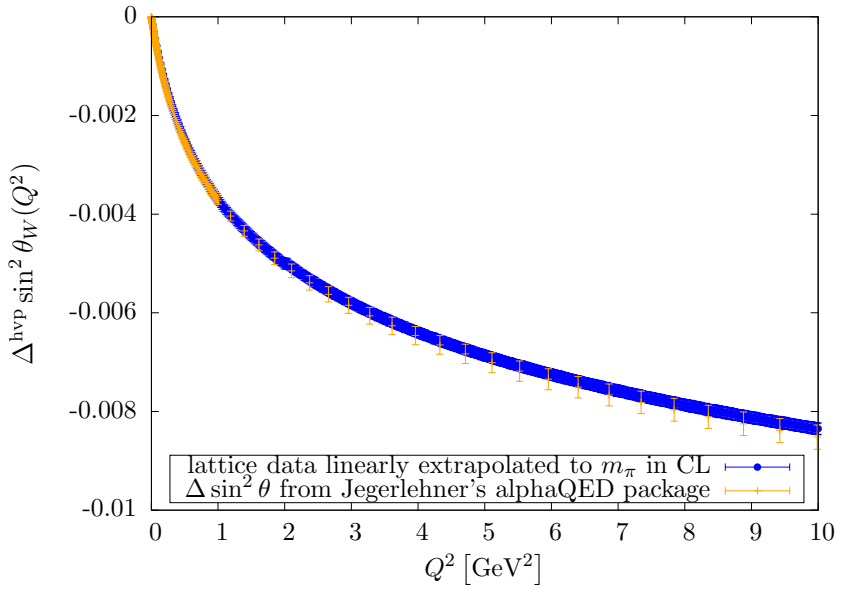

Figure 5.15.: $N_f = 2+1+1$ contribution to the leading-order hadronic contribution $\Delta^{\mathrm{hvp}} \sin\theta_W$ compared to the difference of the data collected in [Jegerlehner 2012]. The lattice data are extrapolated to the physical point and to the continuum limit (CL).

Systematic uncertainties

Since the systematic uncertainties stem from the same sources as for $\Delta\alpha^{\mathrm{hvp}}_{\mathrm{QED}}$ discussed before, the relative errors are the same and only the absolute numbers differ due to the different prefactors of the renormalised vacuum polarisation function. Naturally, also the plots all look very similar. Therefore, we refrain from discussing the systematic effects separately and showing all the figures again and only summarise the general findings.

As before, due to the light quark contribution being an order of magnitude bigger than the contributions from the heavy quarks, we only need to take systematic uncertainties of this part into account. The dominant source of systematic errors is again the choice of the vacuum polarisation fit function as depicted in Fig. 5.16. The only other relevant effect comes from the excited state contamination of the ρ-meson correlator and is shown in Fig. 5.17.

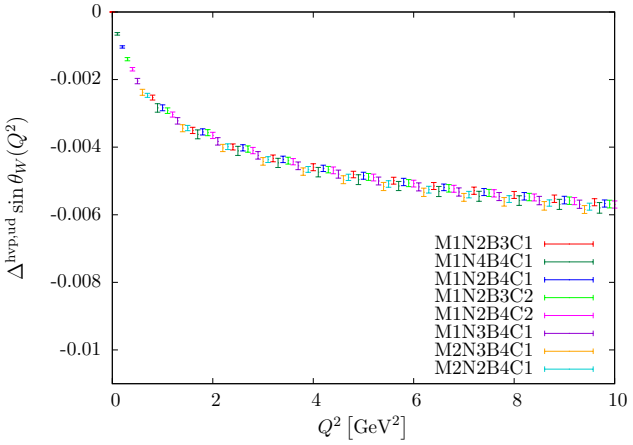

Figure 5.16.: Light quark contribution to $\Delta^{\mathrm{hvp}} \sin\theta_W$ obtained from different fit functions. The standard fit is M1N2B4C1.

Finite volume effects and the usage of rather heavy pion masses in the chiral extrapolation seem to be negligible in our calculation as outlined before. The only unknown systematic effect are the heavy-flavour disconnected contributions which we have neglected here. Since the connected heavy quark pieces are already much smaller than those of the light quarks, it is likely that this does not impair our results at the current level of accuracy. Our analysis of the light-quark disconnected contributions described at the beginning of Sect. 4.1.2 indicates that their contribution is currently below the statistical uncertainty of our results.

Final results for selected momentum values

In Tab. 5.4, we collect our results for $\Delta^{\mathrm{hvp}} \sin^2\theta_W$ with statistical as well as systematic uncertainties for selected momentum values. The systematic uncertainties have been obtained by adding in quadrature the individual systematic uncertainties from the choice of fit function and the excited state contamination of the ρ-correlator for which half the difference between the fit results which are furthest apart has been taken. Additionally, experiments which have measured or will measure the weak mixing angle in the respective momentum region are indicated. Lattice QCD results can directly be used for the theo-

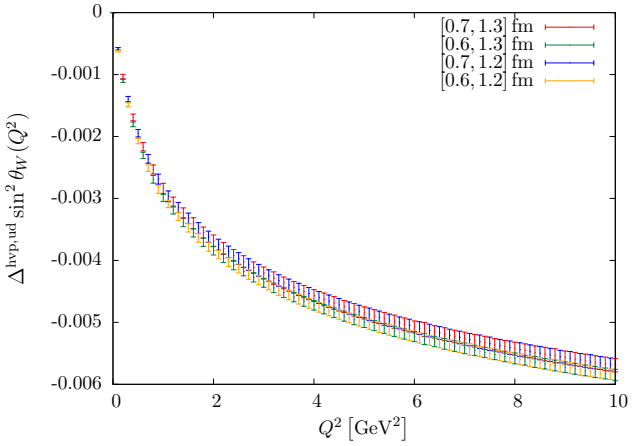

Figure 5.17.: Light quark contribution to $\Delta^{\mathrm{hvp}} \sin\theta_W$ obtained with different fit ranges for the ρ meson properties. The standard fit range is [0.7 fm, 1.2 fm].

Q^2 [GeV^2]	this work	experiment
0.02	$-0.158(05)(08) \cdot 10^{-3}$	E158, Qweak
1.00	$-3.706(83)(127) \cdot 10^{-3}$	PVDIS
2.00	$-5.021(96)(135) \cdot 10^{-3}$	PVDIS
3.00	$-5.801(104)(135) \cdot 10^{-3}$	SoLID
4.00	$-6.398(102)(135) \cdot 10^{-3}$	SoLID
6.00	$-7.251(111)(136) \cdot 10^{-3}$	SoLID
8.00	$-7.867(112)(137) \cdot 10^{-3}$	SoLID
10.0	$-8.352(119)(138) \cdot 10^{-3}$	SoLID

Table 5.4.: $\Delta^{\mathrm{hvp}} \sin^2\theta_W$ for selected values of Q^2. The first error of the lattice results is statistical, the second systematic. Several low-energy experiments sensitive to the respective momentum regions are indicated in the last column.

retical prediction of the outcomes of those experiments due to the studied experimental processes proceeding at spacelike momentum transfers $q^2 < 0$ in the continuum.

The outcome of the E158 experiment at the SLAC linear accelerator [SLAC E158 2005] was the first successful measurement of parity violation in electron-electron (Møller) scattering. The momentum transfer was $Q^2 = 0.026\,\mathrm{GeV}^2$. The Qweak experiment conducted at JLAB in 2012 measured parity violation in electron-proton scattering at almost exactly the same momentum transfer [Qweak 2014]. The data is still being analysed. The predicted final uncertainty is about 5% or $0.7 \cdot 10^{-3}$ taking the central SM value. Another JLAB experiment performed by the PVDIS collaboration determined the weak mixing angle from parity-violating deep inelastic scattering [PVDIS 2014, Wang et al. 2014] which effectively means electron-quark scattering at $Q^2 = 1.085\,\mathrm{GeV}^2$ and $Q^2 = 1.901\,\mathrm{GeV}^2$. The envisioned successor of the PVDIS experiment which also measures parity violation in electron-quark scattering is the SoLID spectrometer proposed at JLAB [SoLID 2014]. It can study about 20 kinematic points with Q^2 ranging from about $2\,\mathrm{GeV}^2$ to about $10\,\mathrm{GeV}^2$. Its target accuracy is $6 \cdot 10^{-4}$. Our results in Tab. 5.4 indicate that it will be essential to take at least the leading QCD correction into account in order to deploy the whole potential of the SoLID experiment in the search for new physics beyond the SM.

5.4. Summary and outlook

Hadronic contributions to the running of electroweak parameters nowadays constitute the major uncertainties of their values and thus necessitate an exact determination in order to fully exploit the potential of the low-energy experiments intended to detect signs for new physics beyond the SM. Even at high energies the uncertainties of the hadronic contributions limit the precision achievable in predictions for future particle colliders. In this chapter, we have considered the running of α_{QED} and of the weak mixing angle which represents one of the most important parameters of the SM and provides a sensitive probe of new physics over a large energy range.

As we have demonstrated in this chapter, lattice QCD provides a most valuable tool to compute these hadronic contributions from first principles alone as it can be used to compute to a good precision the leading-order hadronic contributions to the running of α_{QED} and $\sin^2\theta_W$. In particular, we have carried out the first dynamical four-flavour calculation of the leading-order hadronic contribution to the running of the fine structure constant and the first lattice QCD calculation of the leading hadronic contribution to the shift of the weak mixing angle at energies between 0 and $10\,\mathrm{GeV}^2$. In both cases the chiral as well as continuum extrapolations have been performed. A main effort has been undertaken to assess systematic uncertainties on a quantitative level.

For α_{QED} agreement of our results with a phenomenological determination is observed with an even comparable statistical uncertainty. For α_2, our lattice calculation has identified the perturbatively inspired $SU(2)$ flavour separation neglecting singlet contributions employed in the phenomenological analysis before to be not suitable. This constitutes an important contribution to the dispersive analyses and thus to achieving theoretical predictions which are precise enough to match the envisioned accuracy of future experiments, especially the SoLID experiments for whose success it will be vital to take the hadronic contributions to the running of the weak mixing angle properly into account as we have demonstrated above.

However, we have also found that the systematic effects of the calculations still exceed the statistical errors. The dominant systematic uncertainty has been identified to be the choice of fit function. Thus, methods which try to avoid fitting the vacuum polarisation like the analytic continuation method presented in Sect. 4.2.2 are promising to reduce the overall uncertainty. Further improvement is also expected from increasing the statistical precision which would also more strongly constrain the vacuum polarisation fit. Such improvements might be accomplished by the use of the all-mode-averaging [Blum et al. 2013b] or the exact deflation [Saad 1984, Neff et al. 2001] techniques.

Chapter 6

The lepton anomalous magnetic moments

This chapter is devoted to one of the most active research topics of contemporary lattice field theory, the anomalous magnetic moment of the muon or $(g-2)_\mu$ for short. The reason for the big interest in this quantity is the potential to detect hints for new physics as explained in Sect. 6.1. However, there is more than one lepton in the SM, see chapter 1, and while $(g-2)_\mu$ constitutes a benchmark quantity for the search of new physics, the electron $(g-2)$ is used for a determination of the fine structure constant at zero-momentum transfer and is thus equally important. Thus, we study also the anomalous magnetic moments of the other charged leptons. As we will discuss below, these are important physical quantities in their own right and furthermore provide expedient checks of our parametrisation of the hadronic vacuum polarisation function in different momentum regions. This chapter is to a significant extent based on our articles [Feng et al. 2012b, Burger et al. 2014a, Burger et al. 2014b, Burger et al. 2014c, Burger et al. 2015a].

6.1. Motivation

As mentioned before, the SM contains three electrically charged leptons l (as well as their antileptons), mainly differing in mass, the electron, the muon, and the τ-lepton with $m_e : m_\mu : m_\tau \approx 1 : 207 : 3477$ [PDG 2014]. Their magnetic moments, in particular their so-called anomalous magnetic moments, a_l, control their behaviour in an external magnetic field.

Being the lepton with the smallest mass, the electron is stable. This leads to the electron magnetic moment being one of the most precisely determined quantities in nature. In fact, the latest experimental [Hanneke et al. 2008] and SM values [Aoyama et al. 2012a, Aoyama et al. 2015] agree up to 9 digits, cf. [Giudice et al. 2012] and references therein. This constitutes one of the cornerstone results for quantum field theories to be recognised as the correct mechanism for describing particle interactions.

The very good agreement of the electron magnetic moment between experiment and SM calculations is not matched by the muon anomalous magnetic moment. Here, a long-standing discrepancy between the SM calculation, see e.g. [Jegerlehner and Nyffeler 2009, Miller et al. 2012, Blum et al. 2013a, Brambilla et al. 2014] for a recent review, and its experimental determination [Muon (g-2) 2006, Roberts 2010a] is observed varying between 2.4σ [Davier et al. 2011] and 4.9σ [Benayoun et al. 2012a]. This is illustrated in Fig. 6.1 One reason for the observed discrepancy could be that the magnetic moment of the muon receives larger non-perturbative contributions than the one of the electron. On the other hand, it is supposed to be also more sensitive to beyond the SM physics, since for a large class of theories new physics contributions are expected to be proportional to the squared lepton mass [Czarnecki and Marciano 2001, Jegerlehner 2008b, Jegerlehner and Nyffeler 2009, Miller et al. 2012]. The persistent and often larger than $3\,\sigma$ discrepancy has

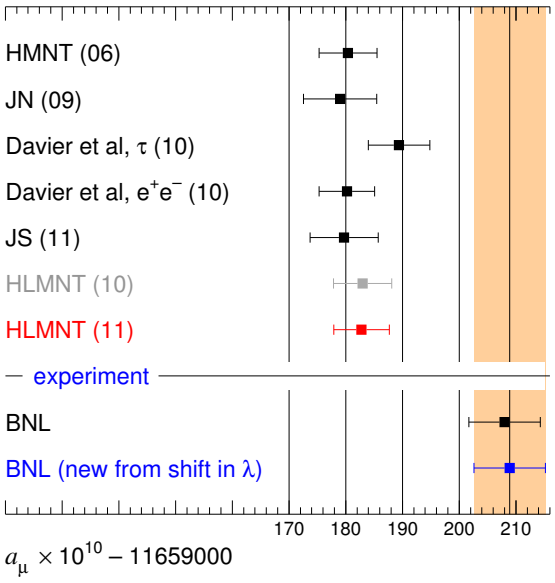

Figure 6.1.: Selection of SM predictions for a_μ compared to the experimental value. The different theoretical values arise from different approaches in the phenomenological analyses used to determine the leading order hadronic contributions. The figure is taken from [Hagiwara et al. 2011]. The phenomenological results indicated by HMNT (06), JN (09), Davier et al. (10), JS (11), HLMNT (10), and HLMNT (11) are from [Hagiwara et al. 2007], [Jegerlehner and Nyffeler 2009], [Davier et al. 2011], [Jegerlehner and Szafron 2011], [Teubner et al. 2011], and [Hagiwara et al. 2011], respectively.

therefore led to an ever increasing interest in this quantity.

Due to the large mass of the τ-lepton this would be the optimal lepton for finding new physics. However, because its lifetime is very short ($\mathcal{O}\left(10^{-13}\right)$ s) and it decays predominantly hadronically, there currently only exist bounds on its anomalous magnetic moment from indirect measurements [DELPHI 2004] which are not precise enough to challenge the SM.

Ever since its emergence, the muon anomaly has been an important constraint for any suggested new physics (NP) model. Additionally, there has been no clear sign for NP found by the LHC experiments so far. Hence, understanding the muon discrepancy becomes even more important. Even if there were any NP signals observed at the LHC, combining these observations with those from $(g-2)_\mu$ can drastically reduce the allowed parameter space for the models, cf. [Miller et al. 2012]. Moreover, the muon anomalous magnetic moment is also sensitive to weakly interacting new particles which might be difficult to observe at the LHC.

Therefore, there are two newly proposed dedicated experiments at Fermilab [Muon (g-2) 2009, Roberts 2010b] and J-PARC [J-PARC New g-2/EDM experiment 2011] which aim to reduce the experimental uncertainty of $(g-2)_\mu$ at least by a factor of four. If this is successful, the comparison between the experimental and SM values will be com-

pletely dominated by the uncertainty of the theoretical evaluation whose by far largest part originates from the leading hadronic contribution as can be seen in Tab. 6.1. The reason is that the QED [Aoyama et al. 2012b, Aoyama et al. 2012a, Aoyama et al. 2015] and the electroweak contributions [Czarnecki et al. 1995, Czarnecki et al. 1996] to the lepton anomalous magnetic moments have been computed reliably in perturbation theory to impressive five and two loops, respectively, and their uncertainties have been found to be small, cf. Tab. 6.1.

type	value $[10^{-10}]$	error $[10^{-10}]$
QCD-LO	694.9	4.3
QCD-NLO	1.8	2.6
QED/EW	11658487.3	0.2
Total	11659184.0	5.9
Experiment	11659208.9	6.3
Discrepancy	24.9	8.7

Table 6.1.: SM contributions to a_μ [Aoyama et al. 2012a]. QCD-LO and QCD-NLO denote the leading-order and next-to-leading order QCD contributions which we will specify in Sect. 6.2 below. The values of the remaining QED and electroweak contributions are taken together and labelled QED/EW.

The above table indicates that the leading-order QCD contribution represents the ideal starting point in order to reduce the overall theoretical uncertainty. Additionally, the variation in the significance of the discrepancy between 2.4σ [Davier et al. 2011] and 4.9σ [Benayoun et al. 2012a] mentioned before results from different phenomenological analyses of the leading QCD contribution, which is mainly caused by choosing different e^+e^- scattering data sets. This is usually not even reflected in the theoretical uncertainty. However, if this deviation of the SM value and experiment remains among the few signs we have for possible extensions of the SM, it is highly desirable to know its exact size and to this end first-principle lattice QCD (LQCD) computations might prove advantageous. In fact, due to the inconsistencies of the various scattering data sets it appears unlikely that the phenomenological determinations can be rendered precise enough to match the envisioned accuracy of the new experiments [Hagiwara et al. 2011], of which the Fermilab one is scheduled to start data taking already in early 2017.

In [Giudice et al. 2012], it has been argued that it might also be feasible to detect deviations from the SM expectation in the electron magnetic moment such that also computing the hadronic contribution to this observable as precisely as possible seems to be advisable. Furthermore, a recalculation of the hadronic contributions to the anomalous magnetic moment of the electron has also been suggested in [Aoyama et al. 2012b], since they are known to be approximately twice as large as the current minor difference between the SM and the experimental values $a_e^{\mathrm{SM}} - a_e^{\mathrm{exp}} = 0.91(0.82) \cdot 10^{-12}$ [Aoyama et al. 2015]. For $(g-2)_e$ the uncertainty of the hadronic contributions is currently comparable to the one of the by far dominant QED contributions.

Even for the τ-lepton, Ref. [Pich 2014] lists several proposals for the first actual measurement of its anomalous magnetic moment, e.g. [Fael et al. 2014]. A first successful measurement in this direction has been reported in [BaBar 2015]. Although the current target accuracy is still below the value for the leading QCD contribution, if a first measurement succeeds it can be expected that this precision might soon be increased such

that having a precise value for the QCD contributions to a_τ might become important as well.

Since the leading-order (LO) hadronic contributions of the lepton anomalous magnetic moments are particularly sensitive to those virtual photon momenta that are of $\mathcal{O}\left(m_l^2\right)$, they are inherently non-perturbative and thus not accessible to perturbation theory. In order to have a purely theoretical prediction of the anomalous magnetic moments from the SM alone, a non-perturbative method needs to be employed and the only such approach we presently know is LQCD which we use here. As we have alluded to in chapter 2, in contrast to the phenomenological results it is in principle straightforward to systematically improve the LQCD values. Hence, this first dynamical four-flavour calculation of the LO QCD contributions to the lepton anomalous magnetic moments might pave the way for surpassing the phenomenological precision and thus providing a theoretical prediction accurate enough to exploit the full potential of the new experiments in the future. To this end, a major effort is made to quantify and disentangle the systematic uncertainties as this enables us to identify which parts of the computations most urgently require improvements.

In this chapter, we present the results of our four-flavour computations of the quark-connected, LO hadronic vacuum polarisation contributions to the electron, muon, and τ-lepton anomalous magnetic moments obtained from the maximally twisted mass formulation of LQCD. One important feature of the present calculation is that we adopt exactly the same strategy for all three leptons including the same fit functions presented in Sect. 4.1.2 and the same chiral and continuum extrapolations. Additionally to the systematic uncertainties discussed in the preceding chapter for $\Delta\alpha^{\text{hvp}}_{\text{QED}}$ and $\Delta^{\text{hvp}}\sin^2\theta_W$, we quantify the influence of the light-quark disconnected contributions on one of our $N_f = 2+1+1$ ensembles. Another very important feature is again that incorporating the complete first two generations of quarks enables us to directly and unambiguously compare our results for the leading hadronic contributions to a_l with the values obtained from phenomenological analyses relying on experimental data and a dispersion relation. We note that the contributions from third-generation quarks can be neglected, since they are smaller than the current theoretical accuracy, as can be inferred e.g. from the data tables of Ref. [Benayoun et al. 2012a]. Recently, the bottom quark contribution to a_μ^{hvp} has been explicitly computed on the lattice [Colquhoun et al. 2015] confirming it to be one order of magnitude smaller than the current uncertainty of the phenomenological determinations of a_μ^{hvp}.

The next section comprises the definitions of the magnetic moment of a particle in general and its LO hadronic contribution in particular. Afterwards, we discuss the muon magnetic moment in Sect. 6.3.1 before repeating the analysis for the electron in Sect. 6.3.2 and the τ-lepton in Sect. 6.3.3. We complete this chapter in Sect. 6.4 with a summary and an outlook.

6.2. Definitions

The magnetic moment $\vec{\mu}$ is an intrinsic property of every charged lepton. It is proportional to the spin $\vec{s}$ of the particle

$$\vec{\mu} = g_l\,\mu_B\,\vec{s}, \tag{6.1}$$

where g_l is the gyromagnetic ratio or g-factor and $\mu_B = \frac{e}{2m_l}$ is known as Bohr's magneton. The magnetic moment governs the response of the particle to an external magnetic field

$\vec{B}$ according to

$$\mathcal{H} = -\vec{\mu} \cdot \vec{B} \,. \tag{6.2}$$

Originally it had been believed that, as for the magnetic moment of the orbital angular momentum, μ_B would be the only proportionality constant needed between magnetic moment and spin [Jegerlehner 2008b]. However, the Dirac theory has, at that time unexpectedly, predicted $g_l = 2$ [Dirac 1928a, Dirac 1928b] for a free lepton which has been experimentally confirmed for the electron soon after [Kinster and Houston 1934]. Quantising the theory, quantum effects also known as radiative corrections appear which lead to the "anomaly", i.e. $g_l > 2$. This is quantified by the anomalous magnetic moment defined to be

$$a_l = \frac{g_l - 2}{2} = \frac{\alpha}{2\pi} + \mathcal{O}(\alpha^2) \,, \tag{6.3}$$

with the leading one-loop QED result given by [Schwinger 1948]

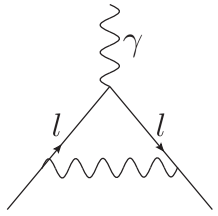

$$= \frac{\alpha}{2\pi} \,.$$

Nowadays those quantum corrections involve contributions from all parts of the Standard Model (SM) and possibly even NP,

$$a_l = a_l^{\mathrm{QED}} + a_l^{\mathrm{EW}} + a_l^{\mathrm{QCD}} (+a_l^{\mathrm{NP}}) \,. \tag{6.4}$$

In particular, due to the formidable accuracy achieved in the latest experimental measurements and the theoretical calculations, we can test the complete SM by looking at just one single number, namely the anomalous magnetic moment of the muon, a_μ. As mentioned before, this can then also provide hints on the nature and the scale of NP.

Since often the connection of a_l with the electromagnetic form factors is invoked, we note here that the magnetic moment can also be defined by the static limit ($q^2 \to 0$) of the general vertex function Γ^μ for lepton-photon interactions with $q = p' - p$, $\overline{u}(p')$ and

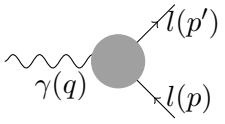

$$= i\, e\, \overline{u}(p')\, \Gamma^\mu(q)\, u(p)$$

$u(p)$ denoting the Dirac spinors of antilepton and lepton, respectively, and

$$\Gamma^\mu = \left[\gamma^\mu F_1(q^2) + \frac{i\sigma^{\mu\nu} q_\nu}{2m_l} F_2(q^2) \right] , \tag{6.5}$$

where $\sigma^{\mu\nu} = \frac{i}{2}[\gamma_\mu, \gamma_\nu]$ denotes the spin-$\frac{1}{2}$ angular momentum tensor. All information about the lepton's interaction with an external electromagnetic field is encoded in the electric or Dirac form factor $F_1(q^2)$ and the magnetic or Pauli form factor $F_2(q^2)$. In the static limit, $F_1(0) = 1$ is the electric charge of the lepton in units of e, known as charge

normalisation condition, while the g-factor is given by

$$g_l = 2F_1(0) + 2F_2(0) = 2(1 + F_2(0))\,. \tag{6.6}$$

Hence, the lepton anomalous magnetic moments are identical to the magnetic form factors in the static limit,

$$a_l = F_2^l(0)\,. \tag{6.7}$$

At tree-level they vanish identically. This is a consequence of the SM being a local, relativistic, and renormalisable quantum field theory [Jegerlehner 2008b] since this implies that the lepton anomalous magnetic moments are no independently adjustable parameters and hence carry unambiguous predictability.

The observable consequence of a non-vanishing anomalous magnetic moment is the Larmor precession of the spin of polarised leptons in an external magnetic field with respect to their momentum at an angular frequency of

$$\vec{\omega}_a = a_l \frac{e\vec{B}}{m_l}\,. \tag{6.8}$$

For $a_l = 0$, the lepton spin would remain parallel to its momentum. This is exploited in the measurements of a_e and a_μ and illustrated for the case of the muon in Fig. 6.2 taken from [Jegerlehner and Nyffeler 2009]. Further details can also be found in the reviews [Jegerlehner 2008b, Miller et al. 2012] and the original experimental articles [Muon (g-2) 2006, Hanneke et al. 2008].

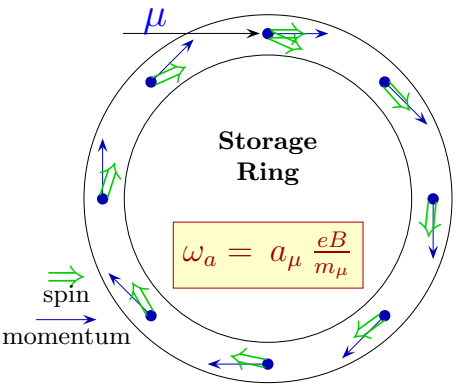

Figure 6.2.: Measurement principle for the determination of a_μ in a muon storage ring from Ref. [Jegerlehner and Nyffeler 2009]. In the BNL storage ring featuring a diameter of 14 m the spin direction changed by approximately 12°/cycle [Muon (g-2) 2006].

The QCD contributions to a_l comprise the leading-order (LO) hadronic contribution at $\mathcal{O}\left(\alpha_0^2\right)$ originating from a single insertion of the hadronic vacuum polarisation (hvp) in the photon propagator of the leading-order QED diagram shown in Fig. 6.3 as well as higher order (HO) contributions in the QED coupling which can be divided into those

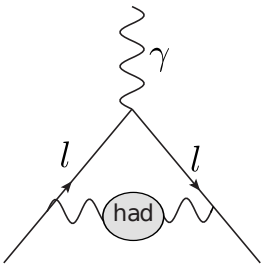

Figure 6.3.: Feynman diagram of leading-order QCD contribution to the $(g-2)$ of the SM leptons.

from multiple insertions of the hadronic vacuum polarisation (hvp) in the above diagram and the light-by-light (lbl) scattering contribution which both start at $\mathcal{O}\left(\alpha_0^3\right)$,

$$a_l^{\mathrm{QCD}} = a_l^{\mathrm{LO,hvp}}(\alpha_0^2) + a_l^{\mathrm{HO,hvp}}(\alpha_0^3) + a_l^{\mathrm{lbl}}(\alpha_0^3)\,. \tag{6.9}$$

This implies that the LO hadronic contribution is more than an order of magnitude larger than the other QCD contributions as we have already seen in Tab. 6.1. Due to the great accuracy achieved by the perturbative calculations of the QED and weak contributions, currently the LO hadronic correction contributes the largest uncertainty to the theoretical determination of a_μ and a_τ. Thus, it appears to be the ideal starting point for improving the SM prediction of these two important quantities. In the following, we will only consider the LO QCD contribution and leave out "LO" to simplify notation.

As Blum has proven based on the work by [Lautrup et al. 1972], the LO hadronic contribution to the lepton anomalous magnetic moments, a_l^{hvp}, can be directly computed in Euclidean space-time by evaluating the Feynman integral depicted in Fig. 6.3 [Blum 2003]. Hence, we simply have to integrate the renormalised hadronic vacuum polarisation function, $\Pi_{\mathrm{R}}(Q^2)$, which we are well acquainted with by now, with a kernel function $w\left(\frac{Q^2}{m_l^2}\right)$ known from the perturbative one-loop QED calculation conducted by Schwinger [Schwinger 1948],

$$a_l^{\mathrm{hvp}} = \alpha_0^2 \int_0^\infty \frac{dQ^2}{Q^2} w\left(\frac{Q^2}{m_l^2}\right) \Pi_{\mathrm{R}}(Q^2)\,. \tag{6.10}$$

α_0 denotes again the fine structure constant at zero momentum transfer, Q^2 the Euclidean momentum, and m_l the lepton mass. As expected from using the LO resonance chiral perturbation theory result for the vacuum polarisation in Eq. (5.4), the definition in Eq. (6.10) results in a highly non-linear pion mass dependence for the light quarks. This can be seen by studying the LO contribution

$$a_l^{\mathrm{hvp,f}} \propto \alpha_0^2 g_V^2 \frac{m_l^2}{m_V^2}\,, \tag{6.11}$$

which corresponds to a typical vector meson term. Phenomenologically, the respective contributions from only the first three vector mesons, ρ, ω, and Φ, have been found to account for over 80% of the total a_μ^{hvp} [Jegerlehner 2008a]. In contrast to g_V, m_V is non-linear in the squared pion mass as we have shown e.g. in Fig. 5.1. This implies that also

a_l^{hvp} determined according to Eq. (6.10) exhibits a non-linear quark mass dependence and can thus not straightforwardly be extrapolated to the physical point. Therefore, in [Feng et al. 2011a, Renner et al. 2012] a modified definition

$$a_l^{\mathrm{hvp}} = \alpha_0^2 \int_0^\infty \frac{dQ^2}{Q^2}\, w\left(\frac{Q^2}{H^2}\frac{H_{\mathrm{phys}}^2}{m_l^2}\right) \Pi_{\mathrm{R}}(Q^2) \tag{6.12}$$

has been proposed, which is in principle very similar to the ones encountered before in Eqs. (5.5) and (5.19) for α_{QED} and α_2, respectively. Again H stands for some hadronic scale determined at unphysically high pion masses. In contrast to the approach for the electroweak coupling constants presented in the previous chapter, we choose as the hadronic scale the lowest lying ρ-meson state m_V for all flavours, since this can also be viewed as a lattice redefinition of the lepton masses

$$m_{\bar{l}} = m_l \cdot \frac{H}{H_{\mathrm{phys}}}\ , \tag{6.13}$$

which should be treated consistently for the contributions of all flavours even those originating from the heavy quark currents. Substituting m_l in Eq. (6.11) by the expression in Eq. (6.13) with $H = m_V$, immediately reveals the advantage the redefinition has for the chiral extrapolation of the light-quark contributions, namely that the non-linear dependence on m_V is cancelled to a large extent and thus the pion mass dependence can be expected to be the linear one of g_V found in Sect. 4.1.3. As before, $H = H_{\mathrm{phys}} = 1$ reproduces the standard definition in Eq. (6.10). Up to lattice artefacts the standard definition is also recovered at the physical value of the pion mass when the ratio H/H_{phys} becomes one. The weight function $w(r)$ which can be written as a function of either $r = \frac{Q^2}{m_l^2}$ or $r = \frac{Q^2}{H^2}\frac{H_{\mathrm{phys}}^2}{m_l^2}$ reads

$$w(r) = \frac{64}{r^2(1+\sqrt{1+4/r})^4\sqrt{1+4/r}} \tag{6.14}$$

and for $r = \frac{Q^2}{H^2}\frac{H_{\mathrm{phys}}^2}{m_l^2}$ it is peaked at

$$Q^2_{\mathrm{peak}} = (\sqrt{5}-2)\frac{H^2}{H^2_{\mathrm{phys}}} m_l^2\ . \tag{6.15}$$

Since the magnitude of the masses of the three charged SM leptons spans four orders of magnitude, the corresponding contributions to the anomalous magnetic moments differ substantially and probe very different energy regions. This is depicted in Fig. 6.4, where the saturation of the integral in Eq. (6.12) for one of our ensembles, namely B55.32 featuring $m_{\mathrm{PS}} \approx 390\,\mathrm{MeV}$, $a \approx 0.08\,\mathrm{fm}$ and $L = 2.5\,\mathrm{fm}$, is shown for all three leptons by plotting

$$R_l(Q^2_{\mathrm{max}}) = \frac{a_l^{\mathrm{hvp}}(Q^2_{\mathrm{max}})}{a_l^{\mathrm{hvp}}(100\,\mathrm{GeV}^2)}\ , \tag{6.16}$$

where $a_l^{\mathrm{hvp}}(Q^2_{\mathrm{max}})$ is the LO hadronic contribution to the lepton anomalous magnetic moment integrated up to Q^2_{max}.

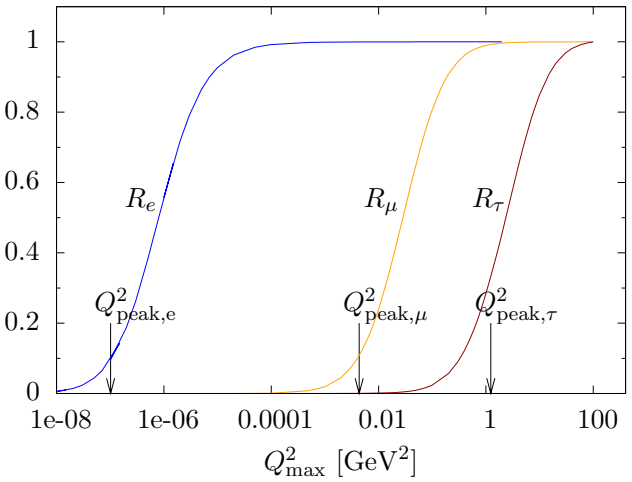

Figure 6.4.: Comparison of the dependence on the upper integration bound in Eq. (6.12) of the four-flavour lepton anomalous magnetic moments. The blue curve represents the ratio defined in Eq. (6.16) for the electron, the orange one for the muon, and the dark red one for the tau. $Q^2_{\text{peak},l}$ denotes the momentum value where the kernel function in Eq. (6.12) attains its maximum.

6.3. Results from twisted mass lattice QCD

6.3.1. Muon $(g-2)$

Triggered by Ref. [Blum 2003], the computation of hadronic contributions to the muon anomalous magnetic moment, a_μ^{hvp}, has recently been a major target of the lattice community, see for instance [QCDSF 2004, Aubin and Blum 2007, Feng et al. 2011a, Boyle et al. 2012, Della Morte et al. 2012, Bernecker and Meyer 2011, Aubin et al. 2012, Renner et al. 2012, Feng et al. 2013]. Due to the potentially big impact these calculations might have for our understanding of the universe, a_μ is considered a prime candidate observable for finding indications of physics beyond the SM. These older computations, however, only took up to $N_f = 2+1$ dynamical quark flavours into account and thus could not unambiguously be compared with the results from the dispersive analyses because those as well as the experimentally obtained values for a_μ at the current level of precision are sensitive to the complete first two generations of quarks. In fact, as we will see below, the charm quark contribution is comparable in magnitude to the complete electroweak and the light-by-light contributions mentioned earlier. Nevertheless, the former LQCD determinations of a_μ^{hvp} put us in the favourable position of actually having lattice data employing other fermion discretisations to compare our intermediate two- and three-flavour results with thereby checking the universality of the obtained values. Hence, in the presentation of our results below we will add the intermediate step of considering $N_f = 2+1$ valence quarks before discussing the full result. As usual we commence with the contribution of up and down quarks.

The light quark contribution, $a_\mu^{\text{hvp,ud}}$

Considering only the light currents, for which the sea quark action is identical to the valence action, provides the contribution of the up and down quarks to the total $a_\mu^{\text{hvp,ud}}$.

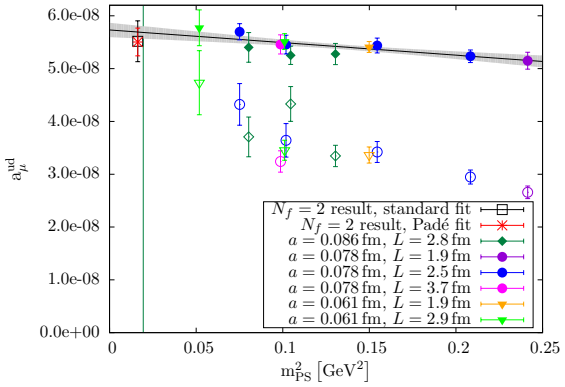

Figure 6.5.: Light-quark contribution to a_μ^{hvp} on $N_f = 2+1+1$ sea. Filled symbols correspond to Eq. (6.12) whereas results marked by open symbols have been obtained with Eq. (6.10).

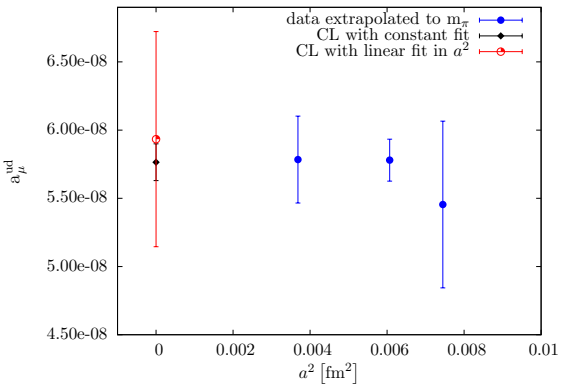

Figure 6.6.: Continuum extrapolation of $a_\mu^{\mathrm{hvp,ud}}$ after the linear extrapolation to the physical pion mass has been performed separately for each lattice spacing.

The pion mass dependence of this light quark portion is shown in Fig. 6.5. To perform the chiral extrapolation we utilise our lattice redefinition $a_{\overline{\mu}}^{\mathrm{hvp,ud}}$, i.e. Eq. (6.12) with $H = m_V$, since this allows for a linear extrapolation in the squared pion mass, m_{PS}^2 (broken black line with light grey error-band) according to

$$a_\mu^{\mathrm{ud}}\left(a, m_{\mathrm{PS}}^2\right) = A + B\, m_{\mathrm{PS}}^2 \tag{6.17}$$

with fit parameters A and B. It has been found that this simple ansatz is sufficient to describe the data.

As shown in Fig. 6.6, with the current precision of our data we do not observe significant lattice spacing artefacts in $a_\mu^{\mathrm{hvp,ud}}$ on the four-flavour ensembles. Therefore, we believe that also at the physical point lattice artefacts will not have a big impact, especially because lattice artefacts are found to be reduced by the introduction of the clover-term in Eq. (4.2) [Abdel-Rehim et al. 2014]. Thus, the light-quark contribution on the four-flavour sea extrapolated to the physical point with the help of the linear fit given in Eq. (6.17) can be compared to the value obtained with only two dynamical quark flavours directly at the physical point

$$\begin{aligned} a_\mu^{\mathrm{hvp,ud}} &= 5.69(12)\cdot 10^{-8} \quad (N_f = 2+1+1) \\ a_\mu^{\mathrm{hvp,ud}} &= 5.52(39)\cdot 10^{-8} \quad (N_f = 2\,\text{physical}) \end{aligned} \tag{6.18}$$

yielding fully compatible results. The same is true when comparing the four-flavour result with the extrapolated value of the old two-flavour calculation [Feng et al. 2011a]

$$a_\mu^{\mathrm{hvp,ud}} = 5.72(16)\cdot 10^{-8}\,. \tag{6.19}$$

This indicates that the impact of the heavy second-generation sea quarks on the light quark contribution to the leading order QCD correction of the muon anomalous magnetic moment is small. The difference between the error of the two extrapolated results is that

the $N_f = 2 + 1 + 1$ uncertainty given above is only of statistical nature whereas the old $N_f = 2$ value involves an estimate of systematic effects. We will estimate the systematic uncertainty of our calculation below and compare the results with full error budgets in Tab. 6.4.

Additionally, in Fig. 6.5 we have indicated the result of a [1,1] Padé fit of the data collected at the physical value of the pion mass for which the upper bound of the fit interval is $Q^2_{\text{max}} = 1.5\,\text{GeV}^2$. Full agreement is observed. However, since especially for low-order Padé approximants it is not clear whether they are reliable up to $Q^2_{\text{max}} = 1.5\,\text{GeV}^2$, cf. the discussion in Sect. 4.2.1, we prefer to confront our results with those of two types of Padé fits for the light quark contribution to the electron $(g-2)$ in Sect. 6.3.2 for which a smaller Q^2_{max} can be used due to the early saturation of the integral in Eq. (6.12) which has been depicted in Fig. 6.4 above.

Briefly returning to the discussion of lattice artefacts, we repeat that the result with four dynamical sea quarks presented above has been obtained by fitting all data from the ensembles listed in Tab. 4.1 simultaneously by a linear fit in m^2_{PS}. Performing a combined fit in m^2_{PS} and a^2 to all the data in Fig. 6.5 yields a coefficient of the a^2-term $1.08\,\sigma$ away from and thus almost compatible with zero. The results from first extrapolating $a_{\overline{\mu}}^{\text{hvp,ud}}$ linearly in m^2_{PS} to the physical point for a fixed value of the lattice spacing and then performing the continuum limit are shown in Fig. 6.6. Here we see that all chirally extrapolated values agree within the errorbars. We can therefore use a constant extrapolation to zero lattice spacing giving $a_\mu^{\text{hvp,ud}} = 5.76(13) \cdot 10^{-8}$ which is compatible with the result quoted in Eq. (6.18). This is why we have stated above that for the present level of precision of our data, we do not observe significant lattice spacing artefacts in $a^{\text{hvp}}_{\mu,\text{ud}}$ and hence the comparison with the ensemble directly at the physical point seems to be admissible. However, this is likely to change once more precise results can be computed.

The three-flavour contribution, $a_\mu^{\text{hvp,uds}}$

For the three-flavour contribution we use again the ρ-meson mass as hadronic scale H in order to have a consistent redefinition of the muon mass on the lattice. It turns out that this leads to larger statistical uncertainties for the strange quark contribution than employing the standard definition of $a_\mu^{\text{hvp,s}}$. In addition, the dependence of $a_\mu^{\text{hvp,s}}$ on the squared pion mass becomes non-linear. However, since the light quark contribution constitutes by far the largest part of a_μ^{hvp}, we still obtain a mild pion mass dependence for $a_\mu^{\text{hvp,uds}}$, the sum of the light and strange quark contributions, as can be seen when looking at the twisted mass points (upper set of data points with filled symbols) in Fig. 6.7.

In this figure we also include data obtained with other fermion actions from the literature naturally possessing different cut-off effects. The orange downward triangles are from [Della Morte et al. 2012] using clover-improved Wilson fermions with two dynamical light and a quenched strange quark. The green upward triangles and diamonds have been computed with $N_f = 2 + 1$ dynamical domain wall fermions [Boyle et al. 2012]. These results from the other groups employ the standard definition for a_μ^{hvp} given in Eq. (6.10). We therefore add also twisted mass points obtained with the standard definition (lower set of twisted mass points with open symbols). We observe overall agreement between the different lattice determinations for the raw data of $a_\mu^{\text{hvp,uds}}$ when the standard definition is used, except for some of the points obtained with domain-wall fermions at higher pion masses. Besides the aforementioned varying cut-off effects, slight differences can also

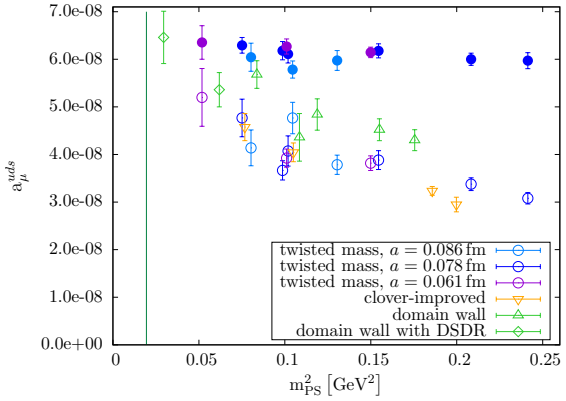

Figure 6.7.: Comparison of three-flavour contribution to $a_\mu^{\rm hvp}$ obtained with different fermion actions.

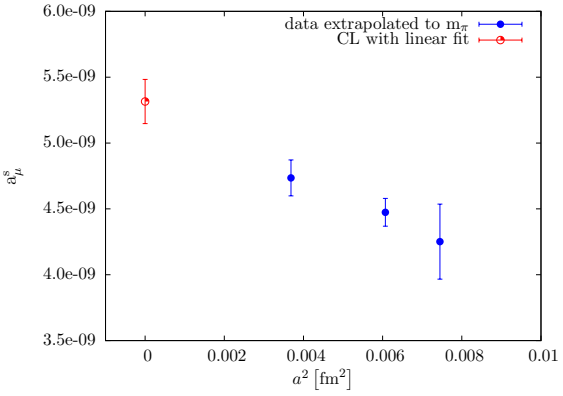

Figure 6.8.: Continuum extrapolation of $a_\mu^{\rm hvp,s}$.

originate from utilising different conditions to determine the strange quark mass used for computing the strange quark contribution to $a_\mu^{\rm hvp,uds}$. It is clear from Fig. 6.7 that the improved definition of $a_\mu^{\rm hvp}$ leads to a smooth and linear extrapolation to the physical point. In contrast, the standard definition of $a_\mu^{\rm hvp}$ needs a more complicated extrapolation resulting in a larger uncertainty as we will see in the comparison of the final results presented in Tab. 6.4.

Since the strange quark is about 19 times heavier than the light quarks [PDG 2014], the size of lattice artefacts is expected to be significantly enhanced for the strange quark contribution. In fact, if we take lattice artefacts into account performing a combined fit in $m_{\rm PS}^2$ and a^2, we find a definitely non-zero value for the coefficient of the a^2-term. The presence of lattice artefacts can also be seen when looking at the lattice spacing dependence of $a_\mu^{\rm hvp,s}$ obtained with the standard definition linearly extrapolated to the physical point as shown in Fig. 6.8. From this figure it is obvious that the limit $a \to 0$ can no longer be obtained by a constant extrapolation.

As a result of this observation it is clear that we have to take an a^2-term into account in order to arrive at a result for $a_\mu^{\rm hvp,uds}$ meaningful also in the continuum theory. We therefore use the the same type of fit function as for $\alpha_{\rm QED}$ and $\sin^2\theta_W$ in the previous chapter to determine $a_\mu^{\rm hvp,uds}$ in the continuum limit at the physical point

$$a_\mu^{\rm hvp,uds}(m_{\rm PS}, a) = A + B\ m_{PS}^2 + C\ a^2 \tag{6.20}$$

with A, B, C denoting the parameters of the fit. Since we add the light quark and the strange contributions before performing the fit, the coefficient C will also contain terms $\sim m_{c,R}^2$, $m_{s,R}^2$ from the renormalised charm and strange quark mass and might also receive contributions from lattice artefacts possibly present in the light quark piece. Let us mention again that we omit a linear term in a since we have shown in Sect. 3.2.2 that automatic $\mathcal{O}(a)$ improvement is retained for our definition of the hadronic vacuum polarisation function at maximal twist. The value resulting from this fit at $m_{\rm PS} = m_\pi$ and zero lattice spacing is represented in Fig. 6.9 by the red triangle slightly displaced from the physical point in order to facilitate the comparison with the phenomenological result. The dashed lines represent $a_\mu^{\rm hvp,uds}(m_{\rm PS}, a)$ at fixed values of the lattice spacing as indicated

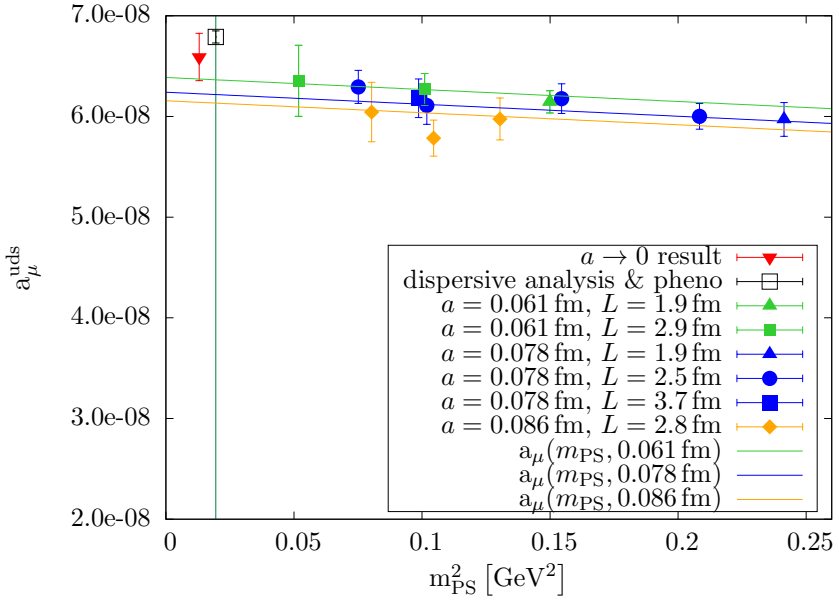

Figure 6.9.: Three-flavour contribution to a_μ^{hvp}. The phenomenological value depicted by the open square is extracted from [Jegerlehner 2008a] assuming quark-hadron duality.

by the colours. We have checked in addition that performing chiral and continuum limit extrapolations independently yields a result compatible with the one obtained from the combined fit.

In order to compare our three-flavour value to a result from a dispersive analysis, we need to disentangle the quark flavours in the phenomenological analysis. To this end, we have to reweight the total a_μ^{hvp}. As alluded to in the context of the determination of the LO QCD contribution to the running of α_2 in the previous chapter, there are various possibilities to carry out such a reweighting. We have decided to reweight the values given in [Jegerlehner 2008a] by the charges of the active flavours. This approach is based on the assumption of quark-hadron duality. For more details and an alternative method see [Petschlies 2013]. Given the ambiguity of such an approach we indicate by the abbreviation "pheno" that a certain extra phenomenological analysis has been employed. Comparing our lattice result with this phenomenological extraction method leads to

$$\begin{aligned} a_\mu^{\text{hvp,uds}} &= 6.59(23) \cdot 10^{-8} \quad (N_f = 2+1+1) \\ a_\mu^{\text{hvp,uds}} &= 6.79(05) \cdot 10^{-8} \quad (\text{pheno}) \end{aligned} \tag{6.21}$$

where we find agreement within the comparatively large error of our LQCD determination. Note, however, that due to our simplified chiral extrapolation this uncertainty is much smaller than that obtained in earlier computations [Boyle et al. 2012, Della Morte et al. 2012]. For a comparison of the final results we again refer to Tab. 6.4.

Given the fact that our extracted phenomenological value is certainly afflicted by an unknown systematic error, we consider it reassuring that our lattice QCD analysis can reproduce the phenomenological value at this level of accuracy. As mentioned in Sect. 6.1, this ambiguity in the comparison of lattice results and those utilising the dispersion relation

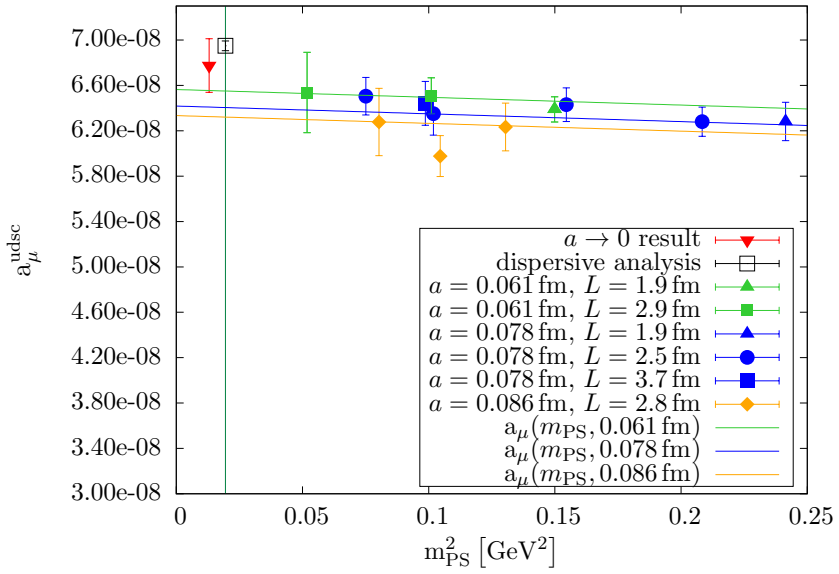

Figure 6.10.: $N_f = 2+1+1$ result for a_μ^{hvp}. This time the phenomenological value is taken from [Hagiwara et al. 2011].

can be removed by the inclusion of the charm quark in the calculation which we want to report on next.

The four-flavour contribution, a_μ^{hvp}

Adding the charm quark contribution according to Eq. (6.12) again using $H = m_V$ we are able to directly compare to experimental values and those from different dispersive analyses. Since the charm quark is even heavier than the strange quark, we again use a combined fit involving an m_{PS}^2- and an a^2-term of the form stated in Eq. (6.20). In this way, we arrive at the picture shown in Fig. 6.10. Here, our result obtained in the continuum limit and at the physical value of the pion mass, represented by the red triangle, can now be unambiguously confronted with the corresponding one from a dispersive analysis [Jegerlehner and Szafron 2011]:

$$\begin{aligned} a_\mu^{\text{hvp}} &= 6.78(24) \cdot 10^{-8} \quad (N_f = 2+1+1) \\ a_\mu^{\text{hvp}} &= 6.91(05) \cdot 10^{-8} \quad \text{(dispersive analysis)} \,. \end{aligned} \tag{6.22}$$

Comparing the value of the total a_μ^{hvp} now a convincing agreement between the two ways of determining this important quantity is found. However, it needs to be noted that at this point our result from twisted mass lattice QCD has a significantly larger statistical error than the one from the dispersive analysis.

Let us briefly remark that the result presented above also agrees with the value

$$a_\mu^{\text{hvp}} = 6.76 \cdot 10^{-8} \tag{6.23}$$

obtained for five flavours with the help of Dyson-Schwinger equations in [Goecke et al. 2011], where the systematic uncertainty of this number has been estimated to be about 10%. Since the discussion of the Dyson-Schwinger approach and its applications is beyond

the scope of this thesis we refer the interested reader to [Alkofer and von Smekal 2001,Maris and Roberts 2003, Fischer 2006] for a review.

Systematic effects

Quantifying the systematic effects constitutes an essential part in every LQCD calculation. Therefore, we provide in this section a comprehensive discussion of the various systematic uncertainties appearing in our calculation.

- *Finite-size effects*
  The systematic uncertainty of finite-size effects appears to be small in our computation. The ensembles employed for our result in Eq. (6.22) feature values of $3.35 < m_{\mathrm{PS}}\ L < 5.93$. Restricting our data to the condition $m_{\mathrm{PS}}\ L > 3.8$ yields a total
  $$a_\mu^{\mathrm{hvp}} = 6.73(25) \cdot 10^{-8}$$
  after combined continuum and chiral extrapolation which is fully compatible with the value quoted in Eq. (6.22).

  Furthermore, the ETMC has generated ensembles to explicitly check the volume dependence of a_μ^{hvp}. For the B35 ensembles with a pion mass of about 320 MeV (see Tab. 4.1) we have two different volumes ($32^3 \times 64$ and $48^3 \times 96$) at our disposal. A comparison is given in Tab. 6.2.

Ensemble	$\left(\frac{L}{a}\right)^3 \cdot \frac{T}{a}$	$a_\mu^{\mathrm{hvp,ud}}$	a_μ^{hvp}
B35.32	$32^3 \times 64$	$5.45(18) \cdot 10^{-8}$	$6.35(19) \cdot 10^{-8}$
B35.48	$48^3 \times 96$	$5.46(18) \cdot 10^{-8}$	$6.44(19) \cdot 10^{-8}$

Table 6.2.: Comparison of the light-quark contribution to a_μ^{hvp} and the total a_μ^{hvp} from two ensembles of different volumes. See Tab. 4.1 for a description of the ensembles used here.

  We conclude that finite size effects are negligible compared to our statistical uncertainty and we therefore do not take them as a systematic error into account. This is again substantiated by the dedicated investigation of the Budapest-Marseille-Wuppertal collaboration [BMW 2015] who used various lattices up to $m_{\mathrm{PS}}\, L \approx 12.3$ and observed only negligible finite size effects when using the renormalised vacuum polarisation in Eq. (3.5). This also justifies neglecting the volume dependence when performing the continuum extrapolation.

- *Chiral extrapolation*
  Also the systematic uncertainty of the chiral extrapolation is small. This has already been indicated by the comparison of the extrapolated result for the light quark contribution to a_μ^{hvp} with the result obtained directly at the physical point which is shown in Fig. 6.5. As we have seen in Sect. 4.1.1, the ensembles utilised to arrive at the result given in Eq. (6.22) have values of $227\,\mathrm{MeV} < m_{\mathrm{PS}} < 491\,\mathrm{MeV}$. Restricting our data to the condition $m_{\mathrm{PS}} < 400$ MeV yields the value
  $$a_\mu^{\mathrm{hvp}} = 6.85(32) \cdot 10^{-8}$$

after combined continuum and chiral extrapolation which is fully compatible with the result quoted in Eq. (6.22). Hence, we do not assign a systematic uncertainty to our way of extrapolating to the physical point.

- *Fit ranges of the vector meson fits*
  As we have seen several times before, the vector meson properties play an important role in our analysis of the vacuum polarisation function. In order to estimate the systematic effect of determining the vector meson masses and decay constants we have varied the fit ranges of the single-state vector meson fits by a) 0.1 fm to the left, b) 0.1 fm to the right, and c) 0.1 fm to the left and to the right.

  With this procedure, we do not find any significant differences in the values for $a_\mu^{\mathrm{hvp,s}}$ and $a_\mu^{\mathrm{hvp,c}}$. For the light quark contribution, however, we observe a systematic shift due to excited state contaminations when including time slices corresponding to a shift of 0.1 fm to the left of our standard fit range. This can be seen in Fig. 6.11.

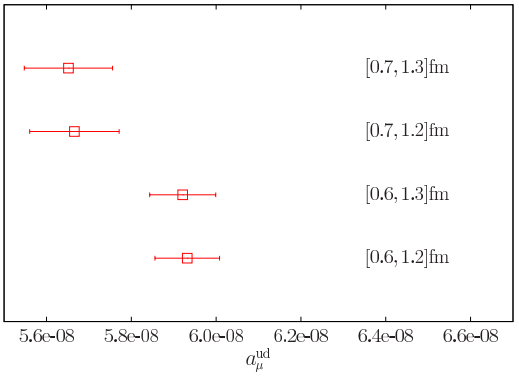

Figure 6.11.: Comparison of the effect of choosing different fit ranges on $a_\mu^{\mathrm{hvp,ud}}$ extrapolated linearly in m_{PS}^2 to the physical pion mass. The standard fit range is $[0.7\,\mathrm{fm}, 1.2\,\mathrm{fm}]$.

  Taking half the difference of $a_{\mu,\mathrm{ud}}^{\mathrm{hvp}}$ values obtained after fitting the ρ-meson in the fit ranges $[0.6\,\mathrm{fm}, 1.2\,\mathrm{fm}]$ and $[0.7\,\mathrm{fm}, 1.2\,\mathrm{fm}]$, we obtain as conservative estimate of systematic uncertainty from the choice of fit range for the vector mesons

$$\Delta_V = 0.13 \cdot 10^{-8} \,. \tag{6.24}$$

- *Fit function*
  For our MNBC fit functions presented in Sec. 4.1.2 different values of M,N, B, and C have been tested with the result that changing B and C does not have noticeable effects as long as a smooth matching between the low-momentum and the high-momentum fit functions is ensured. The reason is, of course, the high weight the kernel function in Eq. (6.10) puts on the low-Q^2 region and the early saturation of the integral shown in Fig. 6.4.

  For the strange and the charm quark contributions to a_μ^{hvp} even choosing different combinations of $M \in 1, 2$ and $N \in 2, 3, 4$ does not result in systematic differences. However, we do see systematic effects when varying M and N for the light quark contribution. This is shown in Fig. 6.12. Thus for the choice of the light quark fit

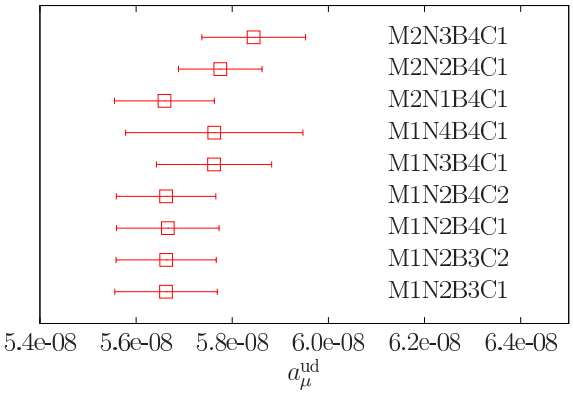

Figure 6.12.: Comparison of the effect of different M, N, B, C values on $a_{\mu,\mathrm{ud}}^{\mathrm{hvp}}$ extrapolated linearly to the physical pion mass. The standard fit is M1N2B4C1.

function we take half the difference of the extrapolated M1N2B4C1 and M2N3B4C1 results as estimate of the systematic uncertainty of choosing specific values for M, N, B, and C:

$$\Delta_{MNBC} = 0.09 \cdot 10^{-8} \,. \tag{6.25}$$

Additionally, we have checked that varying the matching momentum between $1\,\mathrm{GeV}^2$ and $3\,\mathrm{GeV}^2$ gives compatible results for a_μ^{hvp} as long as the transition between the fit functions in the low- and high-momentum regions is smooth. Another criterion has been that the coefficients of the fit polynomial in the high-momentum region, where more data is available, do not influence the coefficients of the fit polynomial in the low-momentum region. Applying these criteria all choices of different functions to combine the two momentum regions have not resulted in significant differences in the final values for a_μ^{hvp} compared to the Heaviside step function that we have used for our quoted result.

- *Osterwalder-Seiler (OS) matching uncertainties*
  Since we use the OS action Eq. (2.36) in the strange and charm quark sector, different values for the corresponding quark masses could be used which, however, have to lead to the physical values of the kaon and D-meson masses in the continuum and chiral limit. Varying the strange and charm quark masses within the uncertainties given for $a\mu_s$ and $a\mu_c$ in Tab. 4.2 has been found to be negligible. Likewise changing μ_s to the value obtained from directly matching with the physical kaon mass instead of $2m_K^2 - m_{\mathrm{PS}}^2$ gives a compatible result. The same is true when using the μ_s and μ_c values procured when allowing for a^2-effects in the fit function employed in the matching.

- *Different strange and charm sea quark masses*
  Additionally to the choice of valence quark masses, our result might be influenced by sea quark masses which for some of the ensembles have not been tuned to their correct physical values. For details see [ETMC 2010a]. By changing the mass splitting parameter μ_δ of the twisted mass action for a non-degenerate fermion doublet Eq. (2.35) for the ensemble with the biggest deviation from the physical strange quark mass, the ETMC has generated an ensemble in which both heavy sea quark masses

are compatible with their physical values. The new ensemble is called A100.24s whereas the old one is A100.24, sharing apart from μ_δ the same parameters. They have both been tuned to maximal twist and possess a pion mass of about 500 MeV and a space-time volume in units of the lattice spacing of $24^3 \times 48$. Due to the large pion mass they are not included in the rest of our analysis. Using the same matching conditions as before for the OS valence quarks, we arrive at consistent values for the single-flavour contributions to a_μ^{hvp} as can be seen in Tab. 6.3. Hence, we conclude that the impact of different sea quark masses in the heavy sector on a_μ^{hvp} is negligible.

Ensemble	$a_{mu}^{\mathrm{hvp,ud}}$	$a_\mu^{\mathrm{hvp,s}}$	$a_\mu^{\mathrm{hvp,c}}$	a_μ^{hvp}
A100.24	$5.18(18) \cdot 10^{-8}$	$8.25(59) \cdot 10^{-9}$	$3.16(24) \cdot 10^{-9}$	$6.32(19) \cdot 10^{-8}$
A100.24s	$5.32(18) \cdot 10^{-8}$	$8.87(55) \cdot 10^{-9}$	$3.16(22) \cdot 10^{-9}$	$6.52(19) \cdot 10^{-8}$

Table 6.3.: Comparison of single-flavour contributions and total a_μ^{hvp} from ensembles having different strange and charm sea quark masses.

- *Disconnected contributions*
  This is a systematic effect we can currently not adequately quantify. There are, however, several reasons for assuming that the disconnected contributions are small. First of all, a dedicated study in the two-flavour case has revealed them to be compatible with zero [Feng et al. 2011a]. This is in accordance with our own analysis of the light quark disconnected contributions on one of the $N_f = 2 + 1 + 1$ ensembles which we report in Sect. 6.3.4. Note, however, that in Refs. [Della Morte and Jüttner 2010, Francis et al. 2013a] the impact of disconnected contributions has been estimated to be -10%, at least in the energy range $2m_\pi < q < 3m_\pi$. Secondly, in the $SU(3)$ flavour limit they are identically zero due to charge cancellation. Thirdly, the disconnected contribution arising from the charm quark has been computed in perturbation theory and shown to be suppressed by a factor $\left(\frac{q^2}{4\ m_c^2}\right)^4$ [Groote and Pivovarov 2002], where q^2 is the relevant energy scale of the problem, i.e. $0.003\,\mathrm{GeV}^2$. Nevertheless, it is mandatory to properly quantify the quark-disconnected contributions involving heavy quarks in the future.

Comparison of the final results with other LQCD determinations

Having analysed the systematic uncertainties of our results, we can now compare them with the outcomes of various other LQCD calculations collected in Tab. 6.4. Here, we have combined statistical and systematic uncertainties in quadrature. Full agreement between all values is found thus indicating that the obtained results are universal, i.e. independent of a particular fermion discretisation as expected in the continuum limit. Additionally, we have quoted the results from a dispersive analysis employing the Hidden Local Symmetry (HLS) model [Benayoun et al. 2012b] from which the two- and three-flavour values have again been obtained by a phenomenological approach assuming quark-hadron duality. Additionally, the effect of successively adding valence quark species can be deduced from Tab. 6.4. Incorporating the complete first two generations of quarks in the lattice computation allows for an unambiguous comparison with the results of phenomenological analyses which we discuss below. Last but not least, comparing the uncertainties of the

twisted mass results to those of the calculations by RBC-UKQCD [Boyle et al. 2012] and Mainz [Della Morte et al. 2012] illustrates the advantage the redefinition in Eq. (6.12) entails for the chiral extrapolation.

	u,d	u, d, s	u, d, s, c
this work	5.69(20)	6.59(28)	6.78(29)
ETMC 2011	5.72(16)	-	-
Mainz 2012	5.46(66)	6.18(64)	-
RBC-UKQCD 2012	-	6.41(46)	-
HLS estimate 2012 (+ flavour weighting)	5.59(04)	6.71(05)	6.83(05)

Table 6.4.: a_μ^{hvp} in 10^{-8} for different numbers of valence quarks compared to the LQCD results from the old $N_f = 2$ ETMC calculation [Feng et al. 2011a], the Mainz group using dynamical light and a quenched strange clover-improved Wilson quark [Della Morte et al. 2012], and RBC-UKQCD [Boyle et al. 2012] employing $N_f = 2+1$ overlap fermions. The HLS estimate is the result of a dispersive analysis [Benayoun et al. 2012b]. The flavour-weighting to obtain the two- and three-flavour results from this value has been performed by us.

Using basically the temporal moment method which we have discussed in Sect. 4.2.2, in Ref. [HPQCD 2014] the HPQCD collaboration has performed a dedicated high-statistics determination of the strange and charm quark contributions to a_μ^{hvp} employing configurations generated by the MILC collaboration highly improved staggered quarks [HPQCD, UKQCD 2007]. For the strange quark piece they used $N_f = 2 + 1 + 1$ configurations [MILC 2013] whereas for the charm quark contribution the sea contained $N_f = 2+1$ fermions [MILC 2010]. In Tab. 6.5 we compare their final results with ours finding full agreement. Note that while HPQCD has analysed up to 1000 configurations per ensemble we typically only took about 150 configurations for the heavy flavours into account because this gave already an uncertainty an order of magnitude smaller than the one obtained for the dominant light-quark contribution, cf. Tab. G.2 in appendix G.

The reader might notice that the results in Tab. 6.5 are not exactly equal to the differences between the various valence quark flavour results in Tab. 6.4 although they are, of course, compatible within the rather large uncertainties of the 3- and 4-flavour results given in Tab. 6.4. The reason is that like HPQCD we have employed the standard definition in Eq. (6.10) for the single strange and charm quark contributions which then only

	$a_\mu^{\mathrm{hvp,s}}$	$a_\mu^{\mathrm{hvp,c}}$
this work	$53.6(1.9) \cdot 10^{-10}$	$14.18(61) \cdot 10^{-10}$
HPQCD 2014	$53.41(59) \cdot 10^{-10}$	$14.42(39) \cdot 10^{-10}$

Table 6.5.: Comparison of continuum and chirally extrapolated strange and charm quark contributions to a_μ obtained with the standard definition Eq. (6.10) from twisted mass and highly-improved staggered fermions presented in [HPQCD 2014].

very mildly depend on the squared pion mass and are therefore easily extrapolated to the physical point whereas for the complete three- and four-flavour results we have utilised the redefinition in Eq. (6.12) with $H = m_V$, the ρ-meson mass, for all single-flavour contributions in order to have a consistent lattice definition of the muon mass. As noted above, this leads to larger uncertainties for the strange and charm quark pieces originating from the uncertainty in the determination of the ρ-meson mass and only allows for a linear extrapolation in the squared pion mass if the heavy quark pieces are added to the dominant light quark contribution.

As we have mentioned when discussing the running of the $SU(2)_I$ coupling constant in Sect. 5.3.2, the charm quark contribution to the vacuum polarisation and thus to the LO hadronic contribution to $(g-2)_\mu$ can also be computed reliably in perturbation theory. Such a calculation has been performed in [Bodenstein et al. 2012] and both lattice results quoted above agree with the perturbative value

$$a_\mu^{\mathrm{hvp,c}} = 14.4(1) \cdot 10^{-10} \, . \tag{6.26}$$

Studying the charm quark LO hadronic vacuum polarisation contribution reveals that it is of the same order of magnitude as the currently accepted value for the hadronic light-by-light scattering contribution [Prades et al. 2009]

$$a_\mu^{\mathrm{lbl}} = 10.5(2.6) \cdot 10^{-10} \tag{6.27}$$

and the electroweak contributions [Jegerlehner and Nyffeler 2009]

$$a_\mu^{\mathrm{EW}} = 15.3(2) \cdot 10^{-10} \tag{6.28}$$

and thus can clearly not be neglected when trying to understand the discrepancy between experimental and theoretical results [Hagiwara et al. 2011]

$$a_\mu^{\mathrm{exp}} - a_\mu^{\mathrm{SM}} = 26.1(8.0) \cdot 10^{-10} \tag{6.29}$$

such that it will be vital for any lattice calculation aiming at an improvement of the results reported above to take the charm quark contribution to a_μ^{hvp} into account.

Comparison of the final results with dispersive analyses

Finally, since this is the first four-flavour lattice determination of a_μ^{hvp} we can also for the first time directly compare our value with the results procured by various phenomenological analyses of e^+e^--scattering and τ-decay data. For the latter isospin relations have to be applied and we refer the interested reader to [Davier and Marciano 2004, Jegerlehner 2008b, Jegerlehner and Nyffeler 2009] for detailed information.

As our main result we provide a comparison to a dispersive analysis which by taking the effects of ρ-γ mixing into account succeeded in obtaining consistent results from e^+e^--scattering as well as τ-decay data [Jegerlehner and Szafron 2011]:

$$\begin{aligned} a_\mu^{\mathrm{hvp}} &= 6.78(24)(16) \cdot 10^{-8} \quad (N_f = 2+1+1) \\ a_\mu^{\mathrm{hvp}} &= 6.91(01)(05) \cdot 10^{-8} \quad (\text{dispersive analysis}) \, . \end{aligned} \tag{6.30}$$

In Fig. 6.13 we also compare the outcome of our first-principle computation with a sum-

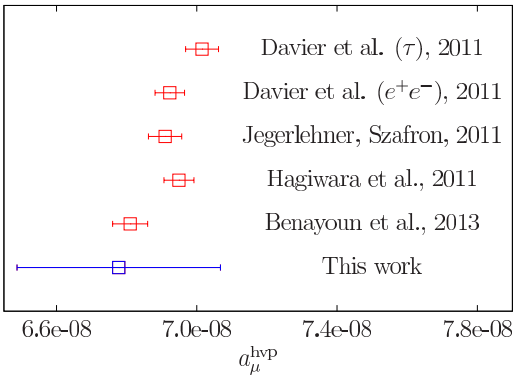

Figure 6.13.: Comparison of the first four-flavour LQCD result for $a_\mu^{\rm hvp}$ with different results based on dispersion relations: Davier et al. [Davier et al. 2011], Jegerlehner and Szafron [Jegerlehner and Szafron 2011], Hagiwara et al. [Hagiwara et al. 2011], and HLS [Benayoun et al. 2012a]

mary of other results obtained utilising the dispersion relation. Here, we have again added statistical and systematic uncertainties in quadrature. Although our lattice QCD determination of $a_\mu^{\rm hvp}$ shows an overall agreement with phenomenology, the lattice QCD result has clearly a significantly larger error being, however, already at the same order of magnitude and systematically improvable as we have discussed in Sect. 2.2.

6.3.2. Electron $(g-2)$

As highlighted in [Giudice et al. 2012], the uncertainty in the comparison between the experimental and the SM value for the electron anomalous magnetic moment is currently dominated by the experimental uncertainties of its determination and of the value for $\alpha_{\rm QED}$ from atomic physics experiments with rubidium atoms which both are to be reduced in the future. Recently, the Harvard group has announced to be working on a more accurate determination of the electron as well as the positron $(g-2)$ [Hoogerheide et al. 2014] thus also testing the CPT theorem [Lüders 1954, Pauli 1955]. According to [Giudice et al. 2012] uncertainties in the sub-10^{-13} region might be expected which would clearly provide the opportunity to also detect NP contributions in the anomalous magnetic moment of the electron and thus to cross-check the muon discrepancy. In this situation it will again be of utmost importance to know the hadronic contributions as precisely as possible. Furthermore, as noted before, due to its sensitivity to the very low momentum region the LQCD determination of the LO hadronic contribution to the electron anomalous magnetic moment, $a_{\rm e}^{\rm hvp}$, serves as a substantial cross-check of the computations performed to determine the muon $(g-2)$ as well as the LO QCD contribution to the running of the coupling constants presented in chapter 5.

From Fig. 6.4 one can deduce that the LO hadronic contribution to $a_{\rm e}$ is dominated by momenta below $10^{-4}\,{\rm GeV}^2$. To a good approximation it can even be determined from the slope of the vacuum polarisation at zero momentum $a_{\rm e} \propto d\Pi/dQ^2(Q^2=0)$. Therefore, we only use the low-momentum part, $\Pi_{\rm low}(Q^2)$, of the hadronic vacuum polarisation function Eq. (4.6). This also implies that for the electron we have to rely largely on the extrapolation of our vacuum polarisation data to the very low momentum region which is also important for the renormalisation of the hadronic vacuum polarisation function and

thus for all physical observables derived from it. The correctness of this extrapolation can be buttressed by a successful comparison of the LQCD and the phenomenological results for a_e^{hvp}.

The light quark contribution, $a_e^{\mathrm{hvp,ud}}$

The contribution from up and down valence quarks is depicted in Fig. 6.14. Here, we compare $a_e^{\mathrm{hvp,ud}}$ with the result at the physical value of the pion mass obtained with the standard definition Eq. (6.10) on the ensembles introduced in Sect. 4.1.1. The physical point result is fully compatible with the value determined by the linear extrapolation of the data procured with the reparametrisation Eq. (6.12).

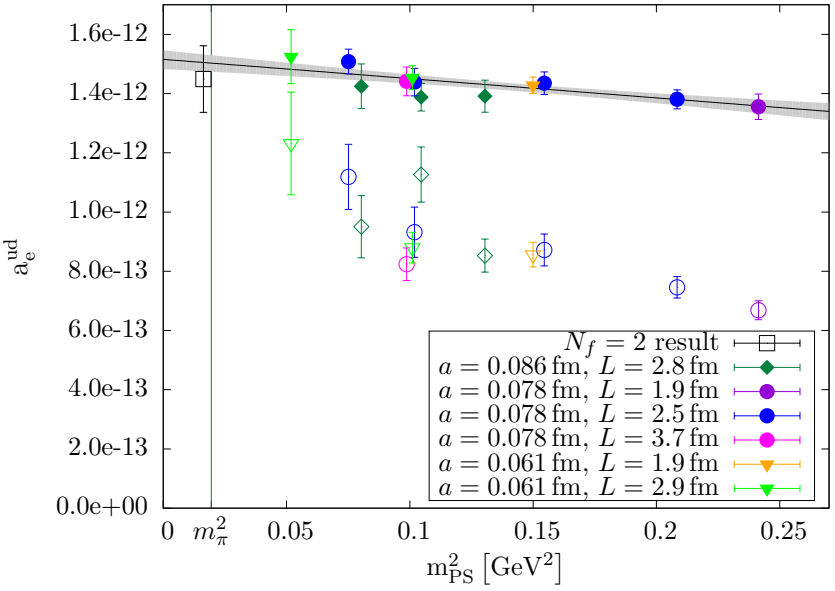

Figure 6.14.: Light-quark contribution to a_e^{hvp} with filled symbols representing points obtained with Eq. (6.12) with $H = m_V$, open symbols refer to those obtained with Eq. (6.10), i.e. $\frac{H}{H_{\mathrm{phys}}} = 1$. In particular, the two-flavour result at the physical point has been computed with the standard definition. The light grey errorband indicates the uncertainty of the linear fit represented by the dotted black line.

Below we additionally compare the results of [0,1] and [1,1] Padé fits introduced in Sect. 4.2.1 with our M1N2 and M1N3 fits up to $Q^2_{\mathrm{max}} = 0.75\,\mathrm{GeV}^2$ on the ensemble featuring the physical value of the pion mass. We have chosen a rather small Q^2_{max} because, as we have discussed in Sect. 4.2.1, especially for low-order Padé fits a small number of points is required to arrive at some kind of multipole approximation. Furthermore, we have observed that the Padé fits only describe the data well at small momenta as has also been concluded in [Golterman et al. 2014]. Thus, we limit the comparison to the case of the electron where the weight function guarantees an early saturation of the integral.

We find first of all that the values for the fitted single pole obtained from MN fits and Padé fits are compatible. Secondly, the results for a_e^{hvp} from the [0,1] Padé and the M1N2 fit (3 free parameters) as well as those from the [1,1] Padé fit and the M1N3 fit (4 free parameters) are mutually consistent. This is no surprise as we expect the results of

	M1N2	M1N3 (standard)	[0,1] Padé fit	[1,1] Padé fit
$a^2\times$ pole	0.154(38)	0.154(38)	0.183(01)	0.188(02)
$a_{\mathrm{e}}^{\mathrm{hvp}}$	$1.45(11)\cdot 10^{-12}$	$1.56(09)\cdot 10^{-12}$	$1.31(05)\cdot 10^{-12}$	$1.67(20)\cdot 10^{-12}$

Table 6.6.: Comparison of the single pole and the value for $a_{\mathrm{e}}^{\mathrm{hvp}}$ obtained from MN and Padé fits with the standard definition Eq. (6.10).

Padé fits and the MN fits with the same number of parameters to only differ by lattice artefacts, since in the MN fits the pole is determined from the temporal correlator whereas in the Padé fits the pole comes from $\Pi(Q^2)$. We thus expect equivalence in the continuum limit provided the same procedure is followed in both cases (same number of parameters, standard definition for a_e^{hvp}, keeping correlations and properly propagating uncertainties from vector meson fits). However, we also see that while the results of the M1N2 and the M1N3 fits are compatible, the results of [0,1] and [1,1] Padé fits are not. Hence, for the example considered here the uncertainty from choosing one particular fit function is larger for the class of Padé approximants than for our standard MN fits.

Adding the strange and the charm quark contributions

When incorporating the heavy, second-generation flavours, we again have to take $\mathcal{O}(a^2)$ lattice artefacts into account. The single-flavour contributions for all ensambles are tabulated in Tab. G.1 in appendix G. We observe that we would have obtained compatible results when only considering the light and the strange quarks. The reason is the high weight put on the very small momentum region by the kernel function in Eq. (6.12). However, already the strange quark contribution exhibits discretisation effects. Hence, as for the muon the four-flavour result for $a_{\mathrm{e}}^{\mathrm{hvp}}$ at the physical point in the continuum limit is obtained with the help of a fit function of the form given in Eq. (6.20). For $a_{\mathrm{e}}^{\mathrm{hvp}}$ the corresponding fit is shown together with the procured data points in Fig. 6.15. Our result with only statistical uncertainty reads

$$a_{\mathrm{e}}^{\mathrm{hvp}} = 1.78(06)\cdot 10^{-12}\,. \tag{6.31}$$

Systematic uncertainties

In this section we give an account of the systematic uncertainties of our result for $a_{\mathrm{e}}^{\mathrm{hvp}}$ given in Eq. (6.31) leaving out some of the uncertainties found negligible in the muon case in Sect. 6.3.1 to avoid unnecessary repetitions. We have investigated finite size effects (FSE), the dependence of our chiral extrapolation on the incorporation of large pion masses, vector meson fit ranges, and the dependence of our results on different vacuum polarisation fit functions.

- *Finite size effects*
  As presented in Sect. 4.1.1, the $N_f = 2{+}1{+}1$ ensembles analysed in this work feature $3.35 < m_{\mathrm{PS}}\, L < 5.93$, where L is the spatial extent of the lattice. Restricting our data to the condition $m_{\mathrm{PS}}L > 3.8$ yields

$$a_{\mathrm{e}}^{\mathrm{hvp}} = 1.77(07)\cdot 10^{-12} \tag{6.32}$$

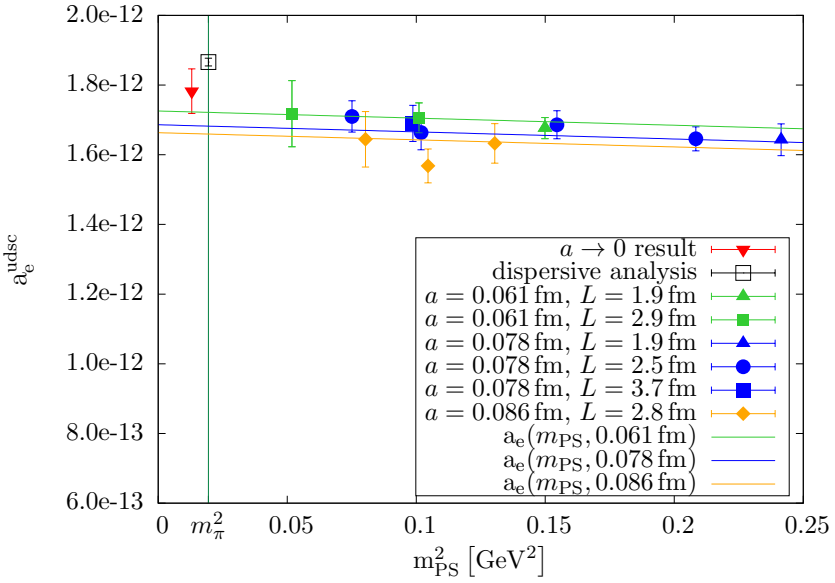

Figure 6.15.: Chiral and continuum extrapolation of the $N_f = 2+1+1$ contribution to a_e^{hvp}. The inverted red triangle shows the value extrapolated to the continuum and to the physical value of the pion mass. It has been displaced to the left to facilitate the comparison with the dispersive result in the black square [Nomura and Teubner 2013].

after combined chiral and continuum extrapolation. This matches the result given in Eq. (6.31) and thus indicates that FSE are negligible in our computation. This finding is supported by comparing the results of two ensembles only differing in lattice size provided in Tab. 6.7. The numbers do not change when restricting the momenta of the larger ensemble to those of the smaller one. The FSE attributed to the lowest achievable momentum being $\frac{2\pi}{L}$ mixes with FSE entering the choice of different fit functions. We take a conservative approach and consider these effects separately.

Ensemble	$\left(\frac{L}{a}\right)^3 \times \frac{T}{a}$	$a_e^{hvp,ud}$	a_e^{hvp}
B35.32	$32^3 \times 64$	$1.44(05) \cdot 10^{-12}$	$1.66(05) \cdot 10^{-12}$
B35.48	$48^3 \times 96$	$1.44(05) \cdot 10^{-12}$	$1.69(05) \cdot 10^{-12}$

Table 6.7.: Comparison of light-quark contribution to a_e^{hvp} and total a_e^{hvp} from ensembles of different volumes.

Let us repeat again that studying lattices up to $m_{PS}\, L \approx 12.3$ the BMW collaboration could also not detect any finite size effects if the subtracted hadronic vacuum polarisation function has been used [BMW 2015].

- *Chiral extrapolation*
  Besides comparing our extrapolated result for the light-quark contribution with the result procured directly at the physical point, we have checked the validity of the

chiral extrapolation by restricting the four-flavour data, comprising pion masses between 227 MeV and 491 MeV, to the condition $m_{\mathrm{PS}} < 400\,\mathrm{MeV}$. The value we obtain

$$a_{\mathrm{e}}^{\mathrm{hvp}} = 1.78(07) \cdot 10^{-12} \tag{6.33}$$

only features a slightly larger uncertainty compared to the result in Eq. (6.31). Thus, we do not assign a systematic uncertainty to the usage of pion masses above 400 MeV.

- *Vector meson fit ranges*
  Our standard computation involves the determination of the masses and decay constants of the vector meson ground states for the different flavours. Their values depend on the choice of fit ranges. We have analysed different fit ranges for the two-point functions of the light, strange, and charm vector currents and propagated the uncertainties to the values for $a_{\mathrm{e}}^{\mathrm{hvp}}$. This shows that excited state contaminations are significant only for m_V and f_V determined from the light vector current-current correlator. Variations of the standard fit ranges by 0.1 fm to the left, right and both simultaneously do not lead to any observable differences in $a_{\mathrm{e}}^{\mathrm{hvp}}$ for the $\bar{s}\gamma_\mu s$- and the J/ψ correlator. Furthermore, the heavy flavour contributions are approximately one order of magnitude smaller than the light quark contribution such that their systematic uncertainties would not noticeably impact the overall uncertainty of $a_{\mathrm{e}}^{\mathrm{hvp}}$ anyway.

  In the left panel of Fig. 6.16 the dependence of the light quark contribution to the electron anomalous magnetic moment on the fitrange for the ρ-correlator is plotted. Taking half the difference of the central values obtained for $[0.6\,\mathrm{fm}, 1.2\,\mathrm{fm}]$ and $[0.7\,\mathrm{fm}, 1.2\,\mathrm{fm}]$ gives a systematic uncertainty of

$$\Delta_V = 0.035 \cdot 10^{-12}\,. \tag{6.34}$$

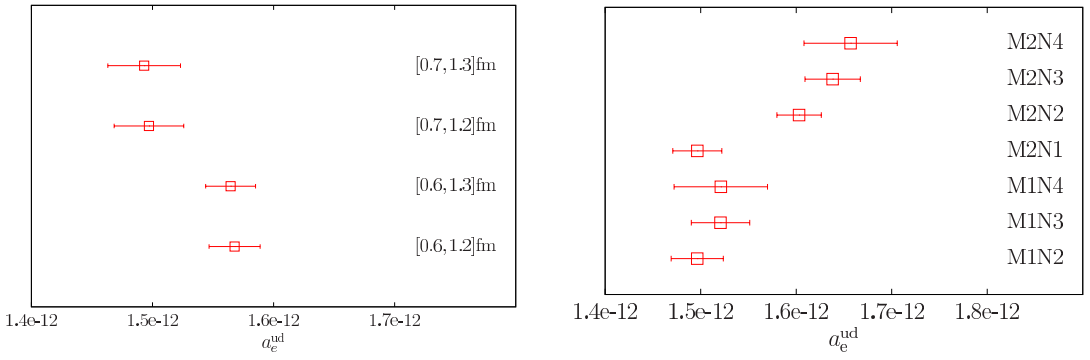

Figure 6.16.: Dependence of $a_{\mathrm{e}}^{\mathrm{ud}}$ on the fitrange of the ρ-correlator (left panel) and on values chosen for M, N in the vacuum polarisation fit function (right panel). The standard ρ-correlator fit range is $[0.7\,\mathrm{fm}, 1.2\,\mathrm{fm}]$ and the standard fit function corresponds to M1N2.

- *Number of terms in MN fit function*
  The number of terms in the fit function Eq. (4.6) is given by M and N. M1N2 is our standard choice. Repeating the whole analysis with different numbers of terms for the light quark contribution leads to the results shown in the right panel of

Fig. 6.16. We observe that the chirally and continuum extrapolated results of fit functions involving one and two poles are not compatible and thus we assign a systematic error by taking half the difference of the central values of the result of the M2N3 and the M1N2 fit. This leads to a systematic uncertainty of

$$\Delta^{\mathrm{ud}}_{MN} = 0.071 \cdot 10^{-12} \,. \tag{6.35}$$

As for $\Delta\alpha^{\mathrm{hvp}}_{\mathrm{QED}}$ and $\Delta^{\mathrm{hvp}} \sin^2\theta_W$, this results in the dominant systematic uncertainty of the determination of a_e^{hvp} and needs to be scrutinised further when more accurate data becomes available. For the strange quark the systematic uncertainty from different values of M and N is

$$\Delta^{\mathrm{s}}_{MN} = 0.007 \cdot 10^{-12} \tag{6.36}$$

which we add to the light quark one. The differences of the results from different fit functions for the charm quark contribution have turned out to be negligible such that the total systematic error originating from employing various numbers of terms in the fit function amounts to

$$\Delta_{MN} = 0.078 \cdot 10^{-12} \,. \tag{6.37}$$

Comparison with a phenomenological value

Adding the quantified systematic uncertainties in quadrature we obtain as final result

$$a_{\mathrm{e}}^{\mathrm{hvp}} = 1.782(64)(86) \cdot 10^{-12} \,. \tag{6.38}$$

This can directly be compared with the phenomenological determination of [Nomura and Teubner 2013]

$$a_{\mathrm{e}}^{\mathrm{hvp}} = 1.866(10)(05) \cdot 10^{-12} \,. \tag{6.39}$$

They are fully compatible with each other although also for $a_{\mathrm{e}}^{\mathrm{hvp}}$ our lattice result is afflicted with larger errors which seems to be difficult to mend for this quantity with our standard approach due to the far extrapolation we have to perform between the available lattice momenta and the momentum region most relevant for $a_{\mathrm{e}}^{\mathrm{hvp}}$. This problem might be alleviated by the use of (partially) twisted boundary conditions as suggested in [De Divitiis et al. 2004, Sachrajda and Villadoro 2005] or by data from much larger lattices. Nevertheless, the consistency of the LQCD and the phenomenological result for this rather challenging quantity confirms the correctness of our computational strategy.

6.3.3. The τ-lepton $(g-2)$

The large mass of the tau lepton, $m_\tau \approx 1.8\,\mathrm{GeV}$, implies a peak of the weight function in the expression for the LO hadronic contribution to its magnetic moment in Eq. (6.10) at $Q^2_{\mathrm{peak}} \approx 0.75\,\mathrm{GeV}^2$. This is very different from the peak position of the weight functions of the two other charged leptons as we have shown in Fig. 6.4. Hence, a_τ^{hvp} is sensitive to a distinctly different part of the vacuum polarisation function, in particular, also the high-momentum piece of our fit function Eq. (4.7) is important here. This could not be properly checked by the calculations of the other two anomalous magnetic moments such

that the determination of a_τ^{hvp} provides another beneficial test of our standard approach. Furthermore, the sensitivity to the high-momentum region also entails a larger charm quark contribution than for the other two lepton anomalous magnetic moments. Additionally, as we have mentioned at the beginning of this chapter, once a true measurement of a_τ succeeds it is likely to exhibit much larger NP contributions than the muon $(g-2)$. As we will see shortly, a_τ^{hvp} is suited best for lattice computations such that compared to the challenges posed by the anomalous magnetic moments of electron and muon it will be easiest for LQCD to exceed the accuracy of the phenomenological analyses of this quantity.

The light quark contribution, $a_\tau^{\mathrm{hvp,ud}}$

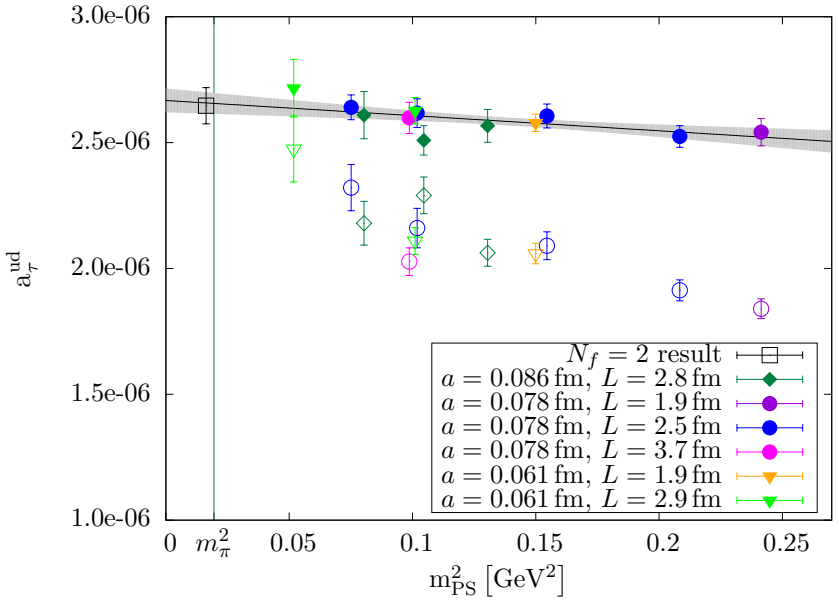

Figure 6.17.: Light-quark contribution to a_τ^{hvp} with filled symbols representing points obtained with Eq. (6.12) with $H = m_V$, open symbols refer to those obtained with Eq. (6.10), i.e. $H = 1$. We note that the two-flavour result at the physical point has been computed with the standard definition. The light grey errorband represents the uncertainty of the linear fit (dotted black line).

As for the electron and the muon, we start the presentation of our LQCD results for a_τ^{hvp} by showing the contribution of the first-generation flavours to a_τ^{hvp} in Fig. 6.17. The data show a qualitatively similar behaviour to those of the electron in Fig. 6.14. Their values differ, however, by six orders of magnitude. In particular, we find that no significant lattice artefacts are present and that the data at unphysical pion masses obtained with Eq. (6.12), can be linearly extrapolated to the physical point. This demonstrates again that the method of including $\frac{H}{H_{\mathrm{phys}}}$ in the weight function is advantageous for the chiral extrapolation. The value extrapolated in this way agrees with our calculation directly at the physical pion mass following the standard procedure shown as the open square in Fig. 6.17. The large Q^2_{peak} prevents the application of a low-order Padé approximant whereas high-order Padé fits cannot be performed due to the limited accuracy of our data. Therefore, it currently appears to be impossible to obtain a_τ^{hvp} from a Padé fit for the ensemble at the physical point.

Adding the strange and the charm quark contributions

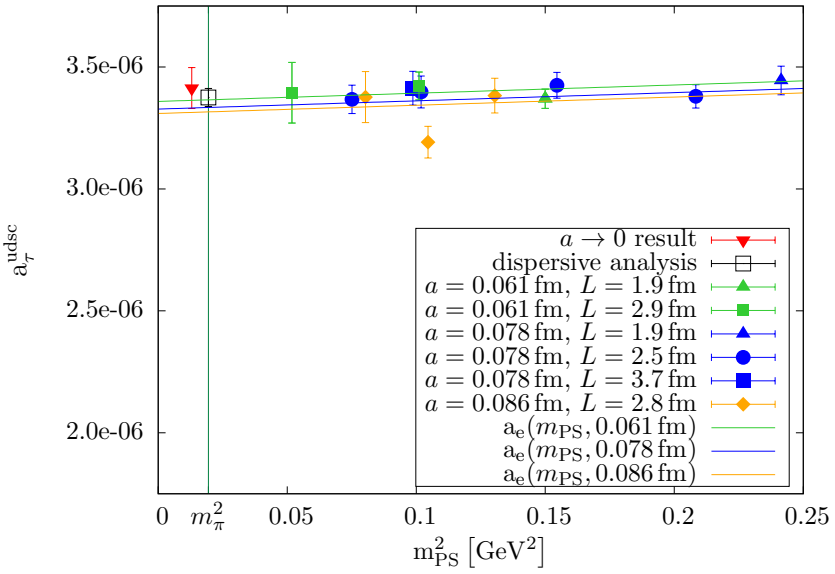

Figure 6.18.: Chiral and continuum extrapolation of the $N_f = 2+1+1$ contribution to a_τ^{hvp}. The inverted red triangle shows the value in the continuum limit at the physical value of the pion mass. It has been displaced to the left to facilitate the comparison with the dispersive result depicted as black square [Eidelman and Passera 2007].

Analogously to the cases of the other leptons, we perform the chiral and continuum extrapolation of the complete four-flavour result using a fit of the form given in Eq. (6.20). This is shown in Fig. 6.18. Comparing this with Fig. 6.15, we see that the lattice artefacts are much smaller than for the electron and the muon such that we would have obtained a compatible result when omitting the a^2 term in Eq. (6.20). As can be seen in Fig. 6.19, for the tau lepton both, the strange and the charm contributions, do not show significant cut-off effects and hence, also for the total contribution a^2 effects are small. In fact, there seems to be even no significant dependence on the pion mass anymore. We nevertheless conduct the continuum and chiral extrapolation as before in order to use exactly the same analysis strategy as for the other leptons. Our resulting four-flavour value with only statistical uncertainty reads

$$a_\tau^{\text{hvp}} = 3.41(8) \cdot 10^{-6}\,. \tag{6.40}$$

Fig. 6.19 and Tab. G.3 in appendix G, which lists the single-flavour contributions obtained on each ensemble, also show that contrary to the other two lepton anomalous magnetic moments for a_τ^{hvp} the contributions of strange and charm quarks are compatible with each other and thus considering the charm quark as active flavour in the calculation is of utmost importance for obtaining reliable results.

Systematic uncertainties

We have investigated the same systematic uncertainties for our determination of a_τ^{hvp} as for the case of the electron. Additionally, the influence of the disconnected contributions on the dominant light-quark contribution will be discussed in Sect. 6.3.4.

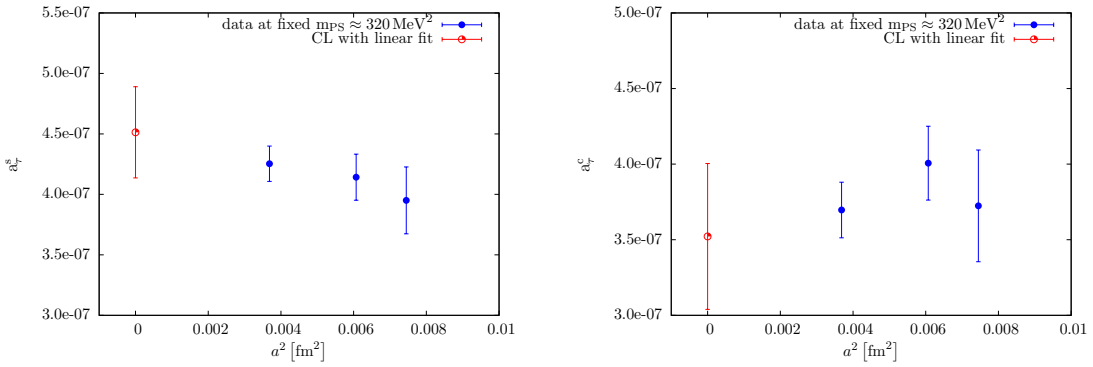

Figure 6.19.: Continuum limit of strange (left panel) and charm (right panel) quark contribution to a_τ^{hvp} at approximately fixed pion mass.

- *Finite size effects*
  Restricting our data to the condition $m_{\mathrm{PS}}L > 3.8$ yields

$$a_\tau^{\mathrm{hvp}} = 3.40(09) \cdot 10^{-6}\,. \tag{6.41}$$

  This is compatible with the result in Eq. (6.40). Comparing again the two ensembles at $m_{\mathrm{PS}} \approx 315\,\mathrm{MeV}$ which only differ in the extent of the lattices also indicates negligible finite size effects as shown in Tab. 6.8. Hence, we do not assign a FSE related systematic uncertainty in accordance with the insights of the Budapest-Marseille-Wuppertal collaboration [BMW 2015].

Ensemble	$\left(\frac{L}{a}\right)^3 \times \frac{T}{a}$	$a_{\tau,\mathrm{ud}}^{\mathrm{hvp}}$	a_τ^{hvp}
B35.32	$32^3 \times 64$	$2.62(06) \cdot 10^{-6}$	$3.40(07) \cdot 10^{-6}$
B35.48	$48^3 \times 96$	$2.60(06) \cdot 10^{-6}$	$3.41(07) \cdot 10^{-6}$

Table 6.8.: Comparison of light-quark contribution to a_τ^{hvp} and total a_τ^{hvp} from ensembles of different volumes.

- *Chiral extrapolation*
  Restricting the analysed ensembles to those featuring pion masses $m_{\mathrm{PS}} < 400\,\mathrm{MeV}$, we get

$$a_\tau^{\mathrm{hvp}} = 3.45(09) \cdot 10^{-6}\,. \tag{6.42}$$

  This is again compatible with the value given in Eq. (6.40). Hence, we do not assign a systematic uncertainty to the fact that ensembles with pion masses above 400 MeV have been employed when extrapolating to the physical value of the pion mass. Again, this is strongly supported by the comparison of the extrapolated value on the $N_f = 2 + 1 + 1$ ensembles for the light-quark contribution to a_τ^{hvp} and the two-flavour result at the physical value of the pion mass in Fig. 6.17.

- *Vector meson fit ranges*
  The situation is very similar to the cases of the electron and the muon reported above. Only the excited state contamination in the ρ-correlator has to be taken into account

as systematic uncertainty. In the left panel of Fig. 6.20 the dependence of the light quark contribution, a_τ^{ud}, on the fit range chosen to extract the spectral information from the ρ-correlator is depicted. Taking half the difference of the central values obtained for $[0.6\,\mathrm{fm}, 1.2\,\mathrm{fm}]$ and our standard fit range $[0.7\,\mathrm{fm}, 1.2\,\mathrm{f}m]$ results in an estimated systematic uncertainty of

$$\Delta_V = 0.046 \cdot 10^{-6} \,. \tag{6.43}$$

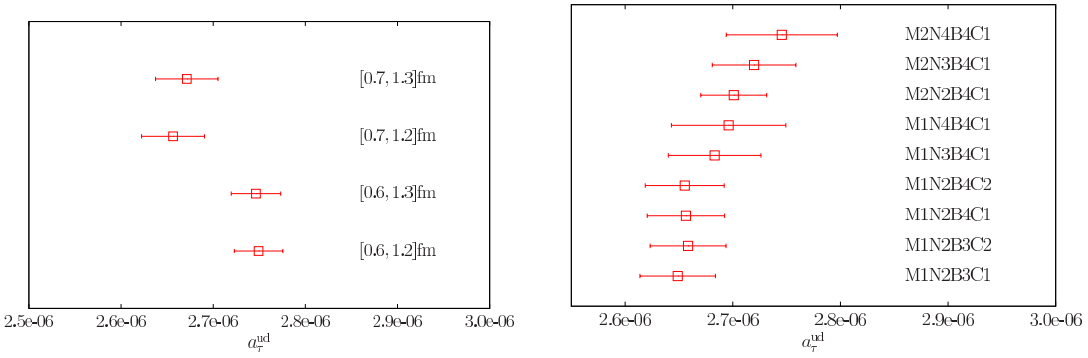

Figure 6.20.: Dependence of a_τ^{ud} on the fit range of the ρ-correlator (left panel) and on the values chosen for M, N, B, and C in the vacuum polarisation fit function (right panel). The standard ρ-correlator fit range is $[0.7\,\mathrm{fm}, 1.2\,\mathrm{fm}]$ and the standard fit function corresponds to M1N2B4C1.

- *Number of terms in MNBC fit function*
  Due to the large Q^2_{peak} we have to take the whole vacuum polarisation function Eq. (4.8) into account, including in particular the high-momentum piece in Eq. (4.7). Thus, we have four different types of terms in the fit function that can have different numbers of summands. We only find observable differences in the light quark sector. But also here the results from different fits are all compatible as shown in the right panel of Fig. 6.20. The reason is, of course, that in contrast to electron and muon we have a lot of lattice data available in the momentum domain where the weight function attains its maximum. Conservatively, we take half the difference between the M2N3B4C1 and M1N2B4C1 fit and assign a systematic uncertainty of

  $$\Delta_{MNBC} = 0.032 \cdot 10^{-6} \tag{6.44}$$

  to our choice of the fit function.

Comparison with a phenomenological value

Including the identified systematic uncertainties added in quadrature, our final four-flavour result reads

$$a_\tau^{\mathrm{hvp}} = 3.41(8)(6) \cdot 10^{-6} \,. \tag{6.45}$$

This agrees with the one obtained by a dispersive analysis [Eidelman and Passera 2007]

$$a_\tau^{\mathrm{hvp}} = 3.38(4) \cdot 10^{-6} \,. \tag{6.46}$$

Compared to the other leptons even better agreement between the lattice and the phenomenological result is observed for the τ-lepton. In this case, the statistical uncertainty of our twisted mass LQCD calculation is only about twice the phenomenological one such that it is likely that LQCD computations will play a major role in the determination of a_τ^{hvp} in the future.

6.3.4. Disconnected contributions

As mentioned when discussing the muon $(g-2)$, leaving out the quark-disconnected contributions is a systematic uncertainty we cannot completely quantify, yet. We have started investigating their magnitude on the B55.32 ensemble, see Tab. 4.1 and the discussion at the beginning of Sect. 4.1.2, and actually have observed a clean signal in the temporal correlator for the isovector current when applying the one-end trick [ETMC 2008]. The isoscalar temporal correlator also exhibits a decrease but is much noisier. Consequently, also the isoscalar part of the hadronic vacuum polarisation function is much noisier than the disconnected contributions obtained for the isovector current as shown in Fig. 6.21. However, the data at least show some momentum dependence, such that it might be expected that a signal can be extracted when improving the statistical accuracy of the results, e.g. by the exact deflation technique [Saad 1984, Neff et al. 2001].

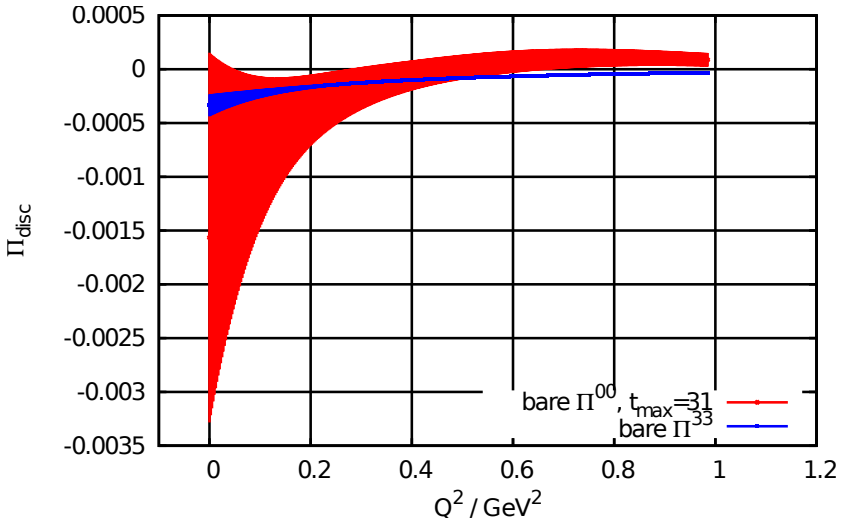

Figure 6.21.: Quark-disconnected contributions to the bare hadronic vacuum polarisation function obtained from local isoscalar and isovector current correlators, Π^{00} and Π^{33}, respectively. The data has been obtained with the method in Sect. 4.2.2 and $t_{\mathrm{max}} = 31$.

The comparison of the magnitude of the connected and disconnected pieces has already been shown in Fig. 4.1. From this we expect only a minor influence of the quark-disconnected contributions on the total anomalous magnetic moments. Such a comparison of the values of $a_l^{\mathrm{hvp,ud}}$ for all three leptons on the B55.32 ensemble with and without incorporating the disconnected contributions is presented in Tab. 6.9. Here, we have combined the connected pieces obtained from the point-split current correlator with the isoscalar part of the disconnected contributions obtained from the local current correlator using the renormalisation constant Z_V determined from the ratio of the connected pieces of the

conserved and the local vector current two-point functions. Therefore and because we only have results for one ensemble, the numbers below can only give hints on the influence of the disconnected pieces. We observe the tendency that for all three leptons $a_l^{\mathrm{hvp,ud}}$ decreases when incorporating the disconnected contributions as has been predicted in [Della Morte and Jüttner 2010]. However, this is statistically not significant. Furthermore, we find that the magnitude of the disconnected contributions is comparable to our current uncertainty. Hence, it will be mandatory to compute them when aiming at more precise results. For the muon the value shifts by $\approx 3\%$, which is also not statistically significant at this stage, but is in accordance with the upper bound of $4-5\%$ given in [Francis et al. 2014b].

	$a_{\mathrm{e}}^{\mathrm{hvp.ud}}$	$a_{\mu}^{\mathrm{hvp,ud}}$	$a_{\tau}^{\mathrm{hvp,ud}}$
without disc	$1.44(04)\cdot 10^{-12}$	$5.42(14)\cdot 10^{-8}$	$1.27(03)\cdot 10^{-6}$
with disc	$1.39(07)\cdot 10^{-12}$	$5.26(25)\cdot 10^{-8}$	$1.24(04)\cdot 10^{-6}$

Table 6.9.: Comparison of light-quark contributions to a_l^{hvp} with and without disconnected pieces in the low-momentum region for the B55.32 ensemble. For all contributions the redefinition Eq. (6.12) and our standard analysis have been used.

From this first investigation we conclude, that at the current level of precision it might be justified to omit the quark-disconnected contributions. However, the disconnected heavy flavour contributions need to be considered as well. We plan to check their size in future calculations. Furthermore, it appears to be obvious that future calculations of the lepton anomalous magnetic moments will have to incorporate a proper determination of the disconnected contributions, at least in the light-quark sector.

6.4. Summary and outlook

In this chapter, we have presented the first four-flavour LQCD computation of the LO HVP contributions to the lepton anomalous magnetic moments. Our results have been obtained with $N_f = 2+1+1$ twisted mass fermions mostly at unphysically large pion masses but, at least for the light quark contribution, also directly at the physical point. We find that for all three leptons the chirally extrapolated values for the light quark contributions agree with the one at the physical point.

For our data at unphysically large values of the pion mass, we have performed the continuum limit and investigated the systematic uncertainties of the method used to obtain our final results. In particular, we have addressed the effects of the finite volumes, the fit range for extracting the vector meson properties, and using different fit functions for the vacuum polarisation function.

As an additional uncertainty, we have investigated the light-quark disconnected contributions by using the local vector current. This led to the first observation of a momentum dependence of the two-point function for the disconnected diagrams whose influence, however, is compatible with zero within our current errors and which we therefore have neglected. This will no longer be justified once the uncertainties of the connected pieces are reduced. Actually, quark disconnected contributions seem to have a larger impact than what is expected from isospin breaking effects [Blum et al. 2012] and thus should be

	$a_{\mathrm{e}}^{\mathrm{hvp}}$	a_{μ}^{hvp}	a_{τ}^{hvp}
this work	$1.782(64)(86)\cdot 10^{-12}$	$6.78(24)(16)\cdot 10^{-8}$	$3.41(8)(6)\cdot 10^{-6}$
dispersive analyses	$1.866(10)(05)\cdot 10^{-12}$	$6.91(01)(05)\cdot 10^{-8}$	$3.38(4)\cdot 10^{-6}$

Table 6.10.: Comparison of our first-principle values for $a_{\mathrm{e}}^{\mathrm{hvp}}$, a_{μ}^{hvp}, and a_{τ}^{hvp} with the phenomenological results of [Nomura and Teubner 2013], [Jegerlehner and Szafron 2011], and, [Eidelman and Passera 2007], respectively.

the first to be examined in an ensuing four-flavour calculation.

Our final results are summarised in Tab. 6.10. They agree with the phenomenological determinations of the LO QCD contributions to the lepton magnetic moments which are also shown there. Let us stress again that the same analysis strategy is employed for all three leptons and the fit functions are identical to those used for the determination of the leading QCD contribution to the running of the electroweak coupling constants presented in the preceding chapter. Thus, we have shown that despite their sensitivity to different momentum regions and the associated different systematics, correct physical results can be obtained from twisted mass LQCD for the leading hadronic contribution of various electroweak observables.

For all three leptons, the errors of our calculations are larger than those from the dispersive analyses quoted above. However, it can be expected that with future LQCD calculations at the physical value of the pion mass, increased statistics, and an even better control over systematic uncertainties the phenomenological error can be matched, if not even beaten. In fact, from the results presented in this chapter it is straightforward to deduce the steps required to achieve this ambitious aim. First of all, it is clear that the next generation of LQCD determinations of the LO hadronic contributions to the lepton anomalous magnetic moments and in particular $(g-2)_{\mu}$ needs to reduce the statistical uncertainties of the connected contributions, e.g. by the use of the all-mode-averaging [Blum et al. 2013b] or the exact deflation [Saad 1984, Neff et al. 2001] techniques. Furthermore, including the charm quark contributions as well as the disconnected contributions of the light quarks, possibly even of all flavours, appears to be necessary. Much larger lattices would allow to apply the theoretically favourable analytic continuation method presented in Sect. 4.2.2 and facilitate the usage of Padé approximants introduced in Sect. 4.2.1. In this way, the systematic uncertainties can be reduced. Having computed the quark-disconnected pieces, the incorporation of isospin breaking and electromagnetic effects due to the charges of the light quarks and their different masses will pose the final challenge, since in order to match the envisioned accuracy of the new muon $(g-2)$ experiments a total uncertainty at the per mille level will be needed. On the other hand, as soon as a proper measurement of $(g-2)_{\tau}$ possibly along the lines of the suggestions collected in [Pich 2014] exists, it will be much easier to obtain a value for a_{τ}^{hvp} from LQCD with the required precision to detect NP. It will probably not take very long before the QCD contribution entering the official SM result will be provided by LQCD.

Chapter 7

Conclusions

It has been the aim of this thesis to perform the first $N_f = 2+1+1$ lattice QCD (LQCD) investigation of the hadronic vacuum polarisation (HVP) function. The importance of LQCD for the HVP results from the fact that it is the only ab initio approach solely based on the QCD part of the SM which is available for calculations in the low-energy regime.

From the HVP function, we have determined the leading-order hadronic contributions both to the anomalous magnetic moments of the SM leptons and to the running of the electroweak coupling constants. An important result is the insight that the respective contribution to the running of the weak mixing angle can be obtained from the same vector current two-point functions that are used for the other quantities. In addition to the muon $(g-2)$, we have thus identified another benchmark observable for physics searches beyond the SM on whose determination LQCD has an important impact. In fact, our results have directly assisted in refining the phenomenological value of the leading order hadronic contribution to the weak mixing angle by demonstrating that the lattice data deviate from the phenomenological results obtained with one particular flavour separation, whereas they clearly prefer another way of assigning the outcome of e^+e^- scattering processes to the quarks in the hard scattering process. This discovery is especially relevant since the inappropriate approach has been used before to compute the SM value [Jegerlehner 2011]. Besides, we have also determined the masses and coupling constants of the vector mesons from the temporal correlation functions and convincing agreement with the experimental values has been found for the ρ- and the J/Ψ mesons.

For our computations we have employed $N_f = 2 + 1 + 1$ gauge field configurations generated by the European Twisted Mass Collaboration featuring strange and charm quark masses close to their physical values and pion masses in the range $230\,\mathrm{MeV} \lesssim m_\pi \lesssim 490\,\mathrm{MeV}$. Considering four active flavours has allowed us to unambiguously compare our results with the various phenomenological analyses of the investigated observables. The electron $(g-2)$ represents an exception since it only receives contributions from very small momenta where heavy flavours are less important. Thus, $N_f = 2+1$ active flavours already yield compatible results for the electron anomalous magnetic moment. Conversely, the τ-lepton anomalous magnetic moment is most sensitive to the charm quark contribution. Nevertheless, the anomalous magnetic moment of the electron provides a very important cross-check of the overall parametrisation of the HVP function, as the value of the HVP function at zero momentum transfer has to be subtracted for all observables. Within our standard approach, $\Pi(0)$ is determined by extrapolating the lattice data obtained at discrete momenta. Hence, verifying the results of this extrapolation by a comparison of the electron $(g-2)$ with its phenomenological value constitutes an essential element for the determination of all observables studied in this thesis.

From our LQCD calculations, we have obtained reliable error estimates for all quantities. This has been achieved by performing the chiral and continuum extrapolations in conjunc-

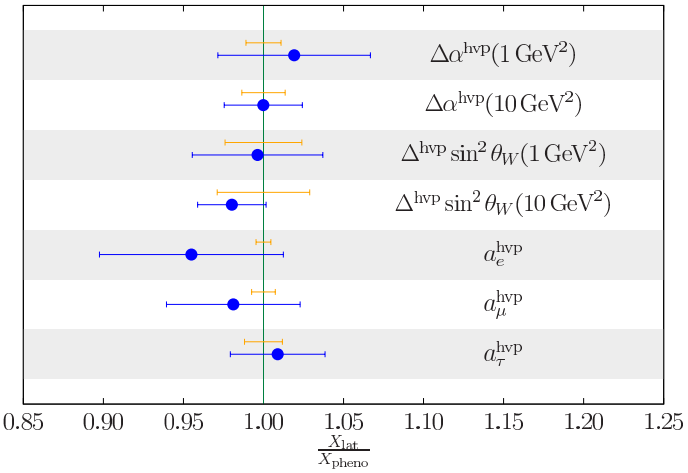

Figure 7.1.: The blue circles depict the ratios of LQCD to phenomenological results of the electroweak parameters indicated on the right. Their error bars represent the combined statistical and systematic uncertainties of our results. The uncertainties of the phenomenological results have been indicated separately by the orange error bars. This figure summarises Tab. 5.2, Tab. 5.4, and Tab. 6.10 whose captions provide the references to the phenomenological values. For the weak mixing angle, we have used the results from [Jegerlehner 2012] obtained with $SU(3)$ flavour separation.

tion with a comprehensive investigation of the systematic uncertainties, including a first estimate of the light-quark disconnected contributions on one of our four-flavour ensembles. Additionally, the results of the chiral extrapolation have been verified by comparing the light quark contributions with those obtained on a $N_f = 2$ twisted mass ensemble at the physical point.

For the muon anomalous magnetic moment, two- and three-flavour LQCD results have also been computed by other collaborations using different fermion actions. A comparison with our two- and three flavour values has revealed convincing agreement as shown in Tab. 6.4. The values obtained with twisted mass fermions typically are more precise, which can be attributed to the lattice redefinitions of the considered quantities [Feng et al. 2011a, Renner et al. 2012]. These redefinitions are inspired by leading-order resonance chiral perturbation theory and considerably facilitate the extrapolation to the physical point. As an important theoretical result, we have analytically proven that automatic $\mathcal{O}(a)$ improvement, characteristic of twisted mass fermions, is retained for our definition of the HVP function despite its short-distance contributions. This ensures that observables derived from the HVP function approach the continuum limit as $\mathcal{O}\left(a^2\right)$ without requiring additional improvement coefficients which have to be computed in other LQCD formulations.

A summary of the obtained results is presented in Fig. 7.1. Here, we compare our continuum and chirally extrapolated values for the electroweak observables X with those of various phenomenological determinations in the form $\frac{X_{\mathrm{lat}}}{X_{\mathrm{pheno}}}$. For α_{QED} and the weak mixing angle, we have chosen two representative momentum values. Full agreement is observed for all quantities with a precision of $2-6\%$. This constitutes a highly non-trivial verification of the phenomenological results from first principles. Moreover, it confirms

the validity of our parametrisation of the HVP function, as we have employed exactly the same computational strategy for all leptons, including the same fit functions that were also used for the investigation of the electroweak coupling constants. The precision of our pilot LQCD investigations with four active flavours is notably lower than the phenomenological accuracy, but it already reaches the same order of magnitude. Our accuracy for the τ-lepton anomalous magnetic moment is within a factor of two of the phenomenological value, as it is most easily accessible on a finite space-time lattice.

As the dominant sources of uncertainty, we have identified both the choice of fit interval to extract the vector meson properties and the choice of fit function for the HVP. The former can potentially be avoided for the electron and the muon anomalous magnetic moments by using Padé approximants. However, doing so requires more momenta in the low-Q^2 region and thus larger lattices as well as drastically improved statistical uncertainties. This would be particularly useful as it would also reduce the dependence on the choice of fit function, our second major uncertainty. If the above-mentioned suggestions are realised, it can be hoped that fitting the HVP function can be avoided altogether by using, for example, the analytic continuation method. It might even be possible to overcome all these issues together with the uncertainty related to the chiral extrapolation by using $N_f = 2 + 1 + 1$ configurations at the physical point, for which large lattices will be needed. In fact, the tuning to maximal twist of a $N_f = 2 + 1 + 1$ ensemble featuring twisted mass fermions with masses all at or very close to their physical values is currently underway. This entails the exciting prospect of a completely physical setup which could be available in the near future.

In order to potentially challenge the precision of the phenomenological computations, additional steps to reduce the LQCD uncertainties are required. As a starting point, we have tried to increase the statistical precision by implementing and testing the all-mode-averaging [Blum et al. 2013b] and the exact deflation techniques [Saad 1984, Neff et al. 2001], where the latter proved to be advantageous, at least for the ensemble at the physical point. Currently, we are repeating our determination of the HVP function at the physical point with exact deflation. Further measures involve computing the complete quark-disconnected contributions and including isospin breaking as well as electromagnetic effects. We have started addressing the former through a dedicated evaluation of the light-quark disconnected contributions on the ensemble with the largest statistics and found an influence of about 3% for the muon $(g-2)$, which is, however, not yet statistically significant. This is larger than the expected 1% effect caused by isospin breaking and suggests that the disconnected contributions can no longer be neglected once the statistical uncertainty is lowered. Once all three aspects mentioned above have been effectuated in order to achieve a sufficiently high accuracy for the leading order QCD contributions, it will be essential to reduce the uncertainties of the next-to-leading order contributions as well. This is of particular importance for the light-by-light contribution entering the computations of the lepton anomalous magnetic moments at $\mathcal{O}\left(\alpha^3\right)$, for which meanwhile several approaches exist, see e.g. [Blum et al. 2015, Green et al. 2015].

Apart from the electroweak observables discussed before, the generated data have also been used to determine the strong coupling constant α_s and the charm quark mass along the lines of [Jansen et al. 2011]. Both quantities represent further fundamental parameters of the SM and are of considerable importance. The strong coupling constant can also be determined by comparing the Adler function, proportional to the first logarithmic derivative of the HVP function, with perturbative calculations in the large-momentum

regime. Moreover, the ρ masses obtained in this thesis have been used to compute the lattice QCD β-function to determine the QCD equation of state via the trace anomaly at finite temperature [Burger et al. 2013]. In addition, the Lamb shift in muonic and ordinary hydrogen is proportional to the first derivative of the HVP function at zero momentum [Friar et al. 1999,Martynenko and Faustov 2001] and could thus be determined from the same lattice data. From this quantity the proton radius can be derived. At present, there is a discrepancy of about seven standard deviations between the value obtained from ordinary hydrogen and that gained from muonic hydrogen known as proton radius puzzle, cf. [Antognini et al. 2013, Carlson 2015].

The computations and tools developed in this thesis have the potential to lead to more precise values for electroweak parameters in the future and could thus assist in the detection of yet-unknown physics. We have computed the leading QCD contributions both to various benchmark quantities for new physics searches and to coupling constants necessary for perturbative calculations while taking for the first time all relevant quark species into account. For all observables, we have obtained fully consistent results with those from dispersive analyses. Compared to the precision achieved by those phenomenological calculations, this pilot lattice QCD investigation still entails larger uncertainties after all extrapolations have been performed and all quantified systematic uncertainties have been addressed. Nevertheless, the presented results have already influenced the next generation of phenomenological determination of the leading hadronic contribution to the running of the $SU(2)_I$ coupling constant α_2 and thus the weak mixing angle by identifying appropriate flavour separations necessary in the dispersive approach. One ingredient that helped to achieve the required precision was the proof of automatic $\mathcal{O}(a)$ improvement for the complete HVP function. Due to ever increasing computational resources as well as algorithmic and conceptual improvements, some of which have already been mentioned in this thesis, it can be hoped that LQCD results will be able to exceed the accuracy of the phenomenological approaches within the coming years.

Appendix A

Symmetry transformations

$$
\begin{array}{rl}
\mathcal{T}_{1,2}: & x \to Tx = (-x_0,\, \vec{x}) \\
& \chi(x) \to i\tau^{1,2}\,\gamma_0\,\gamma_5\,\chi(Tx) \\
& \bar{\chi}(x) \to -i\bar{\chi}(Tx)\,\tau^{1,2}\,\gamma_5\,\gamma_0 \\
& U_0(x) \to U_0(Tx - a\hat{0})^\dagger\,,\; U_i(x) \to U_i(Tx) \\
\mathcal{T} \times [\mu_q \to -\mu_q]: & \\
\text{with } \mathcal{T}: & x \to Tx = (-x_0,\, \vec{x}) \\
& \chi(x) \to i\,\gamma_0\,\gamma_5\,\chi(Tx) \\
& \bar{\chi}(x) \to -i\bar{\chi}(Tx)\,\gamma_5\,\gamma_0 \\
& U_0(x) \to U_0(Tx - a\hat{0})^\dagger\,,\; U_i(x) \to U_i(Tx) \\
\hline
\mathcal{P}_{1,2}: & x \to Px = (x_0,\, -\vec{x}) \\
& \chi(x) \to i\tau^{1,2}\,\gamma_0\,\chi(Px) \\
& \bar{\chi}(x) \to -i\bar{\chi}(Px)\,\tau^{1,2}\,\gamma_0 \\
& U_0(x) \to U_0(Px)\,,\; U_i(x) \to U_i(Px - a\hat{i})^\dagger \\
\mathcal{P} \times [\mu_q \to -\mu_q]: & \\
\text{with } \mathcal{P}: & x \to Px = (x_0,\, -\vec{x}) \\
& \chi(x) \to i\,\gamma_0\,\chi(Px) \\
& \bar{\chi}(x) \to -i\bar{\chi}(Px)\,\gamma_0 \\
& U_0(x) \to U_0(Px)\,,\; U_i(x) \to U_i(Px - a\hat{i})^\dagger \\
\hline
\mathcal{C}: & \chi(x) \to C^{-1}\,\bar{\chi}(x)^T \\
& \bar{\chi}(x) \to -\chi(x)^T\,C \\
& U_\mu(x) \to U_\mu(x)^* \\
\text{with} & C = i\gamma_0\gamma_2 \text{ in representation of [Shindler 2008]}
\end{array}
\tag{A.1}
$$

$\mathcal{P} \times \mathcal{D} \times [m_q \to -m_q] \times [r \to -r]$:

with $\mathcal{D}$: $U_\mu(x) \to U_\mu(-x - a\hat{\mu})^\dagger$

$\chi(x) \to -i\,\chi(-x)$

$\bar{\chi}(x) \to -i\,\bar{\chi}(-x)$

$\mathcal{R}_5^{1,2} \times \mathcal{D} \times [\mu_q \to -\mu_q]$:

with $\mathcal{R}_5^{1,2}$: $\chi(x) \to i\,\gamma_5\,\tau^{1,2}\,\chi(x)$

$\bar{\chi}(x) \to i\,\bar{\chi}(x)\,\gamma_5\,\tau^{1,2}$

Appendix B

Space-time symmetry projections in position space

The momentum projector $P_{\mu\nu}(Q)$ given in Eq. (3.25) transforms like a rank-2-tensor, that is for any discrete space-time transformation Λ we have

$$P_{\mu\nu}(\Lambda Q) = \Lambda_\mu^{\mu'}\, \Lambda_\nu^{\nu'}\, P_{\mu'\nu'}(Q)\,.$$

Λ denotes a representation of the essentially hypercubic lattice symmetry group. We can restrict the set of momenta to a representative set and translate the average over $\mathcal{G}(Q)$ to position space. Moreover, instead of averaging over $\mathcal{G}(Q)$ for a specific momentum Q we can average over the complete space-time transformation group $\mathcal{G}$ [1]and define

$$\begin{aligned}
[\Pi(Q)]^{(\mathrm{av})} &= \frac{1}{N_{\mathcal{G}(Q)}} \sum_{Q\in\mathcal{G}(Q)} \frac{1}{3(\hat{Q}^2)^2}\, P_{\mu\nu}(Q)\, a^4 \sum_x \Pi_{\mu\nu}(x,y)\, \mathrm{e}^{iQ(x+a\hat{\mu}/2-y-a\hat{\nu}/2)} \\
&= \frac{1}{N_{\mathcal{G}}} \sum_{\Lambda\in\mathcal{G}} \frac{1}{3(\hat{Q}^2)^2}\, P_{\mu\nu}(\Lambda Q_{\mathrm{fix}})\, a^4 \sum_x \Pi_{\mu\nu}(x,y)\, \mathrm{e}^{i(\Lambda Q_{\mathrm{fix}})(x+a\hat{\mu}/2-y-a\hat{\nu}/2)} \\
&= \frac{P_{\mu'\nu'}(Q_{\mathrm{fix}})}{3(\hat{Q}^2)^2}\, a^4 \sum_x \frac{1}{N_{\mathcal{G}}} \sum_{\Lambda\in\mathcal{G}} \Lambda_\mu^{\mu'}\, \Lambda_\nu^{\nu'}\, \Pi_{\mu\nu}(x,y)\, \mathrm{e}^{iQ_{\mathrm{fix}}\,\Lambda^{-1}(x+a\hat{\mu}/2-y-a\hat{\nu}/2)}
\end{aligned} \tag{B.1}$$

where Q_{fix} is some fixed reference momentum. We can rewrite the transformed space-time argument in the Fourier phase in Eq. (B.1) as

$$\begin{aligned}
\Lambda^{-1}(x+a\hat{\mu}/2) &= x' + a\hat{\mu}'/2 \\
\mu' &= \sigma_\Lambda(\mu) \\
x' &= \begin{cases} \Lambda^{-1}x & \mu-\text{direction not reflected} \\ \Lambda^{-1}(x+a\hat{\mu}) & \mu-\text{direction reflected} \end{cases},
\end{aligned} \tag{B.2}$$

where σ_Λ is the permutation generated by Λ. Hence, we obtain

$$\begin{aligned}
[\Pi(Q)]^{(\mathrm{av})} &= \frac{1}{3(\hat{Q}^2)^2}\, P_{\mu'\nu'}(Q_{\mathrm{fix}})\, a^4 \sum_{x'} \frac{1}{N_{\mathcal{G}}} \sum_{\Lambda\in\mathcal{G}} \Lambda_\mu^{\mu'}\, \Lambda_\nu^{\nu'}\, \Pi_{\mu\nu}(\Lambda x', \Lambda y')\, \mathrm{e}^{iQ_{\mathrm{fix}}\,(x'+a\hat{\mu}'/2-y'-a\hat{\nu}'/2)} \\
&= \frac{1}{3(\hat{Q}^2)^2}\, P_{\mu'\nu'}(Q_{\mathrm{fix}})\, a^4 \sum_{x'} \left[\Pi_{\mu'\nu'}(x',y')\right]^{(av)}\, \mathrm{e}^{iQ_{\mathrm{fix}}\,(x'+a\hat{\mu}'/2-y'-a\hat{\nu}'/2)}\,.
\end{aligned} \tag{B.3}$$

[1]For any momentum Q the number of elements $N_{\mathcal{G}(Q)}$ divides the number of elements in the whole group $N_{\mathcal{G}}$.

By construction the operator

$$\left[\Pi_{\mu'\nu'}(x',y')\right]^{(av)} = \frac{1}{N_{\mathcal{G}}} \sum_{\Lambda\in\mathcal{G}} \Lambda_{\mu}^{\mu'}\, \Lambda_{\nu}^{\nu'}\, \Pi_{\mu\nu}(\Lambda x', \Lambda y') \tag{B.4}$$

has the same transformation behaviour as the projector $P_{\mu\nu}$; it transforms like a true rank-2 tensor in position space and the trace of the tensor, $\sum_{\mu'} \left[\Pi_{\mu'\mu'}(x',y')\right]^{(av)}$, is a scalar.

Appendix C

Operator listings

The relevant lattice operators which potentially mix with $\Pi_{\mu\nu}$ at short distances are listed in the following tables {C.1}, and {C.2}. The first contains operators not involving derivatives whereas the second accommodates the derivative operators. We note that for obtaining a complete set of operators for any operator $O_{\mu\nu}$ appearing in the tables the diagonal part $\delta_{\mu\nu} O_{\mu\mu}$ (without summation over μ) and the trace $\delta_{\mu\nu} O_{\lambda\lambda}$ must be included separately. Since these have the same quantum numbers as $O_{\mu\nu}$ given in the table (with $I_{\mu\mu} = 1$), we do not repeat those quantum numbers. To indicate the symmetry transformations we use the short-hand notations $[-\mu]$ for $[\mu_q \to -\mu_q]$, $[-m]$ for $[m_q \to -m_q]$, and $[-r]$ for $[r \to -r]$.

Furthermore, to save space the common prefactor $r^k\, m_q^{n_m}\, \mu_q^{n_\mu}$ ($k \in \{0,1\}$, n_m, $n_\mu \in \mathbb{N}_0$), which is essential for counting the dimension of the operator, is omitted for all but the first operator. Its quantum numbers can be inferred from the first line of each table and have to be multiplied with the quantum numbers in the respective column.

The powers of τ^3 and γ_5 appearing in fermion bilinears such as

$$r^k\, m_q^{n_m}\, \mu_q^{n_\mu} \bar{\chi} (\tau^3)^m (\gamma_5)^l \Gamma \chi$$

with $\Gamma \in \{\mathbb{1}, \gamma_\mu, \sigma_{\mu\nu}, \gamma_5\gamma_\mu, \gamma_5\}$ and four-quark operators

$$r^k\, m_q^{n_m}\, \mu_q^{n_\mu} \bar{\chi} (\tau^3)^m (\gamma_5)^l \Gamma \chi \bar{\chi} (\tau^3)^{m'} (\gamma_5)^{l'} \Gamma \chi$$

can only take the values m, m', l, $l' \in \{0,1\}$.

operator	$\mathcal{P}_{1/2}$	$\mathcal{P}\,[-\mu]$	$\mathcal{T}_{1/2}$	$\mathcal{T}\,[-\mu]$	$\mathcal{C}$	$\mathcal{P}\,\mathcal{D}\,[-m]\,[-r]$	$\mathcal{R}_5^{1,2}\,\mathcal{D}\,[-\mu]$
$\delta_{\mu\nu}\, r^k\, m^{n_m}\, \mu^{n_\mu}$	$I_{\mu\nu}$	$(-)^{n_\mu}\, I_{\mu\nu}$	$I_{\mu\nu}$	$(-)^{n_\mu}\, I_{\mu\nu}$	$+1$	$(-)^{n_m+k}\, I_{\mu\nu}$	$(-)^{n_\mu}$
$\delta_{\mu\nu}\, \bar{\chi}\, (\tau^3)^m\, \gamma_5^l\, \chi(x)$	$(-)^{m+l}\, I_{\mu\nu}$	$(-)^l\, I_{\mu\nu}$	$(-)^{m+l}\, I_{\mu\nu}$	$(-)^l\, I_{\mu\nu}$	$+1$	$(-)^{l+1}\, I_{\mu\nu}$	$(-)^m$
$\mathrm{tr}\,[C_{\mu\lambda}\, C_{\lambda\nu}(x)]$	$I_{\mu\nu}$	$I_{\mu\nu}$	$I_{\mu\nu}$	$I_{\mu\nu}$	$+1$	$I_{\mu\nu}$	$+1$
$\mathrm{tr}\left[C_{\mu\lambda}\, \tilde{C}_{\lambda\nu}(x)\right] + [\mu \leftrightarrow \nu]$	$-I_{\mu\nu}$	$-I_{\mu\nu}$	$-I_{\mu\nu}$	$-I_{\mu\nu}$	$+1$	$-I_{\mu\nu}$	$+1$
$\bar{\chi}\, (\tau^3)^m\, \gamma_5^l\, \sigma_{\mu\lambda}\, C_{\lambda\nu}\, \chi(x) + [\mu \leftrightarrow \nu]$	$(-)^{l+m}\, I_{\mu\nu}$	$(-)^l\, I_{\mu\nu}$	$(-)^{l+m}\, I_{\mu\nu}$	$(-)^l\, I_{\mu\nu}$	$+1$	$(-)^{l+1} I_{\mu\nu}$	$(-)^m$
$\bar{\chi}\, (\tau^3)^m\, \gamma_5^l\, \sigma_{\mu\lambda}\, \tilde{C}_{\lambda\nu}\, \chi(x) + [\mu \leftrightarrow \nu]$	$(-)^{l+m+1}\, I_{\mu\nu}$	$(-)^{l+1}\, I_{\mu\nu}$	$(-)^{l+m+1}\, I_{\mu\nu}$	$(-)^{l+1}\, I_{\mu\nu}$	$+1$	$(-)^l I_{\mu\nu}$	$(-)^m$
$\delta_{\mu\nu}\, \bar{\chi}\, (\tau^3)^m\, \gamma_5^l\, \chi\, \bar{\chi}\, (\tau^3)^{m'}\, \gamma_5^{l'}\, \chi(x)$	$(-)^{l+l'+m+m'}\, I_{\mu\nu}$	$(-)^{l+l'}\, I_{\mu\nu}$	$(-)^{l+l'+m+m'}\, I_{\mu\nu}$	$(-)^{l+l'}\, I_{\mu\nu}$	$+1$	$(-)^{l+l'}\, I_{\mu\nu}$	$(-)^{m+m'}$
$\bar{\chi}\, (\tau^3)^m\, \gamma_5^l\, \gamma_\mu\, \chi\, \bar{\chi}\, (\tau^3)^{m'}\, \gamma_5^{l'}\, \gamma_\nu\, \chi(x) + [\mu \leftrightarrow \nu]$	$(-)^{l+l'+m+m'}\, I_{\mu\nu}$	$(-)^{l+l'}\, I_{\mu\nu}$	$(-)^{l+l'+m+m'}\, I_{\mu\nu}$	$(-)^{l+l'}\, I_{\mu\nu}$	$(-)^{l+l'}$	$(-)^{l+l'}\, I_{\mu\nu}$	$(-)^{m+m'}$
$\bar{\chi}\, (\tau^3)^m\, \gamma_5^l\, \sigma_{\mu\lambda}\, \chi\, \bar{\chi}\, (\tau^3)^{m'}\, \gamma_5^{l'}\, \sigma_{\lambda\nu}\, \chi(x) + [\mu \leftrightarrow \nu]$	$(-)^{l+l'+m+m'}\, I_{\mu\nu}$	$(-)^{l+l'}\, I_{\mu\nu}$	$(-)^{l+l'+m+m'}\, I_{\mu\nu}$	$(-)^{l+l'}\, I_{\mu\nu}$	$+1$	$(-)^{l+l'}\, I_{\mu\nu}$	$(-)^{m+m'}$
$\delta_{\mu\nu}\, \bar{\chi}\, (\tau^3)^m\, \gamma_5^l\, t^a\, \chi\, \bar{\chi}\, (\tau^3)^{m'}\, \gamma_5^{l'}\, t^a\, \chi(x)$							
$\bar{\chi}\, (\tau^3)^m\, \gamma_5^l\, \gamma_\mu\, t^a\, \chi\, \bar{\chi}\, (\tau^3)^{m'}\, \gamma_5^{l'}\, \gamma_\nu\, t^a\, \chi(x) + [\mu \leftrightarrow \nu]$							
$\bar{\chi}\, (\tau^3)^m\, \gamma_5^l\, \sigma_{\mu\lambda}\, t^a\, \chi\, \bar{\chi}\, (\tau^3)^{m'}\, \gamma_5^{l'}\, \sigma_{\lambda\nu}\, t^a\, \chi(x) + [\mu \leftrightarrow \nu]$							
$\delta_{\mu\nu}\, \bar{\chi}\, \tau^b\, \gamma_5^l\, \chi\, \bar{\chi}\, \tau^b\, \gamma_5^{l'}\, \chi(x)$	$(-)^{l+l'}\, I_{\mu\nu}$	$(-)^{l+l'}\, I_{\mu\nu}$	$(-)^{l+l'}\, I_{\mu\nu}$	$(-)^{l+l'}\, I_{\mu\nu}$	$+1$	$(-)^{l+l'}\, I_{\mu\nu}$	$+1$
$\bar{\chi}\, \tau^b\, \gamma_5^l\, \gamma_\mu\, \chi\, \bar{\chi}\, \tau^b\, \gamma_5^{l'}\, \gamma_\nu\, \chi(x) + [\mu \leftrightarrow \nu]$	$(-)^{l+l'}\, I_{\mu\nu}$	$(-)^{l+l'}\, I_{\mu\nu}$	$(-)^{l+l'}\, I_{\mu\nu}$	$(-)^{l+l'}\, I_{\mu\nu}$	$(-)^{l+l'}$	$(-)^{l+l'}\, I_{\mu\nu}$	$+1$
$\bar{\chi}\, \tau^b\, \gamma_5^l\, \sigma_{\mu\lambda}\, \chi\, \bar{\chi}\, \tau^b\, \gamma_5^{l'}\, \sigma_{\lambda\nu}\, \chi(x) + [\mu \leftrightarrow \nu]$	$(-)^{l+l'}\, I_{\mu\nu}$	$(-)^{l+l'}\, I_{\mu\nu}$	$(-)^{l+l'}\, I_{\mu\nu}$	$(-)^{l+l'}\, I_{\mu\nu}$	$+1$	$(-)^{l+l'}\, I_{\mu\nu}$	$+1$
$\delta_{\mu\nu}\, \bar{\chi}\, \tau^b\, \gamma_5^l\, t^a\, \chi\, \bar{\chi}\, \tau^b\, \gamma_5^{l'}\, t^a\, \chi(x)$							
$\bar{\chi}\, \tau^b\, \gamma_5^l\, \gamma_\mu\, t^a\, \chi\, \bar{\chi}\, \tau^b\, \gamma_5^{l'}\, \gamma_\nu\, t^a\, \chi(x) + [\mu \leftrightarrow \nu]$							
$\bar{\chi}\, \tau^b\, \gamma_5^l\, \sigma_{\mu\lambda}\, t^a\, \chi\, \bar{\chi}\, \tau^b\, \gamma_5^{l'}\, \sigma_{\lambda\nu}\, t^a\, \chi(x) + [\mu \leftrightarrow \nu]$							

Table C.1.: Transformation properties of operators without covariant derivatives up to mass dimension 6. $C_{\mu\nu}$ is a version of the lattice field strength tensor as appearing in the Sheikholeslami-Wohlert term [Sheikholeslami and Wohlert 1985]. $+1$ indicates that the operator is even under the respective transformation, -1 denotes odd transformation behavior. $I_{\mu\nu} = (-1)^{\delta_{\mu 0}+\delta_{\nu 0}}$.

operator	$\mathcal{P}_{1,2}$	$\mathcal{P}\,[-\mu]$	$\mathcal{T}_{1,2}$	$\mathcal{T}\,[-\mu]$	$\mathcal{C}$	$\mathcal{P}\,\mathcal{D}\,[-m]\,[-r]$	$\mathcal{R}_5^{1,2}\,\mathcal{D}\,[-\mu]$
$r^k m^{n_m} \mu^{n_\mu}$	$+1$	$(-)^{n_\mu}$	$+1$	$(-)^{n_\mu}$	$+1$	$(-)^{n_m}(-)^k$	$(-)^{n_\mu}$
$\mathrm{Tr}\left(\overrightarrow{\nabla}_\mu \overrightarrow{\nabla}_\lambda C_{\lambda\nu}(x) + \overrightarrow{\nabla}_\nu \overrightarrow{\nabla}_\lambda C_{\lambda\mu}(x)\right)$	$I_{\mu\nu}$	$I_{\mu\nu}$	$I_{\mu\nu}$	$I_{\mu\nu}$	$+1$	$I_{\mu\nu}$	$+1$
$\mathrm{Tr}\left(\overrightarrow{\nabla}_\mu \overrightarrow{\nabla}_\lambda \tilde{C}_{\lambda\nu}(x) + \overrightarrow{\nabla}_\nu \overrightarrow{\nabla}_\lambda \tilde{C}_{\lambda\mu}(x)\right)$	$-I_{\mu\nu}$	$-I_{\mu\nu}$	$-I_{\mu\nu}$	$-I_{\mu\nu}$	N	$-I_{\mu\nu}$	$+1$
$\bar{\chi}\,(\tau^3)^m \left(\overleftarrow{\nabla}_\mu \gamma_\nu \gamma_5^l \pm \gamma_5^l \gamma_\nu \overrightarrow{\nabla}_\mu\right) \chi(x) + [\mu \leftrightarrow \nu]$	$(-)^{l+m} I_{\mu\nu}$	$(-)^l I_{\mu\nu}$	$(-)^{l+m} I_{\mu\nu}$	$(-)^l I_{\mu\nu}$	± 1	$(-)^l I_{\mu\nu}$	$(-)^m$
$\bar{\chi}\,(\tau^3)^m \gamma_5^l \left(\overleftarrow{\nabla}_\mu \overleftarrow{\nabla}_\nu \pm \overrightarrow{\nabla}_\mu \overrightarrow{\nabla}_\nu\right) \chi(x) + [\mu \leftrightarrow \nu]$							
$\bar{\chi}\,(\tau^3)^m \left(\overleftarrow{\not{\nabla}} \overleftarrow{\nabla}_\mu \gamma_\nu \gamma_5^l \pm \gamma_5^l \gamma_\nu \overrightarrow{\nabla}_\mu \overrightarrow{\not{\nabla}}\right) \chi(x) + [\mu \leftrightarrow \nu]$							
$\bar{\chi}\,(\tau^3)^m \left(\overleftarrow{\nabla}_\mu \overleftarrow{\not{\nabla}} \gamma_\nu \gamma_5^l \pm \gamma_5^l \gamma_\nu \overrightarrow{\not{\nabla}} \overrightarrow{\nabla}_\mu\right) \chi(x) + [\mu \leftrightarrow \nu]$							
$\bar{\chi}\,(\tau^3)^m \gamma_5^l \left(\overleftarrow{\nabla}_\mu \overrightarrow{\nabla}_\nu\right) \chi(x) + [\mu \leftrightarrow \nu]$							
$\bar{\chi}\,(\tau^3)^m \left(\overleftarrow{\not{\nabla}} \gamma_\nu \gamma_5^l \overrightarrow{\nabla}_\mu \mp \overleftarrow{\nabla}_\mu \gamma_5^l \gamma_\nu \overrightarrow{\not{\nabla}}\right) \chi(x) + [\mu \leftrightarrow \nu]$							
$\bar{\chi}\,(\tau^3)^m \left(\overleftarrow{\nabla}_\mu \overleftarrow{\nabla}_\nu \overleftarrow{\not{\nabla}} \gamma_5^l \mp \gamma_5^l \overrightarrow{\not{\nabla}} \overrightarrow{\nabla}_\nu \overrightarrow{\nabla}_\mu\right) \chi(x) + [\mu \leftrightarrow \nu]$	$(-)^{l+m} I_{\mu\nu}$	$(-)^l I_{\mu\nu}$	$(-)^{l+m} I_{\mu\nu}$	$(-)^l I_{\mu\nu}$	± 1	$(-)^l I_{\mu\nu}$	$(-)^m$
$\bar{\chi}\,(\tau^3)^m \left(\overleftarrow{\nabla}_\mu \overleftarrow{\not{\nabla}} \overleftarrow{\nabla}_\nu \gamma_5^l \mp \gamma_5^l \overrightarrow{\nabla}_\nu \overrightarrow{\not{\nabla}} \overrightarrow{\nabla}_\mu\right) \chi(x) + [\mu \leftrightarrow \nu]$							
$\bar{\chi}\,(\tau^3)^m \left(\overleftarrow{\not{\nabla}} \overleftarrow{\nabla}_\mu \overleftarrow{\nabla}_\nu \gamma_5^l \mp \gamma_5^l \overrightarrow{\nabla}_\nu \overrightarrow{\nabla}_\mu \overrightarrow{\not{\nabla}}\right) \chi(x) + [\mu \leftrightarrow \nu]$							
$\bar{\chi}\,(\tau^3)^m \left(\overleftarrow{\nabla}^2 \overleftarrow{\nabla}_\mu \gamma_\nu \gamma_5^l \mp \gamma_5^l \gamma_\nu \overrightarrow{\nabla}_\mu \overrightarrow{\nabla}^2\right) \chi(x) + [\mu \leftrightarrow \nu]$							
$\bar{\chi}\,(\tau^3)^m \left(\overleftarrow{\nabla} \overleftarrow{\nabla}_\mu \overleftarrow{\nabla} \gamma_\nu \gamma_5^l \mp \gamma_5^l \gamma_\nu \overrightarrow{\nabla} \overrightarrow{\nabla}_\mu \overrightarrow{\nabla}\right) \chi(x) + [\mu \leftrightarrow \nu]$							
$\bar{\chi}\,(\tau^3)^m \left(\overleftarrow{\nabla}_\mu \overleftarrow{\nabla}^2 \gamma_\nu \gamma_5^l \mp \gamma_5^l \gamma_\nu \overrightarrow{\nabla}^2 \overrightarrow{\nabla}_\mu\right) \chi(x) + [\mu \leftrightarrow \nu]$							
$\bar{\chi}\,(\tau^3)^m \left(\overleftarrow{\not{\nabla}}^2 \gamma_\nu \gamma_5^l \mp \gamma_5^l \gamma_\nu \overrightarrow{\not{\nabla}}^2 \overrightarrow{\nabla}_\mu\right) \chi(x) + [\mu \leftrightarrow \nu]$							
$\bar{\chi}\,(\tau^3)^m \left(\overleftarrow{\not{\nabla}} \overleftarrow{\nabla}_\mu \overleftarrow{\not{\nabla}} \gamma_\nu \gamma_5^l \mp \gamma_5^l \gamma_\nu \overrightarrow{\not{\nabla}} \overrightarrow{\nabla}_\mu \overrightarrow{\not{\nabla}}\right) \chi(x) + [\mu \leftrightarrow \nu]$							
$\bar{\chi}\,(\tau^3)^m \left(\overleftarrow{\not{\nabla}}^2 \overleftarrow{\nabla}_\mu \gamma_\nu \gamma_5^l \mp \gamma_5^l \gamma_\nu \overrightarrow{\nabla}_\mu \overrightarrow{\not{\nabla}}^2\right) \chi(x) + [\mu \leftrightarrow \nu]$							

$\bar{\chi}\,(\tau^3)^m\,\left(\overleftarrow{\nabla}^3_\mu\,\gamma_\nu\,\gamma_5^l \mp \gamma_5^l\,\gamma_\nu\,\overrightarrow{\nabla}^3_\mu\right)\,\chi(x) + [\mu \leftrightarrow \nu]$	$(-)^{l+m} I_{\mu\nu} \quad (-)^l I_{\mu\nu}$	$(-)^{l+m} I_{\mu\nu} \quad (-)^l I_{\mu\nu}$	± 1	$(-)^l I_{\mu\nu}$	$(-)^m$
$\bar{\chi}\,(\tau^3)^m\,\left(\overleftarrow{\nabla}^2_\mu\,\overleftarrow{\nabla}_\nu\,\gamma_\mu\,\gamma_5^l \mp \gamma_5^l\,\gamma_\mu\,\overrightarrow{\nabla}_\nu\,\overrightarrow{\nabla}^2_\mu\right)\,\chi(x) + [\mu \leftrightarrow \nu]$					
$\bar{\chi}\,(\tau^3)^m\,\left(\overleftarrow{\nabla}_\mu\,\overleftarrow{\nabla}_\nu\,\overleftarrow{\nabla}_\mu\,\gamma_\mu\,\gamma_5^l \mp \gamma_5^l\,\gamma_\mu\,\overrightarrow{\nabla}_\mu\,\overrightarrow{\nabla}_\nu\,\overrightarrow{\nabla}_\mu\right)\,\chi(x) + [\mu \leftrightarrow \nu]$					
$\bar{\chi}\,(\tau^3)^m\,\left(\overleftarrow{\nabla}_\nu\,\overleftarrow{\nabla}^2_\mu\,\gamma_\mu\,\gamma_5^l \mp \gamma_5^l\,\gamma_\mu\,\overrightarrow{\nabla}^2_\mu\,\overrightarrow{\nabla}_\nu\right)\,\chi(x) + [\mu \leftrightarrow \nu]$					
$\bar{\chi}\,(\tau^3)^m\,\left(\overleftarrow{\nabla}^2_\mu\,\overleftarrow{\not\nabla}\,\gamma_\mu\,\gamma_\nu\,\gamma_5^l \mp \gamma_5^l\,\gamma_\nu\,\gamma_\mu\,\overrightarrow{\not\nabla}\,\overrightarrow{\nabla}^2_\mu\right)\,\chi(x) + [\mu \leftrightarrow \nu]$					
$\bar{\chi}\,(\tau^3)^m\,\left(\overleftarrow{\nabla}_\mu\,\overleftarrow{\not\nabla}\,\overleftarrow{\nabla}_\mu\,\gamma_\mu\,\gamma_\nu\,\gamma_5^l \mp \gamma_5^l\,\gamma_\nu\,\gamma_\mu\,\overrightarrow{\nabla}_\mu\,\overrightarrow{\not\nabla}\,\overrightarrow{\nabla}_\mu\right)\,\chi(x) + [\mu \leftrightarrow \nu]$					
$\bar{\chi}\,(\tau^3)^m\,\left(\overleftarrow{\not\nabla}\,\overleftarrow{\nabla}^2_\mu\,\gamma_\mu\,\gamma_\nu\,\gamma_5^l \mp \gamma_5^l\,\gamma_\nu\,\gamma_\mu\,\overrightarrow{\nabla}^2_\mu\,\overrightarrow{\not\nabla}\right)\,\chi(x) + [\mu \leftrightarrow \nu]$					

$\bar{\chi}\,(\tau^3)^m\,\left(\overleftarrow{\nabla}_\mu\,\overleftarrow{\nabla}_\nu\,\overleftarrow{\not\nabla}\,\gamma_5^l \mp \gamma_5^l\,\overleftarrow{\not\nabla}\,\overrightarrow{\nabla}_\nu\,\overrightarrow{\nabla}_\mu\right)\,\chi(x) + [\mu \leftrightarrow \nu]$	$(-)^{l+m} I_{\mu\nu} \quad (-)^l I_{\mu\nu}$	$(-)^{l+m} I_{\mu\nu} \quad (-)^l I_{\mu\nu}$	± 1	$(-)^l I_{\mu\nu}$	$(-)^m$
$\bar{\chi}\,(\tau^3)^m\,\left(\overleftarrow{\nabla}_\mu\,\overleftarrow{\not\nabla}\,\overrightarrow{\nabla}_\nu\,\gamma_5^l \mp \gamma_5^l\,\overleftarrow{\nabla}_\nu\,\overrightarrow{\not\nabla}\,\overrightarrow{\nabla}_\mu\right)\,\chi(x) + [\mu \leftrightarrow \nu]$					
$\bar{\chi}\,(\tau^3)^m\,\left(\overleftarrow{\not\nabla}\,\overleftarrow{\nabla}_\mu\,\overrightarrow{\nabla}_\nu\,\gamma_5^l \mp \gamma_5^l\,\overleftarrow{\nabla}_\nu\,\overrightarrow{\nabla}_\mu\,\overrightarrow{\not\nabla}\right)\,\chi(x) + [\mu \leftrightarrow \nu]$					
$\bar{\chi}\,(\tau^3)^m\,\left(\overleftarrow{\nabla}^2\,\overrightarrow{\nabla}_\mu\,\gamma_\nu\,\gamma_5^l \mp \gamma_5^l\,\gamma_\nu\,\overleftarrow{\nabla}_\mu\,\overrightarrow{\nabla}^2\right)\,\chi(x) + [\mu \leftrightarrow \nu]$					
$\bar{\chi}\,(\tau^3)^m\,\left(\overleftarrow{\nabla}\,\overleftarrow{\nabla}_\mu\,\overrightarrow{\nabla}\,\gamma_\nu\,\gamma_5^l \mp \gamma_5^l\,\gamma_\nu\,\overleftarrow{\nabla}\,\overrightarrow{\nabla}_\mu\,\overrightarrow{\nabla}\right)\,\chi(x) + [\mu \leftrightarrow \nu]$					
$\bar{\chi}\,(\tau^3)^m\,\left(\overleftarrow{\nabla}_\mu\,\overleftarrow{\nabla}\,\overrightarrow{\nabla}\,\gamma_\nu\,\gamma_5^l \mp \gamma_5^l\,\gamma_\nu\,\overleftarrow{\nabla}\,\overrightarrow{\nabla}\,\overrightarrow{\nabla}_\mu\right)\,\chi(x) + [\mu \leftrightarrow \nu]$					
$\bar{\chi}\,(\tau^3)^m\,\left(\overleftarrow{\nabla}_\mu\,\overleftarrow{\not\nabla}\,\overrightarrow{\not\nabla}\,\gamma_\nu\,\gamma_5^l \mp \gamma_5^l\,\gamma_\nu\,\overleftarrow{\not\nabla}\,\overrightarrow{\not\nabla}\,\overrightarrow{\nabla}_\mu\right)\,\chi(x) + [\mu \leftrightarrow \nu]$					
$\bar{\chi}\,(\tau^3)^m\,\left(\overleftarrow{\not\nabla}\,\overleftarrow{\nabla}_\mu\,\overrightarrow{\not\nabla}\,\gamma_\nu\,\gamma_5^l \mp \gamma_5^l\,\gamma_\nu\,\overleftarrow{\not\nabla}\,\overrightarrow{\not\nabla}_\mu\,\overrightarrow{\not\nabla}\right)\,\chi(x) + [\mu \leftrightarrow \nu]$					
$\bar{\chi}\,(\tau^3)^m\,\left(\overleftarrow{\not\nabla}^2\,\overrightarrow{\nabla}_\mu\,\gamma_\nu\,\gamma_5^l \mp \gamma_5^l\,\gamma_\nu\,\overleftarrow{\not\nabla}^2\,\overrightarrow{\not\nabla}_\mu\right)\,\chi(x) + [\mu \leftrightarrow \nu]$					
$\bar{\chi}\,(\tau^3)^m\,\left(\overleftarrow{\nabla}^2_\mu\,\overrightarrow{\nabla}_\mu\,\gamma_\nu\,\gamma_5^l \mp \gamma_5^l\,\gamma_\nu\,\overleftarrow{\nabla}_\mu\,\overrightarrow{\nabla}^2_\mu\right)\,\chi(x) + [\mu \leftrightarrow \nu]$					
$\bar{\chi}\,(\tau^3)^m\,\left(\overleftarrow{\nabla}^2_\mu\,\overrightarrow{\nabla}_\nu\,\gamma_\mu\,\gamma_5^l \mp \gamma_5^l\,\gamma_\mu\,\overleftarrow{\nabla}_\nu\,\overrightarrow{\nabla}^2_\mu\right)\,\chi(x) + [\mu \leftrightarrow \nu]$					
$\bar{\chi}\,(\tau^3)^m\,\left(\overleftarrow{\nabla}_\mu\,\overleftarrow{\nabla}_\nu\,\overrightarrow{\nabla}_\mu\,\gamma_\mu\,\gamma_5^l \mp \gamma_5^l\,\gamma_\mu\,\overleftarrow{\nabla}_\mu\,\overrightarrow{\nabla}_\nu\,\overrightarrow{\nabla}_\mu\right)\,\chi(x) + [\mu \leftrightarrow \nu]$					

$\bar{\chi}\,(\tau^3)^m \left(\overleftarrow{\nabla}_\nu \overleftarrow{\nabla}_\mu \overrightarrow{\nabla}_\mu \gamma_\mu \gamma_5^l \mp \gamma_5^l \gamma_\mu \overleftarrow{\nabla}_\mu \overrightarrow{\nabla}_\mu \overrightarrow{\nabla}_\nu\right) \chi(x) + [\mu \leftrightarrow \nu]$					
$\bar{\chi}\,(\tau^3)^m \left(\overleftarrow{\nabla}_\mu^2 \overrightarrow{\not{\nabla}} \gamma_\mu \gamma_\nu \gamma_5^l \mp \gamma_5^l \gamma_\nu \gamma_\mu \overleftarrow{\not{\nabla}} \overrightarrow{\nabla}_\mu^2\right) \chi(x) + [\mu \leftrightarrow \nu]$					
$\bar{\chi}\,(\tau^3)^m \left(\overleftarrow{\nabla}_\mu \overleftarrow{\not{\nabla}} \overrightarrow{\nabla}_\mu \gamma_\mu \gamma_\nu \gamma_5^l \mp \gamma_5^l \gamma_\nu \gamma_\mu \overleftarrow{\nabla}_\mu \overrightarrow{\not{\nabla}} \overrightarrow{\nabla}_\mu\right) \chi(x) + [\mu \leftrightarrow \nu]$					
$\bar{\chi}\,(\tau^3)^m \left(\overleftarrow{\not{\nabla}} \overleftarrow{\nabla}_\mu \overrightarrow{\nabla}_\mu \gamma_\mu \gamma_\nu \gamma_5^l \mp \gamma_5^l \gamma_\nu \gamma_\mu \overleftarrow{\nabla}_\mu \overrightarrow{\nabla}_\mu \overrightarrow{\not{\nabla}}\right) \chi(x) + [\mu \leftrightarrow \nu]$					

Table C.2.: Transformation properties of operators including covariant derivatives with same notation as in Tab. C.1.

Appendix D

Symmetry properties of S_7

In Tab. D.1 we list all possible terms of mass dimension 7 appearing in an expansion of the effective action to order a^3. We discuss their transformation properties under the $\mathcal{R}_5^{1,2}$ and $\mathcal{P} \times [\mu_q \to -\mu_q]$ symmetries which are symmetries of the continuum twisted mass action. We restrict the discussion to operators involving the twisted mass μ_q only since the bare quark mass $m_q = 0$ at maximal twist. We note further that neither $\mathcal{R}_5^{1,2}$ nor $\mathcal{P}\times[\mu_q \to -\mu_q]$ is affected by commuting two different derivative operators in a given expression such that we omit the commuted expressions. $G_{\mu\nu}$ and $\tilde{G}_{\mu\nu}$ denote the continuum field strength tensor and its dual, respectively.

In the four fermion operators we have included a generic transformation matrix $T^A = \tau^\mu \times t^a \times \Gamma$ where $\tau \in \{\tau^0, \tau^1, \tau^2, \tau^3\}$, $\Gamma \in \{\mathbb{1}, \gamma_\mu, \sigma_{\mu\nu}, \gamma_5\gamma_\mu, \gamma_5\}$ and t^a are acting in flavor-, Dirac- and color-space, respectively. Their index A used as a short-hand notation for flavor-, Dirac- and color-indices is summed over in the fermion bilinear product. Different Dirac structures are related via Fierz-identities and have the same transformation properties under the symmetries. Since T^A is appearing twice in all products this introduces an even number of both flavor- and Dirac-matrices such that the symmetry transformation is the same as for the trivial product with all matrices equal to the identity.

operator	$\mathcal{R}_5^{1,2}$	$\mathcal{P}\,[-\mu_q]$	operator	$\mathcal{R}_5^{1,2}$	$\mathcal{P}\,[-\mu_q]$
$\mu_q^4\bar{\chi}\chi$	-1	+1	$\mu_q^4\bar{\chi}\gamma_5\tau^3\chi$	+1	-1
$\mu_q^3\bar{\chi}\not{D}\chi$	+1	-1	$\mu_q^3\bar{\chi}\gamma_5\tau^3\not{D}\chi$	-1	+1
$\mu_q^3\mathrm{tr}\,[G_{\mu\nu}G_{\mu\nu}]$	+1	-1	-	-	-
$\mu_q^2\bar{\chi}D^2\chi$	-1	+1	$\mu_q^2\bar{\chi}\gamma_5\tau^3D^2\chi$	+1	-1
$\mu_q^2\bar{\chi}\sigma_{\mu\nu}G_{\mu\nu}\chi$	-1	+1	$\mu_q^2\bar{\chi}\gamma_5\tau^3\sigma_{\mu\nu}G_{\mu\nu}\chi$	+1	-1
$\mu_q(\bar{\chi}T^A\chi)^2$	+1	-1	$\mu_q(\bar{\chi}\gamma_5\tau^3T^A\chi)\,(\bar{\chi}T^A\chi)$	-1	+1
$\mu_q(\bar{\chi}\gamma_5\tau^3T^A\chi)^2$	+1	-1	-	-	-
$\mu_q\bar{\chi}\not{D}\sigma_{\mu\nu}G_{\mu\nu}\chi$	+1	-1	$\mu_q\bar{\chi}\gamma_5\tau^3\not{D}\sigma_{\mu\nu}G_{\mu\nu}\chi$	-1	+1
$\mu_q\bar{\chi}\not{D}D^2\chi$	+1	-1	$\mu_q\bar{\chi}\gamma_5\tau^3\not{D}D^2\chi$	-1	+1
$\mu_q\bar{\chi}\gamma_\mu D_\mu^3\chi$	+1	-1	$\mu_q\bar{\chi}\gamma_5\tau^3\gamma_\mu D_\mu^3\chi$	-1	+1
$\mu_q\bar{\chi}\gamma_\mu[D_\nu,G_{\mu\nu}]\chi$	+1	-1	$\mu_q\bar{\chi}\gamma_5\tau^3\gamma_\mu[D_\nu,G_{\mu\nu}]\chi$	-1	+1
$(\bar{\chi}T^A\chi)(\bar{\chi}\not{D}T^A\chi)$	-1	+1	$(\bar{\chi}\gamma_5\tau^3T^A\chi)(\bar{\chi}\not{D}T^A\chi)$	+1	-1
$(\bar{\chi}\gamma_5\tau^3T^A\chi)(\bar{\chi}\gamma_5\tau^3T^A\not{D}\chi)$	-1	+1	-	-	-
$\bar{\chi}\not{D}\gamma_\mu D_\mu^3\chi$	-1	+1	$\bar{\chi}\gamma_5\tau^3\not{D}\gamma_\mu D_\mu^3\chi$	+1	-1
$\bar{\chi}\not{D}\gamma_\mu[D_\nu,G_{\mu\nu}]\chi$	-1	+1	$\bar{\chi}\gamma_5\tau^3\not{D}\gamma_\mu[D_\nu,G_{\mu\nu}]\chi$	+1	-1
$\bar{\chi}D^2\sigma_{\mu\nu}G_{\mu\nu}\chi$	-1	+1	$\bar{\chi}\gamma_5\tau^3D^2\sigma_{\mu\nu}G_{\mu\nu}\chi$	+1	-1
$\bar{\chi}\sigma_{\kappa\lambda}G_{\kappa\lambda}\sigma_{\mu\nu}G_{\mu\nu}\chi$	-1	+1	$\bar{\chi}\gamma_5\tau^3\sigma_{\kappa\lambda}G_{\kappa\lambda}\sigma_{\mu\nu}G_{\mu\nu}\chi$	+1	-1
$\bar{\chi}(D^2)^2\chi$	-1	+1	$\bar{\chi}\gamma_5\tau^3(D^2)^2\chi$	+1	-1
$\bar{\chi}D^4\chi$	-1	+1	$\bar{\chi}\gamma_5\tau^3D^4\chi$	+1	-1
$\bar{\chi}\gamma_5G_{\mu\nu}\tilde{G}_{\mu\nu}\chi$	-1	+1	$\bar{\chi}\tau^3G_{\mu\nu}\tilde{G}_{\mu\nu}\chi$	+1	-1
$\bar{\chi}G_{\mu\nu}G_{\mu\nu}\chi$	-1	+1	$\bar{\chi}\gamma_5\tau^3G_{\mu\nu}G_{\mu\nu}\chi$	+1	-1
$\bar{\chi}\chi\mathrm{tr}\,[G_{\mu\nu}G_{\mu\nu}]$	-1	+1	$\bar{\chi}\gamma_5\tau^3\chi\mathrm{tr}\,[G_{\mu\nu}G_{\mu\nu}]$	+1	-1
$\bar{\chi}G_{\mu\nu}\tilde{G}_{\mu\nu}\chi$	+1	-1	$\bar{\chi}\gamma_5\tau^3G_{\mu\nu}\tilde{G}_{\mu\nu}\chi$	-1	+1
$\bar{\chi}\chi\mathrm{tr}\left[G_{\mu\nu}\tilde{G}_{\mu\nu}\right]$	+1	-1	$\bar{\chi}\gamma_5\tau^3\chi\mathrm{tr}\left[G_{\mu\nu}\tilde{G}_{\mu\nu}\right]$	-1	+1

Table D.1.: Transformation properties of operators appearing in S_7.

Appendix E

Vector meson properties

Ensemble	f_ρ[GeV]	m_ρ[GeV]	χ^2/dof	$f_{s\bar{s}}$[GeV]	$m_{s\bar{s}}$[GeV]	χ^2/dof
D15.48	0.263(17)	0.933(55)	1.01	0.289(08)	1.129(14)	1.06
D30.48	0.279(12)	0.998(34)	0.21	0.291(10)	1.132(16)	0.79
D45.32sc	0.279(09)	1.003(27)	0.52	0.273(06)	1.112(13)	1.06
B25.32t	0.261(14)	0.903(44)	1.23	0.268(12)	1.112(21)	0.88
B35.32	0.269(15)	0.967(47)	0.47	0.271(09)	1.129(19)	1.28
B35.48	0.288(16)	1.028(44)	1.13	0.286(18)	1.156(35)	1.77
B55.32	0.278(11)	0.996(33)	1.81	0.294(10)	1.144(17)	0.10
B75.32	0.289(10)	1.056(28)	1.02	0.285(15)	1.154(26)	0.15
A30.32	0.264(25)	0.954(68)	1.18	0.284(14)	1.149(27)	1.16
A40.32	0.238(13)	0.863(39)	0.81	0.278(12)	1.135(20)	1.55
A50.32	0.271(16)	0.992(42)	1.50	0.268(12)	1.117(22)	1.08

Table E.1.: ρ- and ϕ-meson masses and decay constants obtained from correlator fits outlined in Sec. 4.1.3.

Ensemble	$f_{J/\Psi}$[GeV]	$m_{J/\Psi}$[GeV]	χ^2/dof
D15.48	0.439(07)	3.079(05)	0.99
D30.48	0.435(06)	3.078(04)	0.44
D45.32sc	0.429(05)	3.070(03)	0.83
B25.32t	0.443(08)	3.057(05)	0.66
B35.32	0.437(08)	3.051(05)	0.95
B35.48	0.412(11)	3.035(08)	1.45
B55.32	0.446(09)	3.053(06)	1.63
B75.32	0.447(12)	3.065(08)	0.93
A30.32	0.438(09)	3.039(06)	2.42
A40.32	0.436(10)	3.041(06)	0.37
A50.32	0.453(09)	3.051(06)	1.50

Table E.2.: J/Ψ masses and decay constants obtained from correlator fits outlined in Sec. 4.1.3.

Appendix F

Contraction formulae

In this appendix we add some details about the actual implementation of the equations which have appeared in the main body of this thesis, in particular in Sect. 3.2.3. All inversions have been performed with the application `invert` provided in the tmLQCD software package [Jansen and Urbach 2009]. For the light quarks, we have chosen the conjugate gradient algorithm whereas for the heavy quarks we have used the multiple mass solver. The reason for the latter is that we have computed the propagators for several strange and charm quark masses in order to check the dependence of the physical quantities on the valence quark masses and also to compute the charm quark mass and the strong coupling constant along the lines of [Jansen et al. 2011].

F.1. Quark-connected contributions with propagators from point sources

For our computations of the connected contributions $C_{\mu\nu}$ in Eq. (3.43), we use point-to-all propagators for each of the introduced quark flavours to obtain $C^f_{\mu\nu}$ given in Eq. (3.44). For the HVP function in the low-momentum region, this has been proven beneficial when compared to the usage of stochastic volume sources. As is well-known, the latter approach entails the introduction of additional source noise. For instance, for the extreme case of the smallest achievable lattice momentum, the uncertainty when using volume sources has been found to be more than 20 times larger than the one obtained by using point sources with the same number of inversions. At larger momenta, volume sources are to be preferred, since in this situation the introduced source noise can be overcompensated by a reduction of the gauge noise. However, this is not the case at low Q^2 which is a very important region for all observables studied in this thesis since they all involve the subtraction of $\Pi^f(0)$.

Hence, for the quark-connected contributions the propagators are obtained by numerically solving the equations

$$D^{f\ ab}_{\mathrm{tm}\,\alpha\beta}(n,p)\Phi_f[\tilde{a},\tilde{\alpha},\tilde{n}]^b_\beta(p) = \eta[\tilde{a},\tilde{\alpha},\tilde{n}]^a_\alpha(n)\ , \tag{F.1}$$

where D^f_{tm} denotes the twisted mass Dirac operator for quark species f and $\alpha = 1,\ldots,4$ the Dirac index, $c = 1,2,3$ the colour index, and $n \in \Lambda$ the source location. The spinor field of the point source is given by

$$\eta[\tilde{a},\tilde{\alpha},\tilde{n}]^a_\alpha(n) = \delta(n-\tilde{n})\delta_{\alpha\tilde{\alpha}}\delta^{a\tilde{a}}\ . \tag{F.2}$$

This implies that the field $\Phi_f[\tilde{a},\tilde{\alpha},\tilde{n}]^b_\gamma(p)$ equals the propagator from $\tilde{n}$ to any other space-

time point p

$$\Phi_f[\tilde{a},\tilde{\alpha},\tilde{n}]^b_\gamma(p) = \left(D^{f\ -1}_{\mathrm{tm}}\right)^{b\tilde{a}}_{\gamma\tilde{\alpha}}(p,\tilde{n}) = \left(S^f\right)^{b\tilde{a}}_{\gamma\tilde{\alpha}}(p,\tilde{n})\ . \tag{F.3}$$

The components of the source field $\eta[\tilde{a},\tilde{\alpha},\tilde{n}]^a_\alpha(n)$, in particular the source location $\tilde{n}$, are chosen randomly to reduce correlations between different gauge field configurations.

Currently, the usage of point sources is only feasible for fixed source locations n of the propagator elements $S^f(m,n)$. Therefore, we utilise the γ_5-hermiticity Eq. (3.33) of the twisted mass Dirac operator which implies

$$S^f(n,m) = \gamma_5 S^{\bar{f}\dagger}(m,n)\gamma_5 \tag{F.4}$$

to exchange the space-time arguments of the propagators in Eq. (3.44). Since this relation mixes the upper and lower components of the flavour doublets, we always have to compute the propagators for both signs of the twisted quark mass in the Dirac operator as has already been indicated in Sect. 3.2.3.

Using Eq. (F.4) in the expression of the quark-connected contributions provided in Eq. (3.44) and exchanging some of the γ-matrices by exploiting the cyclic property of the trace yields

$$\begin{aligned} C^f_{\mu\nu}(m,n) = \ -\frac{1}{4}\,\mathrm{tr}_{\mathrm{cs}}\Big\{ & S^{\bar{f}\dagger}(m+a\hat{\mu},n)^\dagger\gamma_5(1+\gamma_\mu)U^\dagger_\mu(m)S^f(m,n+a\hat{\nu})\gamma_5(1-\gamma_\nu)U^\dagger_\nu(n) \\ & -S^{\bar{f}\dagger}(m+a\hat{\mu},n+a\hat{\nu})\gamma_5(1+\gamma_\mu)U^\dagger_\mu(m)S^f(m,n)\gamma_5(1+\gamma_\nu)U_\nu(n) \\ & -S^{\bar{f}\dagger}(m,n)\gamma_5(1-\gamma_\mu)U_\mu(m)S^f(m+a\hat{\mu},n+a\hat{\nu})\gamma_5(1-\gamma_\nu)U^\dagger_\nu(n) \\ & +S^{\bar{f}\dagger}(m,n+a\hat{\nu})\gamma_5(1-\gamma_\mu)U_\mu(m)S^f(m+a\hat{\mu},n)\gamma_5(1+\gamma_\nu)U_\nu(n)\Big\}\ . \end{aligned} \tag{F.5}$$

Inserting Eq. (F.3) and continuing to neglect spin and colour indices, we arrive at the expression implemented in our calculations

$$\begin{aligned} C^f_{\mu\nu}(m,n) = \ -\frac{1}{4}\,\mathrm{tr}_{\mathrm{cs}}\Big\{ & \Phi^{\bar{f}\dagger}[n](m+a\hat{\mu})\gamma_5(1+\gamma_\mu)U^\dagger_\mu(m)\Phi^f[n+a\hat{\nu}](m)\gamma_5(1-\gamma_\nu)U^\dagger_\nu(n) \\ & -\Phi^{\bar{f}\dagger}[n+a\hat{\nu}](m+a\hat{\mu})\gamma_5(1+\gamma_\mu)U^\dagger_\mu(m)\Phi^f[n](m)\gamma_5(1+\gamma_\nu)U_\nu(n) \\ & -\Phi^{\bar{f}\dagger}[n](m)\gamma_5(1-\gamma_\mu)U_\mu(m)\Phi^f[n+a\hat{\nu}](m+a\hat{\mu})\gamma_5(1-\gamma_\nu)U^\dagger_\nu(n) \\ & +\Phi^{\bar{f}\dagger}[n+a\hat{\nu}](m)\gamma_5(1-\gamma_\mu)U_\mu(m)\Phi^f[n](m+a\hat{\mu})\gamma_5(1+\gamma_\nu)U_\nu(n)\Big\}\ . \end{aligned} \tag{F.6}$$

Again, this explicitly shows that we have to compute the point-to-all propagators at the five source locations $n, n+a\hat{\nu}$, $\nu = 0,\ldots,3$.

The propagators computed for the quark-connected contributions are also used to determine the field in the contact term. The straightforward Wick contraction for a single flavour f results in

$$S^f_\nu(n) = \frac{1}{2}\mathrm{tr}_{\mathrm{cs}}\left\{S^f(n,n+a\hat{\mu})(1+\gamma_\nu)U^\dagger_\nu(n) + S^f(n+a\hat{\nu},n)(1-\gamma_\nu)U_\nu(n)\right\}\ . \tag{F.7}$$

F.2. Quark-disconnected contributions with propagators from stochastic volume sources

Due to the disconnected contributions having the form

$$D_{\mu\nu}(m,n) = L_\mu(m)L_\nu(n) \tag{F.8}$$

with $L_\mu(m)$ representing the Wick contraction of the electromagnetic current, the source location n does not enter the first factor $L_\mu(m)$. Therefore, the propagators needed to compute the quark-disconnected contributions involve propagators from m to $m + a\hat{\mu}$ for all $m \in \Lambda$ which is unfeasible with point sources. Instead, we use stochastic volume sources to compute so-called all-to-all propagators. They are also obtained from solving Eq. (F.1), but this time with stochastic volume sources on the right-hand-side. This entails the introduction of an additional index r labelling the independent source fields. Hence, Eq. (F.1) becomes

$$D^f_{\mathrm{tm}}(n,p)\Phi_f[\tilde{n}]^r(p) = \eta[\tilde{n}]^r(n)\ , \tag{F.9}$$

where we have neglected spin and colour indices. In our calculations the elements of the source fields η^r are independently of each other distributed according to the Gaussian probability distribution

$$p(\xi) = \frac{1}{\sqrt{2\pi}} e^{\frac{-\xi^2}{2}} \tag{F.10}$$

for $\xi = \mathrm{Re}\,(\eta^r[\tilde{a},\tilde{\alpha},\tilde{n}])$ and $\xi = \mathrm{Im}\,(\eta^r[\tilde{a},\tilde{\alpha},\tilde{n}])$, respectively. In this way $24 \cdot V^2$ additional noise terms are introduced which allow to stochastically estimate the quark propagators for all space-time positions (m,n). The expression implemented in our calculations can be obtained from Eq. (3.47) by substituting $S^f(m,n)$ with

$$S^f(m,n) = \Phi_f[n]^r\,(\eta[m]^r)^\dagger\ . \tag{F.11}$$

When using stochastic volume sources, in contrast to the case of point sources also a sum over the source locations can be included in the Fourier transform in Eq. (3.22) which is advantageous to reduce the gauge noise and allows to perform the Fourier transformation separately for each factor $L_\mu(m)$ in Eq. (F.8). Thus, the expression for the Fourier-transformed quark-disconnected contributions to the HVP tensor becomes

$$\Pi^{\mathrm{disc}}_{\mu\nu}(Q) = L_\mu(Q)\,L_\nu(-Q)\ . \tag{F.12}$$

Since products of propagators originating from the same source have to be avoided, we obtain as the averaged estimate

$$\Pi^{\mathrm{disc}}_{\mu\nu}(Q) = \frac{1}{N_s(N_s-1)} \sum_{1\le r<s\le N_s} \left(L^r_\mu(Q)L^s_\nu(-Q) + L^s_\mu(Q)L^r_\nu(-Q)\right) + \mathcal{O}\left(\frac{1}{N_s}\right)\ , \tag{F.13}$$

where N_s denotes the number of volume sources. As indicated above, this estimate is in general expected to become more precise the larger N_s. However, since the terms of $\mathcal{O}\left(\frac{1}{N_s}\right)$ contain coefficients $\propto Q^{-1}$, this is more efficient the higher the momentum transfer under consideration. We have performed inversions with $N_s = 24$ and $N_s = 48$.

Appendix G

Data for lepton anomalous magnetic moments

Ensemble	$a_e^{\mathrm{ud}} \cdot 10^{12}$	# light	$a_e^{\mathrm{s}} \cdot 10^{13}$	# strange	$a_e^{\mathrm{c}} \cdot 10^{14}$	# charm	$a_e^{\mathrm{hvp}} \cdot 10^{12}$
A30.32	1.425(75)	267	1.64(24)	158	5.55(81)	158	1.644(80)
A40.32	1.388(47)	248	1.35(13)	174	4.55(42)	174	1.568(49)
A50.32	1.391(54)	216	1.80(16)	157	6.13(52)	157	1.633(57)
B25.32t	1.508(42)	258	1.52(15)	166	5.01(49)	167	1.710(45)
B35.32	1.439(46)	201	1.68(16)	194	5.72(54)	194	1.664(49)
B35.48	1.441(49)	233	1.87(17)	103	6.22(55)	104	1.690(52)
B55.32	1.435(38)	199	1.91(12)	199	6.01(40)	199	1.686(40)
B75.32	1.381(32)	158	1.99(12)	100	6.63(37)	100	1.646(35)
B85.24	1.355(43)	192	2.14(14)	142	7.41(45)	136	1.643(46)
D15.48	1.525(91)	265	1.50(26)	155	4.34(75)	156	1.718(95)
D30.48	1.454(40)	203	1.95(14)	148	5.69(39)	148	1.706(43)
D45.32.sc	1.428(28)	397	1.91(11)	346	5.78(32)	308	1.676(30)

Table G.1.: Single-flavour contributions to the electron $(g-2)$ including the charge factors as well as total a_e^{hvp} obtained in our calculations together with the number of configurations used to compute the single-flavour contributions. The parameters of the ensembles have been given in Tab. 4.1.

Ensemble	$a_\mu^{\mathrm{ud}} \cdot 10^8$	# light	$a_\mu^{\mathrm{s}} \cdot 10^9$	# strange	$a_\mu^{\mathrm{c}} \cdot 10^9$	# charm	$a_\mu^{\mathrm{hvp}} \cdot 10^8$
A30.32	5.40(28)	267	6.42(89)	158	2.34(34)	158	6.28(30)
A40.32	5.25(17)	248	5.33(48)	174	1.92(18)	174	5.98(18)
A50.32	5.28(20)	216	6.98(58)	157	2.58(22)	157	6.23(21)
B25.32t	5.70(15)	258	5.96(56)	166	2.12(21)	167	6.50(17)
B35.32	5.45(18)	201	6.55(62)	194	2.41(23)	194	6.35(19)
B35.48	5.46(18)	233	7.23(63)	103	2.61(23)	104	6.44(19)
B55.32	5.44(14)	199	7.40(44)	199	2.53(17)	199	6.43(15)
B75.32	5.23(12)	158	7.67(45)	100	2.79(16)	100	6.28(13)
B85.24	5.15(16)	192	8.21(51)	142	3.11(18)	136	6.28(17)
D15.48	5.77(34)	265	5.81(95)	155	1.84(31)	156	6.54(35)
D30.48	5.51(15)	203	7.57(51)	148	2.40(16)	148	6.51(16)
D45.32.sc	5.41(10)	397	7.36(40)	346	2.43(13)	308	6.39(11)

Table G.2.: Single-flavour contributions to the muon $(g-2)$ including the charge factors as well as total a_μ^{hvp} obtained in our calculations together with the number of configurations used to compute the single-flavour contributions. The parameters of the ensembles have been given in Tab. 4.1.

Ensemble	$a_\tau^{\mathrm{ud}} \cdot 10^6$	# light	$a_\tau^{\mathrm{s}} \cdot 10^7$	# strange	$a_\tau^{\mathrm{c}} \cdot 10^7$	# charm	$a_\tau^{\mathrm{hvp}} \cdot 10^6$
A30.32	2.609(94)	267	3.95(28)	158	3.72(37)	158	3.377(104)
A40.32	2.509(59)	248	3.58(17)	174	3.25(22)	174	3.192(65)
A50.32	2.567(65)	216	4.14(18)	157	4.02(23)	157	3.383(71)
B25.32t	2.640(49)	258	3.81(19)	166	3.47(25)	167	3.367(58)
B35.32	2.617(57)	201	4.01(19)	194	3.80(26)	194	3.398(65)
B35.48	2.598(62)	233	4.14(19)	103	4.01(24)	104	3.413(69)
B55.32	2.606(48)	199	4.26(13)	199	3.93(19)	199	3.425(53)
B75.32	2.524(43)	158	4.32(13)	100	4.23(16)	100	3.380(48)
B85.24	2.541(54)	192	4.50(14)	142	4.53(18)	136	3.445(59)
D15.48	2.716(114)	265	3.73(31)	155	3.05(38)	156	3.395(124)
D30.48	2.627(52)	203	4.25(15)	148	3.70(18)	148	3.422(57)
D45.32.sc	2.579(35)	397	4.15(11)	346	3.76(15)	308	3.370(39)

Table G.3.: Single-flavour contributions to the τ-lepton $(g-2)$ including the charge factors as well as total a_μ^{hvp} obtained in our calculations together with the number of configurations used to compute the single-flavour contributions. The parameters of the ensembles have been given in Tab. 4.1.

Acknowledgements

First and foremost, I cordially thank Dr. Karl Jansen and Prof. Michael Müller-Preußker for granting me the opportunity to work on this PhD project and for the great trust they have placed in me when allowing me to work under their supervision. In particular, I am deeply grateful to my scientific supervisor Dr. Jansen for suggesting to me the most interesting topic of all, at least from my subjective point of view. I also want to thank him for guiding this work, the numerous enlightening discussions, the great atmosphere in the Berlin/Zeuthen working groups, and his support not only but also during the preparation of this thesis.

I have very much enjoyed working under the direct supervision of Prof. Müller-Preußker as he has always been supportive and understanding, especially during the time of my parental leave and shortly after when I regularly made use of his generous offer to work from home. I am indebted to him not only for stimulating discussions and sorting out bureaucratic issues but also for his moral support and encouragement and the nice and productive working environment that he provides for his group. He is efficiently assisted in doing so by Sylvia Richter who I also want to thank here.

To complete the list of supervisors, I would like to express my gratitude to my academic supervisor Prof. Marc Wagner for his readiness to accept this responsibility and the great support and many helpful insights, especially during the early stages of this thesis. I have always appreciated our scientific discussions.

This work would not have been the same without the support and the indispensable groundwork provided by Dr. Marcus Petschlies. I am deeply grateful to him not only for passing his contraction and analysis code packages to me but also for sharing part of his broad knowledge on the subject we continued to investigate together. On top of that, I have also appreciated the conversations and activities at a more personal level.

I am indebted to the German National Academic Foundation (Studienstiftung des deutschen Volkes e.V.) for granting me a PhD scholarship after having already financed part of my study. Additionally, I very much enjoyed the meeting of our local group of fellows lead by Prof. Thomas Lohse who has always been very supportive in every respect. Another very important aspect of my two fellowships of the Studienstiftung has been the participation in the working group "Elementary particle physics" under the supervision of Prof. Barbara Schrempp from which I profitted a lot. Especially, I would like to thank all participants who have continued the biannual meetings originally planned for two years for more than six years now. Additional funding has been received from the DFG Corroborative Research Center SFB/TR9 and the DFG-funded Graduate School GK 1504, which is gratefully acknowledged. I am also thankful for the opportunity to participate in the biannual block courses organised by the graduate school.

With respect to the content of this thesis, I first of all would like to thank the members of the European Twisted Mass Collaboration for the generation of the gauge field ensembles employed in this work and the enjoyable collaboration. Without the provided ensemble data it would, of course, not have been possible to arrive at any physically meaningful results. Furthermore, I am grateful to Dr. Andreas Ammon for providing us with the information of the matching K- and D-meson masses in the mixed-action setup with their physical values and for patiently answering all related questions. Special thanks goes to the authors of [Michael et al. 2013] who generously granted us access to their data for the disconnected contributions of the local vector current correlators. Additionally, I

thank Dr. Vincent Drach for helpful discussions on quark-disconnected contributions, and Dr. Elena Garcia Ramos as well as Dr. Krzysztof Cichy for enlightening discussions about the topic of $\mathcal{O}(a)$ improvement.

I am most grateful to Prof. Friedrich Jegerlehner for very instructive discussions regarding electroweak physics in general and the phenomenological computations of the observables investigated in this thesis in particular. Additionally, I would also like to acknowledge his generosity when providing his preliminary data on the electroweak coupling constants we have used for Fig. 5.13.

I would like to thank the scientists that I had the pleasure to collaborate with namely Dr. Marcus Petschlies, Dr. Dru B. Renner, Dr. Xu Feng, and Dr. Florian Burger. Their helpful insights, support, cross-checks, and practical knowledge have been vital for the success of this thesis. Special thanks goes to Dr. Florian Burger for sharing not only the office with me, but also for numerous scientific discussions, his practical help with computational issues, and the many nice conversations not related to physics at all.

Apart from that I would also like to take the opportunity to thank the other members of the Berlin/Zeuthen working groups for the great time we had together and the insightful discussions and seminars, namely Simone Alioli, Andreas Ammon, Krzysztof Cichy, Simon Dinter, Vincent Drach, Patrick Fritzsch, Elena Garcia Ramos, Jenifer Gonzalez Lopez, Alexander Hasselhuhn, Dirk Hesse, Pan Kessel, Piotr Korcyl, Bartosz Kostrzewa, Petra Kovacikova, Marina Marinkovic, Attila Nagy, Ralf Sattler, Julia Volmer, Christian Wiese, and Fabian Wißbrock. I would like to especially mention Attila and Bartek for their moral support during the completion of this thesis and the many lively conversations.

The numerical computations have been performed on the HLRN-II and HLRN-III at the HLRN Supercomputing Service Berlin-Hannover, FZJ/GCS, BG/P, and BG/Q at FZ-Jülich, and the local computers of the Humboldt University. I would like to thank all people involved in the smooth operation of these computing resources. Apart from the tmLQCD software package [Jansen and Urbach 2009] and Marcus' programs, I have used the software packages Lemon [Deuzeman et al. 2012] and R [R Core Team 2012].

Last but not least, I also want to express my deep gratitude to my family and friends for their support, affection, and for simply making me happy. First of all I want to mention my birds of prey: My grandfather Arno Preuß without whom I would never have studied physics, my husband Falko Pientka who always sees more in me than I do, and last but not least my son Milan Pientka for being the cutest and loveliest little boy I could have wished for. His laughter always makes my day. Additionally, I am deeply indebted to my parents Britta and Martin Hotzel and the rest of my relatives, especially my grandmother Elisabeth Preuß. I thank all of them for their love and understanding.

Special thanks goes to the girls Melanie Eyßer, Judith von Falkenhausen, Franziska Hennig, Karin Pritscha, Anika Sieber, Anja Uedsen, and Carolin Zobel for their support, the great time we have together, and their enriching perspectives. For the same reasons I want to also mention the boys Steffen Karalus and Adam Roe. With regard to the preparation of this thesis, I especially thank Judith von Falkenhausen, Maren Peters, Falko Pientka, and Anja Uedsen for reading parts of the manuscript. Falko has also kindly assisted me with adapting the bibtex style. I would not have been able to complete this thesis so quickly without the indispensable support of my parents and our babysitter Armi who took care of Milan on the weekends and other occasions when the child care centre was closed and have thus enabled me to work several extra hours.

I am deeply grateful to everyone who in numerous and diverse ways has supported this work during the last years and feel blessed to have received so much aid and encouragement.

List of Figures

List of Tables

Bibliography

['t Hooft 1971] 't Hooft, G. (1971). Renormalizable Lagrangians for Massive Yang-Mills Fields. *Nucl.Phys.*, B35:167–188.

[ATLAS 2012] **ATLAS Collaboration**, Aad, G. et al. (2012). Observation of a new particle in the search for the Standard Model Higgs boson with the ATLAS detector at the LHC. *Phys.Lett.*, B716:1–29. `arXiv:1207.7214 [hep-ex]`.

[ATLAS 2015] **ATLAS Collaboration**, Aad, G. et al. (2015). Evidence of $W\gamma\gamma$ production in pp collisions at $\sqrt{s} = 8$ TeV and limits on anomalous quartic gauge couplings with the ATLAS detector. `arXiv:1503.03243 [hep-ex]`.

[Abdel-Rehim et al. 2013] Abdel-Rehim, A., Boucaud, P., Carrasco, N., Deuzeman, A., Dimopoulos, P., et al. (2013). A first look at maximally twisted mass lattice QCD calculations at the physical point. *PoS*, LATTICE2013:264. `arXiv:1311.4522 [hep-lat]`.

[Abdel-Rehim et al. 2014] Abdel-Rehim, A., Alexandrou, C., Dimopoulos, P., Frezzotti, R., Jansen, K., et al. (2014). Progress in Simulations with Twisted Mass Fermions at the Physical Point. *PoS*, LATTICE2014:119. `arXiv:1411.6842 [hep-lat]`.

[Alexandrou et al. 2014] Alexandrou, C., Constantinou, M., Koutsou, G., Ottnad, K., and Petschlies, M. (2014). Extraction of the isovector magnetic form factor of the nucleon at zero momentum. `arXiv:1410.8818 [hep-lat]`.

[Alkofer and von Smekal 2001] Alkofer, R. and von Smekal, L. (2001). The Infrared behavior of QCD Green's functions: Confinement dynamical symmetry breaking, and hadrons as relativistic bound states. *Phys.Rept.*, 353:281. `arXiv:hep-ph/0007355 [hep-ph]`.

[Alpha 2001] **Alpha Collaboration**, Frezzotti, R., Grassi, P. A., Sint, S., and Weisz, P. (2001). Lattice QCD with a chirally twisted mass term. *JHEP*, 0108:058. `arXiv:hep-lat/0101001 [hep-lat]`.

[Antognini et al. 2013] Antognini, A., Kottmann, F., Biraben, F., Indelicato, P., Nez, F., et al. (2013). Theory of the 2S-2P Lamb shift and 2S hyperfine splitting in muonic hydrogen. *Annals Phys.*, 331:127–145. `arXiv:1208.2637 [physics.atom-ph]`.

[Aoki 1984] Aoki, S. (1984). New Phase Structure for Lattice QCD with Wilson Fermions. *Phys.Rev.*, D30:2653.

[Aoki and Gocksch 1989] Aoki, S. and Gocksch, A. (1989). Spontaneous Breaking of Parity in Quenched Lattice QCD With Wilson Fermions. *Phys.Lett.*, B231:449.

[Aoyama et al. 2012a] Aoyama, T., Hayakawa, M., Kinoshita, T., and Nio, M. (2012a). Complete Tenth-Order QED Contribution to the Muon g-2. *Phys.Rev.Lett.*, 109:111808. `arXiv:1205.5370 [hep-ph]`.

[Aoyama et al. 2012b] Aoyama, T., Hayakawa, M., Kinoshita, T., and Nio, M. (2012b). Tenth-Order QED Contribution to the Electron g-2 and an Improved Value of the Fine Structure Constant. *Phys.Rev.Lett.*, 109:111807. arXiv:1205.5368 [hep-ph].

[Aoyama et al. 2015] Aoyama, T., Hayakawa, M., Kinoshita, T., and Nio, M. (2015). Tenth-Order Electron Anomalous Magnetic Moment — Contribution of Diagrams without Closed Lepton Loops. *Phys.Rev.*, D91(3):033006. arXiv:1412.8284 [hep-ph].

[Aubin and Blum 2007] Aubin, C. and Blum, T. (2007). Calculating the hadronic vacuum polarization and leading hadronic contribution to the muon anomalous magnetic moment with improved staggered quarks. *Phys.Rev.*, D75:114502. arXiv:hep-lat/0608011 [hep-lat].

[Aubin et al. 2012] Aubin, C., Blum, T., Golterman, M., and Peris, S. (2012). Model-independent parametrization of the hadronic vacuum polarization and g-2 for the muon on the lattice. *Phys.Rev.*, D86:054509. arXiv:1205.3695 [hep-lat].

[BMW 2015] **BMW Collaboration**, Malak, R., Fodor, Z., Hoelbling, C., Lellouch, L., Sastre, A., et al. (2015). Finite-volume corrections to the leading-order hadronic contribution to $g_\mu - 2$. arXiv:1502.02172 [hep-lat].

[BaBar 2015] **BaBar Collaboration**, Oberhof, B. (2015). Measurement of the branching fractions of radiative leptonic τ decays $\tau \to \ell\gamma\nu\bar{\nu}, (\ell = e, \mu)$at $BABAR$. *Nucl.Part.Phys.Proc.*, 260:12–15. arXiv:1502.01810 [hep-ex].

[Baikov et al. 2012] Baikov, P., Chetyrkin, K., Kühn, J., and Rittinger, J. (2012). Vector Correlator in Massless QCD at Order $\mathcal{O}\left(\alpha_s^4\right)$ and the QED beta-function at Five Loop. *JHEP*, 1207:017. arXiv:1206.1284 [hep-ph].

[Baikov et al. 2015] Baikov, P., Chetyrkin, K., and Kühn, J. (2015). Massless Propagators, $R(s)$ and Multiloop QCD. *Nucl.Part.Phys.Proc.*, 261-262:3–18. arXiv:1501.06739 [hep-ph].

[Baker 1969] Baker, G. (1969). Best error bounds for pade approximants to convergent series of stieltjes. *J.Math.Phys.*, 10:814–820.

[Balazs 2014] Balazs, C. (2014). Baryogenesis: A small review of the big picture. arXiv:1411.3398 [hep-ph].

[Bali and Endrődi 2015] Bali, G. and Endrődi, G. (2015). Hadronic vacuum polarization and muon g-2 from magnetic susceptibilities on the lattice. arXiv:1506.08638 [hep-lat].

[Barnsley 1973] Barnsley, M. (1973). The bounding properties of the multipoint pade approximant to a series of stieltjes on the real line. *J.Math.Phys.*, 14:299–313.

[Becker et al. 2013] Becker, D., Gerz, K., Baunack, S., Kumar, K., and Maas, F. (2013). P2 - The weak charge of the proton. *PoS*, Bormio2013:024.

[Benayoun et al. 2012a] Benayoun, M., David, P., DelBuono, L., and Jegerlehner, F. (2012a). An Update of the HLS Estimate of the Muon g-2. arXiv:1210.7184 [hep-ph].

[Benayoun et al. 2012b] Benayoun, M., David, P., DelBuono, L., and Jegerlehner, F. (2012b). Upgraded Breaking Of The HLS Model: A Full Solution to the $\tau^- e^+ e^-$ and ϕ Decay Issues And Its Consequences On g-2 VMD Estimates. *Eur.Phys.J.*, C72:1848. arXiv:1106.1315 [hep-ph].

[Bernecker and Meyer 2011] Bernecker, D. and Meyer, H. B. (2011). Vector Correlators in Lattice QCD: Methods and applications. *Eur.Phys.J.*, A47:148. arXiv:1107.4388 [hep-lat].

[Blum 2003] Blum, T. (2003). Lattice calculation of the lowest order hadronic contribution to the muon anomalous magnetic moment. *Phys. Rev. Lett.*, 91:052001. arXiv:hep-lat/0212018.

[Blum et al. 2012] Blum, T., Hayakawa, M., and Izubuchi, T. (2012). Hadronic corrections to the muon anomalous magnetic moment from lattice QCD. *PoS*, LATTICE2012:022. arXiv:1301.2607 [hep-lat].

[Blum et al. 2013a] Blum, T., Denig, A., Logashenko, I., de Rafael, E., Lee Roberts, B., et al. (2013a). The Muon (g-2) Theory Value: Present and Future. arXiv:1311.2198 [hep-ph].

[Blum et al. 2013b] Blum, T., Izubuchi, T., and Shintani, E. (2013b). New class of variance-reduction techniques using lattice symmetries. *Phys.Rev.*, D88(9):094503. arXiv:1208.4349 [hep-lat].

[Blum et al. 2015] Blum, T., Chowdhury, S., Hayakawa, M., and Izubuchi, T. (2015). Hadronic light-by-light scattering contribution to the muon anomalous magnetic moment from lattice QCD. *Phys.Rev.Lett.*, 114(1):012001. arXiv:1407.2923 [hep-lat].

[Bochicchio et al. 1985] Bochicchio, M., Maiani, L., Martinelli, G., Rossi, G. C., and Testa, M. (1985). Chiral Symmetry on the Lattice with Wilson Fermions. *Nucl.Phys.*, B262:331.

[Bodenstein et al. 2012] Bodenstein, S., Dominguez, C., and Schilcher, K. (2012). Hadronic contribution to the muon g-2: A Theoretical determination. *Phys.Rev.*, D85:014029. arXiv:1106.0427 [hep-ph].

[Boyle et al. 2012] Boyle, P., Del Debbio, L., Kerrane, E., and Zanotti, J. (2012). Lattice Determination of the Hadronic Contribution to the Muon $g-2$ using Dynamical Domain Wall Fermions. *Phys.Rev.*, D85:074504. arXiv:1107.1497 [hep-lat].

[Bradac et al. 2008] Bradac, M., Allen, S. W., Treu, T., Ebeling, H., Massey, R., et al. (2008). Revealing the properties of dark matter in the merging cluster MACSJ0025.4-1222. *Astrophys.J.*, 687:959. arXiv:0806.2320 [astro-ph].

[Brambilla et al. 2014] Brambilla, N., Eidelman, S., Foka, P., Gardner, S., Kronfeld, A., et al. (2014). QCD and Strongly Coupled Gauge Theories: Challenges and Perspectives. *Eur.Phys.J.*, C74(10):2981. arXiv:1404.3723 [hep-ph].

[Burger et al. 2013] Burger, F., Hotzel, G., Müller-Preussker, M., Ilgenfritz, E.-M., and Lombardo, M. P. (2013). Towards thermodynamics with $N_f = 2 + 1 + 1$ twisted mass quarks. *PoS*, Lattice2013:153. arXiv:1311.1631 [hep-lat].

[Burger et al. 2014a] **ETM Collaboration**, Burger, F. et al. (2014a). Four-Flavour Leading-Order Hadronic Contribution To The Muon Anomalous Magnetic Moment. *JHEP*, 1402:099. arXiv:1308.4327 [hep-lat].

[Burger et al. 2014b] Burger, F., Feng, X., Hotzel, G., Jansen, K., Petschlies, M., et al. (2014b). Leading-order hadronic contribution to the anomalous magnetic moment of the muon from $N_f = 2 + 1 + 1$ twisted mass fermions. *PoS*, LATTICE2013:301. arXiv:1311.3885 [hep-lat].

[Burger et al. 2014c] Burger, F., Hotzel, G., Jansen, K., and Petschlies, M. (2014c). Lepton anomalous magnetic moments from twisted mass fermions. *PoS*, LATTICE2014:145. arXiv:1411.0705 [hep-lat].

[Burger et al. 2015a] Burger, F., Hotzel, G., Jansen, K., and Petschlies, M. (2015a). Leading-order hadronic contributions to the electron and tau anomalous magnetic moments. arXiv:1501.05110 [hep-lat].

[Burger et al. 2015b] Burger, F., Hotzel, G., Jansen, K., and Petschlies, M. (2015b). The hadronic vacuum polarization and automatic $\mathcal{O}(a)$ improvement for twisted mass fermions. *JHEP*, 1503:073. arXiv:1412.0546 [hep-lat].

[Burger et al. 2015c] Burger, F., Jansen, K., Petschlies, M., and Pientka, G. (2015c). Leading hadronic contributions to the running of the electroweak coupling constants from lattice QCD. arXiv:1505.03283 [hep-lat].

[CDF 1995] **CDF Collaboration**, Abe, F. et al. (1995). Observation of top quark production in $\bar{p}p$ collisions. *Phys.Rev.Lett.*, 74:2626–2631. arXiv:hep-ex/9503002 [hep-ex].

[CMS 2012] **CMS Collaboration**, Chatrchyan, S. et al. (2012). Observation of a new boson at a mass of 125 GeV with the CMS experiment at the LHC. *Phys.Lett.*, B716:30–61. arXiv:1207.7235 [hep-ex].

[CMS 2015] **CMS Collaboration**, Khachatryan, V. et al. (2015). Study of vector boson scattering and search for new physics in events with two same-sign leptons and two jets. *Phys.Rev.Lett.*, 114(5):051801. arXiv:1410.6315 [hep-ex].

[CP-PACS, JLQCD 2006] **CP-PACS, JLQCD Collaborations**, Aoki, S. et al. (2006). Nonperturbative O(a) improvement of the Wilson quark action with the RG-improved gauge action using the Schrodinger functional method. *Phys.Rev.*, D73:034501. arXiv:hep-lat/0508031 [hep-lat].

[Canetti et al. 2012] Canetti, L., Drewes, M., and Shaposhnikov, M. (2012). Matter and Antimatter in the Universe. *New J.Phys.*, 14:095012. arXiv:1204.4186 [hep-ph].

[Carlson 2015] Carlson, C. E. (2015). The Proton Radius Puzzle. *Prog.Part.Nucl.Phys.*, 82:59–77. arXiv:1502.05314 [hep-ph].

[Chetyrkin et al. 2000] Chetyrkin, K., Harlander, R., and Kühn, J. H. (2000). Quartic mass corrections to R(had) at order alpha**3(s). *Nucl.Phys.*, B586:56–72. arXiv:hep-ph/0005139 [hep-ph].

[Chetyrkin et al. 2012] Chetyrkin, K., Kühn, J., Maier, A., Maierhofer, P., Marquard, P., et al. (2012). Precise Charm- and Bottom-Quark Masses: Theoretical and Experimental Uncertainties. *Theor.Math.Phys.*, 170:217–228. arXiv:1010.6157 [hep-ph].

[Chiarappa et al. 2007] Chiarappa, T., Farchioni, F., Jansen, K., Montvay, I., Scholz, E., et al. (2007). Numerical simulation of QCD with u, d, s and c quarks in the twisted-mass Wilson formulation. *Eur.Phys.J.*, C50:373–383. arXiv:hep-lat/0606011 [hep-lat].

[Clowe et al. 2006] Clowe, D., Bradac, M., Gonzalez, A. H., Markevitch, M., Randall, S. W., et al. (2006). A direct empirical proof of the existence of dark matter. *Astrophys.J.*, 648:L109–L113. arXiv:astro-ph/0608407 [astro-ph].

[Colquhoun et al. 2015] Colquhoun, B., Dowdall, R., Davies, C., Hornbostel, K., and Lepage, G. (2015). Υ and Υ' Leptonic Widths, a_μ^b and m_b from full lattice QCD. *Phys.Rev.*, D91(7):074514. arXiv:1408.5768 [hep-lat].

[Czarnecki and Marciano 2001] Czarnecki, A. and Marciano, W. J. (2001). The Muon anomalous magnetic moment: A Harbinger for 'new physics'. *Phys.Rev.*, D64:013014. arXiv:hep-ph/0102122 [hep-ph].

[Czarnecki et al. 1995] Czarnecki, A., Krause, B., and Marciano, W. J. (1995). Electroweak Fermion loop contributions to the muon anomalous magnetic moment. *Phys.Rev.*, D52:2619–2623. arXiv:hep-ph/9506256 [hep-ph].

[Czarnecki et al. 1996] Czarnecki, A., Krause, B., and Marciano, W. J. (1996). Electroweak corrections to the muon anomalous magnetic moment. *Phys.Rev.Lett.*, 76:3267–3270. arXiv:hep-ph/9512369 [hep-ph].

[D0 1995] **D0 Collaboration**, Abachi, S. et al. (1995). Observation of the top quark. *Phys.Rev.Lett.*, 74:2632–2637. arXiv:hep-ex/9503003 [hep-ex].

[DELPHI 2004] **DELPHI Collaboration**, Abdallah, J. et al. (2004). Study of tau-pair production in photon-photon collisions at LEP and limits on the anomalous electromagnetic moments of the tau lepton. *Eur.Phys.J.*, C35:159–170. arXiv:hep-ex/0406010 [hep-ex].

[Davier and Marciano 2004] Davier, M. and Marciano, W. (2004). The theoretical prediction for the muon anomalous magnetic moment. *Ann.Rev.Nucl.Part.Sci.*, 54:115–140.

[Davier et al. 2011] Davier, M., Hoecker, A., Malaescu, B., and Zhang, Z. (2011). Reevaluation of the Hadronic Contributions to the Muon g-2 and to alpha(M_Z). *Eur.Phys.J.*, C71:1515. arXiv:1010.4180 [hep-ph].

[Della Morte and Jüttner 2010] Della Morte, M. and Jüttner, A. (2010). Quark disconnected diagrams in chiral perturbation theory. *JHEP*, 1011:154. arXiv:1009.3783 [hep-lat].

[Della Morte et al. 2012] Della Morte, M., Jager, B., Juttner, A., and Wittig, H. (2012). Towards a precise lattice determination of the leading hadronic contribution to $(g-2)_\mu$. *JHEP*, 1203:055. arXiv:1112.2894 [hep-lat].

[Del Debbio et al. 2007] Del Debbio, L., Giusti, L., Luscher, M., Petronzio, R., and Tantalo, N. (2007). QCD with light Wilson quarks on fine lattices (I): First experiences and physics results. *JHEP*, 0702:056. arXiv:hep-lat/0610059 [hep-lat].

[Deuzeman et al. 2012] **ETM Collaboration**, Deuzeman, A., Reker, S., and Urbach, C. (2012). Lemon: an MPI parallel I/O library for data encapsulation using LIME. *Comput.Phys.Commun.*, 183:1321–1335. arXiv:1106.4177 [hep-lat].

[De Divitiis et al. 2004] De Divitiis, G., Petronzio, R., and Tantalo, N. (2004). On the discretization of physical momenta in lattice QCD. *Phys.Lett.*, B595:408–413. arXiv:hep-lat/0405002 [hep-lat].

[De Divitiis et al. 2012] De Divitiis, G., Petronzio, R., and Tantalo, N. (2012). On the extraction of zero momentum form factors on the lattice. *Phys.Lett.*, B718:589–596. arXiv:1208.5914 [hep-lat].

[Dirac 1928a] Dirac, P. (1928a). The Quantum theory of electron. *Proc.Roy.Soc.Lond.*, A117:610–624.

[Dirac 1928b] Dirac, P. (1928b). The Quantum theory of electron. 2. *Proc.Roy.Soc.Lond.*, A118:351.

[Dudek and Edwards 2006] Dudek, J. J. and Edwards, R. G. (2006). Two Photon Decays of Charmonia from Lattice QCD. *Phys.Rev.Lett.*, 97:172001. arXiv:hep-ph/0607140 [hep-ph].

[Dudek et al. 2013] **Hadron Spectrum Collaboration**, Dudek, J. J., Edwards, R. G., and Thomas, C. E. (2013). Energy dependence of the ρ resonance in $\pi\pi$ elastic scattering from lattice QCD. *Phys.Rev.*, D87(3):034505. arXiv:1212.0830 [hep-ph].

[Dumbrajs et al. 1983] Dumbrajs, O., Koch, R., Pilkuhn, H., Oades, G., Behrens, H., et al. (1983). Compilation of Coupling Constants and Low-Energy Parameters. 1982 Edition. *Nucl.Phys.*, B216:277–335.

[Dzuba et al. 2012] Dzuba, V., Berengut, J., Flambaum, V., and Roberts, B. (2012). Revisiting parity non-conservation in cesium. *Phys.Rev.Lett.*, 109:203003. arXiv:1207.5864 [hep-ph].

[E288 1977] **E288 Collaboration**, Herb, S., Hom, D., Lederman, L., Sens, J., Snyder, H., et al. (1977). Observation of a Dimuon Resonance at 9.5-GeV in 400-GeV Proton-Nucleus Collisions. *Phys.Rev.Lett.*, 39:252–255.

[E598 1974] **E598 Collaboration**, Aubert, J. et al. (1974). Experimental Observation of a Heavy Particle J. *Phys.Rev.Lett.*, 33:1404–1406.

[ETMC 2008] **ETM Collaboration**, Boucaud, P. et al. (2008). Dynamical Twisted Mass Fermions with Light Quarks: Simulation and Analysis Details. *Comput.Phys.Commun.*, 179:695–715. arXiv:0803.0224 [hep-lat].

[ETMC 2010a] **ETM Collaboration**, Baron, R., Boucaud, P., Carbonell, J., Deuzeman, A., Drach, V., et al. (2010a). Light hadrons from lattice QCD with light (u,d), strange and charm dynamical quarks. *JHEP*, 1006:111. arXiv:arXiv:1004.5284 [hep-lat].

[ETMC 2010b] **ETM Collaboration**, Baron, R. et al. (2010b). Light hadrons from $N_f = 2+1+1$ dynamical twisted mass fermions. *PoS*, LATTICE2010:123. arXiv:1101.0518 [hep-lat].

[ETMC 2011] **ETM Collaboration**, Baron, R. et al. (2011). Computing K and D meson masses with $N_f = 2+1+1$ twisted mass lattice QCD. *Comput.Phys.Commun.*, 182:299–316. arXiv:1005.2042 [hep-lat].

[Ecker et al. 1989] Ecker, G., Gasser, J., Pich, A., and de Rafael, E. (1989). The Role of Resonances in Chiral Perturbation Theory. *Nucl.Phys.*, B321:311.

[Eidelman and Passera 2007] Eidelman, S. and Passera, M. (2007). Theory of the tau lepton anomalous magnetic moment. *Mod.Phys.Lett.*, A22:159–179. arXiv:hep-ph/0701260 [hep-ph].

[Einstein 1916] Einstein, A. (1916). The Foundation of the General Theory of Relativity. *Annalen Phys.*, 49:769–822.

[Englert and Brout 1964] Englert, F. and Brout, R. (1964). Broken Symmetry and the Mass of Gauge Vector Mesons. *Phys.Rev.Lett.*, 13:321–323.

[Erler 2012] Erler, J. (2012). Tests of the Electroweak Standard Model. *J.Phys.Conf.Ser.*, 485:012010. arXiv:1209.3324 [hep-ph].

[Erler and Ramsey-Musolf 2005] Erler, J. and Ramsey-Musolf, M. J. (2005). The Weak mixing angle at low energies. *Phys.Rev.*, D72:073003. arXiv:hep-ph/0409169 [hep-ph].

[Fael et al. 2014] Fael, M., Mercolli, L., and Passera, M. (2014). Towards a determination of the tau lepton dipole moments. *Nucl.Phys.Proc.Suppl.*, 253-255:103–106. arXiv:1301.5302 [hep-ph].

[Farchioni et al. 2005a] Farchioni, F., Frezzotti, R., Jansen, K., Montvay, I., Rossi, G., et al. (2005a). Twisted mass quarks and the phase structure of lattice QCD. *Eur.Phys.J.*, C39:421–433. arXiv:hep-lat/0406039 [hep-lat].

[Farchioni et al. 2005b] Farchioni, F., Jansen, K., Montvay, I., Scholz, E., Scorzato, L., et al. (2005b). The Phase structure of lattice QCD with Wilson quarks and renormalization group improved gluons. *Eur.Phys.J.*, C42:73–87. arXiv:hep-lat/0410031 [hep-lat].

[Feng et al. 2011a] Feng, X., Jansen, K., Petschlies, M., and Renner, D. B. (2011a). Two-flavor QCD correction to lepton magnetic moments at leading-order in the electromagnetic coupling. *Phys.Rev.Lett.*, 107:081802. arXiv:1103.4818 [hep-lat].

[Feng et al. 2011b] Feng, X., Jansen, K., and Renner, D. B. (2011b). Resonance Parameters of the rho-Meson from Lattice QCD. *Phys.Rev.*, D83:094505. arXiv:1011.5288 [hep-lat].

[Feng et al. 2012a] Feng, X., Aoki, S., Fukaya, H., Hashimoto, S., Kaneko, T., et al. (2012a). Two-photon decay of the neutral pion in lattice QCD. *Phys.Rev.Lett.*, 109:182001. arXiv:1206.1375 [hep-lat].

[Feng et al. 2012b] Feng, X., Hotzel, G., Jansen, K., Petschlies, M., and Renner, D. B. (2012b). Leading-order hadronic contributions to a_μ and α_{QED} from $N_f = 2 + 1 + 1$ twisted mass fermions. *PoS*, LATTICE2012:174. arXiv:1211.0828 [hep-lat].

[Feng et al. 2013] Feng, X., Hashimoto, S., Hotzel, G., Jansen, K., Petschlies, M., et al. (2013). Computing the hadronic vacuum polarization function by analytic continuation. *Phys.Rev.*, D88:034505. arXiv:1305.5878 [hep-lat].

[Feynman 1950] Feynman, R. (1950). Mathematical formulation of the quantum theory of electromagnetic interaction. *Phys.Rev.*, 80:440–457.

[Fischer 2006] Fischer, C. S. (2006). Infrared properties of QCD from Dyson-Schwinger equations. *J.Phys.*, G32:R253–R291. arXiv:hep-ph/0605173 [hep-ph].

[Francis et al. 2013a] Francis, A., Jäger, B., Meyer, H. B., and Wittig, H. (2013a). A new representation of the Adler function for lattice QCD. *Phys.Rev.*, D88:054502. arXiv:1306.2532 [hep-lat].

[Francis et al. 2013b] Francis, A., von Hippel, G., Meyer, H. B., and Jegerlehner, F. (2013b). Vector correlator and scale determination in lattice QCD. *PoS*, LATTICE2013:320. arXiv:1312.0035 [hep-lat].

[Francis et al. 2014a] Francis, A., Gülpers, V., Herdoiza, G., Horch, H., Jäger, B., et al. (2014a). The leading hadronic contribution to (g-2) of the muon: The chiral behavior using the mixed representation method. arXiv:1410.7491 [hep-lat].

[Francis et al. 2014b] Francis, A., Gülpers, V., Jäger, B., Meyer, H., von Hippel, G., et al. (2014b). The leading disconnected contribution to the anomalous magnetic moment of the muon. *PoS*, LATTICE2014:128. arXiv:1411.7592 [hep-lat].

[Francis et al. 2014c] Francis, A., Herdoíza, G., Horch, H., Jäger, B., Meyer, H. B., et al. (2014c). Study of the Couplings of QED and QCD from the Adler Function. arXiv:1412.6934 [hep-lat].

[Frezzotti and Rossi 2004a] Frezzotti, R. and Rossi, G. (2004a). Chirally improving Wilson fermions. 1. O(a) improvement. *JHEP*, 0408:007. arXiv:hep-lat/0306014 [hep-lat].

[Frezzotti and Rossi 2004b] Frezzotti, R. and Rossi, G. (2004b). Chirally improving Wilson fermions. II. Four-quark operators. *JHEP*, 0410:070. arXiv:hep-lat/0407002 [hep-lat].

[Frezzotti and Rossi 2004c] Frezzotti, R. and Rossi, G. (2004c). Twisted mass lattice QCD with mass nondegenerate quarks. *Nucl.Phys.Proc.Suppl.*, 128:193–202. arXiv:hep-lat/0311008 [hep-lat].

[Frezzotti et al. 2006] Frezzotti, R., Martinelli, G., Papinutto, M., and Rossi, G. (2006). Reducing cutoff effects in maximally twisted lattice QCD close to the chiral limit. *JHEP*, 0604:038. arXiv:hep-lat/0503034 [hep-lat].

[Friar et al. 1999] Friar, J. L., Martorell, J., and Sprung, D. (1999). Hadronic vacuum polarization and the Lamb shift. *Phys.Rev.*, A59:4061–4063. arXiv:nucl-th/9812053 [nucl-th].

[Fritzsch et al. 1973] Fritzsch, H., Gell-Mann, M., and Leutwyler, H. (1973). Advantages of the Color Octet Gluon Picture. *Phys.Lett.*, B47:365–368.

[Garrett and Duda 2011] Garrett, K. and Duda, G. (2011). Dark Matter: A Primer. *Adv.Astron.*, 2011:968283. `arXiv:1006.2483 [hep-ph]`.

[Gattringer and Lang 2010] Gattringer, C. and Lang, C. B. (2010). *Quantum chromodynamics on the lattice*, volume 788 of *Lect.Notes Phys.* Springer Heidelberg.

[Gell-Mann 1962] Gell-Mann, M. (1962). Symmetries of baryons and mesons. *Phys.Rev.*, 125:1067–1084.

[Gell-Mann et al. 1962] Gell-Mann, M., Sharp, D., and Wagner, W. (1962). Decay rates of neutral mesons. *Phys.Rev.Lett.*, 8:261.

[Giudice et al. 2012] Giudice, G., Paradisi, P., and Passera, M. (2012). Testing new physics with the electron g-2. *JHEP*, 1211:113. `arXiv:1208.6583 [hep-ph]`.

[Glashow 1961a] Glashow, S. (1961a). Partial Symmetries of Weak Interactions. *Nucl.Phys.*, 22:579–588.

[Glashow 1961b] Glashow, S. (1961b). Partial Symmetries of Weak Interactions. *Nucl.Phys.*, 22:579–588.

[Glashow et al. 1970] Glashow, S., Iliopoulos, J., and Maiani, L. (1970). Weak Interactions with Lepton-Hadron Symmetry. *Phys.Rev.*, D2:1285–1292.

[Goecke et al. 2011] Goecke, T., Fischer, C. S., and Williams, R. (2011). Leading-order calculation of hadronic contributions to the muon $g-2$ using the Dyson-Schwinger approach. *Phys.Lett.*, B704:211–217. `arXiv:1107.2588 [hep-ph]`.

[Goldstone 1961] Goldstone, J. (1961). Field Theories with Superconductor Solutions. *Nuovo Cim.*, 19:154–164.

[Goldstone et al. 1962] Goldstone, J., Salam, A., and Weinberg, S. (1962). Broken Symmetries. *Phys.Rev.*, 127:965–970.

[Golterman et al. 2013] Golterman, M., Maltman, K., and Peris, S. (2013). Tests of hadronic vacuum polarization fits for the muon anomalous magnetic moment. *Phys.Rev.*, D88(11):114508. `arXiv:1309.2153 [hep-lat]`.

[Golterman et al. 2014] Golterman, M., Maltman, K., and Peris, S. (2014). New strategy for the lattice evaluation of the leading order hadronic contribution to $(g2)\mu$. *Phys.Rev.*, D90(7):074508. `arXiv:1405.2389 [hep-lat]`.

[Green et al. 2015] Green, J., Gryniuk, O., von Hippel, G., Meyer, H. B., and Pascalutsa, V. (2015). Lattice QCD calculation of hadronic light-by-light scattering. `arXiv:1507.01577 [hep-lat]`.

[Groote and Pivovarov 2002] Groote, S. and Pivovarov, A. (2002). Low-energy gluon contributions to the vacuum polarization of heavy quarks. *JETP Lett.*, 75:221. `arXiv:hep-ph/0103047 [hep-ph]`.

[Gross and Wilczek 1973] Gross, D. J. and Wilczek, F. (1973). Ultraviolet Behavior of Nonabelian Gauge Theories. *Phys.Rev.Lett.*, 30:1343–1346.

[Guralnik et al. 1964] Guralnik, G., Hagen, C., and Kibble, T. (1964). Global Conservation Laws and Massless Particles. *Phys.Rev.Lett.*, 13:585–587.

[HPQCD 2008] **HPQCD Collaboration**, Allison, I. et al. (2008). High-Precision Charm-Quark Mass from Current-Current Correlators in Lattice and Continuum QCD. *Phys.Rev.*, D78:054513. `arXiv:0805.2999 [hep-lat]`.

[HPQCD 2014] **HPQCD Collaboration**, Chakraborty, B. et al. (2014). Strange and charm quark contributions to the anomalous magnetic moment of the muon. *Phys.Rev.*, D89(11):114501. `arXiv:1403.1778 [hep-lat]`.

[HPQCD, UKQCD 2007] **HPQCD, UKQCD Collaborations**, Follana, E. et al. (2007). Highly improved staggered quarks on the lattice, with applications to charm physics. *Phys.Rev.*, D75:054502. `arXiv:hep-lat/0610092 [hep-lat]`.

[Hagiwara et al. 2007] Hagiwara, K., Martin, A., Nomura, D., and Teubner, T. (2007). Improved predictions for g-2 of the muon and alpha(QED) (M**2(Z)). *Phys.Lett.*, B649:173–179. `arXiv:hep-ph/0611102 [hep-ph]`.

[Hagiwara et al. 2011] Hagiwara, K., Liao, R., Martin, A. D., Nomura, D., and Teubner, T. (2011). $(g-2)_\mu$ and alpha(M_Z^2) re-evaluated using new precise data. *J.Phys.*, G38:085003. `arXiv:1105.3149 [hep-ph]`.

[Hanneke et al. 2008] Hanneke, D., Fogwell, S., and Gabrielse, G. (2008). New Measurement of the Electron Magnetic Moment and the Fine Structure Constant. *Phys.Rev.Lett.*, 100:120801. `arXiv:0801.1134 [physics.atom-ph]`.

[Harlander and Steinhauser 2003] Harlander, R. V. and Steinhauser, M. (2003). rhad: A Program for the evaluation of the hadronic R ratio in the perturbative regime of QCD. *Comput.Phys.Commun.*, 153:244–274. `arXiv:hep-ph/0212294 [hep-ph]`.

[Herdoiza et al. 2014] Herdoiza, G., Horch, H., Jger, B., and Wittig, H. (2014). Fitting the Lattice Vacuum Polarisation Function to Perturbation Theory. *PoS*, LATTICE2013:444.

[Hewett et al. 2012] Hewett, J., Weerts, H., Brock, R., Butler, J., Casey, B., et al. (2012). Fundamental Physics at the Intensity Frontier. `arXiv:1205.2671 [hep-ex]`.

[Higgs 1964] Higgs, P. W. (1964). Broken Symmetries and the Masses of Gauge Bosons. *Phys.Rev.Lett.*, 13:508–509.

[Hoogerheide et al. 2014] Hoogerheide, S. F., Dorr, J., Novitski, E., and Gabrielse, G. (2014). High Efficiency Positron Accumulation for High-Precision Measurements. `arXiv:1501.00096 [physics.ins-det]`.

[Iwasaki 1985] Iwasaki, Y. (1985). Renormalization Group Analysis of Lattice Theories and Improved Lattice Action: Two-Dimensional Nonlinear O(N) Sigma Model. *Nucl.Phys.*, B258:141–156.

[J-PARC New g-2/EDM experiment 2011] **J-PARC New g-2/EDM experiment Collaboration**, Iinuma, H. (2011). New approach to the muon g-2 and EDM experiment at J-PARC. *J.Phys.Conf.Ser.*, 295:012032.

[Jansen and Urbach 2009] Jansen, K. and Urbach, C. (2009). tmLQCD: A Program suite to simulate Wilson Twisted mass Lattice QCD. *Comput.Phys.Commun.*, 180:2717–2738. `arXiv:0905.3331 [hep-lat]`.

[Jansen et al. 2009] Jansen, K., McNeile, C., Michael, C., and Urbach, C. (2009). Meson masses and decay constants from unquenched lattice QCD. *Phys. Rev.*, D80:054510. `arXiv:arXiv:0906.4720 [hep-lat]`.

[Jansen et al. 2011] Jansen, K., Petschlies, M., and Urbach, C. (2011). Charm Current-Current Correlators in Twisted Mass Lattice QCD. *PoS*, LATTICE2011:234. `arXiv:1111.5252 [hep-lat]`.

[Jansen et al. 2014] Jansen, K., Feng, X., Hashimoto, S., Hotzel, G., Petschlies, M., et al. (2014). Using analytic continuation for the hadronic vacuum polarization computation. *PoS*, LATTICE2013:464.

[Jegerlehner 1986a] Jegerlehner, F. (1986a). Hadronic Contributions to Electroweak Parameter Shifts: A Detailed Analysis. *Z.Phys.*, C32:195.

[Jegerlehner 1986b] Jegerlehner, F. (1986b). Vector Boson Parameters: Scheme Dependence and Theoretical Uncertainties. *Z.Phys.*, C32:425.

[Jegerlehner 1990] Jegerlehner, F. (1990). Renormalizing the standard model. *Conf.Proc.*, C900603:476–590.

[Jegerlehner 2008a] Jegerlehner, F. (2008a). Muon g - 2 update. *Nucl. Phys. Proc. Suppl.*, 181-182:26–31.

[Jegerlehner 2008b] Jegerlehner, F. (2008b). The anomalous magnetic moment of the muon. *Springer Tracts Mod.Phys.*, 226:1–426.

[Jegerlehner 2008c] Jegerlehner, F. (2008c). The Running fine structure constant alpha(E) via the Adler function. *Nucl.Phys.Proc.Suppl.*, 181-182:135–140. `arXiv:0807.4206 [hep-ph]`.

[Jegerlehner 2011] Jegerlehner, F. (2011). Electroweak effective couplings for future precision experiments. *Nuovo Cim.*, 034C:31–40. `arXiv:1107.4683 [hep-ph]`.

[Jegerlehner 2012] Jegerlehner, F. (2012). alphaQED. *http://www-com.physik.hu-berlin.de/ fjeger/software.html*.

[Jegerlehner 2015] Jegerlehner, F. (2015). *private communication*.

[Jegerlehner and Nyffeler 2009] Jegerlehner, F. and Nyffeler, A. (2009). The Muon g-2. *Phys. Rept.*, 477:1–110. `arXiv:arXiv:0902.3360 [hep-ph]`.

[Jegerlehner and Szafron 2011] Jegerlehner, F. and Szafron, R. (2011). $\rho^0 - \gamma$ mixing in the neutral channel pion form factor F_π^e and its role in comparing e^+e^- with τ spectral functions. *Eur.Phys.J.*, C71:1632. `arXiv:1101.2872 [hep-ph]`.

[Ji and Jung 2001] Ji, X.-d. and Jung, C.-w. (2001). Studying hadronic structure of the photon in lattice QCD. *Phys.Rev.Lett.*, 86:208. arXiv:hep-lat/0101014 [hep-lat].

[Karsten and Smit 1981] Karsten, L. H. and Smit, J. (1981). Lattice Fermions: Species Doubling, Chiral Invariance, and the Triangle Anomaly. *Nucl.Phys.*, B183:103.

[Kinster and Houston 1934] Kinster, L. and Houston, W. (1934). unknown. *Phys.Rev.*, 45:104.

[Kobayashi and Maskawa 1973] Kobayashi, M. and Maskawa, T. (1973). CP Violation in the Renormalizable Theory of Weak Interaction. *Prog.Theor.Phys.*, 49:652–657.

[Kronfeld and Quigg 2010] Kronfeld, A. S. and Quigg, C. (2010). Resource Letter: Quantum Chromodynamics. *Am.J.Phys.*, 78:1081–1116. arXiv:1002.5032 [hep-ph].

[Kumar et al. 2013] Kumar, K., Mantry, S., Marciano, W., and Souder, P. (2013). Low Energy Measurements of the Weak Mixing Angle. *Ann.Rev.Nucl.Part.Sci.*, 63:237–267. arXiv:1302.6263 [hep-ex].

[Kühn et al. 2007] Kühn, J. H., Steinhauser, M., and Sturm, C. (2007). Heavy Quark Masses from Sum Rules in Four-Loop Approximation. *Nucl.Phys.*, B778:192–215. arXiv:hep-ph/0702103 [HEP-PH].

[LEPEWWG 2010] **ALEPH, CDF, D0, DELPHI, L3, OPAL, SLD, LEP Electroweak Working Group, Tevatron Electroweak Working Group, SLD Electroweak and Heavy Flavour Groups**, Group, L. E. W. (2010). Precision Electroweak Measurements and Constraints on the Standard Model. arXiv:1012.2367 [hep-ex].

[Lautrup et al. 1972] Lautrup, B., Peterman, A., and de Rafael, E. (1972). Recent developments in the comparison between theory and experiments in quantum electrodynamics. *Phys.Rept.*, 3:193–260.

[Lellouch and Lüscher 2001] Lellouch, L. and Lüscher, M. (2001). Weak transition matrix elements from finite volume correlation functions. *Commun.Math.Phys.*, 219:31–44. arXiv:hep-lat/0003023 [hep-lat].

[Lüscher et al. 1996] Lüscher, M., Sint, S., Sommer, R., and Weisz, P. (1996). Chiral symmetry and O(a) improvement in lattice QCD. *Nucl.Phys.*, B478:365–400. arXiv:hep-lat/9605038 [hep-lat].

[Lüders 1954] Lüders, G. (1954). On the Equivalence of Invariance under Time Reversal and under Particle-Antiparticle Conjugation for Relativistic Field Theories. *Kong.Dan.Vid.Sel.Mat.Fys.Med.*, 28N5:1–17.

[Lüscher 1977] Lüscher, M. (1977). Construction of a Selfadjoint, Strictly Positive Transfer Matrix for Euclidean Lattice Gauge Theories. *Commun.Math.Phys.*, 54:283.

[Lüscher 1986a] Lüscher, M. (1986a). Volume Dependence of the Energy Spectrum in Massive Quantum Field Theories. 1. Stable Particle States. *Commun.Math.Phys.*, 104:177.

[Lüscher 1986b] Lüscher, M. (1986b). Volume Dependence of the Energy Spectrum in Massive Quantum Field Theories. 2. Scattering States. *Commun.Math.Phys.*, 105:153–188.

[Lüscher 2010] Lüscher, M. (2010). Computational Strategies in Lattice QCD. pages 331–399. `arXiv:1002.4232 [hep-lat]`.

[Lüscher and Weisz 1985] Lüscher, M. and Weisz, P. (1985). On-Shell Improved Lattice Gauge Theories. *Commun.Math.Phys.*, 97:59.

[MILC 2010] **MILC Collaboration**, Bazavov, A. et al. (2010). Scaling studies of QCD with the dynamical HISQ action. *Phys.Rev.*, D82:074501. `arXiv:1004.0342 [hep-lat]`.

[MILC 2013] **MILC Collaboration**, Bazavov, A. et al. (2013). Lattice QCD ensembles with four flavors of highly improved staggered quarks. *Phys.Rev.*, D87(5):054505. `arXiv:1212.4768 [hep-lat]`.

[MOLLER 2014] **MOLLER Collaboration**, Benesch, J. et al. (2014). The MOLLER Experiment: An Ultra-Precise Measurement of the Weak Mixing Angle Using Møller Scattering. `arXiv:1411.4088 [nucl-ex]`.

[Majorana 1937] Majorana, E. (1937). Theory of the Symmetry of Electrons and Positrons. *Nuovo Cim.*, 14:171–184.

[Marciano 1993] Marciano, W. J. (1993). Spin and precision electroweak physics.

[Marciano and Sirlin 1984] Marciano, W. and Sirlin, A. (1984). On Some General Properties of the O(alpha) Corrections to Parity Violation in Atoms. *Phys.Rev.*, D29:75.

[Marinkovic et al. 2015] Marinkovic, M., Boyle, P., Del Debbio, L., Juettner, A., Maltman, K., et al. (2015). Towards the physical point hadronic vacuum polarisation from Moebius DWF. `arXiv:1502.05308 [hep-lat]`.

[Maris and Roberts 2003] Maris, P. and Roberts, C. D. (2003). Dyson-Schwinger equations: A Tool for hadron physics. *Int.J.Mod.Phys.*, E12:297–365. `arXiv:nucl-th/0301049 [nucl-th]`.

[Martinelli et al. 1995] Martinelli, G., Pittori, C., Sachrajda, C. T., Testa, M., and Vladikas, A. (1995). A General method for nonperturbative renormalization of lattice operators. *Nucl.Phys.*, B445:81–108. `arXiv:hep-lat/9411010 [hep-lat]`.

[Martynenko and Faustov 2001] Martynenko, A. and Faustov, R. (2001). Effects of vacuum polarization and of proton polarizability in the Lamb shift of muonic hydrogen. *Phys.Atom.Nucl.*, 64:1282–1287.

[Metropolis 1949] Metropolis, N. (1949). The monte carlo method. *Journal of the American Statistical Association*, 44:335–341.

[Meyer 2011] Meyer, H. B. (2011). Lattice QCD and the Timelike Pion Form Factor. *Phys.Rev.Lett.*, 107:072002. `arXiv:1105.1892 [hep-lat]`.

[Michael et al. 2013] **ETM Collaboration**, Michael, C., Ottnad, K., and Urbach, C. (2013). η and η' mixing from Lattice QCD. *Phys.Rev.Lett.*, 111(18):181602. arXiv:1310.1207 [hep-lat].

[Miller et al. 2012] Miller, J. P., Rafael, E. d., Roberts, B. L., and Stöckinger, D. (2012). Muon (g-2): Experiment and Theory. *Ann.Rev.Nucl.Part.Sci.*, 62:237–264.

[Montvay and Münster 1994] Montvay, I. and Münster, G. (1994). *Quantum fields on a lattice*. Cambridge monographs on mathematical physics. Cambridge University Press.

[Muon (g-2) 2006] **Muon (g-2) Collaboration**, Bennett, G. et al. (2006). Final Report of the Muon E821 Anomalous Magnetic Moment Measurement at BNL. *Phys. Rev.*, D73:072003. arXiv:hep-ex/0602035 [hep-ex].

[Muon (g-2) 2009] **Muon (g-2) Collaboration**, Lynch, K. R. (2009). A next generation muon g-2 experiment. *Nucl.Phys.Proc.Suppl.*, 189:201–207.

[NASA et al. 2013] NASA, ESA, CXC, Bradac, M., and Allen, S. (2013).

[Nambu and Sakurai 1962] Nambu, Y. and Sakurai, J. (1962). Rare Decay Modes of the omega (eta) Meson. *Phys.Rev.Lett.*, 8:79–81.

[Neff et al. 2001] Neff, H., Eicker, N., Lippert, T., Negele, J. W., and Schilling, K. (2001). On the low fermionic eigenmode dominance in QCD on the lattice. *Phys.Rev.*, D64:114509. arXiv:hep-lat/0106016 [hep-lat].

[Nielsen and Ninomiya 1981] Nielsen, H. B. and Ninomiya, M. (1981). Absence of Neutrinos on a Lattice. 1. Proof by Homotopy Theory. *Nucl.Phys.*, B185:20.

[Noether 1918] Noether, E. (1918). Invariant Variation Problems. *Gott.Nachr.*, 1918:235–257. arXiv:physics/0503066 [physics].

[Nomura and Teubner 2013] Nomura, D. and Teubner, T. (2013). Hadronic contributions to the anomalous magnetic moment of the electron and the hyperfine splitting of muonium. *Nucl.Phys.*, B867:236–243. arXiv:1208.4194 [hep-ph].

[Osterwalder and Schrader 1973] Osterwalder, K. and Schrader, R. (1973). Axioms for Euclidean Green's Functions. 1. *Commun.Math.Phys.*, 31:83–112.

[Osterwalder and Schrader 1975] Osterwalder, K. and Schrader, R. (1975). Axioms for Euclidean Green's Functions. 2. *Commun.Math.Phys.*, 42:281.

[Osterwalder and Seiler 1978] Osterwalder, K. and Seiler, E. (1978). Gauge Field Theories on the Lattice. *Annals Phys.*, 110:440.

[PDG 2014] **Particle Data Group**, Olive, K. et al. (2014). Review of Particle Physics. *Chin.Phys.*, C38:090001.

[PVDIS 2014] **PVDIS Collaboration**, Wang, D. et al. (2014). Measurement of parity violation in electronquark scattering. *Nature*, 506(7486):67–70.

[Pauli 1955] Pauli, W. (1955). Exclusion principle, Lorentz group and reflection of space-time and charge. In *Niels Bohr and the development of physics*, pages 30–51.

[Perl et al. 1975] Perl, M. L., Abrams, G., Boyarski, A., Breidenbach, M., Briggs, D., et al. (1975). Evidence for Anomalous Lepton Production in e+ - e- Annihilation. *Phys.Rev.Lett.*, 35:1489–1492.

[Peskin and Schroeder 1995] Peskin, M. E. and Schroeder, D. V. (1995). An Introduction to quantum field theory.

[Petschlies 2013] Petschlies, M. (2013). *Non-perturbative investigation of current correlators in twisted mass lattice QCD*. PhD thesis, Humboldt-Universität zu Berlin.

[Pich 1998] Pich, A. (1998). Effective field theory: Course. pages 949–1049. `arXiv:hep-ph/9806303 [hep-ph]`.

[Pich 2014] Pich, A. (2014). Precision Tau Physics. *Prog.Part.Nucl.Phys.*, 75:41–85. `arXiv:1310.7922 [hep-ph]`.

[Planck 2015] **Planck Collaboration**, Ade, P. et al. (2015). Planck 2015 results. XIII. Cosmological parameters. `arXiv:1502.01589 [astro-ph.CO]`.

[Politzer 1973] Politzer, H. D. (1973). Reliable Perturbative Results for Strong Interactions? *Phys.Rev.Lett.*, 30:1346–1349.

[Prades et al. 2009] Prades, J., de Rafael, E., and Vainshtein, A. (2009). Hadronic Light-by-Light Scattering Contribution to the Muon Anomalous Magnetic Moment. `arXiv:0901.0306 [hep-ph]`.

[QCDSF 2004] **QCDSF Collaboration**, Göckeler, M. et al. (2004). Vacuum polarization and hadronic contribution to muon g-2 from lattice QCD. *Nucl.Phys.*, B688:135–164. `arXiv:hep-lat/0312032 [hep-lat]`.

[Qweak 2014] **Qweak Collaboration**, Armstrong, D. S. (2014). First result from Q_{weak}. *EPJ Web Conf.*, 73:07008.

[R Core Team 2012] R Core Team (2012). *R: A Language and Environment for Statistical Computing*. R Foundation for Statistical Computing, Vienna, Austria. ISBN 3-900051-07-0.

[Reed and Simon 1975] Reed, M. and Simon, B. (1975). *Methods of modern mathematical physics. II. Fourier Analysis, Self-adjointness*. Academic Press [Harcourt Brace Jovanovich Publishers], New York.

[Reisz 1988a] Reisz, T. (1988a). A Power Counting Theorem for Feynman Integrals on the Lattice. *Commun.Math.Phys.*, 116:81.

[Reisz 1988b] Reisz, T. (1988b). Renormalization of Feynman Integrals on the Lattice. *Commun.Math.Phys.*, 117:79.

[Reisz 1989] Reisz, T. (1989). Lattice Gauge Theory: Renormalization to All Orders in the Loop Expansion. *Nucl.Phys.*, B318:417.

[Renner et al. 2012] Renner, Dru B. and Feng, X., Jansen, K., and Petschlies, M. (2012). Nonperturbative QCD corrections to electroweak observables. *PoS*, LATTICE2011:022. `arXiv:1206.3113 [hep-lat]`.

[Roberts 2010a] Roberts, B. L. (2010a). Status of the Fermilab Muon ($g-2$) Experiment. *Chin.Phys.*, C34:741–744. arXiv:1001.2898 [hep-ex].

[Roberts 2010b] Roberts, B. L. (2010b). Status of the Fermilab Muon (g-2) Experiment. *Chin.Phys.*, C34:741–744. arXiv:1001.2898 [hep-ex].

[Rothe 1992] Rothe, H. (1992). *Lattice gauge theories: An Introduction*, volume 43 of *World Sci.Lect.Notes Phys.* World Scientific.

[SLAC E158 2005] **SLAC E158 Collaboration**, Anthony, P. et al. (2005). Precision measurement of the weak mixing angle in Moller scattering. *Phys.Rev.Lett.*, 95:081601. arXiv:hep-ex/0504049 [hep-ex].

[SLAC-SP-017 1974] **SLAC-SP-017 Collaboration**, Augustin, J. et al. (1974). Discovery of a Narrow Resonance in e+ e- Annihilation. *Phys.Rev.Lett.*, 33:1406–1408.

[Saad 1984] Saad, Y. (1984). Tchebyshev Acceleration Techniques for Solving Nonsymmetric Eigenvalue Problems. *Math. Comp.*, 42:567–588.

[Sachrajda and Villadoro 2005] Sachrajda, C. and Villadoro, G. (2005). Twisted boundary conditions in lattice simulations. *Phys.Lett.*, B609:73–85. arXiv:hep-lat/0411033 [hep-lat].

[Sakharov 1967] Sakharov, A. (1967). Violation of CP Invariance, c Asymmetry, and Baryon Asymmetry of the Universe. *Pisma Zh.Eksp.Teor.Fiz.*, 5:32–35.

[Salam 1968] Salam, A. (1968). Weak and Electromagnetic Interactions. *Conf.Proc.*, C680519:367–377.

[Schwinger 1948] Schwinger, J. S. (1948). On Quantum electrodynamics and the magnetic moment of the electron. *Phys.Rev.*, 73:416–417.

[Sharpe and Singleton 1998] Sharpe, S. R. and Singleton, Robert L., J. (1998). Spontaneous flavor and parity breaking with Wilson fermions. *Phys.Rev.*, D58:074501. arXiv:hep-lat/9804028 [hep-lat].

[Sheikholeslami and Wohlert 1985] Sheikholeslami, B. and Wohlert, R. (1985). Improved Continuum Limit Lattice Action for QCD with Wilson Fermions. *Nucl.Phys.*, B259:572.

[Shifman et al. 1979] Shifman, M. A., Vainshtein, A., and Zakharov, V. I. (1979). QCD and Resonance Physics. Sum Rules. *Nucl.Phys.*, B147:385–447.

[Shindler 2008] Shindler, A. (2008). Twisted mass lattice QCD. *Phys.Rept.*, 461:37–110. arXiv:0707.4093 [hep-lat].

[Sint 2007] Sint, S. (2007). Lattice QCD with a chiral twist. arXiv:hep-lat/0702008 [HEP-LAT].

[SoLID 2014] **SoLID Collaboration**, Chen, J., Gao, H., Hemmick, T., Meziani, Z. E., and Souder, P. (2014). A White Paper on SoLID (Solenoidal Large Intensity Device). arXiv:1409.7741 [nucl-ex].

[Srednicki 2007] Srednicki, M. (2007). *Quantum field theory*. Cambridge University Press.

[Symanzik 1966] Symanzik, K. (1966). Euclidean quantum field theory. i. equations for a scalar model. *Journal of Mathematical Physics*, 7(3):510–525.

[Symanzik 1983a] Symanzik, K. (1983a). Continuum Limit and Improved Action in Lattice Theories. 1. Principles and phi**4 Theory. *Nucl.Phys.*, B226:187.

[Symanzik 1983b] Symanzik, K. (1983b). Continuum Limit and Improved Action in Lattice Theories. 2. O(N) Nonlinear Sigma Model in Perturbation Theory. *Nucl.Phys.*, B226:205.

[TASSO 1979] **TASSO Collaboration**, Brandelik, R. et al. (1979). Evidence for Planar Events in e+ e- Annihilation at High-Energies. *Phys.Lett.*, B86:243.

[Teubner et al. 2011] Teubner, T., Hagiwara, K., Liao, R., Martin, A., and Nomura, D. (2011). (g-2)mu and Delta alpha: Recent developments and status report. *AIP Conf.Proc.*, 1343:340–342.

[Tsai 1971] Tsai, Y.-S. (1971). Decay Correlations of Heavy Leptons in $e^+e^- \to \text{lepton}^+\text{lepton}^-$. *Phys.Rev.*, D4:2821.

[UA1 1983] **UA1 Collaboration**, Arnison, G. et al. (1983). Experimental Observation of Isolated Large Transverse Energy Electrons with Associated Missing Energy at s**(1/2) = 540-GeV. *Phys.Lett.*, B122:103–116.

[UA2 1983] **UA2 Collaboration**, Banner, M. et al. (1983). Observation of Single Isolated Electrons of High Transverse Momentum in Events with Missing Transverse Energy at the CERN anti-p p Collider. *Phys.Lett.*, B122:476–485.

[Ukawa 2015] Ukawa, A. (2015). Kenneth Wilson and lattice QCD. `arXiv:1501.04215 [hep-lat]`.

[Wang et al. 2014] Wang, D., Pan, K., Subedi, R., Ahmed, Z., Allada, K., et al. (2014). Measurement of Parity-Violating Asymmetry in Electron-Deuteron Inelastic Scattering. `arXiv:1411.3200 [nucl-ex]`.

[Weinberg 1967] Weinberg, S. (1967). A Model of Leptons. *Phys.Rev.Lett.*, 19:1264–1266.

[Weisz 2010] Weisz, P. (2010). Renormalization and lattice artifacts. pages 93–160. `arXiv:1004.3462 [hep-lat]`.

[Wetzel 1981] Wetzel, W. (1981). The Hadronic Contribution to the W and Z Mass. *Z.Phys.*, C11:117.

[Wick 1954] Wick, G. (1954). Properties of Bethe-Salpeter Wave Functions. *Phys.Rev.*, 96:1124–1134.

[Wightman 1956] Wightman, A. (1956). Quantum Field Theory in Terms of Vacuum Expectation Values. *Phys.Rev.*, 101:860–866.

[Wilson 1969] Wilson, K. G. (1969). Nonlagrangian models of current algebra. *Phys.Rev.*, 179:1499–1512.

[Wilson 1974] Wilson, K. G. (1974). Confinement of Quarks. *Phys.Rev.*, D10:2445–2459.

[Wilson 1975] Wilson, K. G. (1975). Quarks and Strings on a Lattice. page 99.

[Wood et al. 1997] Wood, C., Bennett, S., Cho, D., Masterson, B., Roberts, J., et al. (1997). Measurement of parity nonconservation and an anapole moment in cesium. *Science*, 275:1759–1763.

[XLF 2005a] **XLF Collaboration**, Jansen, K., Papinutto, M., Shindler, A., Urbach, C., and Wetzorke, I. (2005a). Light quarks with twisted mass fermions. *Phys.Lett.*, B619:184–191. `arXiv:hep-lat/0503031 [hep-lat]`.

[XLF 2005b] **XLF Collaboration**, Jansen, K., Papinutto, M., Shindler, A., Urbach, C., and Wetzorke, I. (2005b). Quenched scaling of Wilson twisted mass fermions. *JHEP*, 0509:071. `arXiv:hep-lat/0507010 [hep-lat]`.

[Zweig 1964] Zweig, G. (1964). An SU(3) model for strong interaction symmetry and its breaking. Version 2. pages 22–101.

List of own publications

[1] F. Burger, K. Jansen, M. Petschlies and G. Pientka, "Leading hadronic contributions to the running of the electroweak coupling constants from lattice QCD," submitted to JHEP, arXiv:1505.03283 [hep-lat].

[2] F. Burger, G. Hotzel, K. Jansen and M. Petschlies, "Leading-order hadronic contributions to the electron and tau anomalous magnetic moments," submitted to PLB, arXiv:1501.05110 [hep-lat].

[3] F. Burger, G. Hotzel, K. Jansen and M. Petschlies, "The hadronic vacuum polarization and automatic $\mathcal{O}(a)$ improvement for twisted mass fermions," JHEP **1503** (2015) 073 [arXiv:1412.0546 [hep-lat]].

[4] F. Burger, G. Hotzel, K. Jansen and M. Petschlies, "Lepton anomalous magnetic moments from twisted mass fermions," PoS LATTICE **2014** (2014) 145 [arXiv:1411.0705 [hep-lat]].

[5] K. Jansen, X. Feng, S. Hashimoto, G. Hotzel, M. Petschlies and D. Renner, "Using analytic continuation for the hadronic vacuum polarization computation," PoS LATTICE **2013** (2014) 464.

[6] F. Burger, X. Feng, G. Hotzel, K. Jansen, M. Petschlies and D. B. Renner, "Leading-order hadronic contribution to the anomalous magnetic moment of the muon from $N_f = 2{+}1{+}1$ twisted mass fermions," PoS LATTICE **2013** (2014) 301 [arXiv:1311.3885 [hep-lat]].

[7] F. Burger, G. Hotzel, M. Müller-Preussker, E. M. Ilgenfritz and M. P. Lombardo, "Towards thermodynamics with $N_f = 2 + 1 + 1$ twisted mass quarks," PoS Lattice **2013** (2014) 153 [arXiv:1311.1631 [hep-lat]].

[8] X. Feng, S. Hashimoto, G. Hotzel, K. Jansen, M. Petschlies and D. B. Renner, "Using analytic continuation for the hadronic vacuum polarization computation," PoS Lattice **2013** (2014) 464 arXiv:1311.0652 [hep-lat].

[9] F. Burger, X. Feng, G. Hotzel, K. Jansen, M. Petschlies and D. B. Renner, "Four-Flavour Leading-Order Hadronic Contribution To The Muon Anomalous Magnetic Moment," JHEP **1402** (2014) 099 [arXiv:1308.4327 [hep-lat]].

[10] X. Feng, S. Hashimoto, G. Hotzel, K. Jansen, M. Petschlies and D. B. Renner, "Computing the hadronic vacuum polarization function by analytic continuation," Phys. Rev. D **88** (2013) 034505 [arXiv:1305.5878 [hep-lat]].

[11] X. Feng, G. Hotzel, K. Jansen, M. Petschlies and D. B. Renner, "Leading-order hadronic contributions to a_μ and α_{QED} from $N_f = 2+1+1$ twisted mass fermions," PoS LATTICE **2012** (2012) 174 [arXiv:1211.0828 [hep-lat]].

[12] R. Horsley, G. Hotzel, E. M. Ilgenfritz, R. Millo, H. Perlt, P. E. L. Rakow, Y. Nakamura, G. Schierholz and A. Schiller, "Wilson loops to 20th order numerical stochastic perturbation theory," Phys. Rev. D **86** (2012) 054502 [arXiv:1205.1659 [hep-lat]].

[13] R. Horsley, G. Hotzel, E.-M. Ilgenfritz, Y. Nakamura, H. Perlt, P. E. L. Rakow, G. Schierholz and A. Schiller, "Very high order lattice perturbation theory for Wilson loops," PoS LATTICE **2010** (2010) 264 [arXiv:1010.4674 [hep-lat]].

Selbstständigkeitserklärung

Hiermit erkläre ich, dass ich die vorliegende Dissertation selbstständig und nur unter Verwendung der angegebenen Literatur und Hilfsmittel erarbeitet und verfasst habe.

Grit Pientka

Berlin, 14. Juli 2015